

**STRUCTURAL OPTIMIZATION STRATEGIES
VIA DIFFERENT OPTIMIZATION AND SOLVER CODES
AND AEROSPACE APPLICATIONS**

**A THESIS SUBMITTED TO
THE GRADUATE SCHOOL OF NATURAL AND APPLIED SCIENCES
OF
MIDDLE EAST TECHNICAL UNIVERSITY**

BY

MUSTAFA EKREN

**IN PARTIAL FULFILLMENT OF THE REQUIREMENTS
FOR
THE DEGREE OF MASTER OF SCIENCE
IN
AEROSPACE ENGINEERING**

DECEMBER 2008

Approval of the thesis:

**STRUCTURAL OPTIMIZATION STRATEGIES
VIA DIFFERENT OPTIMIZATION AND SOLVER CODES
AND AEROSPACE APPLICATIONS**

submitted by **MUSTAFA EKREN** in partial fulfillment of the requirements for
the degree of **Master of Science in Aerospace Engineering Department,**
Middle East Technical University by,

Prof. Dr. Canan Özgen _____
Dean, Graduate School of **Natural and Applied Sciences**

Prof. Dr. İsmail Hakkı Tuncer _____
Head of Department, **Aerospace Engineering**

Assoc. Prof. Dr. Altan Kayran _____
Supervisor, **Aerospace Engineering Dept., METU**

Examining Committee Members:

Prof. Dr. Ozan Tekinalp _____
Aerospace Engineering Dept., METU

Assoc. Prof. Dr. Altan Kayran _____
Aerospace Engineering Dept., METU

Asst. Prof. Dr. Melin Şahin _____
Aerospace Engineering Dept., METU

Dr. Güçlü Seber _____
Aerospace Engineering Dept., METU

Dr. Küçük Ayşe İlhan _____
TAI

Date: 05.12.2008

I hereby declare that all information in this document has been obtained and presented in accordance with academic rules and ethical conduct. I also declare that, as required by these rules and conduct, I have fully cited and referenced all material and results that are not original to this work.

Name, Last name: Mustafa EKREN

Signature:

ABSTRACT

STRUCTURAL OPTIMIZATION STRATEGIES VIA DIFFERENT OPTIMIZATION AND SOLVER CODES AND AEROSPACE APPLICATIONS

Ekren, Mustafa

M.Sc., Department of Aerospace Engineering

Supervisor: Assoc. Prof. Dr. Altan Kayran

December 2008, 234 pages

In this thesis, structural optimization study is performed by using three different methods. In the first method, optimization is performed using MSC.NASTRAN Optimization Module, a commercial structural analysis program. In the second method, optimization is performed using the optimization code prepared in MATLAB and MSC.NASTRAN as the solver. As the third method, optimization is performed by using the optimization code prepared in MATLAB and analytical equations as the solver. All three methods provide certain advantages in the solution of optimization problems. Therefore, within the context of the thesis these methods are demonstrated and the interface codes specific to the programs used in this thesis are explained in detail. In order to compare the results obtained by the methods, the verification study has been performed on a cantilever beam with rectangular cross-section. In the verification study, the height and width of the cross-section of the beam are taken as the two design parameters. This way it has been possible to show the design space on the two dimensional graph, and it becomes easier to trace the progress of the optimization methods during each step. In the last section structural optimization of a multi-element wing torque box has been performed by the MSC.NASTRAN optimization module. In this section geometric property

optimization has been performed for constant tip loading and variable loading along the wing span. In addition, within the context of shape optimization optimum rib placement problem has also been solved.

Keywords: Structural Optimization, Geometric Property and Shape Optimization, Aerospace Structures, Finite Element Method

ÖZ

DEĞİŞİK OPTİMİZASYON VE ÇÖZÜCÜ KODLARIYLA YAPISAL OPTİMİZASYON STRATEJİLERİ VE HAVACILIK VE UZAY UYGULAMALARI

Ekren, Mustafa

Yüksek Lisans, Havacılık ve Uzay Mühendisliği Bölümü

Tez Yöneticisi: Doç. Dr. Altan Kayran

Aralık 2008, 234 sayfa

Bu tezde, üç farklı yöntem kullanılarak yapısal optimizasyon çalışması gerçekleştirilmiştir. Birinci yöntemde yapısal optimizasyon problemi ticari bir yapısal analiz programı olan MSC.NASTRAN optimizasyon modülü kullanılarak yapılmıştır. İkinci yöntemde MATLAB ortamında hazırlanmış optimizasyon kodu ile çözücü olarak MSC.NASTRAN kullanılarak optimizasyon problemi çözülmüştür. Üçüncü yöntem ise MATLAB ortamında hazırlanmış optimizasyon kodu ve analitik denklemler çözücü olarak kullanılmak suretiyle optimizasyon yapılmıştır. Her üç yöntemde günümüzde optimizasyon problemlerinin çözülmesinde çeşitli avantajlar sağlayabilmektedir. Bu nedenle bu tez kapsamında her üç yöntemin gösterimi gerçekleştirilmiş ve kullanılan programlara özel arayüz kodları da tez içinde detaylıca açıklanmıştır. Her üç yöntem ile elde edilen sonuçların kıyaslanmasını yapabilmek için doğrulama çalışmaları dikdörtgen kesitli ankestre giriş problemi üzerinde gerçekleştirilmiştir. Doğrulama çalışmasında kesit alanın yükseklik ve genişliği olmak üzere iki adet tasarım değişkeni kullanılmıştır. Bu sayede tasarım uzayının iki boyutlu grafik üzerinde görsel olarak gösterilmesi mümkün olmakta ve optimizasyon yöntemlerinin her adımdaki gelişiminin izlenebilmesi

kolaylaşmaktadır. Son bölümde ise çok elemanlı bir kanat tork kutu yapısının optimizasyonu MSC.NASTRAN optimizasyon modülü kullanılarak yapılmıştır. Bu kısımda sabit uç yük, kanat boyunca değişken yük durumları için geometrik özellik optimizasyonu gerçekleştirilmiştir. Ayrıca, şekil optimizasyonu kapsamında ise kanat sinir pozisyonlarının optimum yerleşim problemi çözülmüştür.

Anahtar Kelimeler: Yapısal Optimizasyon, Geometrik Özellik ve Şekil Optimizasyonu, Hava Aracı Yapıları , Sonlu Elemanlar Yöntemi,

To my wife, Pınar and to my parents, İsmet and Hasibe EKREN

ACKNOWLEDGMENTS

I would like to express my deepest gratitude and appreciation to my supervisor Assoc. Prof. Dr. Altan KAYRAN for his guidance, valuable suggestions and deepest knowledge and support at all levels of this study.

I would also like to thank to my colleagues for their assistance and patience. And of course to my company TAI.

I would like to also express my thanks for their friendship and support to, my brother Mehmet, my cousin Elif, and I also want to thank to Melih for his friendship and support.

TABLE OF CONTENTS

| | |
|---|------|
| ABSTRACT | iv |
| ÖZ | vi |
| ACKNOWLEDGMENTS | ix |
| TABLE OF CONTENTS | x |
| LIST OF FIGURES | xiii |
| LIST OF TABLES | xix |
| LIST OF SYMBOLS AND ABBREVIATIONS | xxi |
| CHAPTERS | |
| 1. INTRODUCTION | 1 |
| 1.1 OPTIMIZATION METHODS | 3 |
| 1.2 MAIN APPLICATION AREAS OF OPTIMIZED STRUCTURES ... | 4 |
| 1.2.1 AERONAUTICS | 4 |
| 1.2.2 SPACE | 5 |
| 1.2.3 MARINE | 7 |
| 1.2.4 AUTOMOTIVE | 8 |
| 1.3 ADVANTAGES OF OPTIMIZING STRUCTURES | 9 |
| 2. OPTIMIZATION THEORY FOR GRADIENT BASED METHODS | 10 |
| 2.1 ONE DIMENSIONAL OPTIMIZATION METHODS | 11 |
| 2.1.1 NEWTON RAPHSON METHOD | 12 |
| 2.1.2 BISECTION METHOD | 12 |
| 2.1.3 GOLDEN SECTION METHOD | 13 |
| 2.2 UNCONSTRAINED OPTIMIZATION WITH GRADIENT BASED METHODS | 14 |
| 2.2.1 STEEPEST DESCENT METHOD | 15 |
| 2.2.2 CONJUGATE GRADIENT METHOD | 16 |
| 2.2.3 DAVIDON-FLETCHER-POWELL METHOD | 16 |
| 2.3 CONSTRAINED OPTIMIZATION WITH GRADIENT BASED METHODS | 17 |
| 2.3.1 PENALTY FUNCTION METHOD | 17 |
| 2.3.2 AUGMENTED LAGRANGE MULTIPLIER METHOD | 18 |
| 3. OPTIMIZATION CODE IN MATLAB® | 20 |
| 3.1 AUGMENTED LAGRANGIAN MULTIPLIER METHOD SECTION | 22 |
| 3.2 DAVIDON FLETCHER POWEL METHOD SECTION | 23 |
| 3.3 GOLDEN SECTION METHOD SECTION | 23 |
| 3.4 OBJECTIVE FUNCTION SECTION FOR ANALYTIC SOLVER .. | 26 |
| 3.4.1 OBJECTIVE FUNCTION SECTION | 26 |
| 3.4.2 EQUALITY CONSTRAINT SECTION | 26 |
| 3.4.3 INEQUALITY CONSTRAINT SECTION | 26 |

| | | |
|--------|---|-----|
| 3.4.4 | UNCONSTRAINED OBJECTIVE FUNCTION SECTION | 27 |
| 3.5 | OBJECTIVE FUNCTION SECTION FOR MSC.NASTRAN [®] SOLVER | 27 |
| 3.6 | GRADIENT FUNCTION SECTION | 28 |
| 4. | OPTIMIZATION STRATEGIES WITH DIFFERENT OPTIMIZATION AND SOLVER CODES..... | 29 |
| 4.1 | OPTIMIZATION VIA USER DEVELOPED OPTIMIZATION AND SOLVER CODES | 30 |
| 4.2 | OPTIMIZATION USING AN OPTIMIZATION CODE IN MATLAB [®] AND MSC.NASTRAN [®] AS SOLVER | 32 |
| 4.3 | OPTIMIZATION USING THE OPTIMIZATION MODULE OF MSC.NASTRAN [®] | 34 |
| 4.3.1 | CREATING A BDF-FILE | 36 |
| 4.3.2 | MSC.NASTRAN [®] RUN | 39 |
| 4.3.3 | POSTPROCESSING..... | 39 |
| 5. | SAMPLE STUDIES TO DEMONSTRATE DIFFERENT OPTIMIZATION STRATEGIES | 40 |
| 5.1 | OPTIMIZATION OF CANTILEVER BEAM WITH RECTANGULAR CROSS SECTION..... | 40 |
| 5.1.1 | OPTIMIZATION USING THE OPTIMIZATION CODE IN MATLAB [®] AND ANALYTIC FUNCTIONS AS SOLVER..... | 47 |
| 5.1.2 | CANTILEVER BEAM OPTIMIZATION USING THE OPTIMIZATION CODE IN MATLAB [®] AND MSC.NASTRAN [®] AS THE SOLVER..... | 53 |
| 5.1.3. | CANTILEVER BEAM OPTIMIZATION USING MSC.NASTRAN [®] OPTIMIZATION TOOL | 58 |
| 5.1.4. | COMPARISON OF THE THREE DIFFERENT OPTIMIZATION STRATEGIES | 65 |
| 5.2 | CANTILEVER BEAM WITH I CROSS SECTION | 67 |
| 5.2.1 | OPTIMIZATION USING THE OPTIMIZATION CODE IN MATLAB [®] AND ANALYTIC FUNCTIONS AS SOLVER..... | 69 |
| 5.2.2 | CANTILEVER BEAM OPTIMIZATION USING THE OPTIMIZATION CODE IN MATLAB [®] AND MSC.NASTRAN [®] AS THE SOLVER..... | 77 |
| 5.2.3. | CANTILEVER BEAM OPTIMIZATION USING OPTIMIZATION MODULE OF MSC.NASTRAN [®] | 85 |
| 5.2.4. | COMPARISON OF THE THREE DIFFERENT OPTIMIZATION STRATEGIES | 95 |
| 6. | OPTIMIZATION OF A WING TORQUE BOX..... | 97 |
| 6.1 | OPTIMIZATION OF THE WING WITH TIP LOADING..... | 118 |
| 6.2 | OPTIMIZATION OF THE WING WITH DISTRIBUTED LOADING 138 | |
| 6.3 | OPTIMIZATION OF THE WING TORQUE BOX WITH DISTRIBUTED LOADING INCLUDING SHAPE OPTIMIZATION..... | 158 |
| 6.3.1. | ONE VARIABLE OPTIMIZATION..... | 162 |
| 6.3.2. | MULTI VARIABLE OPTIMIZATION | 167 |

| | | |
|-----|---|-----|
| 6.4 | COMPARISON OF OPTIMIZATION STUDIES OF THE WING TORQUE BOX | 185 |
| 7. | CONCLUDING REMARKS AND FUTURE WORK..... | 187 |
| | REFERENCES..... | 192 |
| | APPENDICES | |
| | NEWTON-RAPHSON METHOD | 194 |
| | BISECTION METHOD | 195 |
| | GOLDEN SECTION METHOD | 196 |
| | STEEPEST DESCENT METHOD..... | 197 |
| | CONJUGATE GRADIENT METHOD..... | 198 |
| | DAVIDON-FLETCHER-POWELL METHOD..... | 199 |
| | PENALTY FUNCTION METHOD | 200 |
| | AUGMENTED LAGRANGE MULTIPLIER METHOD..... | 202 |
| | USER INTERFACE OF MATLAB [®] CODE DEVELOPED FOR OPTIMIZATION | 204 |
| | MATLAB [®] TO MSC.NASTRAN [®] INTERFACE | 207 |
| | MESH DENSITY COMPARISON FOR RECTANGULAR CROSS SECTION CANTILEVER BEAM | 213 |
| | MESH DENSITY COMPARISON FOR I SHAPED CROSS SECTION CANTILEVER BEAM | 215 |
| | COMPARISON TABLES FOR WING TORQUE BOX OPTIMIZATION... | 217 |
| | SAMPLE BDF-FILE FOR PROPERTY OPTIMIZATION..... | 222 |
| | SAMPLE BDF-FILE FOR SHAPE OPTIMIZATION | 227 |

LIST OF FIGURES

| | | |
|-------------|--|----|
| Figure 1.1 | A typical aircraft Structure [4] | 5 |
| Figure 1.2 | Initial satellite structure [5] | 6 |
| Figure 1.3 | Optimized satellite structure [5]..... | 6 |
| Figure 1.4 | Optimized satellite structure on test [5] | 7 |
| Figure 1.5 | Sail boats [6]..... | 8 |
| Figure 1.6 | FE model for optimization | 9 |
| Figure 2.1 | Golden section search technique [7] | 13 |
| Figure 3.1 | Main algorithm of the optimization code..... | 21 |
| Figure 4.1 | MSC.NASTRAN [®] implementation of structural optimization [10] | 35 |
| Figure 5.1 | Cantilever beam with rectangular cross section..... | 41 |
| Figure 5.2 | Variation of the objective function with respect to iteration number..... | 48 |
| Figure 5.3 | Variation of width of cross section “B” with respect to iteration number..... | 49 |
| Figure 5.4 | Variation of height of cross section “H” with respect to iteration number..... | 49 |
| Figure 5.5 | Variation of stress at the root of the beam with respect to iteration number | 50 |
| Figure 5.6 | Variation of displacement at the tip of the beam with respect to iteration number | 50 |
| Figure 5.7 | Variation of H/B with respect to the iteration number..... | 51 |
| Figure 5.8 | Variation of objective function with respect to iteration number | 54 |
| Figure 5.9 | Variation of width of cross section “B” with respect to iteration number..... | 55 |
| Figure 5.10 | Variation of height of cross section “H” with respect to iteration number..... | 55 |
| Figure 5.11 | Variation of stress at the root of the beam with respect to iteration number..... | 56 |
| Figure 5.12 | Variation of displacement at the tip of the beam with respect to iteration number | 56 |
| Figure 5.13 | Variation of H/B with respect to iteration number..... | 57 |
| Figure 5.14 | Cantilever beam finite element model | 58 |
| Figure 5.15 | Initial cantilever beam model with equivalent inertia..... | 59 |
| Figure 5.16 | Initial cantilever beam cross section properties | 59 |
| Figure 5.17 | Cantilever beam initial displacement | 60 |
| Figure 5.18 | Cantilever beam initial stress distribution..... | 60 |
| Figure 5.19 | Final cantilever beam model with equivalent inertia | 61 |

| | | |
|-------------|--|----|
| Figure 5.20 | Final cantilever beam cross section properties..... | 61 |
| Figure 5.21 | Displacement distribution in the optimized beam..... | 62 |
| Figure 5.22 | Stress distribution in the optimized beam..... | 62 |
| Figure 5.23 | History of the objective function..... | 63 |
| Figure 5.24 | History of the design variable “B”..... | 63 |
| Figure 5.25 | History of the design variable “H”..... | 64 |
| Figure 5.26 | History of the maximum constraint value..... | 64 |
| Figure 5.27 | Cantilever beam with I cross section..... | 67 |
| Figure 5.28 | Variation of the objective function with respect to iteration number..... | 71 |
| Figure 5.29 | Variation of the height of cross section “H” with respect to iteration number..... | 72 |
| Figure 5.30 | Variation of the width of flanges “Wf” with respect to iteration number..... | 72 |
| Figure 5.31 | Variation of the web thickness “tw” with respect to iteration number..... | 73 |
| Figure 5.32 | Variation of the flange thickness “tf” with respect to iteration number..... | 73 |
| Figure 5.33 | Variation of maximum bending stress at the root of the beam with respect to iteration number..... | 74 |
| Figure 5.34 | Variation of maximum shear stress at the root of the beam with respect to iteration number..... | 75 |
| Figure 5.35 | Variation of maximum displacement with respect to iteration number..... | 75 |
| Figure 5.36 | Variation of tf / tw with respect to iteration number..... | 76 |
| Figure 5.37 | Variation of the objective function with respect to iteration number..... | 79 |
| Figure 5.38 | Variation of the height of cross section “H” with respect to iteration number..... | 80 |
| Figure 5.39 | Variation of the width of flanges “Wf” with respect to iteration number..... | 80 |
| Figure 5.40 | Variation of the web thickness “tw” with respect to iteration number..... | 81 |
| Figure 5.41 | Variation of the flange thickness “tf” with respect to iteration number..... | 81 |
| Figure 5.42 | Variation of maximum bending stress at the root of the beam with respect to iteration number..... | 82 |
| Figure 5.43 | Variation of maximum shear stress at the root of the beam with respect to iteration number..... | 82 |
| Figure 5.44 | Variation of the maximum displacement with respect to iteration number..... | 83 |
| Figure 5.45 | Variation of tf / tw with respect to iteration number..... | 83 |
| Figure 5.46 | Cantilever I beam model..... | 86 |
| Figure 5.47 | Initial cantilever I beam model with equivalent inertia..... | 86 |
| Figure 5.48 | Initial cantilever I beam section properties..... | 87 |
| Figure 5.49 | Cantilever I beam initial displacement..... | 87 |

| | | |
|-------------|---|-----|
| Figure 5.50 | Cantilever I beam initial bending stress distribution..... | 88 |
| Figure 5.51 | Final cantilever I beam model with equivalent inertia..... | 89 |
| Figure 5.52 | Final cantilever I beam section properties..... | 89 |
| Figure 5.53 | Displacement distribution in the optimized beam..... | 90 |
| Figure 5.54 | Bending stress distribution in the optimized beam | 90 |
| Figure 5.55 | History of the objective function..... | 91 |
| Figure 5.56 | History of the design variable “H”(height of the beam) | 92 |
| Figure 5.57 | History of the design variable “Wf” (width of the flange)..... | 92 |
| Figure 5.58 | History of the design variable “tw” (thickness of the web) | 93 |
| Figure 5.59 | History of the design variable “tf” (thickness of the flange)..... | 93 |
| Figure 5.60 | Cantilever beam problem history of the maximum constraint value | 94 |
| Figure 6.1 | The wing model studied in optimization study | 99 |
| Figure 6.2 | Geometry and finite element of the wing..... | 100 |
| Figure 6.3 | Elements of the wing model..... | 101 |
| Figure 6.4 | Elements of the front spar | 103 |
| Figure 6.5 | Elements of the rear spar | 104 |
| Figure 6.6 | Upper skin elements | 105 |
| Figure 6.7 | Lower skin elements..... | 106 |
| Figure 6.8 | Elements of rib 1 | 107 |
| Figure 6.9 | Elements of rib 2 | 108 |
| Figure 6.10 | Elements of rib 3 | 108 |
| Figure 6.11 | Elements of rib 4 | 109 |
| Figure 6.12 | Elements of rib 5 | 109 |
| Figure 6.13 | Elements of rib 6 | 110 |
| Figure 6.14 | Elements of rib 7 | 110 |
| Figure 6.15 | Applied displacement boundary condition..... | 111 |
| Figure 6.16 | Elements to be optimized | 112 |
| Figure 6.17 | Spanwise aerodynamic lift force distribution..... | 113 |
| Figure 6.18 | Spanwise aerodynamic pitching moment distribution | 113 |
| Figure 6.19 | Initial wing model with tip loading | 118 |
| Figure 6.20 | Initial axial stresses on the flanges..... | 119 |
| Figure 6.21 | Initial Von Mises stresses on the skins and the webs..... | 120 |
| Figure 6.22 | Initial Von Mises stresses on the skins and the webs interior view | 121 |
| Figure 6.23 | Initial deflection of the wing | 121 |
| Figure 6.24 | Final flange areas on the wing model..... | 122 |
| Figure 6.25 | Final upper skin thicknesses of the wing model | 123 |
| Figure 6.26 | Final lower skin thicknesses of the wing model | 123 |
| Figure 6.27 | Final front spar thicknesses of the wing model..... | 124 |
| Figure 6.28 | Final rear spar thicknesses of the wing model | 124 |
| Figure 6.29 | Final rib web thicknesses of the wing model | 125 |
| Figure 6.30 | Final axial stresses on the flanges | 126 |
| Figure 6.31 | Final Von Mises stresses on the skins and the webs..... | 126 |
| Figure 6.32 | Final Von Mises stresses on the skins and the webs interior view | 127 |

| | | |
|-------------|--|-----|
| Figure 6.33 | Final deflection of the wing | 127 |
| Figure 6.34 | History of objective function (in kg)..... | 128 |
| Figure 6.35 | History of lower skin thicknesses (in mm)..... | 129 |
| Figure 6.36 | History of upper skin thicknesses (in mm)..... | 129 |
| Figure 6.37 | History of front spar web thicknesses (in mm) | 130 |
| Figure 6.38 | History of rear spar web thicknesses (in mm)..... | 130 |
| Figure 6.39 | History of rib web thicknesses (in mm) | 131 |
| Figure 6.40 | History of upper flange areas of front spar (in mm ²)..... | 131 |
| Figure 6.41 | History of lower flange areas of front spar (in mm ²)..... | 132 |
| Figure 6.42 | History of upper flange areas of rear spar (in mm ²)..... | 132 |
| Figure 6.43 | History of lower flange areas of rear spar (in mm ²)..... | 133 |
| Figure 6.44 | History of flange areas of rib 1 (in mm ²) | 133 |
| Figure 6.45 | History of flange areas of rib 2 (in mm ²) | 134 |
| Figure 6.46 | History of flange areas of rib 3 (in mm ²) | 134 |
| Figure 6.47 | History of flange areas of rib 4 (in mm ²) | 135 |
| Figure 6.48 | History of flange areas of rib 5 (in mm ²) | 135 |
| Figure 6.49 | History of flange areas of rib 6 (in mm ²) | 136 |
| Figure 6.50 | History of flange areas of rib 7 (in mm ²) | 136 |
| Figure 6.51 | History of maximum constraint value | 137 |
| Figure 6.52 | Initial wing model with distributed loading | 138 |
| Figure 6.53 | Initial axial stresses on the flanges | 139 |
| Figure 6.54 | Initial Von Mises stresses on the skins and the webs..... | 139 |
| Figure 6.55 | Initial Von Mises stresses on the skins and the webs interior view | 140 |
| Figure 6.56 | Initial deflection of the wing model | 140 |
| Figure 6.57 | Final flange areas on the wing model..... | 141 |
| Figure 6.58 | Final upper skin thicknesses of the wing model | 142 |
| Figure 6.59 | Final lower skin thicknesses of the wing model | 142 |
| Figure 6.60 | Final front spar thicknesses of the wing model..... | 143 |
| Figure 6.61 | Final rear spar thicknesses of the wing model | 143 |
| Figure 6.62 | Final rib web thicknesses of the wing model | 144 |
| Figure 6.63 | Final overall thicknesses of the wing model | 144 |
| Figure 6.64 | Final web thicknesses of the wing model interior view | 145 |
| Figure 6.65 | Final axial stresses on the flanges | 146 |
| Figure 6.66 | Final Von Mises stresses on the skins and the webs..... | 146 |
| Figure 6.67 | Final Von Mises stresses on the skins and the webs interior view | 147 |
| Figure 6.68 | Final deflection of the wing model | 147 |
| Figure 6.69 | History of objective function (in kg)..... | 148 |
| Figure 6.70 | History of lower skin thicknesses (in mm)..... | 149 |
| Figure 6.71 | History of upper skin thicknesses (in mm)..... | 149 |
| Figure 6.72 | History of front spar web thicknesses (in mm) | 150 |
| Figure 6.73 | History of rear spar web thicknesses (in mm)..... | 150 |
| Figure 6.74 | History of rib web thicknesses (in mm) | 151 |
| Figure 6.75 | History of upper flange areas of front spar (in mm ²)..... | 151 |
| Figure 6.76 | History of lower flange areas of front spar (in mm ²) | 152 |

| | | |
|--------------|---|-----|
| Figure 6.77 | History of upper flange areas of rear spar (in mm ²)..... | 152 |
| Figure 6.78 | History of lower flange areas of rear spar (in mm ²)..... | 153 |
| Figure 6.79 | History of flange areas of rib 1 (in mm ²) | 153 |
| Figure 6.80 | History of flange areas of rib 2 (in mm ²) | 154 |
| Figure 6.81 | History of flange areas of rib 3 (in mm ²) | 154 |
| Figure 6.82 | History of flange areas of rib 4 (in mm ²) | 155 |
| Figure 6.83 | History of flange areas of rib 5 (in mm ²) | 155 |
| Figure 6.84 | History of flange areas of rib 6 (in mm ²) | 156 |
| Figure 6.85 | History of flange areas of rib 7 (in mm ²) | 156 |
| Figure 6.86 | History of maximum constraint value | 157 |
| Figure 6.87 | Load case 1 in auxiliary model | 159 |
| Figure 6.88 | Load case 2 in auxiliary model | 159 |
| Figure 6.89 | Load case 3 in auxiliary model | 160 |
| Figure 6.90 | Load case 4 in auxiliary model | 160 |
| Figure 6.91 | Load case 5 in auxiliary model | 161 |
| Figure 6.92 | Initial wing model with distributed loading | 163 |
| Figure 6.93 | Final location of the rib 2 on the wing model | 164 |
| Figure 6.94 | Final Von Mises stress on the element 110030..... | 164 |
| Figure 6.95 | History of objective function (in kg)..... | 165 |
| Figure 6.96 | History of rib 2 location (in 100 mm) | 166 |
| Figure 6.97 | History of the maximum constraint value | 166 |
| Figure 6.98 | Initial wing model with distributed loading | 167 |
| Figure 6.99 | Final rib locations on the wing model | 168 |
| Figure 6.100 | Final flange areas of the wing model | 169 |
| Figure 6.101 | Final lower skin thicknesses of the wing model | 169 |
| Figure 6.102 | Final upper skin thicknesses of the wing model | 170 |
| Figure 6.103 | Final front spar thicknesses of the wing model..... | 170 |
| Figure 6.104 | Final rear spar thicknesses of the wing model | 171 |
| Figure 6.105 | Final rib web thicknesses of the wing model | 171 |
| Figure 6.106 | Final rib web thicknesses of the wing model | 172 |
| Figure 6.107 | Final Rib web thicknesses of the wing model interior view | 172 |
| Figure 6.108 | Final axial stresses on the flanges | 173 |
| Figure 6.109 | Final Von Mises stresses on the skins and the webs..... | 174 |
| Figure 6.110 | Final Von Mises stresses on the skins and the webs interior view | 174 |
| Figure 6.111 | Final deflection of the wing model | 175 |
| Figure 6.112 | History of objective function | 176 |
| Figure 6.113 | History of lower skin thicknesses (in mm) | 176 |
| Figure 6.114 | History of upper skin thicknesses (in mm) | 177 |
| Figure 6.115 | History of front spar web thicknesses (in mm)..... | 177 |
| Figure 6.116 | History of rear spar web thicknesses (in mm)..... | 178 |
| Figure 6.117 | History of rib web thicknesses (in mm) | 178 |
| Figure 6.118 | History of upper flange areas of front spar (in mm ²) | 179 |
| Figure 6.119 | History of lower flange areas of front spar (in mm ²) | 179 |
| Figure 6.120 | History of upper flange areas of rear spar (in mm ²)..... | 180 |
| Figure 6.121 | History of lower flange areas of rear spar (in mm ²)..... | 180 |

| | | |
|--------------|--|-----|
| Figure 6.122 | History of flange areas of rib 1 (in mm ²) | 181 |
| Figure 6.123 | History of flange areas of rib 2 (in mm ²) | 181 |
| Figure 6.124 | History of flange areas of rib 3 (in mm ²) | 182 |
| Figure 6.125 | History of flange areas of rib 4 (in mm ²) | 182 |
| Figure 6.126 | History of flange areas of rib 5 (in mm ²) | 183 |
| Figure 6.127 | History of flange areas of rib 6 (in mm ²) | 183 |
| Figure 6.128 | History of flange areas of rib 7 (in mm ²) | 184 |
| Figure 6.129 | History of maximum constraint value | 184 |
| Figure B.1 | Starting AugLagMet in MATLAB [®] command window | 204 |
| Figure B.2 | Entering initial values in MATLAB [®] command window | 205 |
| Figure B.3 | Result in MATLAB [®] command window | 206 |
| Figure B.4 | Open with a bdf-file in Microsoft.WINDOWS [®] | 209 |
| Figure B.5 | Location of “nastran.exe” | 209 |
| Figure B.6 | “nastran.exe” file in ./bin/ directory | 210 |
| Figure B.7 | Open a “bdf-file” allways with “nastran.exe” | 210 |
| Figure B.8 | MATLAB [®] command window | 211 |
| Figure B.9 | MSC.NASTRAN [®] run window | 212 |
| Figure B.10 | MATLAB [®] command window | 212 |
| Figure C.1 | Finite element models for rectangular cross section cantilever beam with different mesh densities | 213 |
| Figure C.2 | Finite element models for I shaped cross section cantilever beam with different mesh densities | 215 |

LIST OF TABLES

| | | |
|------------|---|-----|
| Table 5.1 | Objective function variation in the unconstrained design space | 42 |
| Table 5.2 | Variation of maximum stress in the design space | 43 |
| Table 5.3 | Variation of maximum deflection in the design space | 44 |
| Table 5.4 | Variation of slenderness ratio in the design space | 45 |
| Table 5.5 | Variation of the value of the objective function in the design space after all the constraints are imposed | 46 |
| Table 5.6 | Comparison of results of three different optimization approaches | 65 |
| Table 5.7 | Comparison of results for the I-Beam | 95 |
| Table 6.1 | Element properties and design variables of the front spar | 102 |
| Table 6.2 | Element properties and design variables of the rear spar | 102 |
| Table 6.3 | Element Properties and Design Variables of Upper Skin | 104 |
| Table 6.4 | Element properties and design variables of lower skin | 105 |
| Table 6.5 | Element properties and design variables of rib 1 | 107 |
| Table 6.6 | Element Properties and Design Variables of Rib 2 | 108 |
| Table 6.7 | Element properties and design variables of rib 3 | 108 |
| Table 6.8 | Element properties and design variables of rib 4 | 109 |
| Table 6.9 | Element properties and design variables of rib 5 | 109 |
| Table 6.10 | Element properties and design variables of rib 6 | 110 |
| Table 6.11 | Element properties and design variables of rib 7 | 110 |
| Table 6.12 | Design constraints related to front spar | 114 |
| Table 6.13 | Design constraints related to rear spar | 114 |
| Table 6.14 | Design constraints related to upper skin | 115 |
| Table 6.15 | Design constraints related to lower skin | 115 |
| Table 6.16 | Design constraints related to rib 1 | 115 |
| Table 6.17 | Design constraints related to rib 2 | 115 |
| Table 6.18 | Design constraints related to rib 3 | 116 |
| Table 6.19 | Design constraints related to rib 4 | 116 |
| Table 6.20 | Design constraints related to rib 5 | 116 |
| Table 6.21 | Design constraints related to rib 6 | 116 |
| Table 6.22 | Design constraints related to rib 7 | 117 |
| Table 6.23 | Design constraints related to displacements at rib 7 | 117 |
| Table 6.24 | Comparison of linear static analyses of the wing with rib 2 at different spanwise locations | 162 |
| Table 6.25 | Comparison of results of three optimization processes | 185 |
| Table C.1 | Comparison of optimization results of rectangular cross section cantilever beam with different mesh densities | 214 |
| Table C.2 | Comparison of optimization results of shaped cross section cantilever beam with different mesh densities | 216 |

| | | |
|------------|--|-----|
| Table C.3 | Comparison of front spar results of three optimization processes . | 217 |
| Table C.4 | Comparison of rear spar results of three optimization processes... | 218 |
| Table C.5 | Comparison of upper skin results of three optimization processes | 218 |
| Table C.6 | Comparison of lower skin results of three optimization processes | 219 |
| Table C.7 | Comparison of rib 1 results of three optimization processes ... | 219 |
| Table C.8 | Comparison of rib 2 results of three optimization processes ... | 219 |
| Table C.9 | Comparison of rib 3 results of three optimization processes ... | 220 |
| Table C.10 | Comparison of rib 4 results of three optimization processes ... | 220 |
| Table C.11 | Comparison of rib 5 results of three optimization processes ... | 220 |
| Table C.12 | Comparison of rib 6 results of three optimization processes ... | 221 |
| Table C.13 | Comparison of rib 7 results of three optimization processes ... | 221 |

LIST OF SYMBOLS AND ABBREVIATIONS

| | |
|---------------|------------------------------------|
| x | Design variables |
| FE | Finite Element |
| FEM | Finite Element Method |
| FOC | First Order Condition |
| SOC | Second Order Condition |
| α | Step size in 1-D search |
| τ | Tolerance |
| ε | Tolerance |
| L | Length |
| Δ | Change in value |
| ∇ | Gradient of function |
| c | Maximum distance from neutral axis |
| E | Modulus of Elasticity |
| I | Moment of Inertia |
| H | Height of the Beam |
| B | Width of the Beam |
| M | Applied Moment |
| σ | Stress value |
| P | Applied Force |
| W | Weight |
| ν | Poisson's Ratio |
| δ | Displacement |
| D.R. | Design Response |
| D.V. | Design Variable |
| D.C. | Design Constraint |

CHAPTER 1

INTRODUCTION

Optimization has vital importance in every field of modern world.

“Nothing takes place in the world whose meaning is not that of some maximum or minimum.” said by Euler.

Optimization is defined as the procedure used to make a system or design as effective or functional as possible. Today, optimization forms a major necessary part of design activity in all major disciplines and those disciplines are not limited only to engineering. There is hardly any area where optimization has not proven itself to be effective. These areas include everything that are seen around or used in daily lives. It is unthinkable that the products that are seen everyday, like cars, houses, electronic or non-electronic devices that are produced today are not designed optimally in one way or another. The will to produce maximum quality products with minimum possible cost is the driving force behind the rapid development of the optimization methods.

The theory of optimization has its roots from ancient times. Throughout history, there had always been a huge number of geometrical and mechanical problems, which are optimization problems in fact but has been solved by using geometrical knowledge since the optimization techniques were not known by then. [1]

Optimization techniques are being used for more than a century. At first, the basic tool used to find the extremum of functions was differential calculus [2]. It is the World War II that has played a very important role for the development of optimization. In mid-1940s, Simplex Method has been developed for solving linear programming problems. Linear Programming has been used to solve war

problems at first but afterwards, it was found out that this technique was very useful in solving problems in economics, business and engineering sciences. In 1951, H.W. Kuhn and A.W. Tucker developed the Lagrangian multiplier rule for convex and other non-linear programming problems which also involved inequality constraints. The Kuhn-Tucker optimality conditions became very useful and important for developing algorithms in solving convex and other non-linear programming problems with differentiable functions. After World War II, in late 1950s, non-linear programming has been emphasized with the development of a powerful method for unconstrained optimization developed by W.C. Davidon. Afterwards, his work has been further developed by M.J.D. Powell and R. Fletcher and it lead to the rise of powerful Quasi-Newton methods. The development of computer science made it possible to simplify programming and thus to easily solve great optimization problems which is nearly impossible to solve by hand. Early computers provided accessibility, responsiveness, autonomy and fixed cost while recent models added large memory, high precision and impressive speed. At present, optimization is a developing subject with many newly explored areas of theory and application [1].

There is no doubt that there is a widespread practical usage of optimization methods in many different fields – aerospace industry being one of the earliest disciplines to use these methods most significantly. Driven by the need to lower the burden of the unnecessary weight in aerospace vehicles in order to minimize the tremendous cost associated with this weight, it is not hard to understand why the application of the optimization methods is such a big necessity for aerospace industry. Minimum weight vehicles together with the savings in fuel consumption with optimal trajectory design without any deviations from aviation safety is the main target to reach through optimization.

In the following sections of this chapter, general information on the optimization methods of aerospace structures will be discussed. In chapter 2, optimization theory is introduced. In chapter 3, optimization technique used in the developed MATLAB[®] code will be presented. In chapter 4, three different approaches of

the structural optimization used in the present thesis will be described including the description of the interface codes specific to MATLAB[®] and MSC.NASTRAN[®]. In chapter 5, two case studies are performed with different optimization techniques both for verification and demonstration purposes. In chapter 6, a complex aerospace structure optimization is performed. In this section both geometric property and shape optimization studies are performed for a wing torque box. Finally, in the last chapter, conclusion of the studies is given and researchers interested in the subject matter are encouraged to do further work.

1.1 OPTIMIZATION METHODS

There are many optimization methods used in solving problems in engineering and other disciplines. These methods can be classified mainly in two groups. First group is the genetic algorithms [3] and second group is the gradient based algorithms. In this thesis gradient based algorithms are used for the solution of structural optimization problems. Gradient based algorithms are also divided into two major groups which are the unconstrained and constrained optimization problems. Some examples of methods for gradient based algorithms are given below.

1. Unconstrained Optimization

- Steepest Descent Method
- Conjugate Gradient Method
- Davidon-Fletcher-Powell Method

2. Constrained Optimization

- Penalty Function Method
- Augmented Lagrange Multiplier Method

1.2 MAIN APPLICATION AREAS OF OPTIMIZED STRUCTURES

Optimized structures can be found in many disciplines in engineering. However, structural optimization is especially critical in the design of aerospace structures. Weight of an aerospace vehicle is not only related to the performance of the vehicle but weight savings also induce significant cost savings during the design stage and directly affects the fuel consumption during the operation of the vehicle. Therefore, aerospace companies use low margins of safety in their design to achieve weight savings. The use of low margins of safety in structural design can be best accomplished by performing structural optimization. Common types of optimization performed in the structure area are:

- Property optimization: Cross-section dimensions, thicknesses, geometric dimensions etc.
- Shape optimization: Changing the locations of certain structural members like ribs, changing the shape of a cut-out etc.
- Topology optimization: Optimal distribution of material

In the following section, some examples will be given for the optimized structures used in different fields of engineering.

1.2.1 AERONAUTICS

Almost in all aeronautical vehicles optimization is used, because weight has direct impact on the performance of the air vehicle as well as the operating cost as discussed above. Therefore, aerospace structures are usually composed of stiffened thin walled structural members. The use of stiffened thin walled members assures weight savings as well as structural integrity if the structural design is performed in the right way. Wings and fuselage of aircraft are two main substructures where significant weight savings can be achieved if optimization techniques are implemented in the design stage. For instance in Figure 1.1, a section of the fuselage of an aircraft structure is presented.

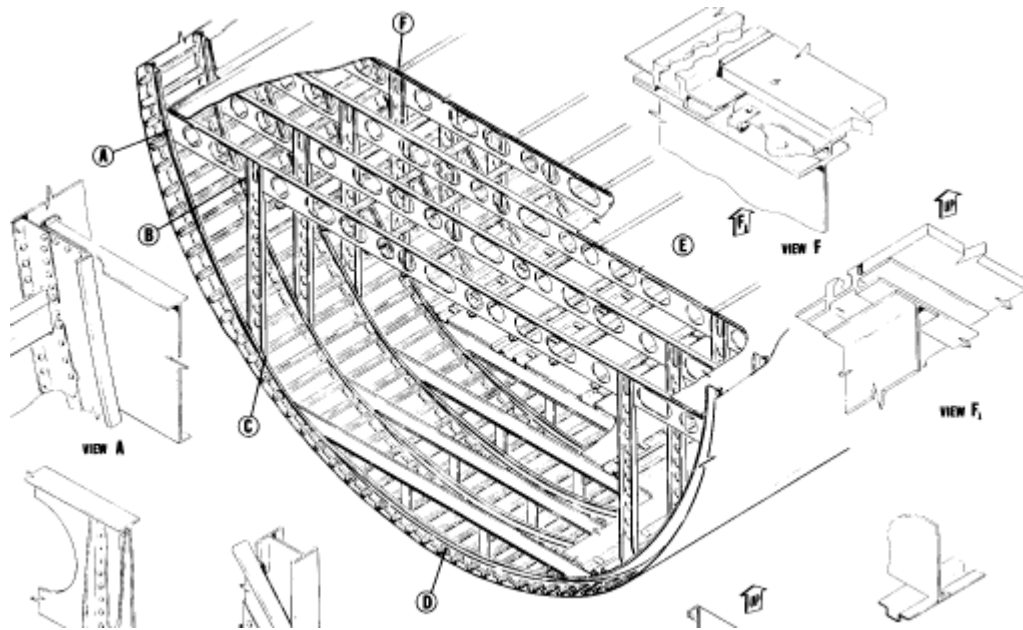


Figure 1.1 A typical aircraft Structure [4]

As it can be seen from Figure 1.1, many structural members exist in the fuselage frame and one can imagine the great amount of weight savings that can be achieved if optimization techniques are used in the design stage of such a fuselage frame.

1.2.2 SPACE

Satellite structures are also becoming very popular with the technological advancement that takes place in space technologies. Today many countries possess their own satellite structures in space and these spacecraft serve for different purposes ranging from telecommunication to earth observation and remote sensing etc. Weight saving in satellite structures is also very critical because the launch cost of satellites are directly related to the weight of the satellite. In addition, orbit performance of the satellites can be improved by weight savings. Figure 1.2 and 1.3 show the initial and optimized shape of a

frame of a satellite structure. Figure 1.4 shows the test of the optimized structure. [5]

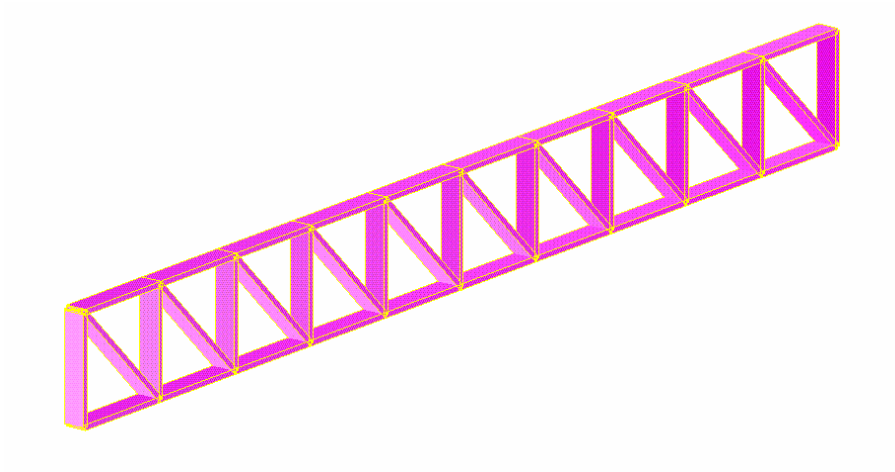


Figure 1.2 Initial satellite structure [5]

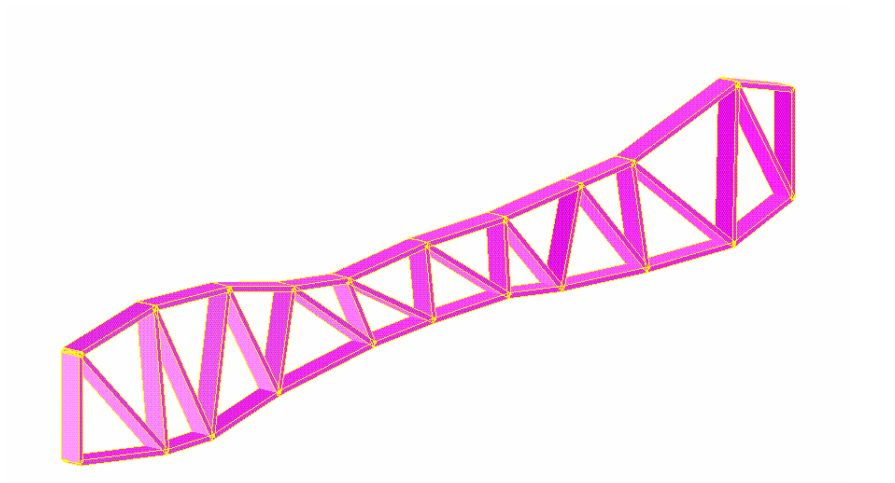


Figure 1.3 Optimized satellite structure [5]



Figure 1.4 Optimized satellite structure on test [5]

1.2.3 MARINE

In the marine industry weight savings are also as important as in aerospace industry. By designing weight efficient ships significant performance gains can be obtained and fuel consumption can be significantly reduced. To increase performance gains nowadays personal yachts are manufactured from composite materials which present significant weight savings. Race sail boats are other examples of marine structures for which weight saving directly affects the success in the race due to performance gains achieved by weight reduction. In Figure 1.5 two racing sail boats are shown. Structural optimization in hull structures has vital importance to achieve excellent strength-to-weight ratios.



Figure 1.5 Sail boats [6]

1.2.4 AUTOMOTIVE

Structural optimization also has vital importance in the automotive industry. Weight reduction in automobiles is especially critical in having reduced emissions. Low emission of combustion products is directly related to the weight of the automobile. Today in many countries around the world, low emission regulations are prepared to force the automobile manufacturers to manufacture automobiles which comply with these regulations. Besides the improvements in the engine technology, weight reduction achieved by means of optimization of the structure of the automobile is also an important factor to consider in having lower emissions. Structural optimization is the only way to design structures with minimum weight by satisfying the prescribed constraints imposed on the structural integrity. As an example of optimization in automobile industry, Figure 1.6 shows the finite element model of the structure of an automobile frame used in the optimization study.

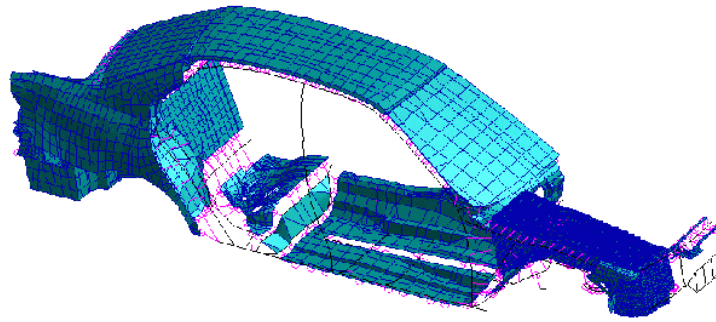


Figure 1.6 FE model for optimization

1.3 ADVANTAGES OF OPTIMIZING STRUCTURES

Although performing optimization studies requires initial investment such as high performance computers and additional engineering cost, there are many advantages gained by optimizing structures. Some of these advantages can be listed as:

- reduced weight ,
- reduced manufacturing cost,
- improved efficiency,
- improved service life
- reduced operating costs (less fuel, less repair costs),
- reduced environmental effect

It is deemed that the advantages gained by optimizing structures outweighs the investment costs related with establishing the infra-structure to perform optimization studies. By implementing optimization early in design stages, companies can manufacture products with superior performance with reduced cost. Especially, for industries involved in series manufacturing, optimization can result in huge cost savings. Today, companies strive to continue to exist in the market with competitive products, and in this respect optimization presents a very powerful tool in achieving the production of competitive products.

CHAPTER 2

OPTIMIZATION THEORY FOR GRADIENT BASED METHODS

Optimization means minimization (or maximization) of a function. In aerospace industry, weight is one of the best example for the function to minimize. It depends on the volume and density of the structure and therefore mostly volume minimization is performed in structural optimization provided that material choice is not included in the optimization study.

In a general structural optimization problem there are always some restrictions that allows no further weight reduction, such as stress values must be below a certain level or the maximum deflections must be below a certain value. In addition, the outer shape of aircraft sub-structures is usually determined by aerodynamics and flight mechanics considerations and unless a multidisciplinary approach is followed in the optimization, the outer dimensions can be taken as constants but not as design variables. For instance, thickness of the profile of a lifting surface may be a fixed value and for a fixed spar location the spar height will be constant. In optimization problems, the design variables usually have an upper and a lower bound. In structural optimization problems these bounds, on some of the design variables, exist because of the available structural elements from which the selection has to be made during the manufacturing.

To handle an optimization problem mathematically, there is a need for a statement. General statement of optimization problems is given as:

$$\begin{aligned}
 \text{Minimize} \quad & f(x_1, x_2, x_3, \dots, x_n) \\
 \text{Subject to} \quad & h_k(x_1, x_2, x_3, \dots, x_n) = 0 \quad k = 1, 2, \dots, l \\
 & g_j(x_1, x_2, x_3, \dots, x_n) \leq 0 \quad j = 1, 2, \dots, m \\
 & x_i^l \leq x_i \leq x_i^u \quad i = 1, 2, \dots, n
 \end{aligned}$$

where,

$$\begin{aligned}
 h_k(x_1, x_2, x_3, \dots, x_n) = 0 \quad k = 1, 2, \dots, l & \text{ represents the equality constraints.} \\
 g_j(x_1, x_2, x_3, \dots, x_n) \leq 0 \quad j = 1, 2, \dots, m & \text{ represents the inequality constraints} \\
 x_i^l \leq x_i \leq x_i^u \quad i = 1, 2, \dots, n & \text{ represents the upper and lower bounds}
 \end{aligned}$$

This chapter introduces optimization methods. One-dimensional optimization methods are explained in the first part. In the second part, unconstrained optimization methods for multivariable optimization problems are investigated. In the last part of the this chapter, implementation of constraints is presented.

2.1 ONE DIMENSIONAL OPTIMIZATION METHODS

Finding global minimum of the function with one variable in a given range can be stated as one dimensional optimization problem. There are many numerical methods for solution of one dimensional optimization problems. These are called as one dimensional search or line search methods. Following three methods will be mentioned in this chapter:

- Newton Raphson Method
- Bisection Method
- Golden Section Method

2.1.1 NEWTON RAPHSON METHOD

Newton Raphson method is used to find the root of a function. At optimum point the derivative of the function is zero. Therefore, this method can be applied to find the optimum point by searching the roots of derivative, instead of original function itself.

The idea is very simple. First the function Φ is evaluated at a point α . Then that point is moved by an amount of $\Delta\alpha$ and the function is evaluated at a new location. This procedure is continued until the condition $\Phi(\alpha) = 0$ is satisfied.

Calculation of increment in α value ($\Delta\alpha$) is as follows:

$$\Phi(\bar{\alpha}) = \Phi(\alpha + \Delta\alpha) = \Phi(\alpha) + \frac{d\Phi}{d\alpha} \Delta\alpha = 0 \quad (2.1)$$

$$\Delta\alpha = -\frac{\Phi(\alpha)}{d\Phi/d\alpha} = -\left[\frac{d\Phi}{d\alpha}\right]^{-1} \Phi(\alpha) \quad (2.2)$$

New α value is determined by incrementing α by $\Delta\alpha$, and the whole process repeated until solution is reached.

The drawback of Newton-Raphson method is the need to have an initial guess near the true solution. Algorithm of this method is given in detail in Appendix A.1.

2.1.2 BISECTION METHOD

Like Newton Raphson method, bisection method is also used to find the roots of the function. This method is based on the reduction of the search interval.

In this method function values are evaluated at incremental values of the independent variable α , and sign change of the function value is searched for. Assuming that an interval is determined at upper bound α_b and lower bound α_a of the interval, the sign of the function must be different. In such a case, a continuous function will have at least one root in the interval.

Next step is evaluating the function in the middle of the interval. The sign of the function will be different from either the sign of the function at the lower bound or the sign of the function at the upper bound. Thus, the search interval is halved

and the whole process is repeated until the interval is less than a prescribed very small value. Middle point of the interval can be obtained by using the formula below.

$$\alpha = \alpha_a + (\alpha_b - \alpha_a)/2 \tag{2.3}$$

Algorithm of this method is given in detail in Appendix A.2.

2.1.3 GOLDEN SECTION METHOD

This method is used to find the minimum or the maximum of a function within a certain interval. The method is similar to bisection method but the intervals are derived from golden section ratio 1.61803 from Fibonacci series [7]. The brief explanation of the method is given below.

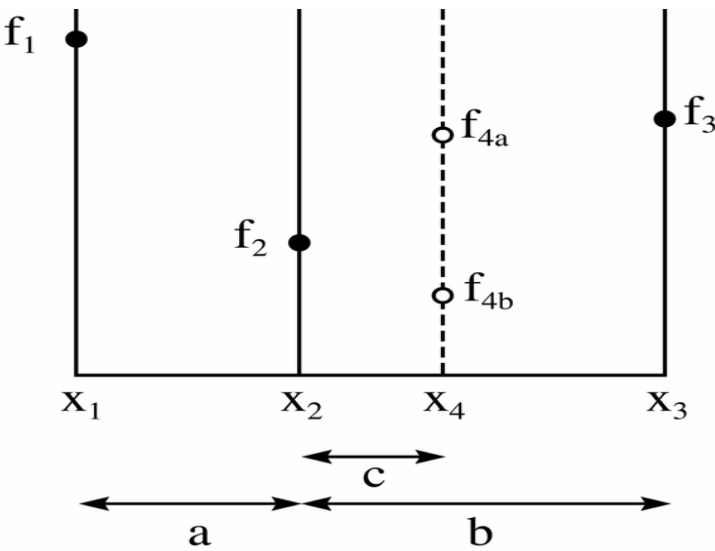


Figure 2.1 Golden section search technique [7]

In Figure 2.1, horizontal axis is used for the independent variable x and the vertical axis is used for the value of the function f(x). The lower value of the search interval is x1 and the upper value is x3. The function is evaluated at three

points x_1 , x_3 and x_2 , where f_1 , f_3 and f_2 are the corresponding function values respectively. If the value of f_2 is smaller than either f_1 or f_3 , the interval contains a minimum. To reduce the search interval one more evaluation at x_4 , located between x_2 and x_3 , has to be performed and the result is f_4 . If the value of f_4 is greater than f_2 , then the interval x_1 and x_4 contains a minimum. The lower value of the new interval is x_1 and the upper value is x_4 . Three points are now x_1 , x_2 and x_4 . However, if the value of f_4 is smaller than f_2 , then the interval x_2 and x_3 contains a minimum. The lower value of the new interval is x_2 and the upper value is x_3 . Three points are then x_2 , x_4 and x_3 .

To reduce the interval by the same fraction at each iteration the location of x_2 and x_4 should be chosen based on the golden section ratio, 1.61803.

$$\frac{b}{a} = \frac{a}{c} = 1.61803 \quad (2.4)$$

The derivation of this ratio can be found in reference [7]. Algorithm of this method is given in detail in Appendix A.3.

2.2 UNCONSTRAINED OPTIMIZATION WITH GRADIENT BASED METHODS

In this class of optimization problems, the function to be optimized may have more than one design variable and there is no restriction on the design variables. Therefore, this type of optimization problems is called as unconstrained optimization.

‘First Order Conditions’ (FOC) should be satisfied at optimum. These conditions are also known as Kuhn Tucker conditions or necessary conditions [8].

$$\nabla f = 0 \quad (2.5)$$

However, ‘First Order Conditions’ does not guarantee the optimum. Therefore, ‘Second Order Conditions’ should also be satisfied.

$$\Delta f = \frac{1}{2} \cdot \Delta \mathbf{x}^T \cdot \mathbf{H}(\mathbf{x}^*) \cdot \Delta \mathbf{x} > 0 \quad (2.6)$$

where,

' $\mathbf{H}(\mathbf{x}^*)$ ' is Hessian matrix which includes second order derivatives of objective function 'f' at solution.

' \mathbf{x} ' is the vector of design variables.

Equation (2.6) is the second order term of Taylor Series expansion. If the right hand side of the equation (2.6) is greater than zero, the extremum at that point is a minima.

Following gradient based methods are commonly used for the solution of optimization problems.

- Steepest Descent Method
- Conjugate Gradient Method
- Davidon-Fletcher-Powell (DFP) Method

2.2.1 STEEPEST DESCENT METHOD

The steepest descent method is the simplest of the gradient based methods. The idea behind this method stems from the definition of the gradient of a function. The objective function increases most rapidly in the direction of the gradient. Therefore, by reversing the direction of the gradient the search direction \mathbf{s}_i is obtained at a given point \mathbf{x}_i . Once the search direction is obtained, the next action to take is to decide how far to go in that direction. At this point any one of the one dimensional optimization methods can be used to solve this problem, and a factor α_i for the search direction is the output of one dimensional search. Next point \mathbf{x}_{i+1} is obtained using formula below.

$$\mathbf{x}_{i+1} = \mathbf{x}_i + \alpha_i \mathbf{s}_i \quad (2.7)$$

This iteration continues until the optimum point is reached.

This method is very simple and easy to apply. It is guaranteed to reach local minimum if there is any. The disadvantage of the steepest descent method is that it is very slow.

An algorithm for this method is given in Appendix A.4. Further information can be found in reference[9].

2.2.2 CONJUGATE GRADIENT METHOD

This method is very similar to the steepest descent method. The only difference is in constructing the search direction. In this method on top of the search direction of the to steepest descent method, a certain fraction of previous search direction is added to the negative of the gradient [9].

$$\mathbf{s}_i = -\nabla \mathbf{f}(\mathbf{x}_i) + \beta \mathbf{s}_{i-1} \quad (2.8)$$

The fraction of the previous search direction is the ratio of squares of the current and the previous gradient vectors.

$$\beta = \frac{\nabla \mathbf{f}(\mathbf{x}_i)^T \nabla \mathbf{f}(\mathbf{x}_i)}{\nabla \mathbf{f}(\mathbf{x}_{i-1})^T \nabla \mathbf{f}(\mathbf{x}_{i-1})} \quad (2.9)$$

The advantage of this method is its robustness compared to the steepest descent method. It should be noted that the magnitude of gradient of the objective function ($\nabla \mathbf{f}$) at optimum approaches to zero. Therefore, if the previous design variable \mathbf{x} is closer to optimum than the current design variable \mathbf{x} , the value of β is large. This means that previous iteration is dominant.

An algorithm for this method is given in Appendix A.5. Further information can be found in reference [9].

2.2.3 DAVIDON-FLETCHER-POWELL METHOD

In ‘Conjugate Gradient Method’ only the information from the previous iteration is included in the determination of the search direction. However, Davidon Fletcher Powell method uses information from all past iterations. This information is kept in a $n \times n$ matrix \mathbf{H} which is called as metric, where n is the number of the design variables. Therefore, this method is called as variable metric method. The search direction is stated as follows [7].

$$\mathbf{s}_i = -\mathbf{H}_i \cdot \nabla \mathbf{f}(\mathbf{x}_i) \quad (2.10)$$

The initial metric \mathbf{H}_0 must be symmetric positive definite. Usually, identity matrix is chosen as the initial metric. It is updated in every iteration according to the following formula [7].

$$\mathbf{H}_{i+1} = \mathbf{H}_i + \frac{\Delta \mathbf{x}_i \cdot \Delta \mathbf{x}_i^T}{\Delta \mathbf{x}_i^T \cdot \Delta[\nabla \mathbf{f}(\mathbf{x}_i)]} - \frac{\{\mathbf{H}_i \cdot \Delta[\nabla \mathbf{f}(\mathbf{x}_i)]\} \cdot \{\mathbf{H}_i \cdot \Delta[\nabla \mathbf{f}(\mathbf{x}_i)]\}^T}{\Delta[\nabla \mathbf{f}(\mathbf{x}_i)]^T \cdot \mathbf{H}_i \cdot \Delta[\nabla \mathbf{f}(\mathbf{x}_i)]} \quad (2.11)$$

\mathbf{H} matrix is symmetric positive definite in all iterations. As \mathbf{x} approaches to the optimum, \mathbf{H} matrix converges to the Hessian of the function. For quadratic functions DFP method converges in less than n iterations.

An algorithm for this method is given in Appendix A.6. Further information can be found in reference [9]

2.3 CONstrained Optimization with Gradient Based Methods

If there are some constraints introduced to the unconstrained optimization problem, the resulting optimization problem is called as constrained optimization. However, a constrained optimization problem can be converted to an unconstrained optimization problem. In this thesis two methods, which convert the constrained optimization problem into unconstrained optimization problem, are introduced. These methods are:

1. Penalty Function Method.
2. Augmented Lagrange Multiplier Method

In the thesis ‘Augmented Lagrange Multiplier Method’ is implemented in the proceeding sections.

2.3.1 PENALTY FUNCTION METHOD

The penalty function method is the modification of objective function $f(\mathbf{x})$ in such a way that it includes the constraints. Then, it can be solved by using algorithms used for unconstrained problems. Modification is very simple. A penalty function $P(\mathbf{x})$ is added to the objective function.

$$f(\mathbf{x}, r_h, r_g) = f(\mathbf{x}) + P(\mathbf{x}, r_h, r_g) \quad (2.12)$$

Where, r_g and r_h are the penalty function multipliers used in equation (2.13).

This additional function should penalize the objective function only outside the feasible region. In order to achieve this, penalty function can be chosen as follows [8].

$$P(\mathbf{x}, r_h, r_g) = r_h \cdot \sum_{k=1}^l h_k(\mathbf{x})^2 + r_g \cdot \sum_{j=1}^m \max(0, g_j(\mathbf{x}))^2 \quad (2.13)$$

where,

$h_k(\mathbf{x})$ defines an equality constraint.

$g_j(\mathbf{x})$ defines an inequality constraint.

This assures that when the constraints are violated the new objective function becomes large. Also, constants “ r_h ” and “ r_g ” are used to adjust the weight of the penalty function. These constants are called weighting factors or penalty parameters and it is not necessary to change them in each iteration.

An algorithm for this method is given in Appendix A.7. Further information can be found in reference [9].

2.3.2 AUGMENTED LAGRANGE MULTIPLIER METHOD

Another method of solving constrained optimization problem is Augmented Lagrange Multiplier (ALM) Method. This method is based on the same idea as ‘Penalty Function Method’. An additional function is added to the original objective function to penalize it when the constraints are violated. New objective function can be stated as follows [8].

$$\begin{aligned} f(\mathbf{x}, \lambda, \beta, r_h, r_g) = & f(\mathbf{x}) + r_h \cdot \sum_{k=1}^l h_k(\mathbf{x})^2 + r_g \cdot \sum_{j=1}^m \left[\max\left(g_j(\mathbf{x}), -\frac{\beta_j}{2 \cdot r_g}\right) \right]^2 \\ & + \sum_{k=1}^l \lambda_k \cdot h_k(\mathbf{x}) + \sum_{j=1}^m \beta_j \cdot \left[\max\left(g_j(\mathbf{x}), -\frac{\beta_j}{2 \cdot r_g}\right) \right] \end{aligned} \quad (2.14)$$

Vectors λ and β are multipliers for equality and inequality constraints respectively. Variables r_g and r_h are the penalty parameters. Vectors λ and β are updated in every iteration by using the formulas below,

$$\lambda = \lambda + 2 \cdot r_h \cdot h(\mathbf{x}) \quad (2.15)$$

$$\beta = \beta + 2 \cdot r_g \cdot \left(\max\left[g(\mathbf{x}), -\frac{\beta}{2 \cdot r_g}\right] \right) \quad (2.16)$$

Main advantage of this method is its robustness. At the solution, this method provides information about lagrange multipliers.

An algorithm for this method is given in Appendix A.8. Further information can be found in reference [9].

CHAPTER 3

OPTIMIZATION CODE IN MATLAB[®]

MATLAB[®] is a very useful tool to create codes for optimization. Because, in optimization problems matrix operations are needed frequently and implementing matrix operations is very easy in MATLAB[®] environment. Also, separation of tasks is quite simple in MATLAB[®] by implementing different code segments in different M files. There are many examples of solution of optimization problems with MATLAB[®]. In this thesis, general structure of the optimization code written by Venkataraman [8] is taken and modifications are incorporated to come up with the optimization code used in the demonstration of the three different ways solving structural optimization problems.

The optimization code includes three nested loops. Outermost loop is used to convert constrained optimization problem to unconstrained one and ‘Augmented Lagrange Multiplier Method’ is used to perform this task. In the inner loop, Davidon Fletcher Powell method is chosen to obtain solution for unconstrained optimization problem. This loop provides a search direction to be solved by a one dimensional search algorithm. Finally, innermost loop provides a solution for one dimensional search problem with golden section method.

Each loop is written in a different M-file. Evaluation of the objective function, equality constraints, inequality constraints, construction of unconstrained objective function and evaluation of the gradient of the function is written in separate M-files. Separation of M-files allows easy adaptation of MSC.NASTRAN[®] as a solver in the optimization.

Main flowchart of the optimization code written in MATLAB® environment is given in Figure 3.1

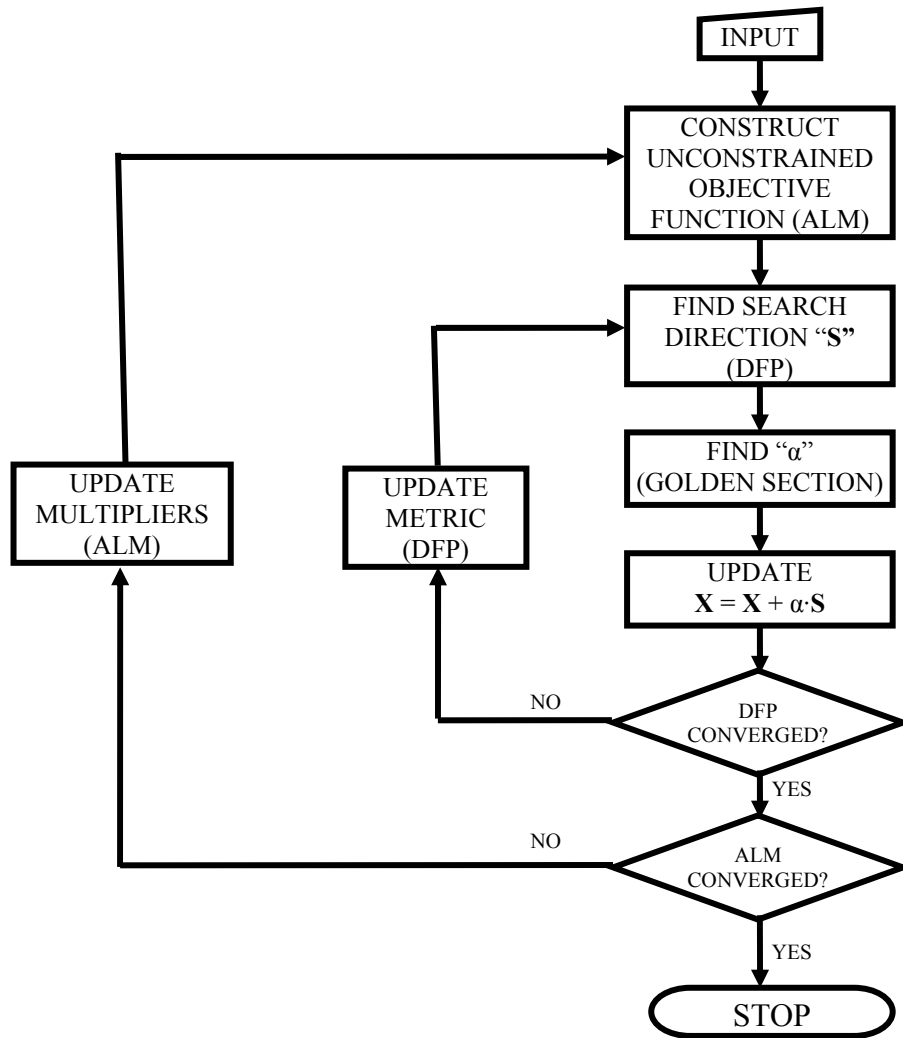


Figure 3.1 Main algorithm of the optimization code

3.1 AUGMENTED LAGRANGIAN MULTIPLIER METHOD SECTION

In this section, the outermost loop of the code is implemented. The augmented lagrangian multiplier method is composed of three main parts.

The first part is the input section where initial values of design variables, upper and lower bounds of the design variables, number of equality and inequality constraints and their initial multipliers are input. In addition, tolerances for convergence and maximum number of iterations are stated. At the end of input section objective function, equality and inequality constraints and newly constructed unconstrained objective function is evaluated and their values are stored.

In the second part, unconstrained optimization problem is solved. Davidon Fletcher Powell method is called and in this part a solution for unconstrained optimization problem is obtained. Similar to the end of the first part, objective function, equality and inequality constraints and newly constructed unconstrained objective function is evaluated and their values are stored.

In third part, convergence criteria is checked. If convergence criteria is achieved the code stops. However, in the code there are also other criteria to stop the execution of the code. These additional criteria include a check on the values of the design variables “ \mathbf{x} ” and maximum number of iterations. If the design variables do not change appreciably or the maximum number of iterations is exceeded, the code stops execution. If any one of the stopping criteria is not satisfied, penalty multipliers “ r_g ”, “ r_h ”, and lagrange multipliers “ λ ”, “ β ” are updated.

If the code stops with a violated constraint because design variables “ \mathbf{x} ” are not changing, in that case the stopping criteria which checks the values of the design variables “ \mathbf{x} ” can be omitted. This allows making further improvements in the multipliers and the weight of the violated constraint will be increased so that the constraint will not be violated. By adjusting the weights of the constraints the code tries to satisfy all constraints.

3.2 DAVIDON FLETCHER POWEL METHOD SECTION

This section of the code implements Davidon Fletcher Powell method to solve the unconstrained optimization problem. The unconstrained objective function, current value of design variable vector “ \mathbf{x} ”, upper and lower bounds of the design variable vector “ \mathbf{x} ” and maximum iteration number are taken from the ALM section. Tolerances for the convergence were stated at the beginning of the section. For the first iteration, identity matrix is used as the initial metric. Subsequently, gradient of the unconstrained objective function is calculated in an external M-file. Next step is determining the search direction “ \mathbf{s} ” which is found by negative of the dot product of the metric by the gradient. Once the search direction is determined, an M-file containing the golden section method is called to solve the one dimensional problem. This M-file provides a multiplier “ α ” for the search direction, updated design variable vector “ \mathbf{x} ” and the corresponding unconstrained objective function value. Square of the length of the gradient of the unconstrained objective function is calculated with the updated “ \mathbf{x} ” for the convergence check. If the square is less than the previously specified tolerance value, the algorithm is converged to a solution and the code stops execution. Otherwise, metric is updated based on DFP method and the whole process is repeated. As an exception, if the search direction is modified in the one dimensional search, metric is reset to the identity matrix. Other stopping criteria, which are the no appreciable change in the design variable vector “ \mathbf{x} ” and no appreciable change in the objective function value, are also checked respectively. If the code does not stop, it repeats all the steps starting from the determination of the search direction until the convergence or until one of the stopping criteria is achieved.

3.3 GOLDEN SECTION METHOD SECTION

This section is composed of two parts. These are determination of upper and lower bound for variable “ α ” which is factor for search direction “ \mathbf{s} ” which is written differently from and the implementation of golden section method.

Since the golden section method needs an interval to work on, determination of upper and lower bound for “ α ” is performed in the first part. Objective of this part is to keep the design variable vector “ \mathbf{x} ” within its lower and upper boundaries which are given as input in the beginning of the ALM section. At first, lower bound for “ α ” is set to zero. For this case the first component of the search direction “ \mathbf{s} ” is zero and the upper bound is set to a very high value such as 10^{12} . Then, for each component of “ \mathbf{x} ” (x_i), its position with respect to the boundaries and corresponding component of “ \mathbf{s} ” (s_i) are checked. There are six possibilities for the position of the design variable x_i .

First, x_i can be between its boundaries and the corresponding search direction is negative. Lower bound of “ α ” remains as is. Upper bound of “ α ” is set to the ratio of the distance to the lower boundary of x_i divided by s_i .

Second, x_i can be between its boundaries and corresponding search direction is positive. Lower bound of “ α ” remains as is. Upper bound of “ α ” is set to the ratio of the distance to the upper boundary of x_i divided by s_i .

Third, x_i can be less than its lower boundary and corresponding search direction is positive. Lower bound of “ α ” is set to the ratio of the distance to the lower boundary of x_i divided by s_i . Upper bound of “ α ” is set to the ratio of the distance to the upper boundary of x_i divided by s_i .

Fourth, x_i can be less than its lower bound and corresponding search direction is negative. For this case the search direction s_i must be reversed. This means a modification in the search direction and requires a reset in metric in DFP section. Lower bound of “ α ” is set to negative value of the ratio of the distance to the lower boundary of x_i divided by original s_i . Upper bound of “ α ” is set to the negative value of the ratio of the distance to the upper boundary of x_i divided by original s_i .

Fifth, x_i can be greater than its upper boundary and corresponding search direction is positive. For this case the search direction s_i must be reversed. This means a modification in the search direction and requires a reset in metric in DFP section. Lower bound of “ α ” is set to the negative value of the ratio of the distance to the upper boundary of x_i divided by original s_i . Upper bound of “ α ”

is set to the negative value of the ratio of the distance to the lower boundary of x_i divided by original s_i .

Sixth, x_i can be greater than its upper boundary and corresponding search direction is negative. Lower bound of “ α ” is set to the ratio of the distance to the upper boundary of x_i divided by s_i . Upper bound of “ α ” is set to the ratio of the distance to the lower boundary of x_i divided by s_i .

After checking for all components of the design variable vector “ \mathbf{x} ”, the minimum value of the calculated upper bound of “ α ” and the maximum value of the calculated lower bound of “ α ” is used as the new upper bound and lower bounds of “ α ”, respectively. This reduces the search interval and ensures staying within the boundaries of the variable “ \mathbf{x} ”.

If the value for the lower bound is greater than the upper bound, it means that the search direction in design space does not pass through the region bounded by lower and upper bounds of the design variable vector “ \mathbf{x} ”. For this case upper and lower bounds are inverted. Therefore, updated “ \mathbf{x} ” is guaranteed to be close to its boundaries in next iterations.

In the second part of this section, golden section algorithm is implemented directly. A tolerance and maximum iteration number are calculated by using upper and lower bounds of “ α ”. In the code the maximum iteration number is limited by 1000. Then, reduction of the interval continues until it becomes less than the tolerance or the maximum number of iterations is reached.

Average of the final lower and upper bound of variable “ α ” is chosen as final “ α ” to be multiplied by search direction “ \mathbf{s} ”.

At the end of the section, design variable vector “ \mathbf{x} ” is updated by the addition of search direction “ \mathbf{s} ” multiplied by “ α ” to the previous “ \mathbf{x} ”. And, finally the corresponding unconstrained objective function value is calculated.

3.4 OBJECTIVE FUNCTION SECTION FOR ANALYTIC SOLVER

This section introduces objective function and constraints of the optimization algorithm. It is composed of four subsections. These are the objective function, equality constraints, inequality constraints and unconstrained objective function section.

3.4.1 OBJECTIVE FUNCTION SECTION

The aim of the optimization is to minimize the objective function. In this section, main objective function is evaluated. The M-file which is dedicated to this function is called “Ofun.m”. Design variable vector “ \mathbf{x} ”, which is a row vector, is the only input to the objective function evaluation. Output is a scalar which is function value.

3.4.2 EQUALITY CONSTRAINT SECTION

An optimization problem might have equality constraints. If there is no equality constraints, this section is skipped. Otherwise, the M-file called “Hfun.m” is used to calculate their value(s). Design variable vector “ \mathbf{x} ” is the only input to this section. Output is a column vector in which each row is allocated for a different constraint value. At the solution, all the values of the output vector must be zero within a prescribed tolerance because the equality constraints are expressed by relations which are set to zero.

3.4.3 INEQUALITY CONSTRAINT SECTION

Similarly, an optimization problem might have inequality constraints. If there are no inequality constraints, this section is skipped as well. The M-file for the calculation of the values of inequality constraints is called “Gfun.m”. Design variable vector “ \mathbf{x} ” is the only input to this section. Output is a column vector in which each row is allocated for a different constraint value. At the solution, all the values of the output vector must be equal to or less than zero. Similar to

equality constraints, inequality constraints are expressed by ‘less than or equal to’ relations.

3.4.4 UNCONSTRAINED OBJECTIVE FUNCTION SECTION

This section constructs the unconstrained objective function for the augmented lagrangian method. The name of the M-file for this subsection is “FALM.m”. Design variable vector “ \mathbf{x} ”, lagrange multipliers λ for equality and β for inequality constraints and penalty multipliers r_h and r_g for equality and inequality constraints are given as inputs. Output is a scalar which is the value of unconstrained function.

In the beginning of the section, the main objective function is called. If there are no constraints, this value is the output value. In order to take constraints into account, first existence of equality constraints is checked. If there is at least one, an additional value which is calculated according to the augmented lagrangian method is added to the main objective function. This procedure is repeated for inequality constraints and final value of unconstrained function is obtained.

3.5 OBJECTIVE FUNCTION SECTION FOR MSC.NASTRAN[®] SOLVER

Like in the previous section, the purpose of this section is to introduce an objective function and constraints to the algorithm. The difference is that in this case values of inequality constraints are obtained from a MSC.NASTRAN[®] solution. Main objective function is calculated in M-file “Ofun.m” which is the same as used in the previous section. Evaluation of equality and inequality constraints, construction of the unconstrained objective function is performed in M-file “nastfunc.m”. Modification of the MSC.NASTRAN[®] input file .bdf for the current design variable vector “ \mathbf{x} ”, executing MSC.NASTRAN[®] and reading results for inequality constraints from the MSC.NASTRAN[®] output file .f06 are performed in the beginning of the “nastfunc.m”.

3.6 GRADIENT FUNCTION SECTION

To find a search direction in each iteration, the gradient of unconstrained objective function at the current design variable vector “ \mathbf{x} ” is needed. The M-file for this task is called “gradfunction.m”. Objective function name and current “ \mathbf{x} ” are used as inputs. For each element of “ \mathbf{x} ” first forward finite difference technique is applied. Results are stored in a row matrix, which is the output.

CHAPTER 4

OPTIMIZATION STRATEGIES WITH DIFFERENT OPTIMIZATION AND SOLVER CODES

Optimization process can be divided into two main sub-processes which are the optimization process and the evaluation of objective function and constraints. Therefore, an optimizer code and a solver are used to perform the optimization process and to evaluate the objective function and constraints, respectively. In this chapter, three different methods are presented to perform structural optimization with different optimization and solver codes. These methods are typically used to solve structural optimization problems in different engineering fields. In the first technique, structural optimization is performed by using the optimization code prepared in MATLAB[®] and analytical equations as the solver. This method actually corresponds to having an optimization and solver code which are developed by the user, and therefore user has complete control over the source codes. In this thesis to demonstrate the method, optimization code developed is used in conjunction with an analytical solver applicable to a cantilever beam problem. In general in this method a finite element code developed by the user can be used as the solver code. In the second technique, optimization is performed using the optimization code prepared in MATLAB[®] and commercial finite element solver MSC.NASTRAN[®] as the solver. The use of a commercial finite element code as the solver is also very common in solving structural optimization problems. Commercial finite element codes present a variety of element types with proven accuracy and most analyst have access to these codes. Therefore, during the solution of the optimization problem one can exploit the advantages of the commercial finite element codes and use

them as their solver codes and concentrate more on the optimization source code. As the third technique, optimization is performed using MSC.NASTRAN® Optimization Module. In this method optimization and solver source codes are not within the reach of the user and user solely relies on the optimization module of a commercial finite element program. This method requires experience in preparing the input files to define the optimization problem. In addition, effective use of optimization modules of the commercial finite element codes usually takes time because in some commercial finite element codes, preprocessing of the optimization problems is not user friendly. However, these optimization modules are often used by the engineers dealing with solving practical optimization problems.

The use of three different strategies, discussed above, to solve the same optimization problem also allows one to make mutual comparison studies. Thus, the solutions obtained with different methods can be compared with each other to further substantiate the results obtained for the optimization problem. Moreover, knowledge of alternative routes to solve the same optimization problem gives the user a chance to optimize their optimization and/or solver codes.

4.1 OPTIMIZATION VIA USER DEVELOPED OPTIMIZATION AND SOLVER CODES

In this technique optimizer code described in chapter three is used. To perform the optimization process, Augmented Lagrange Multiplier method is implemented with Davidon Fletcher Powell algorithm as the unconstrained optimizer. For the determination of the search direction, ‘Golden Section Method’ is chosen in the one dimensional search. To calculate the gradient of the unconstrained objective function, which is required by the Davidon Fletcher Powell algorithm, first forward finite difference technique is used. Each method is written in a different M-file and a total of four main M-files are developed to

perform the optimization process. These M files are named as “AugLagMet.m”, “DFP.m”, “golden.m” and “gradfunction.m” respectively.

The four main M-files are supported with other M-files which perform evaluation of the objective function, and constraints, and construction of the unconstrained objective function. Evaluation of the objective function and constraints are implemented in separate M-files. In M-file “Ofun.m”, main objective function is evaluated. MATLAB[®] files “Gfun.m” and “Hfun.m” are used to evaluate inequality and equality constraints, respectively. Files “Ofun.m”, “Gfun.m” and “Hfun.m” comprise the solver code because in structural optimization problems the objective function evaluation usually requires the calculation of weight, and equality and inequality constraints usually require the solution of certain field variables such as stresses, displacements etc. for the particular optimization problem defined. Finally, in the M-file called “FALM.m” unconstrained objective function is constructed in accordance with Augmented Lagrangian Multiplier Method. Detailed information about the code was given in chapter 3.

This technique is applicable to the problems for which user developed optimization and solver codes are used. For demonstration purposes, Euler beam relations are used as the analytical expressions to calculate field variables such as stresses, displacements etc. The advantage of this technique is that user has full control on optimization and solver process. It should be noted that if a finite element code is developed by the user then this code could be incorporated in “Gfun.m” which evaluates the inequality constraints. In structural optimization problems the inequality constraints are usually defined on field variables such as deflection, stress or on eigen-values defined in structural stability problems such as natural frequency or buckling loads. Thus, the current structure of the code allows expansion in implementing a user developed finite element code as the solver. This expansion is elaborated in the next section. The user interface of this technique is given in Appendix B.1.

4.2 OPTIMIZATION USING AN OPTIMIZATION CODE IN MATLAB[®] AND MSC.NASTRAN[®] AS SOLVER

In structural analysis, for the solution of problems involving complex geometries and loading, analytical solutions are usually not available. Therefore, in such problems finite element method can be used to obtain results for the field quantities such as deflections, stress values, etc.. In the optimization process of such complex problems, finite element method can be implemented as the solver as stated above. In this section, a strategy which uses an optimization code in MATLAB[®] as the optimizer and MSC.NASTRAN[®] as solver is presented.

In this technique, the optimization process is same as described previously. The M-files “AugLagMet.m”, “DFP.m”, “golden.m” and “gradfunction.m” are used without any change in algorithms. Therefore, this technique differs from the previous one only in the evaluation of the objective function and constraints.

Usually, the main objective function to be minimized is the weight or volume. The evaluation of the weight is a simple task. Analytical methods can be used for this task and it is performed in “Ofun.m” which is the same MATLAB[®] file as described in the previous method. However, for checking whether the constraints are satisfied or not, usually a finite element solution is required. For instance, in structural optimization problems the constraints are usually imposed on stress values and displacements, or on natural frequencies and on buckling loads etc. And, calculation of stresses, displacements, natural frequencies, buckling loads etc. usually requires finite element solution to be performed for complex geometry and loading problems defined in aerospace structures. Therefore, in this method the M-file “nastfunc.m” is developed to perform the construction of the unconstrained objective function by using the commercial finite element solver MSC.NASTRAN[®].

In this method, the existing input file bdf-file is modified at the beginning of “nastfunc.m”, In other words the design variables are updated in accordance with

the output of the optimization code and old variables are replaced with the new ones in `bdf_file`. Then, MSC.NASTRAN[®] is called from MATLAB[®] inside the MATLAB[®] file “`nastfunc.m`” to execute a finite element run and the solution is written in the MSC.NASTRAN[®] output file which is `.f06`-file. After the MSC.NASTRAN[®] job is finished, “`nastfunc.m`” file reads the required output from the `.f06`-file. The required output are those quantities which are used in the evaluation of the objective function and constraints. Finally, construction of the unconstrained objective function is performed in accordance with the ‘Augmented Lagrange Multiplier method’. The output of the M-file “`nastfunc.m`” is the value of unconstrained objective function.

To be able to perform these tasks, a run must be executed by MSC.NASTRAN[®] before starting the optimization process to find out the format of the MSC.NASTRAN[®] input and output files for the particular structural problem, and to locate the positions of the variables which will be used in the evaluation of the unconstrained objective function. The position of the variables in the input `.bdf`-file, and required results in the output `.f06`-file should be spotted beforehand to perform the reading and modification of the particular fields in the MSC.NASTRAN[®] input and output files. A detailed procedure for this technique is given in Appendix B.2.

To summarize, the functions of “`FALM.m`” in analytical solver technique and “`nastfunc.m`” in MSC.NASTRAN[®] solver technique are the same. Both take the current variables as input, perform the construction of the unconstrained objective function and evaluate its value. The output of both M-files is the value of unconstrained objective function calculated by using the current value of the design variables.

4.3 OPTIMIZATION USING THE OPTIMIZATION MODULE OF MSC.NASTRAN®

MSC.NASTRAN® is widely used in aerospace industry. It has not only a very powerful finite element solver, but also contains a module for optimization which can be used in structural optimization problems. In this section, property optimization and shape optimization capability of the optimization module of MSC.NASTRAN® is introduced for linear structural analysis. It should be noted that the use of optimization modules of commercial finite element codes presents the user an alternative method to check the results of the optimization/solver codes developed by the users themselves. In aerospace structures margins of safety of structural elements are usually kept low in order to reduce the overall weight of the aerospace vehicle. Structural optimization is especially important in aerospace structures because of the significant impact that the weight reduction induces on the performance and cost of aerospace vehicles. However, since the margins of safety have to be low, in order not to risk any failure the results of the structural optimization must be highly reliable. Therefore, cross-check of the results produced by the user developed optimization/solver codes and by the optimization modules of commercial finite element codes is very important in using the results of the optimization codes in the design of aerospace structures with an increased level of confidence. Optimization process of MSC.NASTRAN® is given in Figure 4.1.

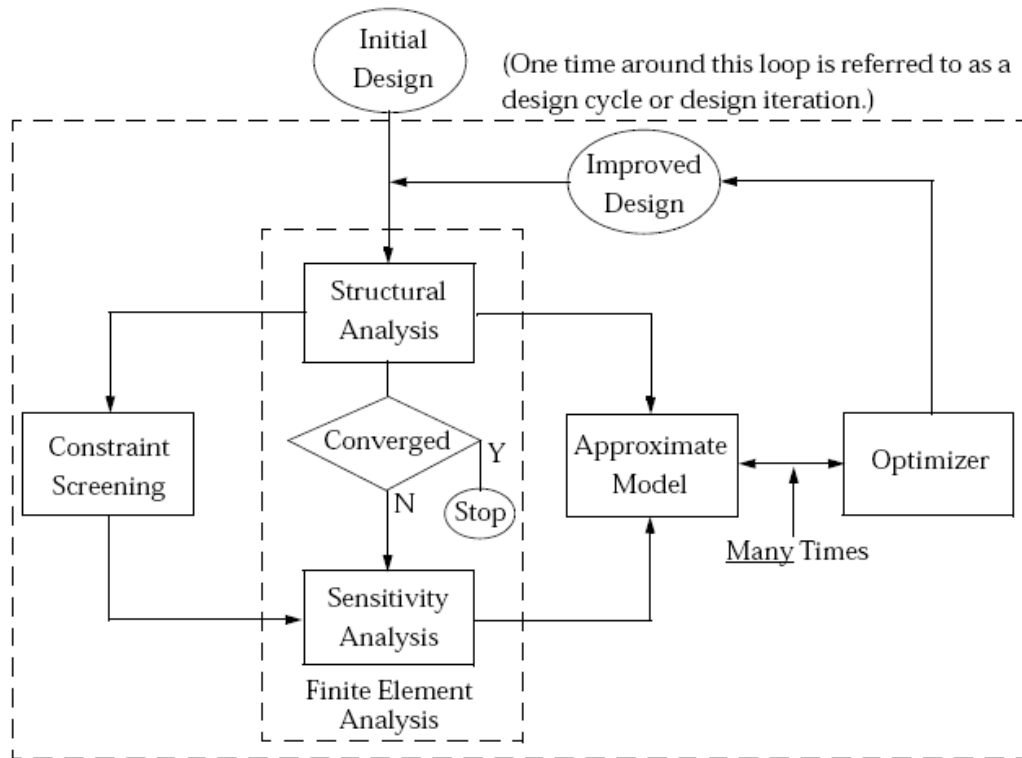


Figure 4.1 MSC.NASTRAN[®] implementation of structural optimization [10]

Initial design is composed of two parts. First part is the analysis model, in which grid locations, element structure and properties, material information, loads, boundary conditions and load cases are described. Second part is the design model. Defining the design variables, relating design variables to element properties, defining the design responses, constraints and objectives are described in design model. The initial design is the input to the MSC.NASTRAN[®] optimization process.

First activity of MSC.NASTRAN[®] optimization process is to perform a finite element analysis. Next, in the constraint screening activity the constraints that are violated or likely to be violated are identified. These are set to be as active constraints.

In sensitivity analysis, the sensitivities such as the rates of change of structural response quantities or a change in constraint values with respect to changes in

design variables are computed. These are partial derivatives and provide essential information to the optimizer.

An approximate model is constructed by using the information from finite element analysis and sensitivity analysis. This model involves approximations to finite element results to reduce the number of full scale finite element analyses. Optimizer performs optimization process by using the approximate model. By default, gradient based methods are used to construct improved design. Other available methods are sequential linear programming and sequential quadratic programming.

The improved model is compared with the previous model. If the changes are below the desired value, this means that soft convergence is achieved. Then, after the finite element analysis, one more convergence test for hard convergence is performed. Detailed information about MSC.NASTRAN[®] sensitivity analysis and optimization process is given in Reference [11].

There are three steps to perform an optimization task using MSC.NASTRAN[®] optimization tools. These are:

1. Creating an input .bdf-file
2. Executing a MSC.NASTRAN[®] run
3. Post processing of the results

4.3.1 CREATING A BDF-FILE

A standard input .bdf-file is composed of four sections which are the file management, executive control, case control and bulk data, respectively. The following paragraphs define these sections. Further information about creating bdf-file can be found in Reference [10].

4.3.1.1 FILE MANAGEMENT SECTION

File management section is used for the attachment and initialization of database sets and external files. Usually, in MSC.NASTRAN[®] jobs, no file management statements are required. But, for shape optimization problems DBLOCATE

statement is used for introducing auxiliary model to the design model. Also, user defined beam libraries or external responses can be introduced in this section.

4.3.1.2 EXECUTIVE CONTROL SECTION

In executive control, the only required statement is “SOL 200” which implies design optimization

4.3.1.3 CASE CONTROL SECTION

In case control section, four tasks are performed for design sensitivity analysis and optimization. These tasks are the analysis discipline definition, design task definition, design response characterization and shape basis vector computation, respectively.

In analysis discipline definition, solution sequences that are used in optimization process are defined. The applicable solution sequences are linear statics, normal modes, buckling, direct frequency, modal frequency, modal transient, direct complex eigenvalue analysis, static aeroelasticity, static aeroelastic divergence and flutter. In this thesis only linear statics is used.

In design task definition, design objective function and design constraint sets are identified.

Design response characterization is used to resolve design response ambiguities. For example, for plate element stresses, maximum shear stress and von Mises stress use the same item code ID. By using the statement “STRESS(VONMISES)=15” or “STRESS(SHEAR)=15” it is clearly identified which stress to be used in analysis and optimization.

Shape basis vector computation is applicable only when analytic boundary shape method is used for shape optimization. Analytic boundary shape method is not used in this thesis.

4.3.1.4 BULK DATA SECTION

Bulk data contains the analysis model and design model. MSC/PATRAN[®] is a very useful tool to construct an analysis model. There are also other commercial tools such as MSC.SOFY[®] or NX.NASTRAN[®]. Design model is located below the analysis model.

At the beginning of the design model section, design variables are identified with their initial values and upper and lower bounds.

Next, the relations between design variables and element properties, displacements or shape basis vectors are defined. For shape optimization, an auxiliary model is required. This model describes change in grid positions when corresponding design variable is changed. It is prepared by a separate finite element analysis of the model for the desired displacements and it should be introduced in the file management section.

Next, design responses are created which are used as basis of defining design objective function and constraints. There are three types of responses. First type is first level responses which are available directly from an MSC.NASTRAN[®] analysis. Structural weight, displacements at grid points, element stresses, and so on, are all examples of first level responses. Second type is second level responses which are called as user-defined since they utilize the equation input feature in MSC.NASTRAN[®]. Third type is third level responses which can be regarded as an extension of the second level responses. This type allows one to introduce an external process to the MSC.NASTRAN[®] design sensitivity and optimization process.

Next, design objective and design constraints are stated. Design objective is a scalar quantity to be minimized by the optimizer. “DESOBJ” statement is used to identify which design response is related to the design objective. Design constraints are defined by “ DCONSTR” statements. This statement points a design response and gives upper and lower limits for the corresponding design response.

At the end of the bulk data section output control parameters are stated. These parameters affect either the frequency or level of detail of the output.

4.3.2 MSC.NASTRAN® RUN

After completing MSC.NASTRAN® input file.bdf, MSC.NASTRAN® job is submitted. Output is written in .f06, .pch (punch) and .op2-files. Xdb file can also be used instead of op2 file. At the end of the solution, the output file .f06-file must be investigated for errors and warnings before post processing the results.

4.3.3 POSTPROCESSING

Two ways of post processing is presented in this section. First one is importing the op2-files into MSC/PATRAN®. Using post processor tool of MSC/PATRAN® history of each variables, objective function and constraints can be plotted on graphs. The results of structural analysis such as stress distribution, displacements, grid point forces can be viewed not only at the final solution but also at each step of the optimization process.

Another way of getting the same data is through the output .f06-files. F06-files contain similar information as op2-files but in formatted text form.

Additionally, pch-file includes outputs from the MSC.NASTRAN® analysis such as final grid locations or final element properties. These outputs can be conveniently used as input into another computer analysis. A sample bdf-file for the optimization process is presented in Appendix B.3

CHAPTER 5

SAMPLE STUDIES TO DEMONSTRATE DIFFERENT OPTIMIZATION STRATEGIES

In this chapter, optimizations of two sample problems are presented to demonstrate the application of the three different strategies described in the previous section. Both problems are cantilever beam problems subjected to a vertical force at the free end. In the first problem a rectangular cross section is chosen with two design variables. The height and width of the cross-section of the beam are taken as the two design parameters. This way it has been possible to show the design space on the two dimensional graph, and thus it becomes easier to trace the progress of the optimization methods during each step.

In the second problem I cross section beam is chosen with 4 design variables. Since analytical solution for stresses and deflections are available for the cantilever beam problems, the three optimization strategies are implemented in solving the optimization problems defined.

5.1 OPTIMIZATION OF CANTILEVER BEAM WITH RECTANGULAR CROSS SECTION

In this sample problem, to illustrate the optimization process a simple optimization problem is solved. A cantilever beam subject to vertical force "P" at the end will be optimized. In this problem two design variables are used, because this way the design space can be shown on a two dimensional graph. The beam is assumed to have rectangular cross section which does not vary along the length. The width "B" and the height "H" are chosen as design

variables. Their dimensions are given in mm. The length of the beam is fixed. Figure 5.1 shows the cantilever beam to be optimized.

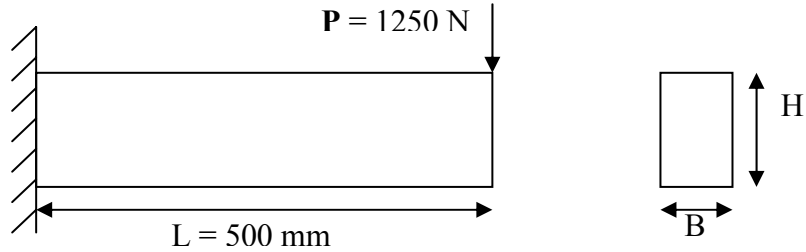


Figure 5.1 Cantilever beam with rectangular cross section

The objective of this problem is to minimize the weight of the beam subject to certain constraints. High strength aluminum is used as the material of the beam. Since density of aluminum is constant, minimizing weight is the same as minimizing the volume.

The beam is subjected to three constraints. First constraint is maximum normal stress due to bending at the root, second one is the maximum tip deflection due to tip loading and the third one is height to width ratio to ensure the stability of the beam.

Based on above explanations the optimization problem can be stated as follows:

Minimize:

$$V = B \cdot H \cdot L \quad (5.1)$$

Subject to:

$$\sigma = \frac{M \cdot c}{I} = \frac{6 \cdot P \cdot L}{B \cdot H^2} \leq 700 \text{ MPa} \quad (5.2)$$

$$\delta = \frac{P \cdot L^3}{3 \cdot E \cdot I} = \frac{4 \cdot P \cdot L^3}{E \cdot B \cdot H^3} \leq 25.4 \text{ mm} \quad (5.3)$$

$$\frac{H}{B} \leq 5 \quad (5.4)$$

where the bounds of the design variables are specified as:

$$1 \leq B \leq 20 \quad (5.5)$$

$$20 \leq H \leq 50 \quad (5.6)$$

The design space for this problem is defined by the lower and upper bounds of the design variables “B” and “H”. To make a one to one correspondence with the optimization solutions, the value of the unconstrained objective function in the design space is given in Table 5.1. Horizontal axis represents width “B” of the cross section and vertical axis represents the height “H” of the cross section. The minimum value of objective function in the design space is at the lower bounds of both design variables. In the Table 5.1 the final optimum value of objective function and its location is marked with blue background. This value is the optimum value considering the constraints imposed on the problem.

Table 5.1 Objective function variation in the unconstrained design space

| Design Space (Volume, Objective Function) (1000 mm ³) | | | | | | | | | | | | | | | | | | | | |
|---|------|------|------|-------|-------|-------|-------|-------|-------|-------|-------|-------|-------|-------|-------|-------|-------|-------|-------|-------|
| HB (mm) | 1 | 2 | 3 | 4 | 5 | 6 | 7 | 8 | 9 | 10 | 11 | 12 | 13 | 14 | 15 | 16 | 17 | 18 | 19 | 20 |
| 20 | 10.0 | 20.0 | 30.0 | 40.0 | 50.0 | 60.0 | 70.0 | 80.0 | 90.0 | 100.0 | 110.0 | 120.0 | 130.0 | 140.0 | 150.0 | 160.0 | 170.0 | 180.0 | 190.0 | 200.0 |
| 21 | 10.5 | 21.0 | 31.5 | 42.0 | 52.5 | 63.0 | 73.5 | 84.0 | 94.5 | 105.0 | 115.5 | 126.0 | 136.5 | 147.0 | 157.5 | 168.0 | 178.5 | 189.0 | 199.5 | 210.0 |
| 22 | 11.0 | 22.0 | 33.0 | 44.0 | 55.0 | 66.0 | 77.0 | 88.0 | 99.0 | 110.0 | 121.0 | 132.0 | 143.0 | 154.0 | 165.0 | 176.0 | 187.0 | 198.0 | 209.0 | 220.0 |
| 23 | 11.5 | 23.0 | 34.5 | 46.0 | 57.5 | 69.0 | 80.5 | 92.0 | 103.5 | 115.0 | 126.5 | 138.0 | 149.5 | 161.0 | 172.5 | 184.0 | 195.5 | 207.0 | 218.5 | 230.0 |
| 24 | 12.0 | 24.0 | 36.0 | 48.0 | 60.0 | 72.0 | 84.0 | 96.0 | 108.0 | 120.0 | 132.0 | 144.0 | 156.0 | 168.0 | 180.0 | 192.0 | 204.0 | 216.0 | 228.0 | 240.0 |
| 25 | 12.5 | 25.0 | 37.5 | 50.0 | 62.5 | 75.0 | 87.5 | 100.0 | 112.5 | 125.0 | 137.5 | 150.0 | 162.5 | 175.0 | 187.5 | 200.0 | 212.5 | 225.0 | 237.5 | 250.0 |
| 26 | 13.0 | 26.0 | 39.0 | 52.0 | 65.0 | 78.0 | 91.0 | 104.0 | 117.0 | 130.0 | 143.0 | 156.0 | 169.0 | 182.0 | 195.0 | 208.0 | 221.0 | 234.0 | 247.0 | 260.0 |
| 27 | 13.5 | 27.0 | 40.5 | 54.0 | 67.5 | 81.0 | 94.5 | 108.0 | 121.5 | 135.0 | 148.5 | 162.0 | 175.5 | 189.0 | 202.5 | 216.0 | 229.5 | 243.0 | 256.5 | 270.0 |
| 28 | 14.0 | 28.0 | 42.0 | 56.0 | 70.0 | 84.0 | 98.0 | 112.0 | 126.0 | 140.0 | 154.0 | 168.0 | 182.0 | 196.0 | 210.0 | 224.0 | 238.0 | 252.0 | 266.0 | 280.0 |
| 29 | 14.5 | 29.0 | 43.5 | 58.0 | 72.5 | 87.0 | 101.5 | 116.0 | 130.5 | 145.0 | 159.5 | 174.0 | 188.5 | 203.0 | 217.5 | 232.0 | 246.5 | 261.0 | 275.5 | 290.0 |
| 30 | 15.0 | 30.0 | 45.0 | 60.0 | 75.0 | 90.0 | 105.0 | 120.0 | 135.0 | 150.0 | 165.0 | 180.0 | 195.0 | 210.0 | 225.0 | 240.0 | 255.0 | 270.0 | 285.0 | 300.0 |
| 31 | 15.5 | 31.0 | 46.5 | 62.0 | 77.5 | 93.0 | 108.5 | 124.0 | 139.5 | 155.0 | 170.5 | 186.0 | 201.5 | 217.0 | 232.5 | 248.0 | 263.5 | 279.0 | 294.5 | 310.0 |
| 32 | 16.0 | 32.0 | 48.0 | 64.0 | 80.0 | 96.0 | 112.0 | 128.0 | 144.0 | 160.0 | 176.0 | 192.0 | 208.0 | 224.0 | 240.0 | 256.0 | 272.0 | 288.0 | 304.0 | 320.0 |
| 33 | 16.5 | 33.0 | 49.5 | 66.0 | 82.5 | 99.0 | 115.5 | 132.0 | 148.5 | 165.0 | 181.5 | 198.0 | 214.5 | 231.0 | 247.5 | 264.0 | 280.5 | 297.0 | 313.5 | 330.0 |
| 34 | 17.0 | 34.0 | 51.0 | 68.0 | 85.0 | 102.0 | 119.0 | 136.0 | 153.0 | 170.0 | 187.0 | 204.0 | 221.0 | 238.0 | 255.0 | 272.0 | 289.0 | 306.0 | 323.0 | 340.0 |
| 35 | 17.5 | 35.0 | 52.5 | 70.0 | 87.5 | 105.0 | 122.5 | 140.0 | 157.5 | 175.0 | 192.5 | 210.0 | 227.5 | 245.0 | 262.5 | 280.0 | 297.5 | 315.0 | 332.5 | 350.0 |
| 36 | 18.0 | 36.0 | 54.0 | 72.0 | 90.0 | 108.0 | 126.0 | 144.0 | 162.0 | 180.0 | 198.0 | 216.0 | 234.0 | 252.0 | 270.0 | 288.0 | 306.0 | 324.0 | 342.0 | 360.0 |
| 37 | 18.5 | 37.0 | 55.5 | 74.0 | 92.5 | 111.0 | 129.5 | 148.0 | 166.5 | 185.0 | 203.5 | 222.0 | 240.5 | 259.0 | 277.5 | 296.0 | 314.5 | 333.0 | 351.5 | 370.0 |
| 38 | 19.0 | 38.0 | 57.0 | 76.0 | 95.0 | 114.0 | 133.0 | 152.0 | 171.0 | 190.0 | 209.0 | 228.0 | 247.0 | 266.0 | 285.0 | 304.0 | 323.0 | 342.0 | 361.0 | 380.0 |
| 39 | 19.5 | 39.0 | 58.5 | 78.0 | 97.5 | 117.0 | 136.5 | 156.0 | 175.5 | 195.0 | 214.5 | 234.0 | 253.5 | 273.0 | 292.5 | 312.0 | 331.5 | 351.0 | 370.5 | 390.0 |
| 40 | 20.0 | 40.0 | 60.0 | 80.0 | 100.0 | 120.0 | 140.0 | 160.0 | 180.0 | 200.0 | 220.0 | 240.0 | 260.0 | 280.0 | 300.0 | 320.0 | 340.0 | 360.0 | 380.0 | 400.0 |
| 41 | 20.5 | 41.0 | 61.5 | 82.0 | 102.5 | 123.0 | 143.5 | 164.0 | 184.5 | 205.0 | 225.5 | 246.0 | 266.5 | 287.0 | 307.5 | 328.0 | 348.5 | 369.0 | 389.5 | 410.0 |
| 42 | 21.0 | 42.0 | 63.0 | 84.0 | 105.0 | 126.0 | 147.0 | 168.0 | 189.0 | 210.0 | 231.0 | 252.0 | 273.0 | 294.0 | 315.0 | 336.0 | 357.0 | 378.0 | 399.0 | 420.0 |
| 43 | 21.5 | 43.0 | 64.5 | 86.0 | 107.5 | 129.0 | 150.5 | 172.0 | 193.5 | 215.0 | 236.5 | 258.0 | 279.5 | 301.0 | 322.5 | 344.0 | 365.5 | 387.0 | 408.5 | 430.0 |
| 44 | 22.0 | 44.0 | 66.0 | 88.0 | 110.0 | 132.0 | 154.0 | 176.0 | 198.0 | 220.0 | 242.0 | 264.0 | 286.0 | 308.0 | 330.0 | 352.0 | 374.0 | 396.0 | 418.0 | 440.0 |
| 45 | 22.5 | 45.0 | 67.5 | 90.0 | 112.5 | 135.0 | 157.5 | 180.0 | 202.5 | 225.0 | 247.5 | 270.0 | 292.5 | 315.0 | 337.5 | 360.0 | 382.5 | 405.0 | 427.5 | 450.0 |
| 46 | 23.0 | 46.0 | 69.0 | 92.0 | 115.0 | 138.0 | 161.0 | 184.0 | 207.0 | 230.0 | 253.0 | 276.0 | 299.0 | 322.0 | 345.0 | 368.0 | 391.0 | 414.0 | 437.0 | 460.0 |
| 47 | 23.5 | 47.0 | 70.5 | 94.0 | 117.5 | 141.0 | 164.5 | 188.0 | 211.5 | 235.0 | 258.5 | 282.0 | 305.5 | 329.0 | 352.5 | 376.0 | 399.5 | 423.0 | 446.5 | 470.0 |
| 48 | 24.0 | 48.0 | 72.0 | 96.0 | 120.0 | 144.0 | 168.0 | 192.0 | 216.0 | 240.0 | 264.0 | 288.0 | 312.0 | 336.0 | 360.0 | 384.0 | 408.0 | 432.0 | 456.0 | 480.0 |
| 49 | 24.5 | 49.0 | 73.5 | 98.0 | 122.5 | 147.0 | 171.5 | 196.0 | 220.5 | 245.0 | 269.5 | 294.0 | 318.5 | 343.0 | 367.5 | 392.0 | 416.5 | 441.0 | 465.5 | 490.0 |
| 50 | 25.0 | 50.0 | 75.0 | 100.0 | 125.0 | 150.0 | 175.0 | 200.0 | 225.0 | 250.0 | 275.0 | 300.0 | 325.0 | 350.0 | 375.0 | 400.0 | 425.0 | 450.0 | 475.0 | 500.0 |

The values of the maximum stress at the root of the beam in the design space is given in Table 5.2. According to the first constraint, maximum stress value must be less than 700 MPa. The region where stress values are higher than 700 MPa marked with red background. This region is the restricted region. Therefore, a feasible region must be defined in the design space where constraints are not violated. If there were no constraints, the feasible region would be the design space itself. From Table 5.2 it can be concluded that the feasible region is reduced by the stress constraint.

Table 5.2 Variation of maximum stress in the design space

| Design Space (Maximum Normal Stress, Constraint 1 \leq 700MPa) | | | | | | | | | | | | | | | | | | | | |
|--|------|------|------|------|------|------|------|------|------|-----|-----|-----|-----|-----|-----|-----|-----|-----|-----|-----|
| HB (mm) | 1 | 2 | 3 | 4 | 5 | 6 | 7 | 8 | 9 | 10 | 11 | 12 | 13 | 14 | 15 | 16 | 17 | 18 | 19 | 20 |
| 20 | 9375 | 4688 | 3125 | 2344 | 1875 | 1563 | 1339 | 1172 | 1042 | 938 | 852 | 781 | 721 | 670 | 625 | 586 | 551 | 521 | 493 | 469 |
| 21 | 8503 | 4252 | 2834 | 2126 | 1701 | 1417 | 1215 | 1063 | 945 | 850 | 773 | 709 | 654 | 607 | 567 | 531 | 500 | 472 | 448 | 425 |
| 22 | 7748 | 3874 | 2583 | 1937 | 1550 | 1291 | 1107 | 968 | 861 | 775 | 704 | 646 | 596 | 553 | 517 | 484 | 456 | 430 | 408 | 387 |
| 23 | 7089 | 3544 | 2363 | 1772 | 1418 | 1181 | 1013 | 886 | 788 | 709 | 644 | 591 | 545 | 506 | 473 | 443 | 417 | 394 | 373 | 354 |
| 24 | 6510 | 3255 | 2170 | 1628 | 1302 | 1085 | 930 | 814 | 723 | 651 | 592 | 543 | 501 | 465 | 434 | 407 | 383 | 362 | 343 | 326 |
| 25 | 6000 | 3000 | 2000 | 1500 | 1200 | 1000 | 857 | 750 | 667 | 600 | 545 | 500 | 462 | 429 | 400 | 375 | 353 | 333 | 316 | 300 |
| 26 | 5547 | 2774 | 1849 | 1387 | 1109 | 925 | 792 | 693 | 616 | 555 | 504 | 462 | 427 | 396 | 370 | 347 | 326 | 308 | 292 | 277 |
| 27 | 5144 | 2572 | 1715 | 1286 | 1029 | 857 | 735 | 643 | 572 | 514 | 468 | 429 | 396 | 367 | 343 | 322 | 303 | 286 | 271 | 257 |
| 28 | 4783 | 2392 | 1594 | 1196 | 957 | 797 | 683 | 598 | 531 | 478 | 435 | 399 | 368 | 342 | 319 | 299 | 281 | 266 | 252 | 239 |
| 29 | 4459 | 2229 | 1486 | 1115 | 892 | 743 | 637 | 557 | 495 | 446 | 405 | 372 | 343 | 318 | 297 | 279 | 262 | 248 | 235 | 223 |
| 30 | 4167 | 2083 | 1389 | 1042 | 833 | 694 | 595 | 521 | 463 | 417 | 379 | 347 | 321 | 298 | 278 | 260 | 245 | 231 | 219 | 208 |
| 31 | 3902 | 1951 | 1301 | 976 | 780 | 650 | 557 | 488 | 434 | 390 | 355 | 325 | 300 | 279 | 260 | 244 | 230 | 217 | 205 | 195 |
| 32 | 3662 | 1831 | 1221 | 916 | 732 | 610 | 523 | 458 | 407 | 366 | 333 | 305 | 282 | 262 | 244 | 229 | 215 | 203 | 193 | 183 |
| 33 | 3444 | 1722 | 1148 | 861 | 689 | 574 | 492 | 430 | 383 | 344 | 313 | 287 | 265 | 246 | 230 | 215 | 203 | 191 | 181 | 172 |
| 34 | 3244 | 1622 | 1081 | 811 | 649 | 541 | 463 | 405 | 360 | 324 | 295 | 270 | 250 | 232 | 216 | 203 | 191 | 180 | 171 | 162 |
| 35 | 3061 | 1531 | 1020 | 765 | 612 | 510 | 437 | 383 | 340 | 306 | 278 | 255 | 235 | 219 | 204 | 191 | 180 | 170 | 161 | 153 |
| 36 | 2894 | 1447 | 965 | 723 | 579 | 482 | 413 | 362 | 322 | 289 | 263 | 241 | 223 | 207 | 193 | 181 | 170 | 161 | 152 | 145 |
| 37 | 2739 | 1370 | 913 | 685 | 548 | 457 | 391 | 342 | 304 | 274 | 249 | 228 | 211 | 196 | 183 | 171 | 161 | 152 | 144 | 137 |
| 38 | 2597 | 1298 | 866 | 649 | 519 | 433 | 371 | 325 | 289 | 260 | 236 | 216 | 200 | 185 | 173 | 162 | 153 | 144 | 137 | 130 |
| 39 | 2465 | 1233 | 822 | 616 | 493 | 411 | 352 | 308 | 274 | 247 | 224 | 205 | 190 | 176 | 164 | 154 | 145 | 137 | 130 | 123 |
| 40 | 2344 | 1172 | 781 | 586 | 469 | 391 | 335 | 293 | 260 | 234 | 213 | 195 | 180 | 167 | 156 | 146 | 138 | 130 | 123 | 117 |
| 41 | 2231 | 1115 | 744 | 558 | 446 | 372 | 319 | 279 | 248 | 223 | 203 | 186 | 172 | 159 | 149 | 139 | 131 | 124 | 117 | 112 |
| 42 | 2126 | 1063 | 709 | 531 | 425 | 354 | 304 | 266 | 236 | 213 | 193 | 177 | 164 | 152 | 142 | 133 | 125 | 118 | 112 | 106 |
| 43 | 2028 | 1014 | 676 | 507 | 406 | 338 | 290 | 254 | 225 | 203 | 184 | 169 | 156 | 145 | 135 | 127 | 119 | 113 | 107 | 101 |
| 44 | 1937 | 968 | 646 | 484 | 387 | 323 | 277 | 242 | 215 | 194 | 176 | 161 | 149 | 138 | 129 | 121 | 114 | 108 | 102 | 97 |
| 45 | 1852 | 926 | 617 | 463 | 370 | 309 | 265 | 231 | 206 | 185 | 168 | 154 | 142 | 132 | 123 | 116 | 109 | 103 | 97 | 93 |
| 46 | 1772 | 886 | 591 | 443 | 354 | 295 | 253 | 222 | 197 | 177 | 161 | 148 | 136 | 127 | 118 | 111 | 104 | 98 | 93 | 89 |
| 47 | 1698 | 849 | 566 | 424 | 340 | 283 | 243 | 212 | 189 | 170 | 154 | 141 | 131 | 121 | 113 | 106 | 100 | 94 | 89 | 85 |
| 48 | 1628 | 814 | 543 | 407 | 326 | 271 | 233 | 203 | 181 | 163 | 148 | 136 | 125 | 116 | 109 | 102 | 96 | 90 | 86 | 81 |
| 49 | 1562 | 781 | 521 | 390 | 312 | 260 | 223 | 195 | 174 | 156 | 142 | 130 | 120 | 112 | 104 | 98 | 92 | 87 | 82 | 78 |
| 50 | 1500 | 750 | 500 | 375 | 300 | 250 | 214 | 188 | 167 | 150 | 136 | 125 | 115 | 107 | 100 | 94 | 88 | 83 | 79 | 75 |

The values of the maximum displacement at the tip of the beam in the design space is given in Table 5.3. According to the second constraint, maximum displacement value must be less than 25.4 mm. The region where displacement values are higher than 25.4 mm marked with red background. This region is restricted region. Therefore, feasible region in the design space is also reduced by the displacement constraint. Again, the cell with the blue background color shows the location of the optimum solution.

Table 5.3 Variation of maximum deflection in the design space

| Design Space (Displacement, Constraint 2 ≤ 25.4 mm) | | | | | | | | | | | | | | | | | | | | |
|---|--------|-------|-------|-------|-------|-------|-------|-------|-------|-------|-------|------|------|------|------|------|------|------|------|------|
| HB (mm) | 1 | 2 | 3 | 4 | 5 | 6 | 7 | 8 | 9 | 10 | 11 | 12 | 13 | 14 | 15 | 16 | 17 | 18 | 19 | 20 |
| 20 | 1116.1 | 558.0 | 372.0 | 279.0 | 223.2 | 186.0 | 159.4 | 139.5 | 124.0 | 111.6 | 101.5 | 93.0 | 85.9 | 79.7 | 74.4 | 69.8 | 65.7 | 62.0 | 58.7 | 55.8 |
| 21 | 964.1 | 482.1 | 321.4 | 241.0 | 192.8 | 160.7 | 137.7 | 120.5 | 107.1 | 96.4 | 87.6 | 80.3 | 74.2 | 68.9 | 64.3 | 60.3 | 56.7 | 53.6 | 50.7 | 48.2 |
| 22 | 838.5 | 419.3 | 279.5 | 209.6 | 167.7 | 139.8 | 119.8 | 104.8 | 93.2 | 83.9 | 76.2 | 69.9 | 64.5 | 59.9 | 55.9 | 52.4 | 49.3 | 46.6 | 44.1 | 41.9 |
| 23 | 733.8 | 366.9 | 244.6 | 183.5 | 146.8 | 122.3 | 104.8 | 91.7 | 81.5 | 73.4 | 66.7 | 61.2 | 56.4 | 52.4 | 48.9 | 45.9 | 43.2 | 40.8 | 38.6 | 36.7 |
| 24 | 645.9 | 322.9 | 215.3 | 161.5 | 129.2 | 107.6 | 92.3 | 80.7 | 71.8 | 64.6 | 58.7 | 53.8 | 49.7 | 46.1 | 43.1 | 40.4 | 38.0 | 35.9 | 34.0 | 32.3 |
| 25 | 571.4 | 285.7 | 190.5 | 142.9 | 114.3 | 95.2 | 81.6 | 71.4 | 63.5 | 57.1 | 51.9 | 47.6 | 44.0 | 40.8 | 38.1 | 35.7 | 33.6 | 31.7 | 30.1 | 28.6 |
| 26 | 508.0 | 254.0 | 169.3 | 127.0 | 101.6 | 84.7 | 72.6 | 63.5 | 56.4 | 50.8 | 46.2 | 42.3 | 39.1 | 36.3 | 33.9 | 31.7 | 29.9 | 28.2 | 26.7 | 25.4 |
| 27 | 453.6 | 226.8 | 151.2 | 113.4 | 90.7 | 75.6 | 64.8 | 56.7 | 50.4 | 45.4 | 41.2 | 37.8 | 34.9 | 32.4 | 30.2 | 28.4 | 26.7 | 25.2 | 23.9 | 22.7 |
| 28 | 406.7 | 203.4 | 135.6 | 101.7 | 81.3 | 67.8 | 58.1 | 50.8 | 45.2 | 40.7 | 37.0 | 33.9 | 31.3 | 29.1 | 27.1 | 25.4 | 23.9 | 22.6 | 21.4 | 20.3 |
| 29 | 366.1 | 183.0 | 122.0 | 91.5 | 73.2 | 61.0 | 52.3 | 45.8 | 40.7 | 36.6 | 33.3 | 30.5 | 28.2 | 26.1 | 24.4 | 22.9 | 21.5 | 20.3 | 19.3 | 18.3 |
| 30 | 330.7 | 165.3 | 110.2 | 82.7 | 66.1 | 55.1 | 47.2 | 41.3 | 36.7 | 33.1 | 30.1 | 27.6 | 25.4 | 23.6 | 22.0 | 20.7 | 19.5 | 18.4 | 17.4 | 16.5 |
| 31 | 299.7 | 149.9 | 99.9 | 74.9 | 59.9 | 50.0 | 42.8 | 37.5 | 33.3 | 30.0 | 27.2 | 25.0 | 23.1 | 21.4 | 20.0 | 18.7 | 17.6 | 16.7 | 15.8 | 15.0 |
| 32 | 272.5 | 136.2 | 90.8 | 68.1 | 54.5 | 45.4 | 38.9 | 34.1 | 30.3 | 27.2 | 24.8 | 22.7 | 21.0 | 19.5 | 18.2 | 17.0 | 16.0 | 15.1 | 14.3 | 13.6 |
| 33 | 248.5 | 124.2 | 82.8 | 62.1 | 49.7 | 41.4 | 35.5 | 31.1 | 27.6 | 24.8 | 22.6 | 20.7 | 19.1 | 17.7 | 16.6 | 15.5 | 14.6 | 13.8 | 13.1 | 12.4 |
| 34 | 227.2 | 113.6 | 75.7 | 56.8 | 45.4 | 37.9 | 32.5 | 28.4 | 25.2 | 22.7 | 20.7 | 18.9 | 17.5 | 16.2 | 15.1 | 14.2 | 13.4 | 12.6 | 12.0 | 11.4 |
| 35 | 208.2 | 104.1 | 69.4 | 52.1 | 41.6 | 34.7 | 29.7 | 26.0 | 23.1 | 20.8 | 18.9 | 17.4 | 16.0 | 14.9 | 13.9 | 13.0 | 12.2 | 11.6 | 11.0 | 10.4 |
| 36 | 191.4 | 95.7 | 63.8 | 47.8 | 38.3 | 31.9 | 27.3 | 23.9 | 21.3 | 19.1 | 17.4 | 15.9 | 14.7 | 13.7 | 12.8 | 12.0 | 11.3 | 10.6 | 10.1 | 9.6 |
| 37 | 176.3 | 88.1 | 58.8 | 44.1 | 35.3 | 29.4 | 25.2 | 22.0 | 19.6 | 17.6 | 16.0 | 14.7 | 13.6 | 12.6 | 11.8 | 11.0 | 10.4 | 9.8 | 9.3 | 8.8 |
| 38 | 162.7 | 81.4 | 54.2 | 40.7 | 32.5 | 27.1 | 23.2 | 20.3 | 18.1 | 16.3 | 14.8 | 13.6 | 12.5 | 11.6 | 10.8 | 10.2 | 9.6 | 9.0 | 8.6 | 8.1 |
| 39 | 150.5 | 75.3 | 50.2 | 37.6 | 30.1 | 25.1 | 21.5 | 18.8 | 16.7 | 15.1 | 13.7 | 12.5 | 11.6 | 10.8 | 10.0 | 9.4 | 8.9 | 8.4 | 7.9 | 7.5 |
| 40 | 139.5 | 69.8 | 46.5 | 34.9 | 27.9 | 23.3 | 19.9 | 17.4 | 15.5 | 14.0 | 12.7 | 11.6 | 10.7 | 10.0 | 9.3 | 8.7 | 8.2 | 7.8 | 7.3 | 7.0 |
| 41 | 129.5 | 64.8 | 43.2 | 32.4 | 25.9 | 21.6 | 18.5 | 16.2 | 14.4 | 13.0 | 11.8 | 10.8 | 10.0 | 9.3 | 8.6 | 8.1 | 7.6 | 7.2 | 6.8 | 6.5 |
| 42 | 120.5 | 60.3 | 40.2 | 30.1 | 24.1 | 20.1 | 17.2 | 15.1 | 13.4 | 12.1 | 11.0 | 10.0 | 9.3 | 8.6 | 8.0 | 7.5 | 7.1 | 6.7 | 6.3 | 6.0 |
| 43 | 112.3 | 56.1 | 37.4 | 28.1 | 22.5 | 18.7 | 16.0 | 14.0 | 12.5 | 11.2 | 10.2 | 9.4 | 8.6 | 8.0 | 7.5 | 7.0 | 6.6 | 6.2 | 5.9 | 5.6 |
| 44 | 104.8 | 52.4 | 34.9 | 26.2 | 21.0 | 17.5 | 15.0 | 13.1 | 11.6 | 10.5 | 9.5 | 8.7 | 8.1 | 7.5 | 7.0 | 6.6 | 6.2 | 5.8 | 5.5 | 5.2 |
| 45 | 98.0 | 49.0 | 32.7 | 24.5 | 19.6 | 16.3 | 14.0 | 12.2 | 10.9 | 9.8 | 8.9 | 8.2 | 7.5 | 7.0 | 6.5 | 6.1 | 5.8 | 5.4 | 5.2 | 4.9 |
| 46 | 91.7 | 45.9 | 30.6 | 22.9 | 18.3 | 15.3 | 13.1 | 11.5 | 10.2 | 9.2 | 8.3 | 7.6 | 7.1 | 6.6 | 6.1 | 5.7 | 5.4 | 5.1 | 4.8 | 4.6 |
| 47 | 86.0 | 43.0 | 28.7 | 21.5 | 17.2 | 14.3 | 12.3 | 10.7 | 9.6 | 8.6 | 7.8 | 7.2 | 6.6 | 6.1 | 5.7 | 5.4 | 5.1 | 4.8 | 4.5 | 4.3 |
| 48 | 80.7 | 40.4 | 26.9 | 20.2 | 16.1 | 13.5 | 11.5 | 10.1 | 9.0 | 8.1 | 7.3 | 6.7 | 6.2 | 5.8 | 5.4 | 5.0 | 4.7 | 4.5 | 4.2 | 4.0 |
| 49 | 75.9 | 37.9 | 25.3 | 19.0 | 15.2 | 12.6 | 10.8 | 9.5 | 8.4 | 7.6 | 6.9 | 6.3 | 5.8 | 5.4 | 5.1 | 4.7 | 4.5 | 4.2 | 4.0 | 3.8 |
| 50 | 71.4 | 35.7 | 23.8 | 17.9 | 14.3 | 11.9 | 10.2 | 8.9 | 7.9 | 7.1 | 6.5 | 6.0 | 5.5 | 5.1 | 4.8 | 4.5 | 4.2 | 4.0 | 3.8 | 3.6 |

The ratio of the “H/B” in the design space is given in Table 5.4. According to the third constraint, the ratio “H/B” must be less than 5. The region where the ratio “H/B” ratio is greater than 5 is marked with red background. This region is the restricted region. Therefore, feasible region in design space is further reduced by the slenderness ratio constraint. The cell with the blue background show the position of the optimum solution.

Table 5.4 Variation of slenderness ratio in the design space

| Design Space (Slenderness, Constraint 3 ≤ 5) | | | | | | | | | | | | | | | | | | | | |
|--|----|----|----|----|----|---|---|---|---|----|----|----|----|----|----|----|----|----|----|----|
| H/B (mm) | 1 | 2 | 3 | 4 | 5 | 6 | 7 | 8 | 9 | 10 | 11 | 12 | 13 | 14 | 15 | 16 | 17 | 18 | 19 | 20 |
| 20 | 20 | 10 | 7 | 5 | 4 | 3 | 3 | 3 | 2 | 2 | 2 | 2 | 2 | 1 | 1 | 1 | 1 | 1 | 1 | 1 |
| 21 | 21 | 11 | 7 | 5 | 4 | 4 | 3 | 3 | 2 | 2 | 2 | 2 | 2 | 2 | 1 | 1 | 1 | 1 | 1 | 1 |
| 22 | 22 | 11 | 7 | 6 | 4 | 4 | 3 | 3 | 2 | 2 | 2 | 2 | 2 | 2 | 1 | 1 | 1 | 1 | 1 | 1 |
| 23 | 23 | 12 | 8 | 6 | 5 | 4 | 3 | 3 | 3 | 2 | 2 | 2 | 2 | 2 | 2 | 1 | 1 | 1 | 1 | 1 |
| 24 | 24 | 12 | 8 | 6 | 5 | 4 | 3 | 3 | 3 | 2 | 2 | 2 | 2 | 2 | 2 | 2 | 1 | 1 | 1 | 1 |
| 25 | 25 | 13 | 8 | 6 | 5 | 4 | 4 | 3 | 3 | 3 | 2 | 2 | 2 | 2 | 2 | 2 | 1 | 1 | 1 | 1 |
| 26 | 26 | 13 | 9 | 7 | 5 | 4 | 4 | 3 | 3 | 3 | 2 | 2 | 2 | 2 | 2 | 2 | 2 | 1 | 1 | 1 |
| 27 | 27 | 14 | 9 | 7 | 5 | 5 | 4 | 3 | 3 | 3 | 2 | 2 | 2 | 2 | 2 | 2 | 2 | 2 | 1 | 1 |
| 28 | 28 | 14 | 9 | 7 | 6 | 5 | 4 | 4 | 3 | 3 | 3 | 2 | 2 | 2 | 2 | 2 | 2 | 2 | 1 | 1 |
| 29 | 29 | 15 | 10 | 7 | 6 | 5 | 4 | 4 | 3 | 3 | 3 | 2 | 2 | 2 | 2 | 2 | 2 | 2 | 2 | 1 |
| 30 | 30 | 15 | 10 | 8 | 6 | 5 | 4 | 4 | 3 | 3 | 3 | 3 | 2 | 2 | 2 | 2 | 2 | 2 | 2 | 2 |
| 31 | 31 | 16 | 10 | 8 | 6 | 5 | 4 | 4 | 3 | 3 | 3 | 3 | 2 | 2 | 2 | 2 | 2 | 2 | 2 | 2 |
| 32 | 32 | 16 | 11 | 8 | 6 | 5 | 5 | 4 | 4 | 3 | 3 | 3 | 2 | 2 | 2 | 2 | 2 | 2 | 2 | 2 |
| 33 | 33 | 17 | 11 | 8 | 7 | 6 | 5 | 4 | 4 | 3 | 3 | 3 | 3 | 2 | 2 | 2 | 2 | 2 | 2 | 2 |
| 34 | 34 | 17 | 11 | 9 | 7 | 6 | 5 | 4 | 4 | 3 | 3 | 3 | 3 | 2 | 2 | 2 | 2 | 2 | 2 | 2 |
| 35 | 35 | 18 | 12 | 9 | 7 | 6 | 5 | 4 | 4 | 4 | 3 | 3 | 3 | 3 | 2 | 2 | 2 | 2 | 2 | 2 |
| 36 | 36 | 18 | 12 | 9 | 7 | 6 | 5 | 5 | 4 | 4 | 3 | 3 | 3 | 3 | 2 | 2 | 2 | 2 | 2 | 2 |
| 37 | 37 | 19 | 12 | 9 | 7 | 6 | 5 | 5 | 4 | 4 | 3 | 3 | 3 | 3 | 2 | 2 | 2 | 2 | 2 | 2 |
| 38 | 38 | 19 | 13 | 10 | 8 | 6 | 5 | 5 | 4 | 4 | 3 | 3 | 3 | 3 | 2 | 2 | 2 | 2 | 2 | 2 |
| 39 | 39 | 20 | 13 | 10 | 8 | 7 | 6 | 5 | 4 | 4 | 4 | 3 | 3 | 3 | 2 | 2 | 2 | 2 | 2 | 2 |
| 40 | 40 | 20 | 13 | 10 | 8 | 7 | 6 | 5 | 4 | 4 | 4 | 3 | 3 | 3 | 3 | 2 | 2 | 2 | 2 | 2 |
| 41 | 41 | 21 | 14 | 10 | 8 | 7 | 6 | 5 | 5 | 4 | 4 | 3 | 3 | 3 | 3 | 2 | 2 | 2 | 2 | 2 |
| 42 | 42 | 21 | 14 | 11 | 8 | 7 | 6 | 5 | 5 | 4 | 4 | 4 | 3 | 3 | 3 | 2 | 2 | 2 | 2 | 2 |
| 43 | 43 | 22 | 14 | 11 | 9 | 7 | 6 | 5 | 5 | 4 | 4 | 4 | 3 | 3 | 3 | 3 | 2 | 2 | 2 | 2 |
| 44 | 44 | 22 | 15 | 11 | 9 | 7 | 6 | 6 | 5 | 4 | 4 | 4 | 3 | 3 | 3 | 3 | 2 | 2 | 2 | 2 |
| 45 | 45 | 23 | 15 | 11 | 9 | 8 | 6 | 6 | 5 | 5 | 4 | 4 | 3 | 3 | 3 | 3 | 3 | 2 | 2 | 2 |
| 46 | 46 | 23 | 15 | 12 | 9 | 8 | 7 | 6 | 5 | 5 | 4 | 4 | 4 | 3 | 3 | 3 | 3 | 2 | 2 | 2 |
| 47 | 47 | 24 | 16 | 12 | 9 | 8 | 7 | 6 | 5 | 5 | 4 | 4 | 4 | 3 | 3 | 3 | 3 | 2 | 2 | 2 |
| 48 | 48 | 24 | 16 | 12 | 10 | 8 | 7 | 6 | 5 | 5 | 4 | 4 | 4 | 3 | 3 | 3 | 3 | 3 | 2 | 2 |
| 49 | 49 | 25 | 16 | 12 | 10 | 8 | 7 | 6 | 5 | 5 | 4 | 4 | 4 | 4 | 3 | 3 | 3 | 3 | 2 | 2 |
| 50 | 50 | 25 | 17 | 13 | 10 | 8 | 7 | 6 | 6 | 5 | 5 | 4 | 4 | 4 | 3 | 3 | 3 | 3 | 2 | 2 |

The feasible region in design space is reduced by each constraint. In the optimization process all the constraints must be satisfied. Therefore, intersection

set of all three feasible regions which are restricted by constraints must be used as the final feasible region where an optimum solution resides. In Table 5.5 the values of the objective function in the design space are shown. The overall restricted region is marked with red background. The final optimum value of objective function and its location is marked with blue background. For the integer values of the design variables with increments of one, at the optimum solution the objective function value is about 144000, the optimum ‘B’ value is about 8 and the optimum ‘H’ value is about 36. Thus, in the optimization solutions which will be performed next, one can compare the solutions with these figures to see how close are the solutions to the true optimum solution.

Table 5.5 Variation of the value of the objective function in the design space after all the constraints are imposed

| Design Space (Volume, Objective Function) (1000 mm ³) | | | | | | | | | | | | | | | | | | | | |
|---|------|------|------|-------|-------|-------|-------|-------|-------|-------|-------|-------|-------|-------|-------|-------|-------|-------|-------|-------|
| H/B (mm) | 1 | 2 | 3 | 4 | 5 | 6 | 7 | 8 | 9 | 10 | 11 | 12 | 13 | 14 | 15 | 16 | 17 | 18 | 19 | 20 |
| 20 | 10.0 | 20.0 | 30.0 | 40.0 | 50.0 | 60.0 | 70.0 | 80.0 | 90.0 | 100.0 | 110.0 | 120.0 | 130.0 | 140.0 | 150.0 | 160.0 | 170.0 | 180.0 | 190.0 | 200.0 |
| 21 | 10.5 | 21.0 | 31.5 | 42.0 | 52.5 | 63.0 | 73.5 | 84.0 | 94.5 | 105.0 | 115.5 | 126.0 | 136.5 | 147.0 | 157.5 | 168.0 | 178.5 | 189.0 | 199.5 | 210.0 |
| 22 | 11.0 | 22.0 | 33.0 | 44.0 | 55.0 | 66.0 | 77.0 | 88.0 | 99.0 | 110.0 | 121.0 | 132.0 | 143.0 | 154.0 | 165.0 | 176.0 | 187.0 | 198.0 | 209.0 | 220.0 |
| 23 | 11.5 | 23.0 | 34.5 | 46.0 | 57.5 | 69.0 | 80.5 | 92.0 | 103.5 | 115.0 | 126.5 | 138.0 | 149.5 | 161.0 | 172.5 | 184.0 | 195.5 | 207.0 | 218.5 | 230.0 |
| 24 | 12.0 | 24.0 | 36.0 | 48.0 | 60.0 | 72.0 | 84.0 | 96.0 | 108.0 | 120.0 | 132.0 | 144.0 | 156.0 | 168.0 | 180.0 | 192.0 | 204.0 | 216.0 | 228.0 | 240.0 |
| 25 | 12.5 | 25.0 | 37.5 | 50.0 | 62.5 | 75.0 | 87.5 | 100.0 | 112.5 | 125.0 | 137.5 | 150.0 | 162.5 | 175.0 | 187.5 | 200.0 | 212.5 | 225.0 | 237.5 | 250.0 |
| 26 | 13.0 | 26.0 | 39.0 | 52.0 | 65.0 | 78.0 | 91.0 | 104.0 | 117.0 | 130.0 | 143.0 | 156.0 | 169.0 | 182.0 | 195.0 | 208.0 | 221.0 | 234.0 | 247.0 | 260.0 |
| 27 | 13.5 | 27.0 | 40.5 | 54.0 | 67.5 | 81.0 | 94.5 | 108.0 | 121.5 | 135.0 | 148.5 | 162.0 | 175.5 | 189.0 | 202.5 | 216.0 | 229.5 | 243.0 | 256.5 | 270.0 |
| 28 | 14.0 | 28.0 | 42.0 | 56.0 | 70.0 | 84.0 | 98.0 | 112.0 | 126.0 | 140.0 | 154.0 | 168.0 | 182.0 | 196.0 | 210.0 | 224.0 | 238.0 | 252.0 | 266.0 | 280.0 |
| 29 | 14.5 | 29.0 | 43.5 | 58.0 | 72.5 | 87.0 | 101.5 | 116.0 | 130.5 | 145.0 | 159.5 | 174.0 | 188.5 | 203.0 | 217.5 | 232.0 | 246.5 | 261.0 | 275.5 | 290.0 |
| 30 | 15.0 | 30.0 | 45.0 | 60.0 | 75.0 | 90.0 | 105.0 | 120.0 | 135.0 | 150.0 | 165.0 | 180.0 | 195.0 | 210.0 | 225.0 | 240.0 | 255.0 | 270.0 | 285.0 | 300.0 |
| 31 | 15.5 | 31.0 | 46.5 | 62.0 | 77.5 | 93.0 | 108.5 | 124.0 | 139.5 | 155.0 | 170.5 | 186.0 | 201.5 | 217.0 | 232.5 | 248.0 | 263.5 | 279.0 | 294.5 | 310.0 |
| 32 | 16.0 | 32.0 | 48.0 | 64.0 | 80.0 | 96.0 | 112.0 | 128.0 | 144.0 | 160.0 | 176.0 | 192.0 | 208.0 | 224.0 | 240.0 | 256.0 | 272.0 | 288.0 | 304.0 | 320.0 |
| 33 | 16.5 | 33.0 | 49.5 | 66.0 | 82.5 | 99.0 | 115.5 | 132.0 | 148.5 | 165.0 | 181.5 | 198.0 | 214.5 | 231.0 | 247.5 | 264.0 | 280.5 | 297.0 | 313.5 | 330.0 |
| 34 | 17.0 | 34.0 | 51.0 | 68.0 | 85.0 | 102.0 | 119.0 | 136.0 | 153.0 | 170.0 | 187.0 | 204.0 | 221.0 | 238.0 | 255.0 | 272.0 | 289.0 | 306.0 | 323.0 | 340.0 |
| 35 | 17.5 | 35.0 | 52.5 | 70.0 | 87.5 | 105.0 | 122.5 | 140.0 | 157.5 | 175.0 | 192.5 | 210.0 | 227.5 | 245.0 | 262.5 | 280.0 | 297.5 | 315.0 | 332.5 | 350.0 |
| 36 | 18.0 | 36.0 | 54.0 | 72.0 | 90.0 | 108.0 | 126.0 | 144.0 | 162.0 | 180.0 | 198.0 | 216.0 | 234.0 | 252.0 | 270.0 | 288.0 | 306.0 | 324.0 | 342.0 | 360.0 |
| 37 | 18.5 | 37.0 | 55.5 | 74.0 | 92.5 | 111.0 | 129.5 | 148.0 | 166.5 | 185.0 | 203.5 | 222.0 | 240.5 | 259.0 | 277.5 | 296.0 | 314.5 | 333.0 | 351.5 | 370.0 |
| 38 | 19.0 | 38.0 | 57.0 | 76.0 | 95.0 | 114.0 | 133.0 | 152.0 | 171.0 | 190.0 | 209.0 | 228.0 | 247.0 | 266.0 | 285.0 | 304.0 | 323.0 | 342.0 | 361.0 | 380.0 |
| 39 | 19.5 | 39.0 | 58.5 | 78.0 | 97.5 | 117.0 | 136.5 | 156.0 | 175.5 | 195.0 | 214.5 | 234.0 | 253.5 | 273.0 | 292.5 | 312.0 | 331.5 | 351.0 | 370.5 | 390.0 |
| 40 | 20.0 | 40.0 | 60.0 | 80.0 | 100.0 | 120.0 | 140.0 | 160.0 | 180.0 | 200.0 | 220.0 | 240.0 | 260.0 | 280.0 | 300.0 | 320.0 | 340.0 | 360.0 | 380.0 | 400.0 |
| 41 | 20.5 | 41.0 | 61.5 | 82.0 | 102.5 | 123.0 | 143.5 | 164.0 | 184.5 | 205.0 | 225.5 | 246.0 | 266.5 | 287.0 | 307.5 | 328.0 | 348.5 | 369.0 | 389.5 | 410.0 |
| 42 | 21.0 | 42.0 | 63.0 | 84.0 | 105.0 | 126.0 | 147.0 | 168.0 | 189.0 | 210.0 | 231.0 | 252.0 | 273.0 | 294.0 | 315.0 | 336.0 | 357.0 | 378.0 | 399.0 | 420.0 |
| 43 | 21.5 | 43.0 | 64.5 | 86.0 | 107.5 | 129.0 | 150.5 | 172.0 | 193.5 | 215.0 | 236.5 | 258.0 | 279.5 | 301.0 | 322.5 | 344.0 | 365.5 | 387.0 | 408.5 | 430.0 |
| 44 | 22.0 | 44.0 | 66.0 | 88.0 | 110.0 | 132.0 | 154.0 | 176.0 | 198.0 | 220.0 | 242.0 | 264.0 | 286.0 | 308.0 | 330.0 | 352.0 | 374.0 | 396.0 | 418.0 | 440.0 |
| 45 | 22.5 | 45.0 | 67.5 | 90.0 | 112.5 | 135.0 | 157.5 | 180.0 | 202.5 | 225.0 | 247.5 | 270.0 | 292.5 | 315.0 | 337.5 | 360.0 | 382.5 | 405.0 | 427.5 | 450.0 |
| 46 | 23.0 | 46.0 | 69.0 | 92.0 | 115.0 | 138.0 | 161.0 | 184.0 | 207.0 | 230.0 | 253.0 | 276.0 | 299.0 | 322.0 | 345.0 | 368.0 | 391.0 | 414.0 | 437.0 | 460.0 |
| 47 | 23.5 | 47.0 | 70.5 | 94.0 | 117.5 | 141.0 | 164.5 | 188.0 | 211.5 | 235.0 | 258.5 | 282.0 | 305.5 | 329.0 | 352.5 | 376.0 | 399.5 | 423.0 | 446.5 | 470.0 |
| 48 | 24.0 | 48.0 | 72.0 | 96.0 | 120.0 | 144.0 | 168.0 | 192.0 | 216.0 | 240.0 | 264.0 | 288.0 | 312.0 | 336.0 | 360.0 | 384.0 | 408.0 | 432.0 | 456.0 | 480.0 |
| 49 | 24.5 | 49.0 | 73.5 | 98.0 | 122.5 | 147.0 | 171.5 | 196.0 | 220.5 | 245.0 | 269.5 | 294.0 | 318.5 | 343.0 | 367.5 | 392.0 | 416.5 | 441.0 | 465.5 | 490.0 |
| 50 | 25.0 | 50.0 | 75.0 | 100.0 | 125.0 | 150.0 | 175.0 | 200.0 | 225.0 | 250.0 | 275.0 | 300.0 | 325.0 | 350.0 | 375.0 | 400.0 | 425.0 | 450.0 | 475.0 | 500.0 |

5.1.1 OPTIMIZATION USING THE OPTIMIZATION CODE IN MATLAB[®] AND ANALYTIC FUNCTIONS AS SOLVER

First, optimization of the cantilever beam with the rectangular cross section is performed by using first strategy explained in Chapter 4. In this method optimization code written in MATLAB[®] is used together with the analytical beam equations as the solver. The M-file called “AugLagMet.m” is executed in MATLAB[®] environment. “AugLagMet.m” asks the user for inputs which are listed below. The lower and upper bounds of the design variables as well as the other inputs are specified as:

1. Initial values of design variables [B,H]: [10 35]
2. Lower bounds of design variables [B,H]: : [1 20]
3. Upper bounds of design variables [B,H]: : [20 50]
4. Number of equality constraints: 0
5. Number of inequality constraints: 3
6. Initial values of lagrange multipliers “ λ ”
for equality constraints: 0
7. Initial values of lagrange multipliers “ β ”
for inequality constraints : [10 10 10]

where, lagrange multipliers “ β ” is given by $[\beta_1, \beta_2, \beta_3]$;

- β_1 is the multiplier for the constraint given in equation (5.2) used for upper bound of the stress value at the root of the beam.
- β_2 is the multiplier for the constraint given in equation (5.3) used for the displacement value at the tip of the beam.
- β_3 is the multiplier for the constraint given in equation (5.4) used for the slenderness ratio.

The M-files “Ofun.m”, “Gfun.m” and “Hfun.m” which evaluate volume, inequality constraints and equality constraints respectively are modified specific to this problem. Since there is no equality constraints, “Hfun.m” is never called during this problem.

The optimization process is converged to the solution in 8 iterations, where one iteration is one outermost cycle in the main algorithm shown in figure 3.1. In Figures 5.2 – 5.7 change of objective function, design variables and constraints with respect to iteration number are shown. Results are tabulated and comparisons are made in section 5.1.4 with the results obtained by the other two methods.

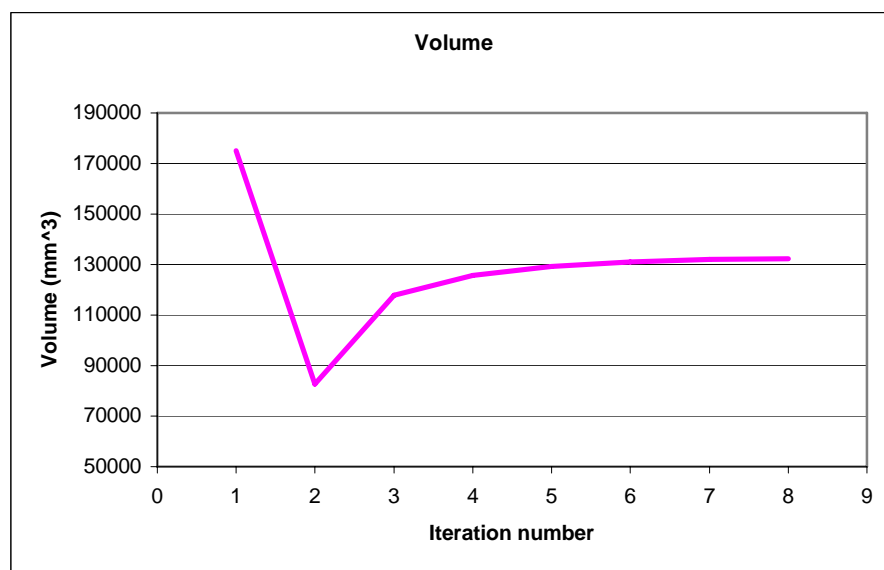


Figure 5.2 Variation of the objective function with respect to iteration number

As it can be seen from Figure 5.2 the objective function initially decreases but then starts to increase to satisfy the constraints.

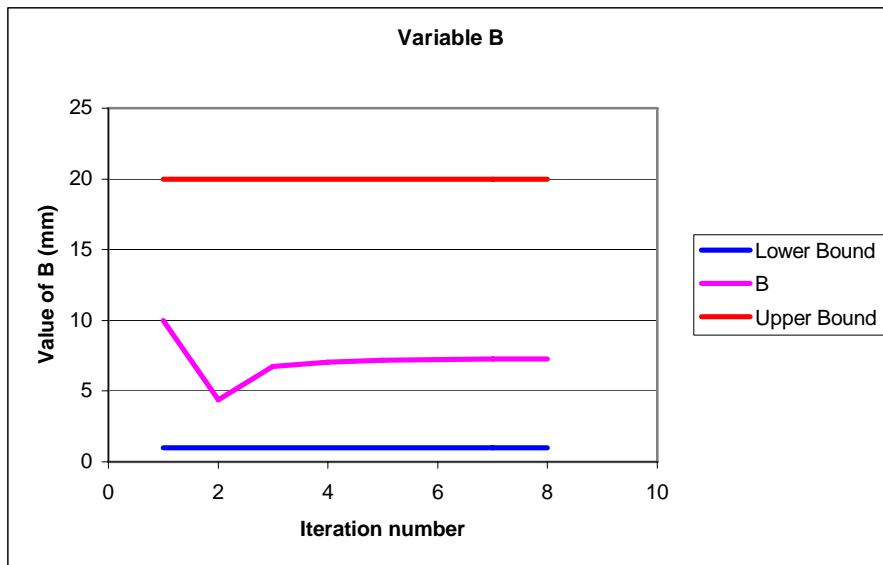


Figure 5.3 Variation of width of cross section “B” with respect to iteration number

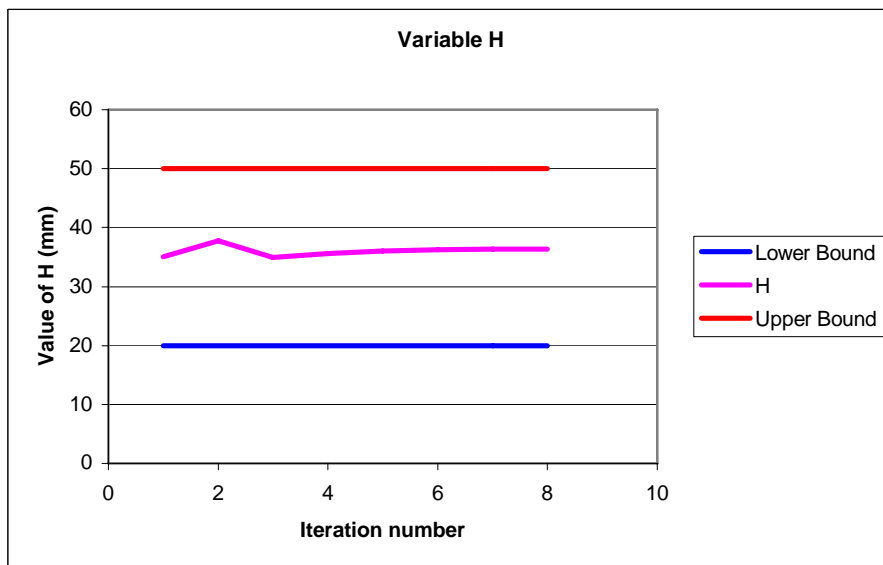


Figure 5.4 Variation of height of cross section “H” with respect to iteration number

Figures 5.3 and 5.4 show that the design variables ‘B’ and ‘H’ are within specified upper and lower bounds.

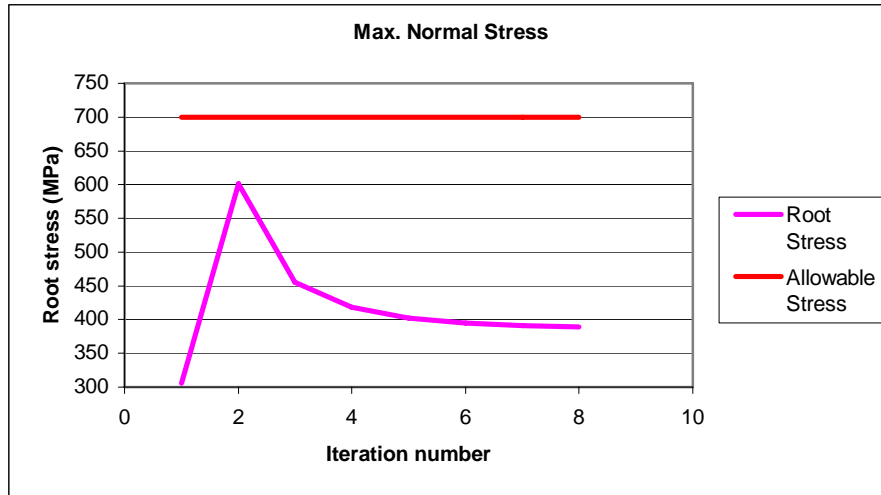


Figure 5.5 Variation of stress at the root of the beam with respect to iteration number

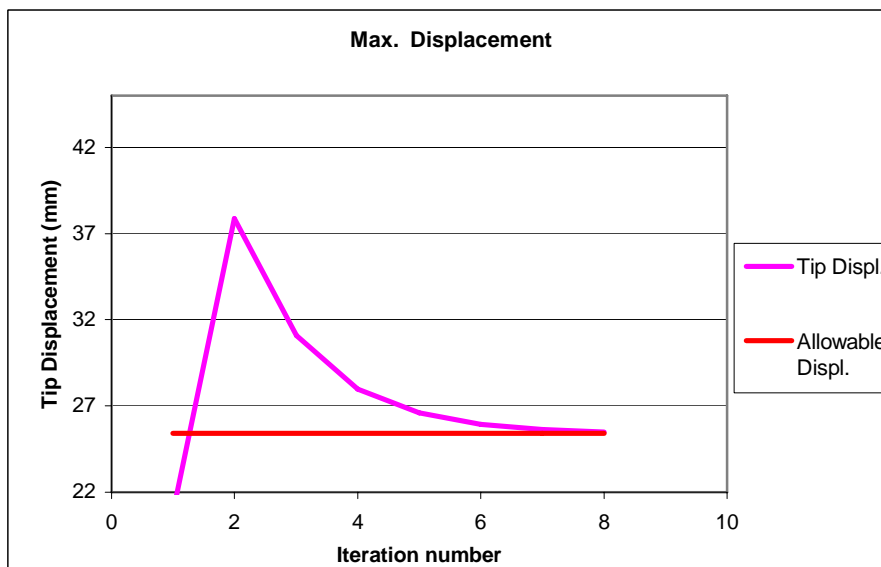


Figure 5.6 Variation of displacement at the tip of the beam with respect to iteration number

Figures 5.5 and 5.6 show that stress constraint is not violated at any iteration until optimum solution is reached. However, in the initial iterations the displacement constraint is violated and the optimization code makes adjustments until the constraint is satisfied. It should be noted that if displacement constraint did not exist, the weight of the beam could be reduced even further because stresses are below the allowable specified for this problem. It is seen that in this particular problem the maximum tip deflection constraint is the more restricting constraint.

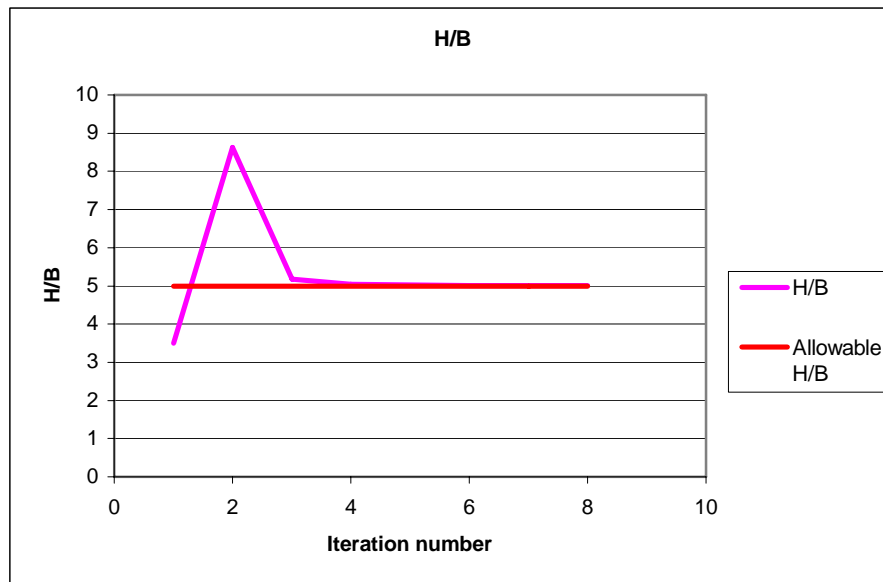


Figure 5.7 Variation of H/B with respect to the iteration number

Figure 5.7 shows that the 'H/B' stress constraint is also violated at the initial steps but eventually it settles down until the constraint is satisfied. Existence of a constraint on the 'H/B' ratio prevents one to increase the height of the beam freely within the bounds specified. Therefore, it becomes harder to satisfy the maximum deflection constraint compared to stress constraint. Because, as it can

be seen from Equation (5.3), the tip deflection is inversely proportional to the cube of the height of the beam, whereas the maximum stress is inversely proportional to the square of the height of the beam.

5.1.2 CANTILEVER BEAM OPTIMIZATION USING THE OPTIMIZATION CODE IN MATLAB® AND MSC.NASTRAN® AS THE SOLVER

Next, optimization of the same cantilever beam with rectangular cross section is performed by using the second strategy described in Chapter 4. In this method optimization code written in MATLAB® is used together with the commercial finite element solver MSC.NASTRAN®. The M-file called “AugLagMet.m” is again executed in MATLAB® environment. “AugLagMet.m” asks the user for inputs which are given below with the corresponding the values for this example.

1. Initial values of design variables [B,H]: : [10 35]
2. Lower bounds of design variables [B,H]: : [1 20]
3. Upper bounds of design variables [B,H]: : [20 50]
4. Number of equality constraints: 0
5. Number of inequality constraints: 3
6. Initial values of lagrange multipliers “ λ ”
for equality constraints: 0
7. Initial values of lagrange multipliers “ β ”
for inequality constraints : [10 10 10]

Where, lagrange multipliers “ β ” is given by [$\beta_1, \beta_2, \beta_3$] ;

- β_1 is the multiplier for the constraint given in equation (5.2) used for upper bound of the stress value at the root of the beam.
- β_2 is the multiplier for the constraint given in equation (5.3) used for the displacement value at the tip of the beam.
- β_3 is the multiplier for the constraint given in equation (5.4) used for the slenderness ratio.

The M-files “Ofun.m”, Gfun.m”and “nastfunc.m” which evaluate volume, inequality constraints and constructs the unconstrained objective function respectively. Since there is no equality constraints, “Hfun.m” is neither modified nor called during this problem. A bdf-file called “cantbeam1.bdf” which is the

input file for the finite element model of the cantilever beam for linear static analysis is created before the start of the optimization process. Whenever the unconstrained objective function or inequality constraints are evaluated, first “cantbeam1.bdf” is modified by using current value of the design variables. In the solution sequence linear static analysis is performed by MSC.NASTRAN[®]. Finally, maximum stress value at the root and maximum displacement at the tip is read from MSC.NASTRAN[®] output file .f06-file. The finite element model is described in section 5.1.3. In section 5.1.3 the solution performed by the MSC.NASTRAN[®] optimization module will be described. The initial analysis model used for MSC.NASTRAN[®] optimization is used as the finite element model of the beam here.

The optimization process is converged to the solution in 12 iterations, where one iteration is one outermost cycle in the main algorithm shown in figure 3.1. In Figures 5.8 – 5.13 change of objective function, design variables and constraints with respect to iteration number are shown. Results are tabulated and comparisons are made in section 5.1.4 with the results obtained by the other two methods.

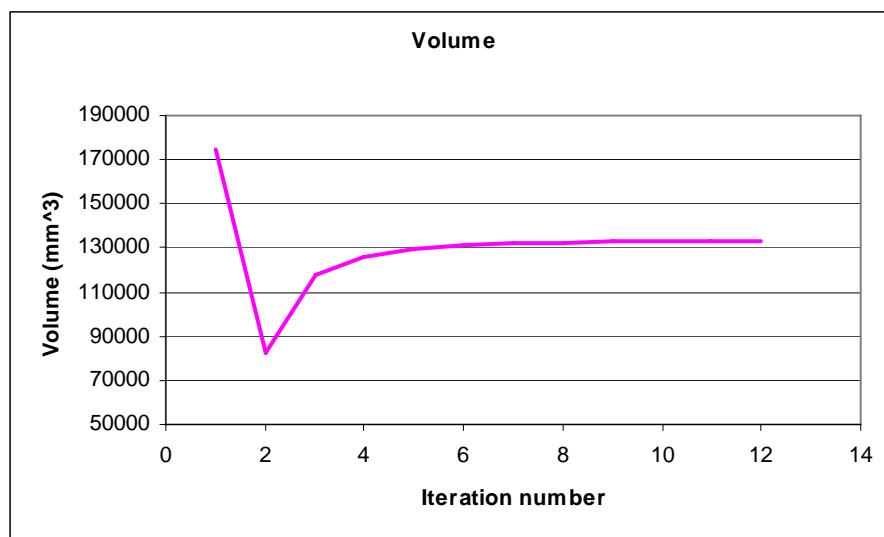


Figure 5.8 Variation of objective function with respect to iteration number

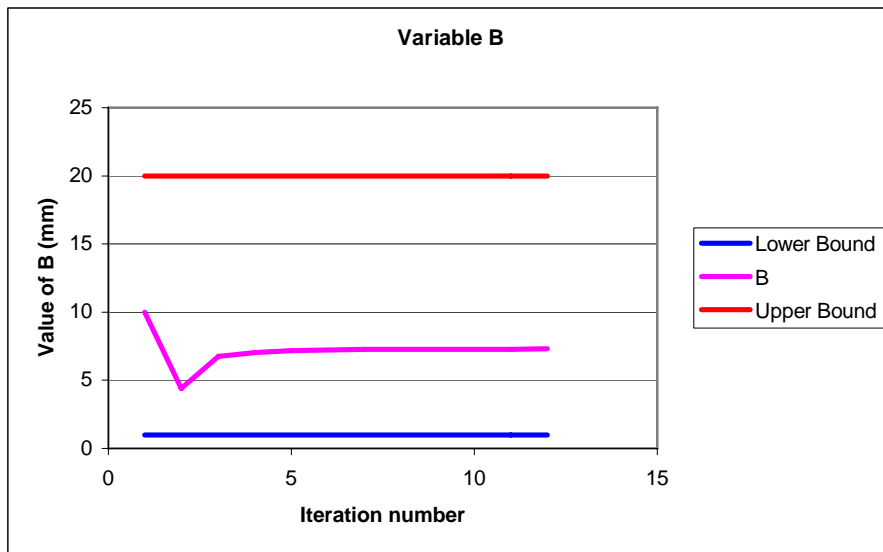


Figure 5.9 Variation of width of cross section “B” with respect to iteration number

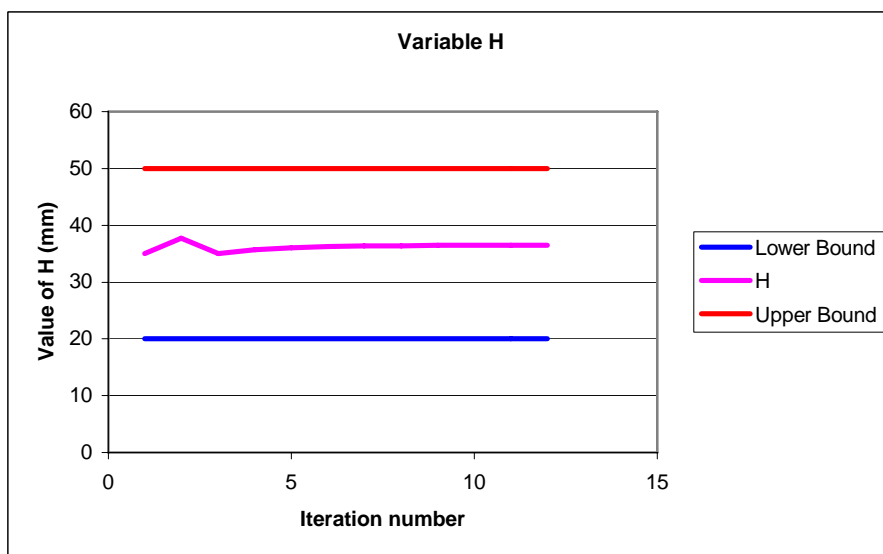


Figure 5.10 Variation of height of cross section “H” with respect to iteration number

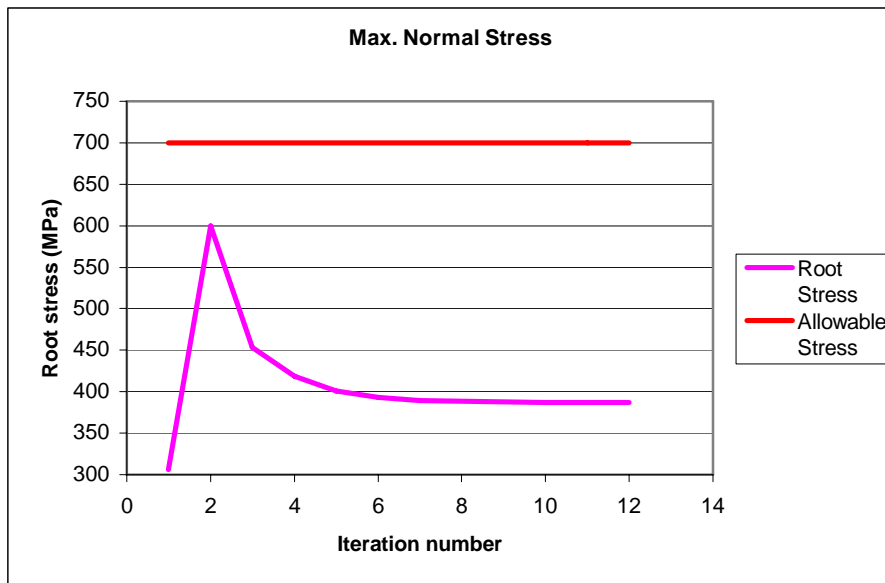


Figure 5.11 Variation of stress at the root of the beam with respect to iteration number

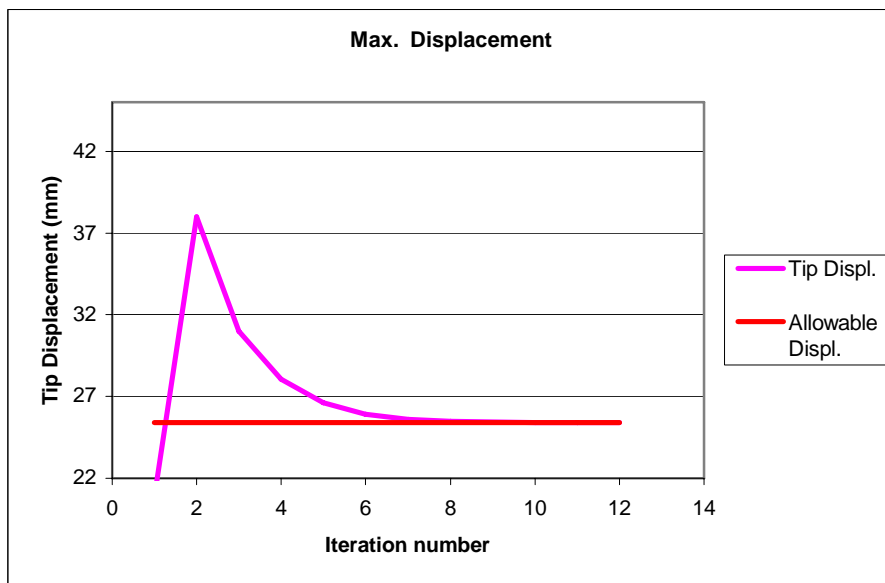


Figure 5.12 Variation of displacement at the tip of the beam with respect to iteration number



Figure 5.13 Variation of H/B with respect to iteration number

Figures 5.8-5.13 show that variations of the objective function, design variables and the constraints with iteration number depict similar behavior as in the first strategy where the solver was the analytical relations for the cantilever beam problem for the maximum axial stress and maximum tip deflection. This example in a way proves that the incorporation of MSC.NASTRAN[®] as the solver of the optimization code developed in MATLAB[®] has been successful.

5.1.3. CANTILEVER BEAM OPTIMIZATION USING MSC.NASTRAN[®] OPTIMIZATION TOOL

Finally, optimization of the cantilever beam with rectangular cross section is performed by using third method explained in chapter 4. In this method optimization module of MSC.NASTRAN[®] is used. It should be noted that during the execution of the optimization solution with the optimization module of MSC.NASTRAN[®], MSC.NASTRAN[®] solver is frequently called internally. Before the optimization process, the cantilever beam problem is modeled in MSC.PATRAN[®].

The beam is modeled with 10 CBAR elements which can be used for the beam cross sections for which the shear center and the centroidal axis coincide. Rectangular cross section is assigned to the beam elements as the element property. At the root 6 degree of freedom (U_x , U_y , U_z , R_x , R_y and R_z) of the node is fixed. At the tip 1250 N force is applied in negative (-) “y” direction as shown in figure 5.14.

Initial finite element model and cross section properties are shown in figures 5.14-5.16.

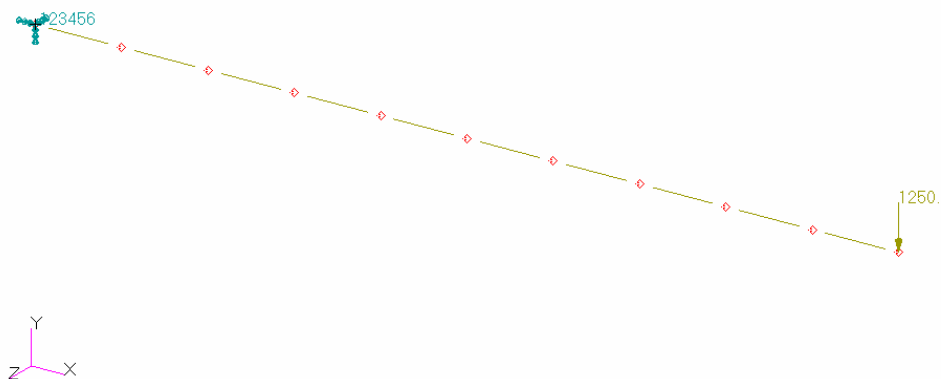


Figure 5.14 Cantilever beam finite element model

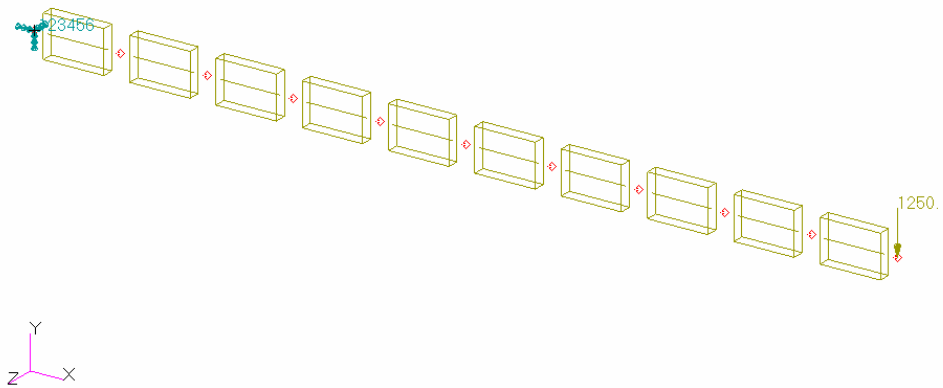


Figure 5.15 Initial cantilever beam model with equivalent inertia

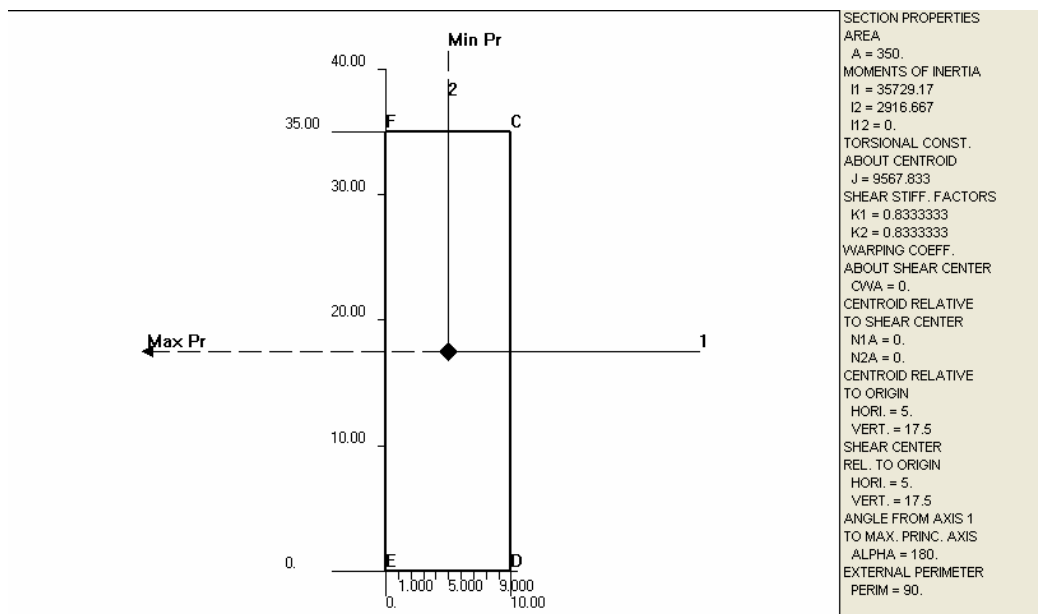


Figure 5.16 Initial cantilever beam cross section properties

To make comparisons with the optimized beam, initial finite element analysis results are presented in Figures 5.17-5.18. Figure 5.17 shows the displacement distribution and Figure 5.18 shows the axial stress distribution along the span of the beam.

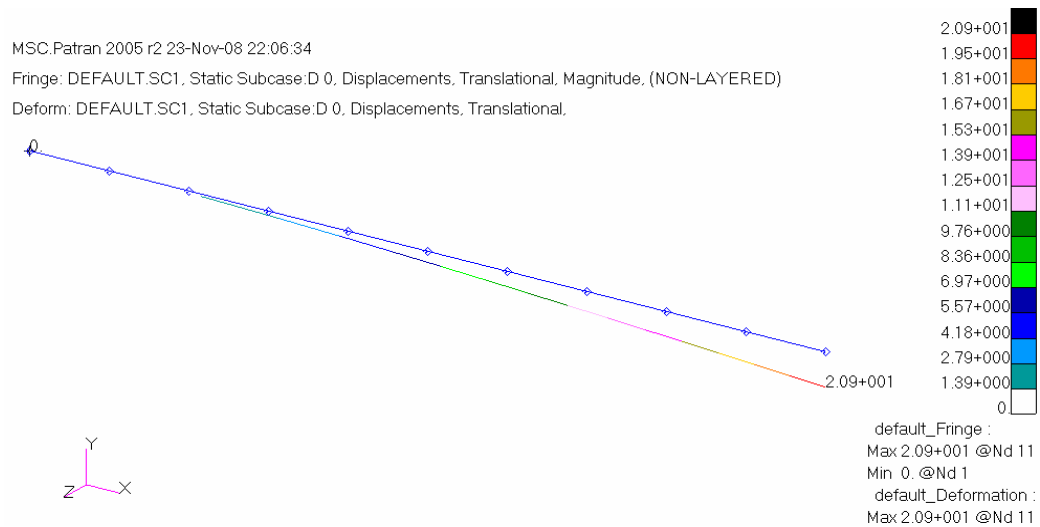


Figure 5.17 Cantilever beam initial displacement



Figure 5.18 Cantilever beam initial stress distribution

Optimized finite element model and the cross-section of the optimized beam are shown in Figures 5.19 and 5.20 respectively. From Figure 5.19 one can not identify the difference between the initial and final optimized beam configuration but Figure 5.20 shows the optimized cross-section clearly. It can be seen that the height of the beam does not change much from its initial value but the width is reduced from its initial value.

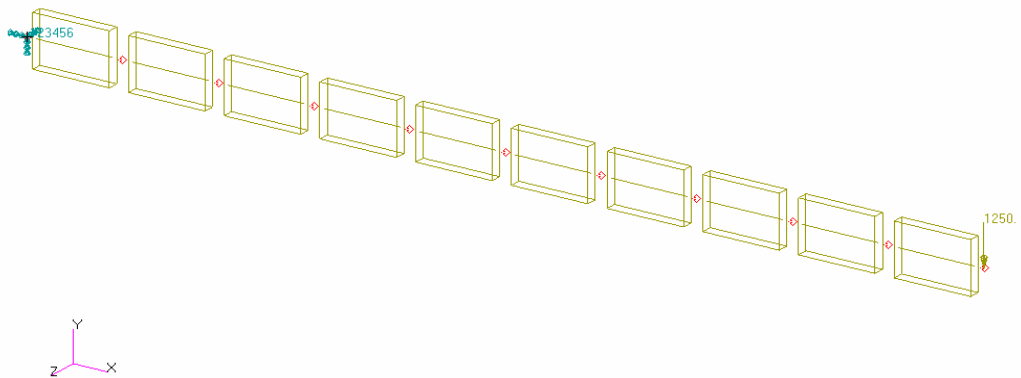


Figure 5.19 Final cantilever beam model with equivalent inertia

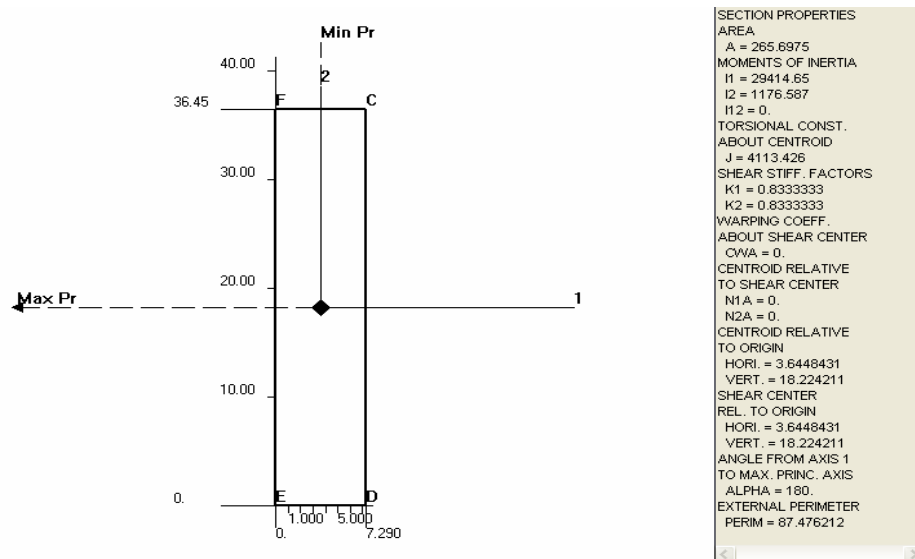


Figure 5.20 Final cantilever beam cross section properties

Final finite element analysis results for the optimized beam are presented in Figures 5.21-5.22. Figure 5.21 shows the displacement distribution and Figure 5.22 shows the axial stress distribution along the span of the beam.



Figure 5.21 Displacement distribution in the optimized beam

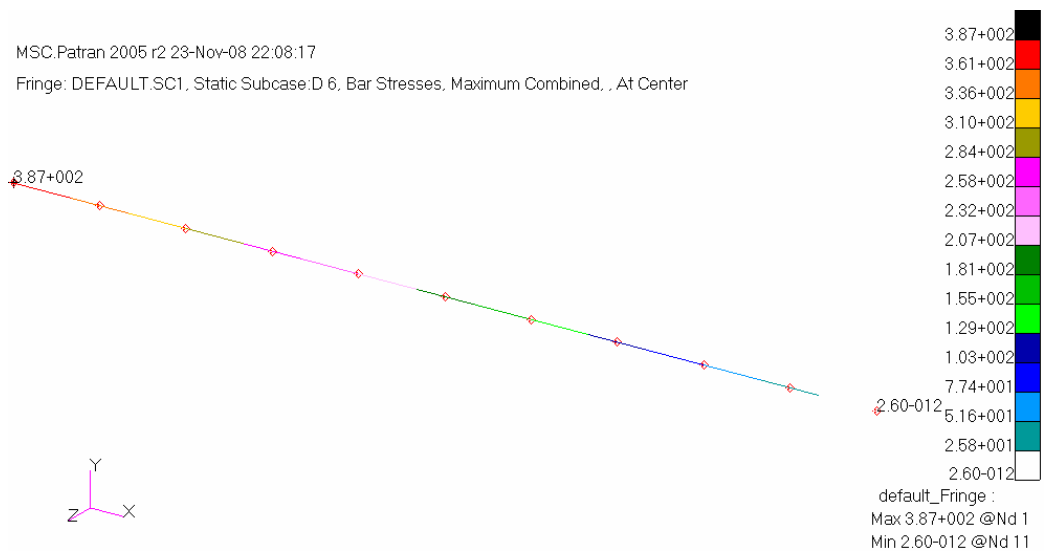


Figure 5.22 Stress distribution in the optimized beam

Variation of the objective function, each design variable and the maximum constraint value are shown in Figures 5.23-5.26. Maximum constraint value is the highest value of the normalized constraints constructed internally in MSC.NASTRAN[®]. In each iteration different constraint may have highest value. MSC.NASTRAN[®] optimization module arrives at the optimum solution in six design cycles as shown in Figures 5.23-5.26.

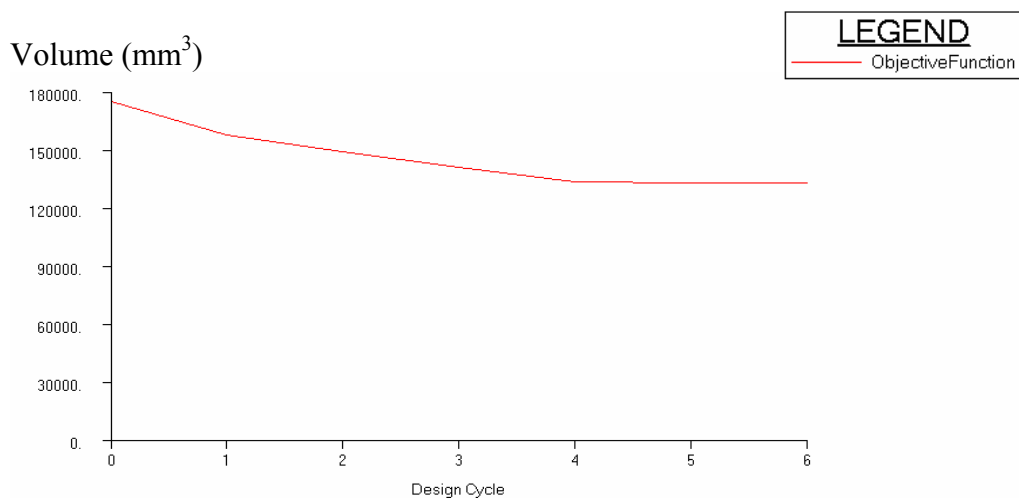


Figure 5.23 History of the objective function

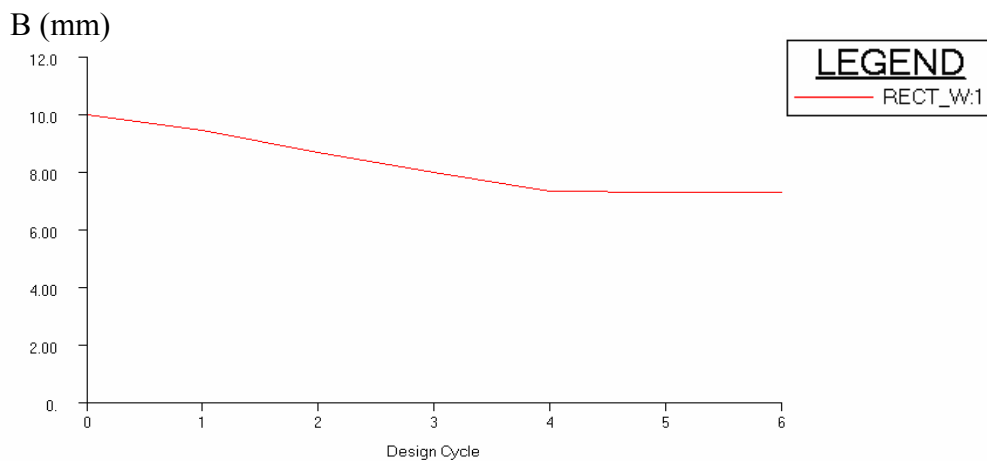


Figure 5.24 History of the design variable "B"

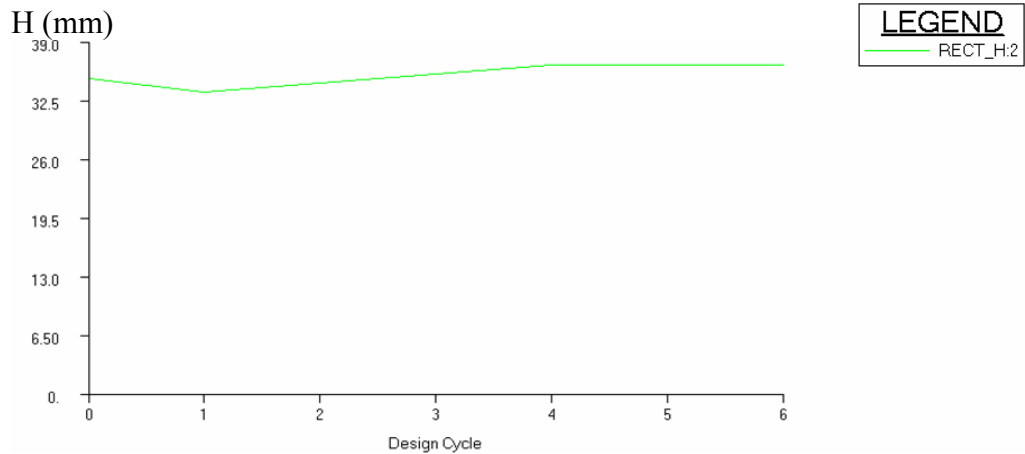


Figure 5.25 History of the design variable ‘H’

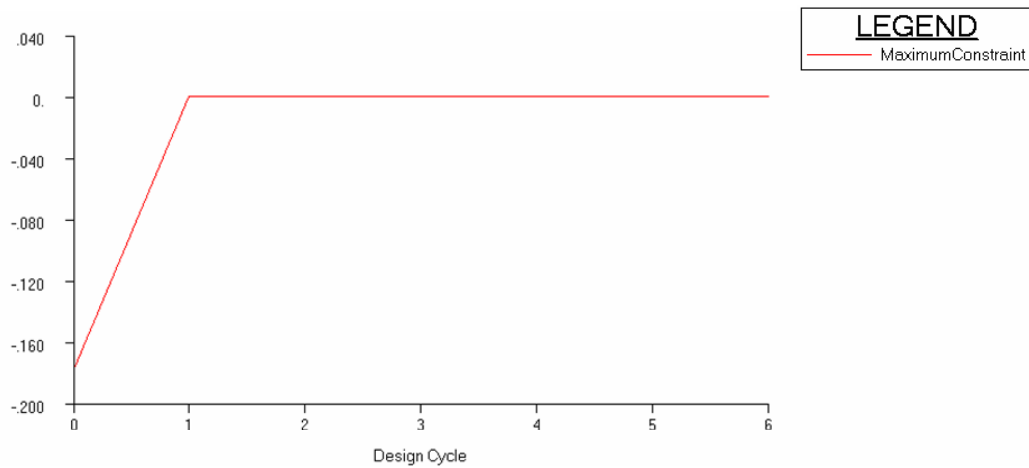


Figure 5.26 History of the maximum constraint value

It is observed that history of the design variables ‘B’ and ‘H’ show similar behaviour as the history of the design variables in the other two strategies with slight differences in the initial phases of the optimization process.

Results of the MSC.NASTRAN[®] optimization module are also tabulated and comparisons are made in section 5.1.4 with the results obtained by the other two methods. The effect of mesh density on results is presented in appendix C.1.

5.1.4. COMPARISON OF THE THREE DIFFERENT OPTIMIZATION STRATEGIES

In this section, results of the three different optimization strategies are compared with each other in Table 5.6.

For the first and second technique, number of iterations indicates evaluation of outer most loop of optimization process shown in figure 3.1. For the third technique, it indicates the evaluation of loop of optimization process shown in figure 4.1.

Table 5.6 Comparison of results of three different optimization approaches

| | | 1st Technique | 2nd Technique | 3rd Technique |
|--|----------------------|------------------|------------------|------------------|
| Number of iterations | | 8 | 12 | 6 |
| B (mm) | Initial value | 10 | 10 | 10 |
| | Final value | 7.274 | 7.294 | 7.290 |
| H (mm) | Initial value | 35 | 35 | 35 |
| | Final value | 36.381 | 36.443 | 36.448 |
| Objective function (mm³) | Initial value | 175000 | 175000 | 175000 |
| | Final value | 132317 | 132914 | 132849 |
| Max axial stress at the root (Mpa) | Initial value | 306.1 | 306.1 | 306.1 |
| | Final value | 389.5 | 387.1 | 387.2 |
| Max. tip deflection (mm) | Initial value | 20.825 | 20.906 | 20.906 |
| | Final value | 25.491 | 25.397 | 25.402 |
| H/B | Initial value | 3.500 | 3.500 | 3.500 |
| | Final value | 5.002 | 4.996 | 5.000 |

It can be seen from Table 5.6 that in all methods the design variables have converged to almost the same values. These values compare well with the values given in Table 5.5. In Table 5.5 only the integer values of the design variables are listed, therefore optimum values given in Table 5.6 are slightly different from the optimum listed in Table 5.5. Since initial values were chosen close to the optimum values optimization processes have converged very quickly in all

techniques. The fastest solution is obtained with optimization module of MSC.NASTRAN[®]. It should be noted that optimization module of MSC.NASTRAN[®] uses sensitivity analysis which speeds up the solution time drastically. First technique is slightly slower than the MSC.NASTRAN[®] optimization module, and the solutions are obtained within seconds. However, second technique is very slow, because during the optimization process MSC.NASTRAN[®] is called whenever the evaluation of the unconstrained function is needed. The optimizer waits MSC.NASTRAN[®] job for some time which is required to ask for the license and finish the execution of a run. For this reason, hours are required to arrive at the solution with this technique. Therefore, this approach should only be used for problems with complex geometry and loading conditions which require finite element analysis. In complex geometry and loading situations if the user wants to have full control over the optimization code, he can choose to use a commercial finite element solver to work in conjunction with the optimization code developed by the user. In such cases it is recommended to use parallel computing to speed up the arriving at the optimum solution. In all optimization approaches weight is reduced by 24 percent without violating any constraint. All techniques show that maximum deflection at the tip and “H/B” ratio are the active or more restricting constraints at the optimum.

The results obtained in this section shows that all three approaches can be successfully applied in the solution of an optimization problem. The optimization approach to be used depends on the availability of resources as well as background on optimization theory. For instance, optimization module of MSC.NASTRAN[®] can be effectively used by those who do not have sufficient background on optimization theory. In engineering applications sometimes engineers are faced to solve problems for which they have little background. Therefore, optimization modules of commercial finite element codes provide such an alternative tool to be used in design optimization studies.

5.2 CANTILEVER BEAM WITH I CROSS SECTION

The second example undertaken is the optimization of a cantilever beam with an I shaped cross-section. In this example the number of design variables is increased to four. Similar to the first beam example cantilever beam is subjected to a vertical force "P" at the end and the beam will be optimized in a similar manner as in rectangular cross-section beam. The beam cross section is assumed to be constant along the span of the beam. Height "H", flange width "Wf", web thickness "tw" and flange thickness "tf" are taken as the design variables, respectively. The dimensions of the design variables are in mm. The length of the beam is fixed and thus only the cross-sectional properties of the beam are included in the design variable list. Figure 5.27 shows the cantilever beam with I cross section to be optimized.

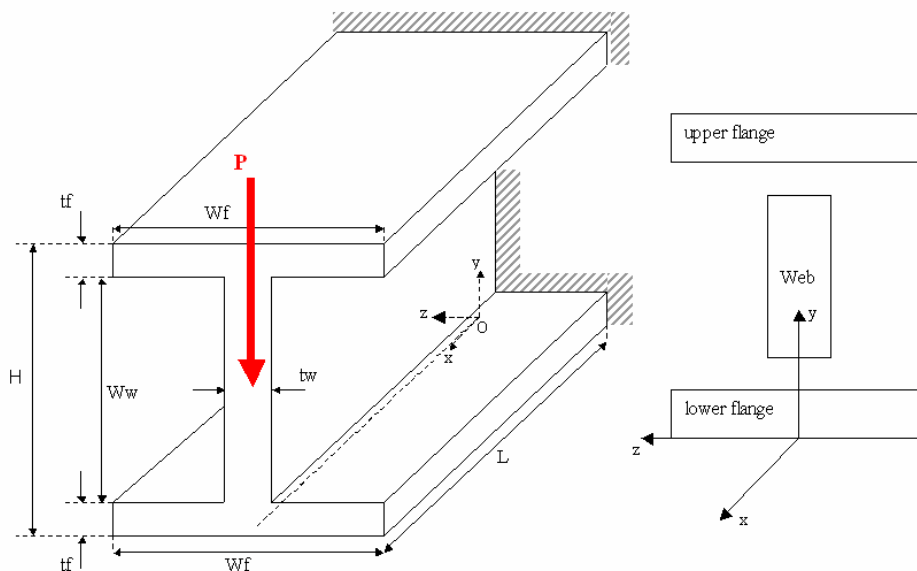


Figure 5.27 Cantilever beam with I cross section

The objective of this problem is again to minimize the weight of the beam. Like in the previous problem high strength aluminum is used as the material of the beam.

The beam is subject to three inequality constraints. First inequality constraint is maximum bending stress at the root, second one is maximum tip deflection due to tip loading and the third one is taken as the maximum shear stress in the web of the beam. Based on the problem definition the optimization problem can be stated as follows:

Minimize:

$$V = (2 \cdot W_f \cdot t_f + W_w \cdot t_w) \cdot L \quad (5.7)$$

Subject to:

$$-700 \text{ MPa} \leq \sigma = \frac{M \cdot c}{I} \leq 700 \text{ MPa} \quad (5.8)$$

$$\delta = \frac{P \cdot L^3}{3 \cdot E \cdot I} \leq 25.4 \text{ mm} \quad (5.9)$$

$$\tau = \frac{P \cdot Q}{I \cdot t_w} \leq 350 \text{ MPa} \quad (5.10)$$

$$0.4 \leq \frac{t_f}{t_w} \leq 2.5 \quad (5.11)$$

where

$$1 \leq W_f \leq 40 \quad (5.12)$$

$$0.5 \leq t_f \leq 20 \quad (5.13)$$

$$0.5 \leq t_w \leq 20 \quad (5.14)$$

$$10 \leq H \leq 40 \quad (5.15)$$

$$I = \frac{1}{6} \cdot W_f \cdot t_f^3 + \frac{1}{2} \cdot t_f \cdot W_f \cdot (H - t_f)^2 + \frac{1}{12} \cdot t_w \cdot (H - 2 \cdot t_f)^2 \quad (5.16)$$

$$Q = \frac{1}{2} \cdot t_f \cdot W_f \cdot (H - t_f)^2 + \frac{1}{8} \cdot t_w \cdot (H - 2 \cdot t_f)^2 \quad (5.17)$$

5.2.1 OPTIMIZATION USING THE OPTIMIZATION CODE IN MATLAB[®] AND ANALYTIC FUNCTIONS AS SOLVER

First, optimization of the cantilever beam with I cross section is performed by using first method explained in Chapter 4. In this method optimization code written in MATLAB[®] is used together with the analytical solver. The M-file called “AugLagMet.m” is executed in MATLAB[®] environment. “AugLagMet.m” asks user for inputs which are given below with the corresponding the values for this example.

1. Initial values of the design variable vector “**x**”: [20 12 3 1.5]
2. Lower bounds of the design variable vector “**x**”: [10 1 0.5 0.5]
3. Upper bounds of the design variable vector “**x**”: [50 50 20 20]
4. Number of equality constraints: 0
5. Number of inequality constraints: 10
6. Initial values of lagrange multipliers “**λ**”
for equality constraints: 0
7. Initial values of lagrange multipliers “**β**”
for inequality constraints : [10000 10000 10000
10000 10000 10000
10000 100 100
10000]

Where the design variable vector “**x**” is given by [H, Wf, tw, tf]. Lagrange multipliers “**β**” are given by [$\beta_1, \beta_2, \beta_3, \beta_4, \beta_5, \beta_6, \beta_7, \beta_8, \beta_9, \beta_{10}$];

- β_1 is the multiplier for the constraint given in equation (5.8) used for upper bound of the stress value which is calculated in upper flange at the root of the beam.
- β_2 is the multiplier for the constraint given in equation (5.8) used for lower bound of the stress value which is calculated in upper flange at the root of the beam.

- β_3 is the multiplier for the constraint given in equation (5.8) used for upper bound of the stress value which is calculated in lower flange at the root of the beam.
- β_4 is the multiplier for the constraint given in equation (5.8) used for lower bound of the stress value which is calculated in lower flange at the root of the beam.
- β_5 is the multiplier for the constraint given in equation (5.11) used for upper bound of the inequality.
- β_6 is the multiplier for the constraint given in equation (5.11) used for lower bound of the inequality.
- β_7 is the multiplier for the constraint given in equation (5.10) used for the shear stress value which is calculated at the centroid at the root of the beam.
- β_8 is the multiplier for the artificial constraint, which is built for the upper bound of the height given in equation (5.15).
- β_9 is the multiplier for the artificial constraint, which is built for the upper bound of the flange width given in equation (5.12)..
- β_{10} is the multiplier for the constraint given in equation (5.9) used for the displacement value at the tip of the beam.

It should be noted that the upper bound of height “H” and the flange width “Wf” are input higher than desired values. The height “H” and the flange width “Wf” values are then restricted by the inequality constraints. The initial multipliers for these constraints “ β_8 ” and “ β_9 ” are chosen less than other multipliers to reduce the impact of these artificial constraints at the beginning of the process.

The M-files “Ofun.m”, Gfun.m”and “Hfun.m” which evaluate volume, inequality constraints and equality constraints respectively, and they are modified accordingly.

The optimization process is converged to the optimum solution in 71 iterations, where one iteration is one outermost cycle in the main algorithm shown in figure 3.1. In Figures 5.28 – 5.36 change of the objective function, design variables

and constraints with respect to iteration number are shown. Results are tabulated and comparisons are made in section 5.2.4 with the results obtained by the other two methods.

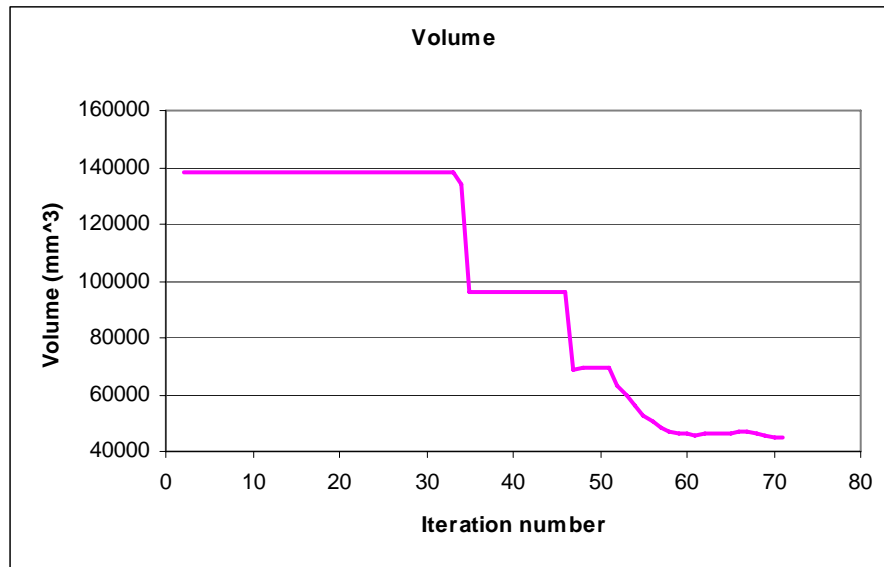


Figure 5.28 Variation of the objective function with respect to iteration number

It is seen that in this problem the objective function decreases considerably in the optimum solution. However, it is also observed that the optimization process is resistant, in other words during the initial phases of the optimization process it is seen that there is almost no variation of the objective function.

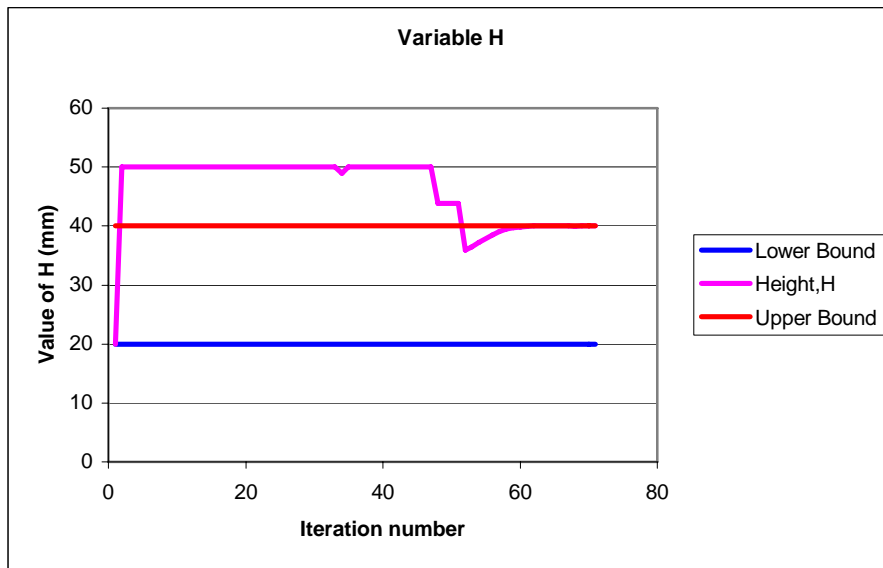


Figure 5.29 Variation of the height of cross section “H” with respect to iteration number

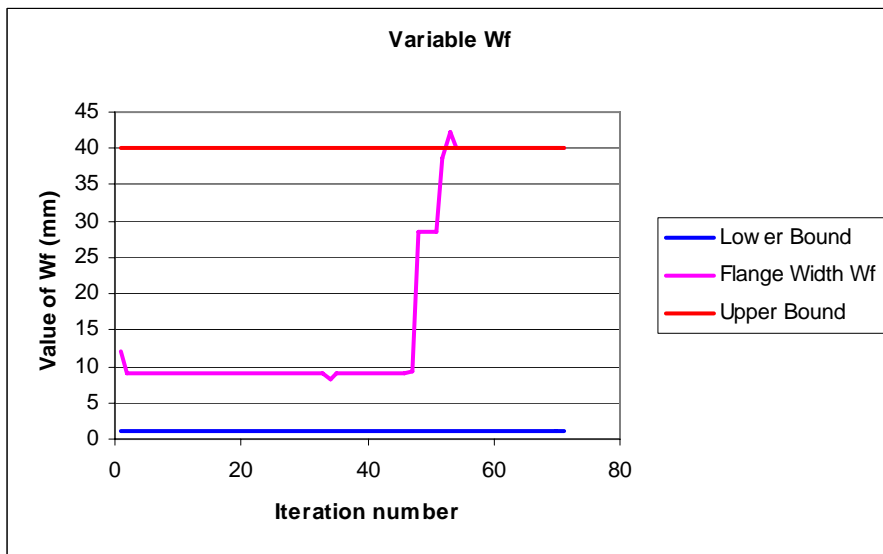


Figure 5.30 Variation of the width of flanges “Wf” with respect to iteration number

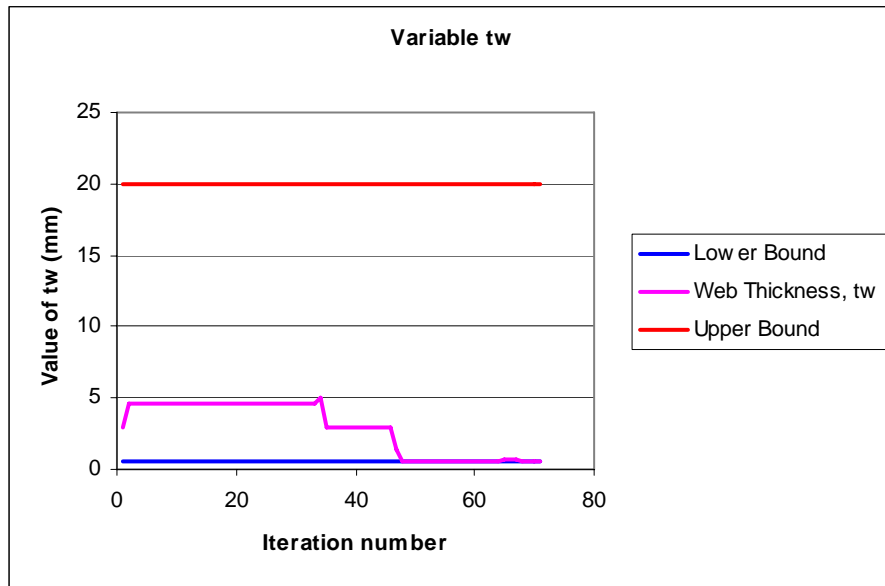


Figure 5.31 Variation of the web thickness “tw” with respect to iteration number

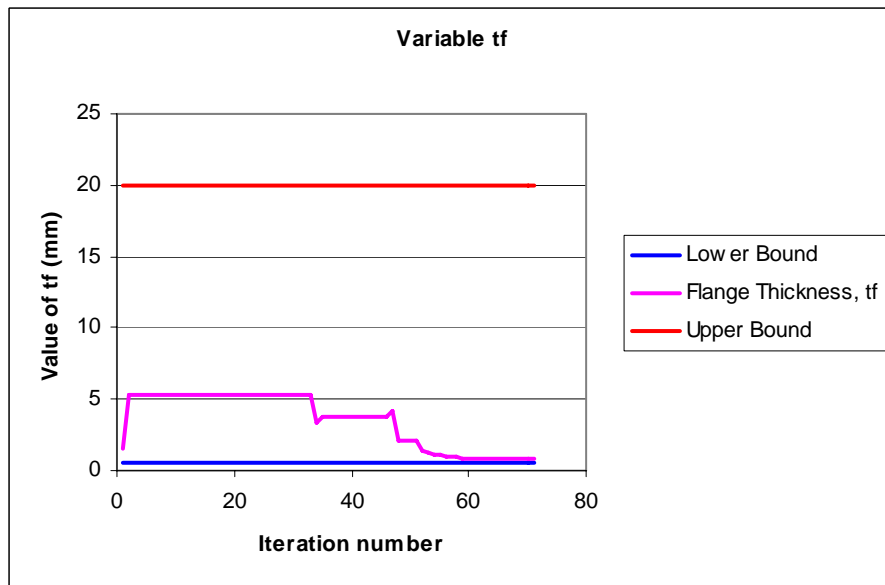


Figure 5.32 Variation of the flange thickness “tf” with respect to iteration number

The variation of the design variables reveals that flange and web thicknesses approach to their lower limit in the optimized solution whereas the flange width and the beam height approach to their upper limit in the optimized solution. It is also observed that the height of the beam violated the upper bound during the initial phase of the iterations and in a way persists to stay in the restricted zone. However, in the end it is forced to enter into the feasible region.

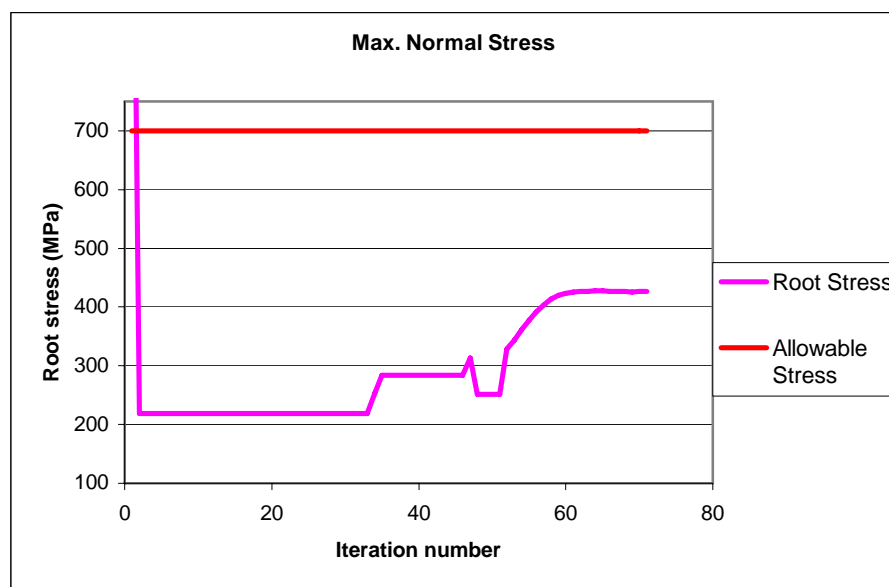


Figure 5.33 Variation of maximum bending stress at the root of the beam with respect to iteration number

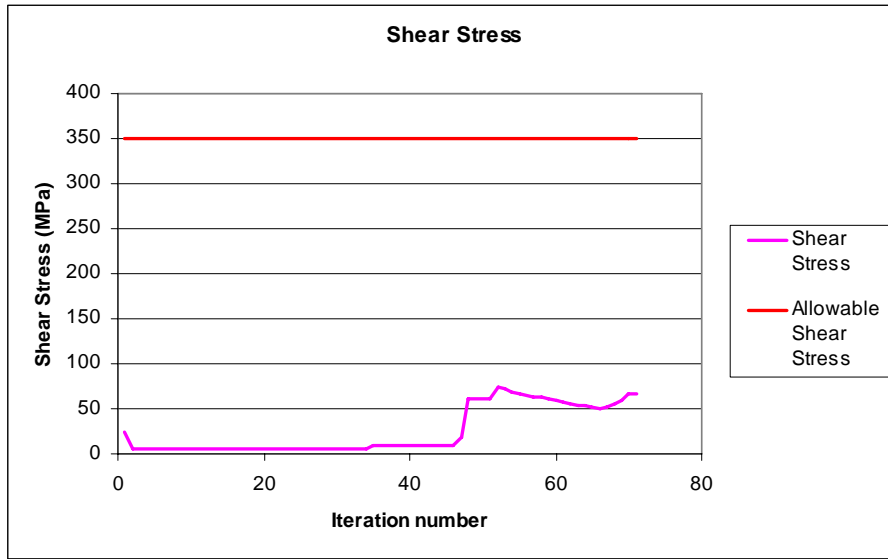


Figure 5.34 Variation of maximum shear stress at the root of the beam with respect to iteration number

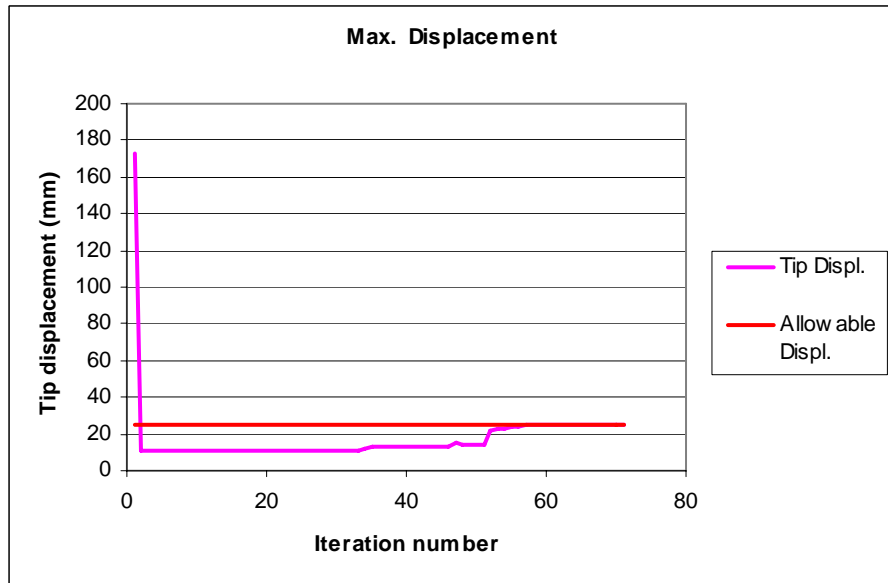


Figure 5.35 Variation of maximum displacement with respect to iteration number

Observation of the stress and deflection constraints shows that the displacement constraint is a gain the more restricting constraint in this problem like in the rectangular beam problem. It is seen that the stress values in the optimum solution are far below the maximum allowable values, however the maximum tip deflection is almost the same as the maximum allowable value in the optimized solution. It is obvious that if there were no displacement constraint defined in this problem, the stress values would increase due to the decreases in the design variables, and more reduction in the objective function, which the total volume, would be obtained.

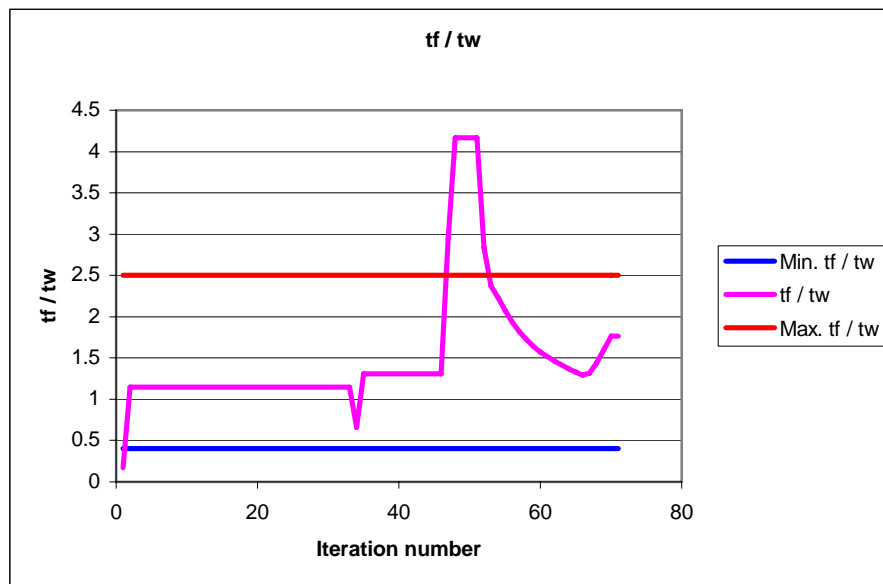


Figure 5.36 Variation of tf / tw with respect to iteration number

Figure 5.36 shows the variation of the constraint on the ratio of the flange thickness to the web thickness. The constraint is violated towards end of the optimization process but eventually the constraint is satisfied at the optimum solution.

5.2.2 CANTILEVER BEAM OPTIMIZATION USING THE OPTIMIZATION CODE IN MATLAB® AND MSC.NASTRAN® AS THE SOLVER

In this section optimization of the cantilever beam with I cross section is performed by using second strategy explained in Chapter 4. In this method optimization code written in MATLAB® is used together with the commercial finite element solver MSC.NASTRAN®. The M-file called “AugLagMet.m” is executed in MATLAB® environment. “AugLagMet.m” asks user for inputs which are given below with the corresponding the values for this example.

- | | |
|---|--|
| 1. Initial values of design variable “ \mathbf{x} ”: | [20 12 3 1.5] |
| 2. Lower bounds of design variable “ \mathbf{x} ”: | [10 1 0.5 0.5] |
| 3. Upper bounds of design variable “ \mathbf{x} ”: | [50 50 20 20] |
| 4. Number of equality constraints: | 0 |
| 5. Number of inequality constraints: | 10 |
| 6. Initial values of lagrange multipliers “ λ ” for equality constraints: | 0 |
| 7. Initial values of lagrange multipliers “ β ” for inequality constraints : | [10000 10000 10000 10000 10000 10000 10000 100 100 10000] |

Where the design variable vector “ \mathbf{x} ” is given by [H, Wf, tw, tf]. Lagrange multipliers “ β ” is given by [$\beta_1, \beta_2, \beta_3, \beta_4, \beta_5, \beta_6, \beta_7, \beta_8, \beta_9, \beta_{10}$];

- β_1 is the multiplier for the constraint given in equation (5.8) used for upper bound of the stress value which is calculated in upper flange at the root of the beam.
- β_2 is the multiplier for the constraint given in equation (5.8) used for lower bound of the stress value which is calculated in upper flange at the root of the beam.

- β_3 is the multiplier for the constraint given in equation (5.8) used for upper bound of the stress value which is calculated in lower flange at the root of the beam.
- β_4 is the multiplier for the constraint given in equation (5.8) used for lower bound of the stress value which is calculated in lower flange at the root of the beam.
- β_5 is the multiplier for the constraint given in equation (5.11) used for upper bound of the inequality.
- β_6 is the multiplier for the constraint given in equation (5.11) used for lower bound of the inequality.
- β_7 is the multiplier for the constraint given in equation (5.10) used for the shear stress value which is calculated at the centroid at the root of the beam.
- β_8 is the multiplier for the artificial constraint, which is built for the upper bound of the height given in equation (5.15).
- β_9 is the multiplier for the artificial constraint, which is built for the upper bound of the flange width given in equation (5.12)..
- β_{10} is the multiplier for the constraint given in equation (5.9) used for the displacement value at the tip of the beam.

It should again be noted that the upper bound of height “H” and the flange width “Wf” are input higher than desired values. The height “H” and the flange width “Wf” values are then restricted by the inequality constraints. The initial multipliers for these constraints “ β_8 ” and “ β_9 ” are chosen less than other multipliers to reduce the impact of these artificial constraints at the beginning of the process.

The M-files “Ofun.m”, “Gfun.m” and “Hfun.m” which evaluate volume, inequality constraints and equality constraints respectively, and they are modified accordingly.

The optimization process is converged to the solution again in 71 iterations, where one iteration is one outermost cycle in the main algorithm shown in figure

3.1. In Figures 5.37 – 5.45 change of objective function, variables and constraints with respect to the iteration number are shown. Results are tabulated and comparisons are made in section 5.2.4 with the results obtained by the other two methods.

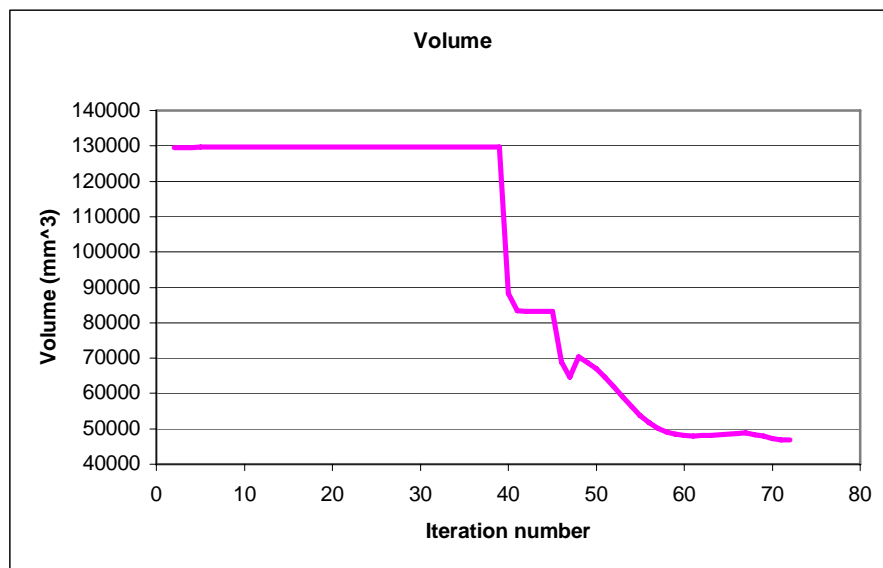


Figure 5.37 Variation of the objective function with respect to iteration number

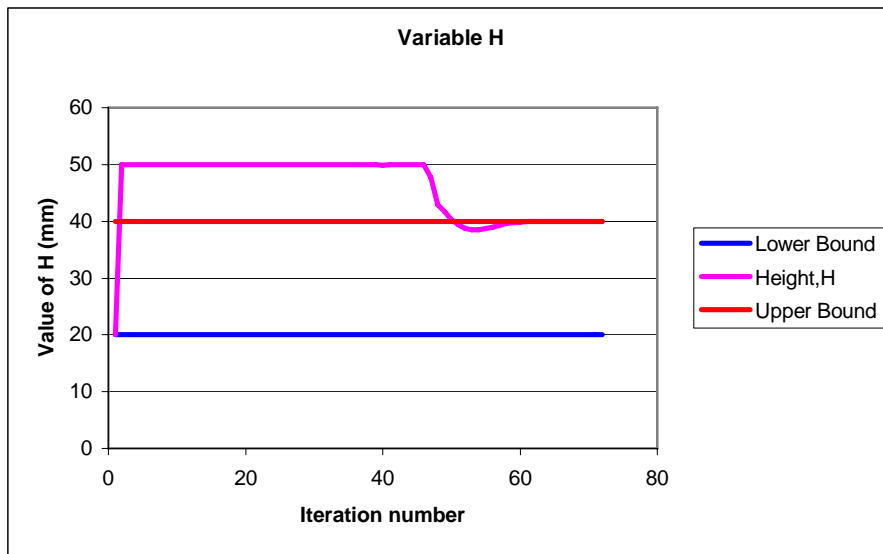


Figure 5.38 Variation of the height of cross section “H” with respect to iteration number

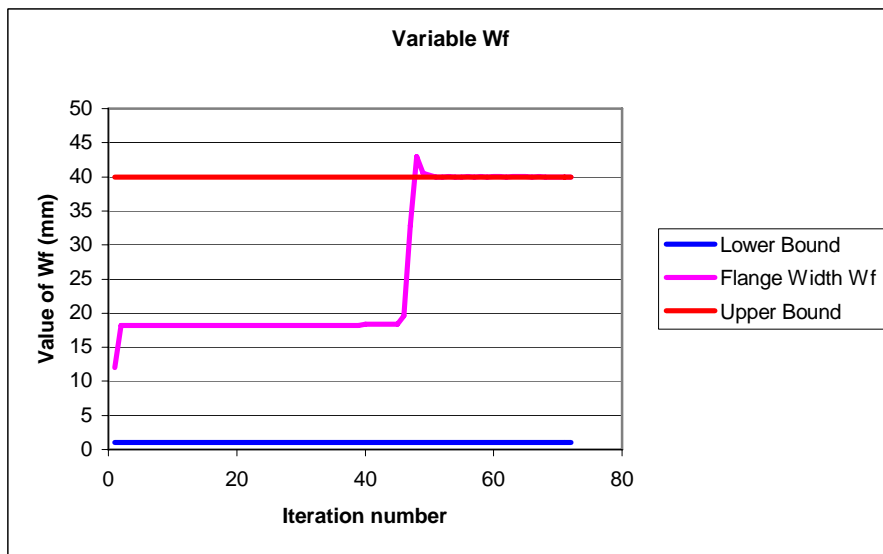


Figure 5.39 Variation of the width of flanges “Wf” with respect to iteration number

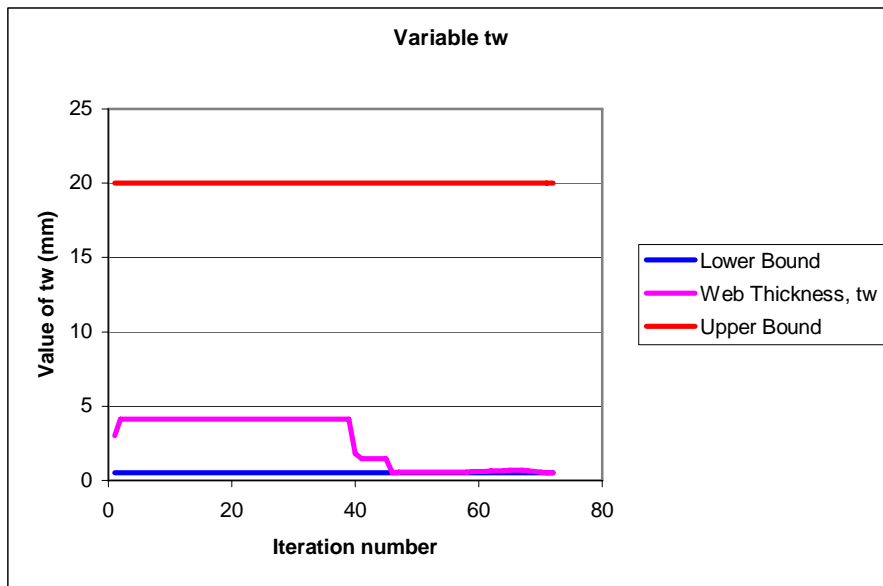


Figure 5.40 Variation of the web thickness “tw” with respect to iteration number

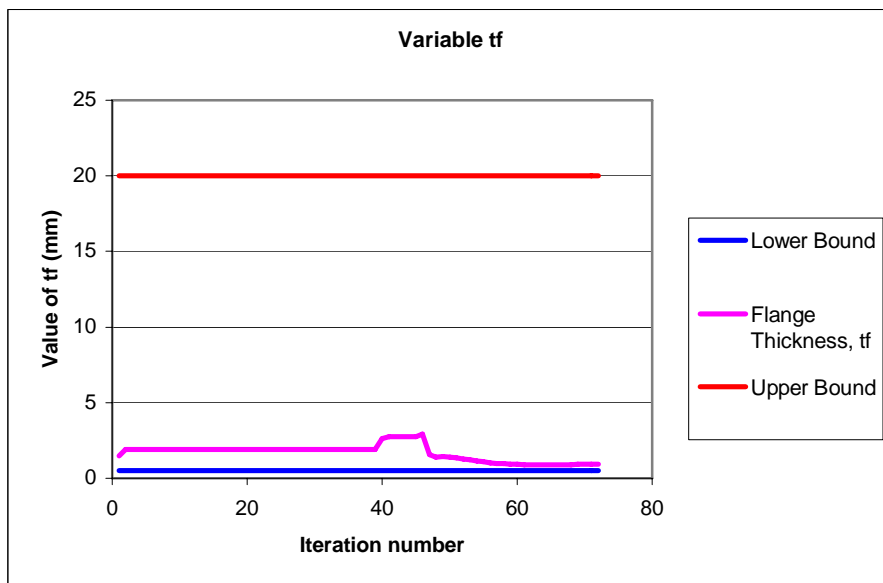


Figure 5.41 Variation of the flange thickness “tf” with respect to iteration number

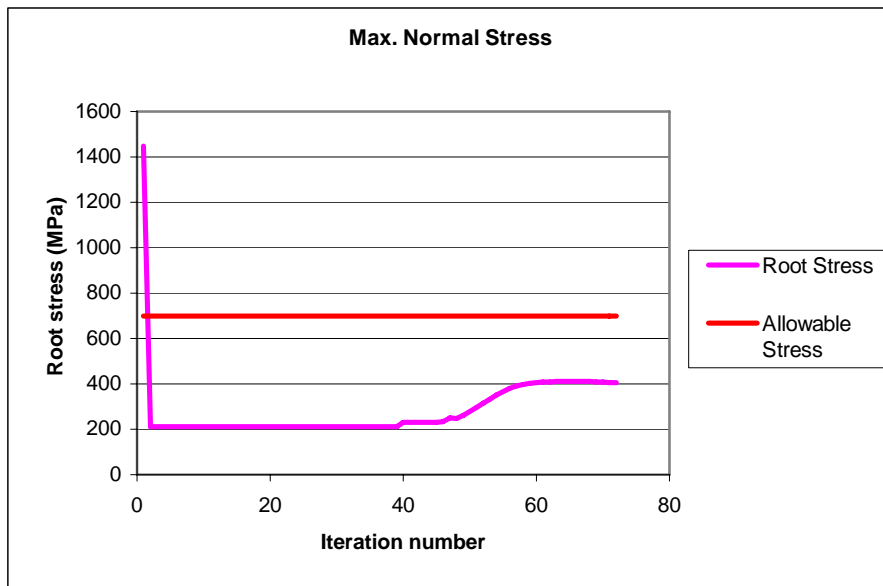


Figure 5.42 Variation of maximum bending stress at the root of the beam with respect to iteration number



Figure 5.43 Variation of maximum shear stress at the root of the beam with respect to iteration number

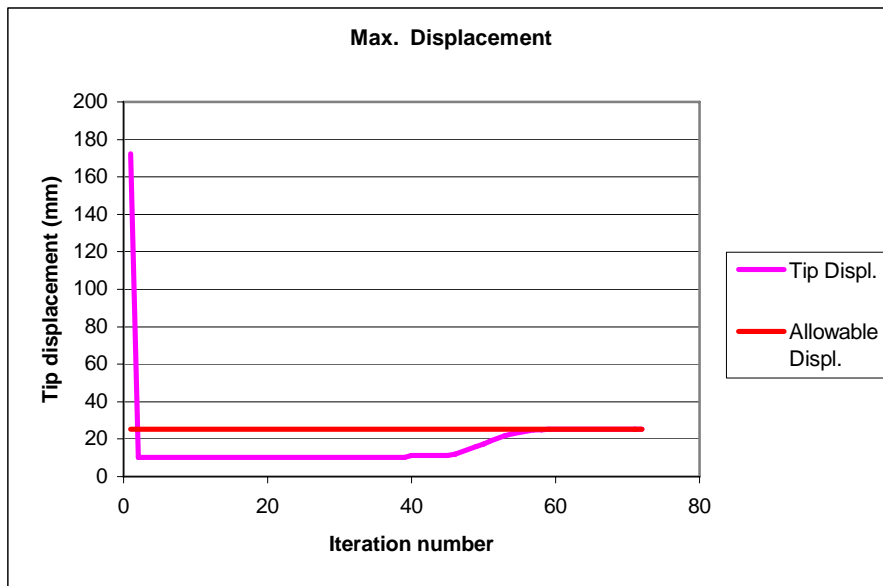


Figure 5.44 Variation of the maximum displacement with respect to iteration number

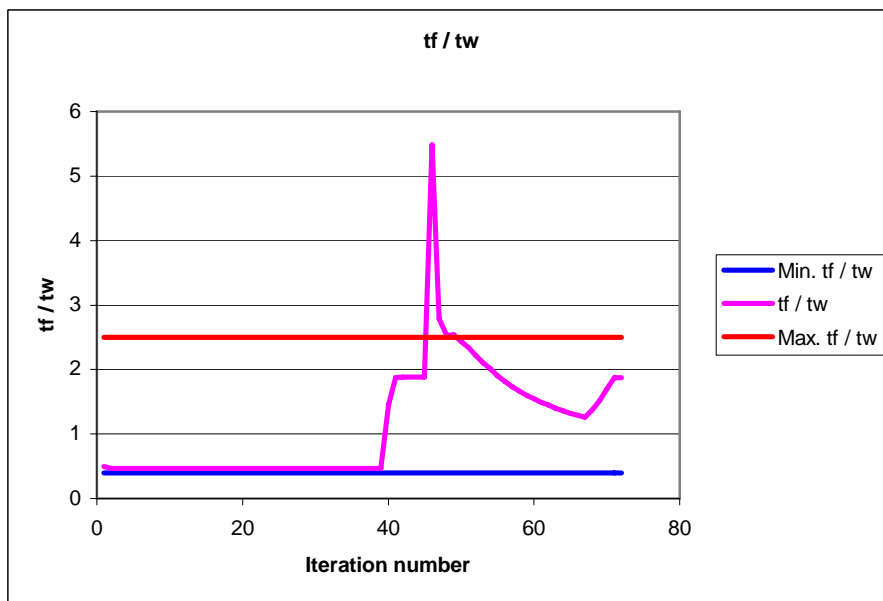


Figure 5.45 Variation of tf / tw with respect to iteration number

Figures 5.37-5.45 show that variations of the objective function, design variables and the constraints with iteration number depict similar behavior as in the first method where the solver was the analytical relations for the cantilever beam problem for the maximum axial stress, maximum shear stress and maximum tip deflection. Moreover, this problem has four design variables. This example also shows that the incorporation of MSC.NASTRAN[®] as the solver of the optimization code developed in MATLAB[®] has been successful.

It should be noted that since the same optimization code are used in both methods discussed above, one should expect to get similar variations in the history of the design variables.

5.2.3. CANTILEVER BEAM OPTIMIZATION USING OPTIMIZATION MODULE OF MSC.NASTRAN[®]

Finally, optimization of the cantilever beam with the I cross section is performed by using the optimization module of MSC.NASTRAN[®]. It should be noted that during the execution of the optimization solution with the optimization module of MSC.NASTRAN[®], MSC.NASTRAN[®] solver is frequently called internally. Before the optimization process, the cantilever beam problem is modeled in MSC.PATRAN[®].

The beam is modeled with 10 CBAR elements similar to the modeling of the rectangular cross-section beam. I cross section is assigned as the element's cross-sectional property. At the root 6 degree of freedom (Ux, Uy, Uz, Rx, Ry and Rz) of the node is fixed. At the tip 1250 N force is applied in negative (-) “y” direction as shown in figure 5.46.

Initial finite element model and cross section properties are shown in figures 5.46-5.48. Initial values are;

- Height of the beam: 20 mm
- Width of the beam: 12 mm
- Thickness of the web: 3 mm
- Thickness of the flanges: 1.5 mm.

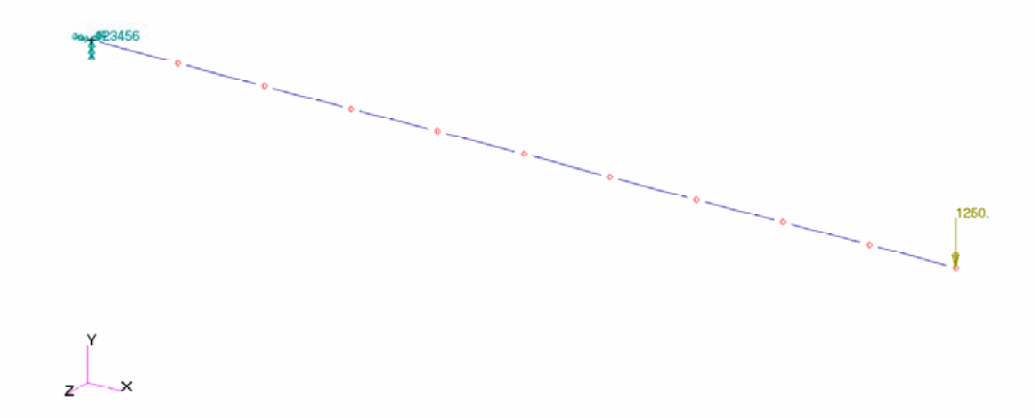


Figure 5.46 Cantilever I beam model

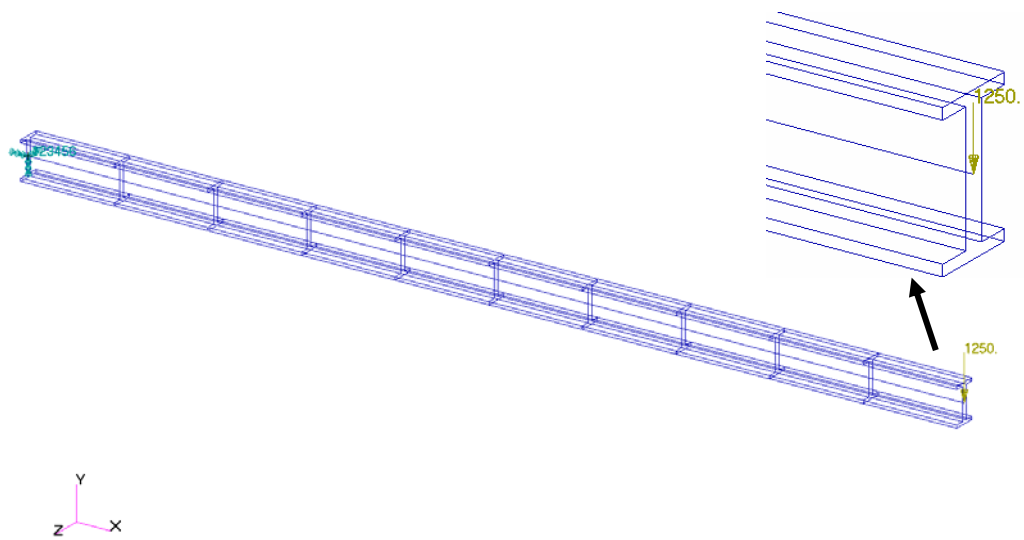


Figure 5.47 Initial cantilever I beam model with equivalent inertia

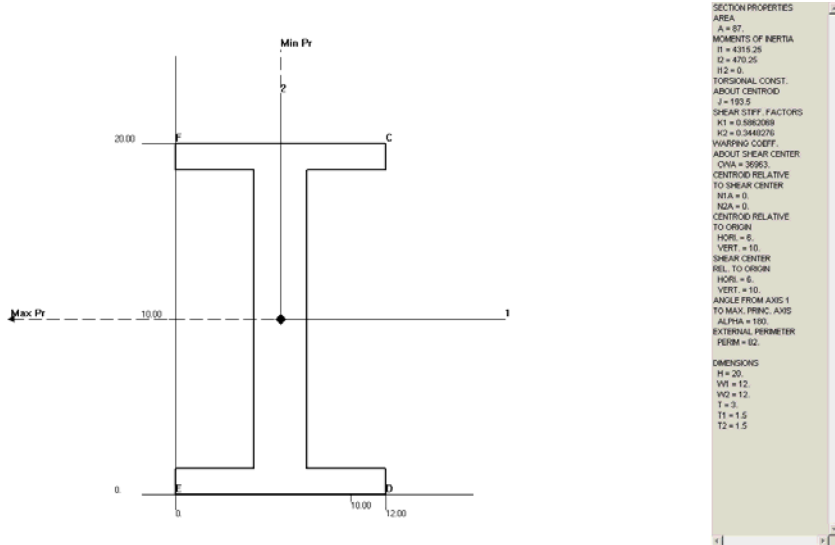


Figure 5.48 Initial cantilever I beam section properties

Initial finite element analysis results are presented in Figures 5.49-5.50. In Figure 5.49 displacement distribution and in Figure 5.50 maximum axial stress distribution due to bending are shown.

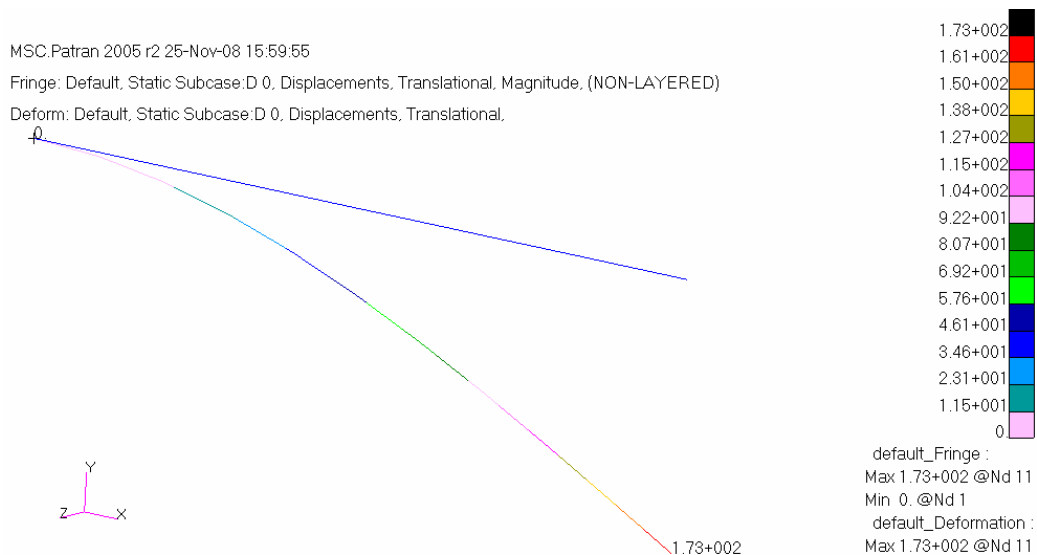


Figure 5.49 Cantilever I beam initial displacement



Figure 5.50 Cantilever I beam initial bending stress distribution

Optimized finite element model and the cross-section of the optimized beam are shown in Figures 5.51 and 5.52 respectively. From Figure 5.51 one can not identify the difference between the initial and final optimized beam configuration but Figure 5.52 shows the optimized cross-section clearly. It can be seen that the height of the beam does not change much from its initial value but the flange width and thickness of the flange and the web are reduced from its initial value.

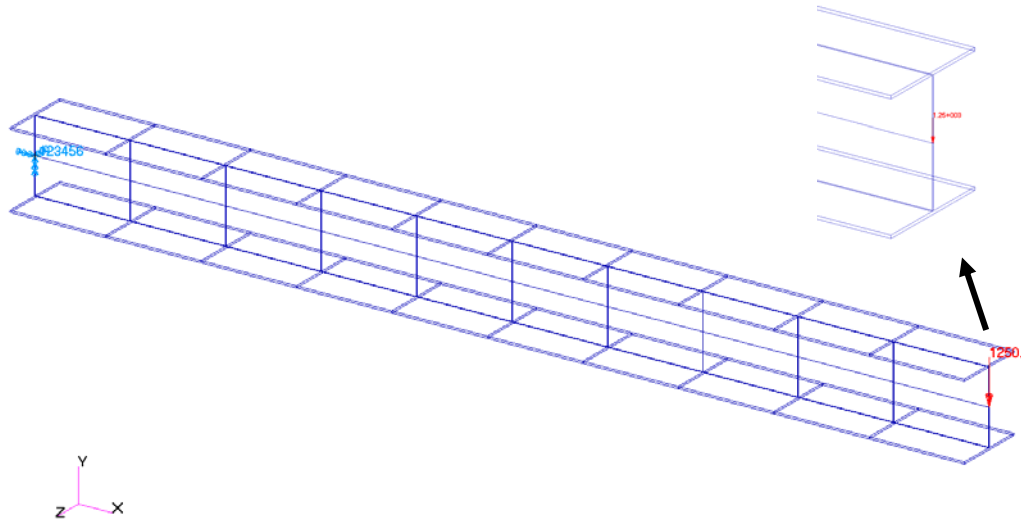


Figure 5.51 Final cantilever I beam model with equivalent inertia

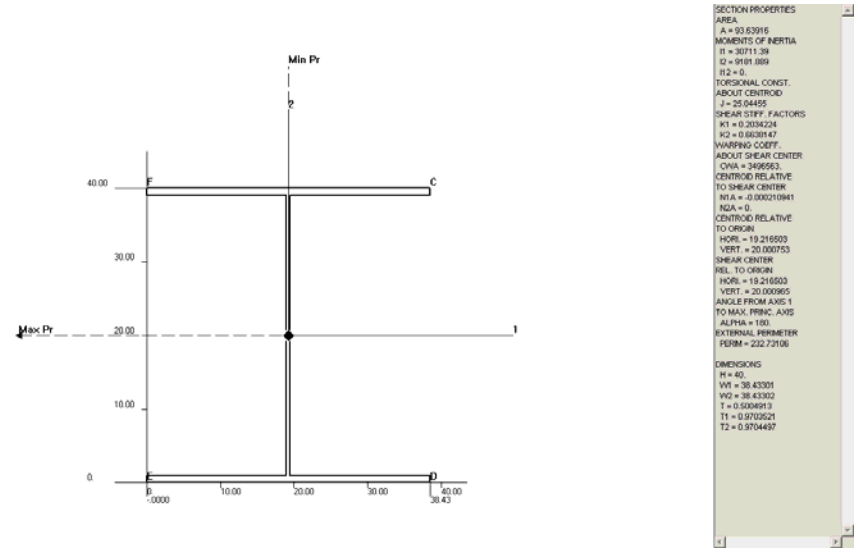


Figure 5.52 Final cantilever I beam section properties

Final finite element analysis results for the optimized beam are presented in Figures 5.53-5.54. Figure 5.53 shows the displacement distribution and Figure

5.54 shows the axial stress distribution due to bending along the span of the beam.

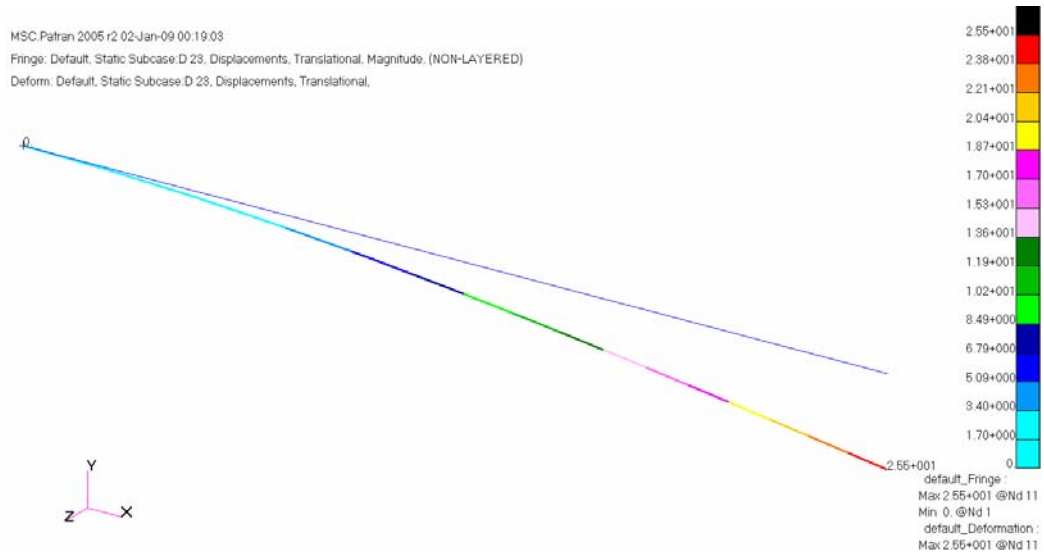


Figure 5.53 Displacement distribution in the optimized beam

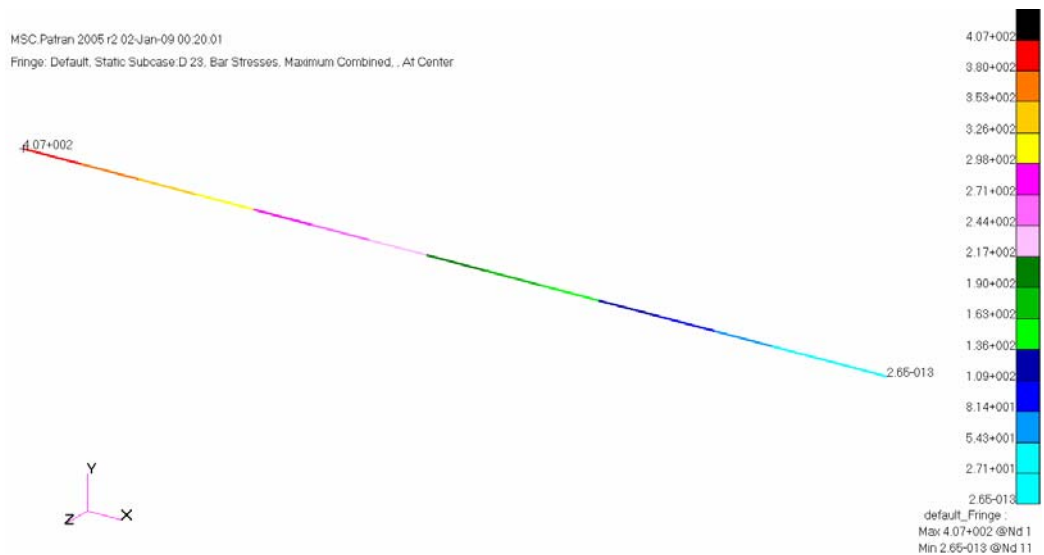


Figure 5.54 Bending stress distribution in the optimized beam

Variation of the objective function, each design variable and the maximum constraint value are shown in Figures 5.55-5.60. Maximum constraint value is the highest value of the normalized constraints constructed internally in MSC.NASTRAN[®]. In each iteration different constraint may have highest value. MSC.NASTRAN[®] optimization module arrives at the optimum solution in twenty design cycles as shown in Figures 5.55-5.60.

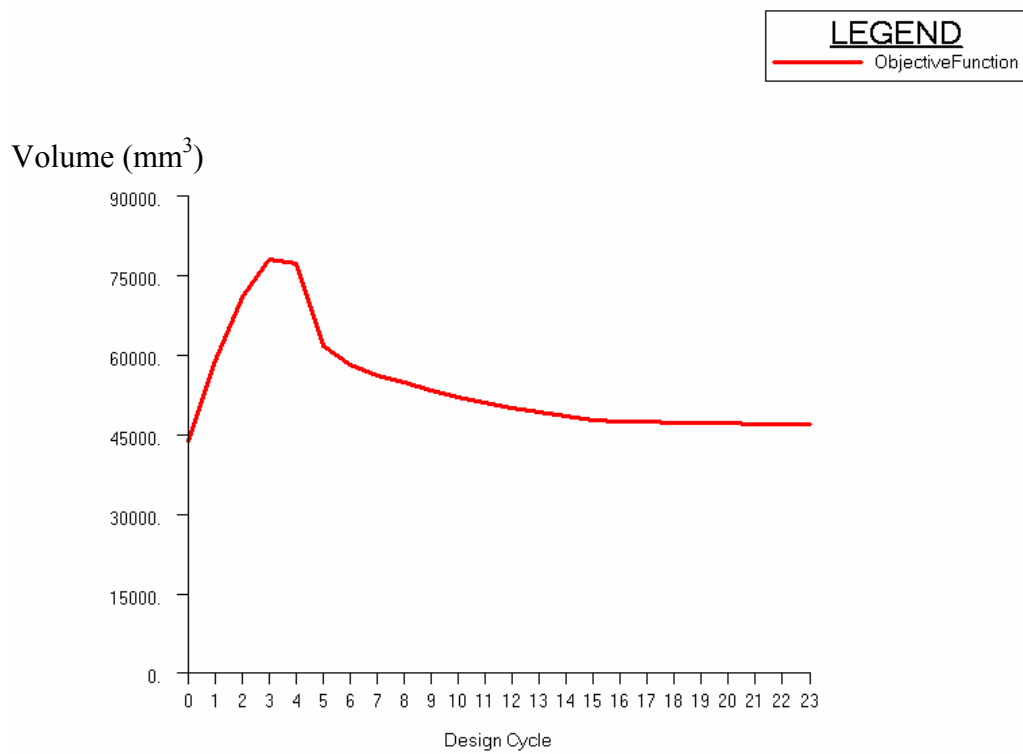


Figure 5.55 History of the objective function

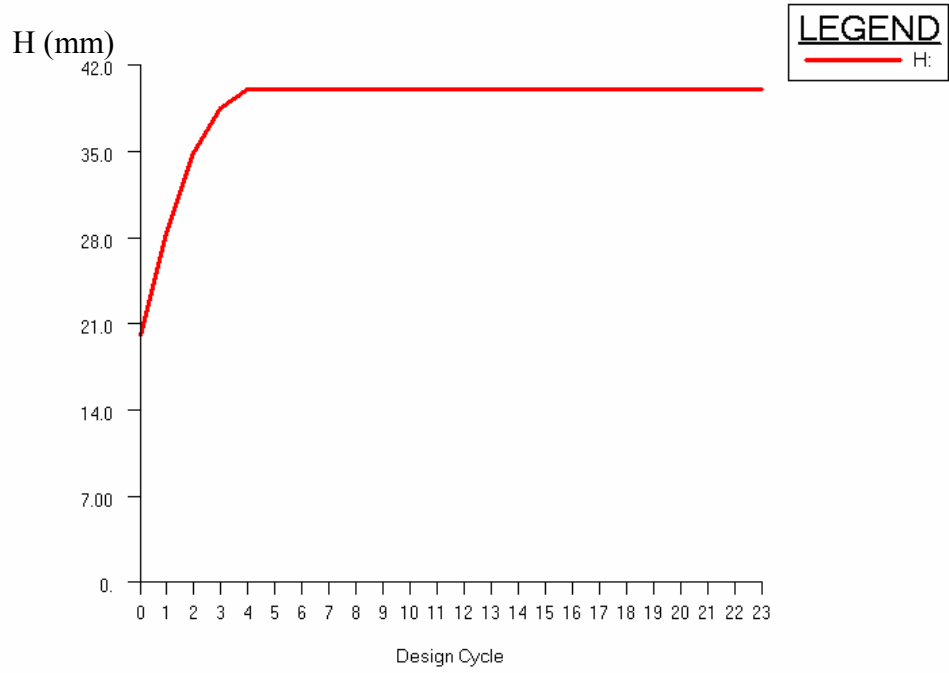


Figure 5.56 History of the design variable "H"(height of the beam)

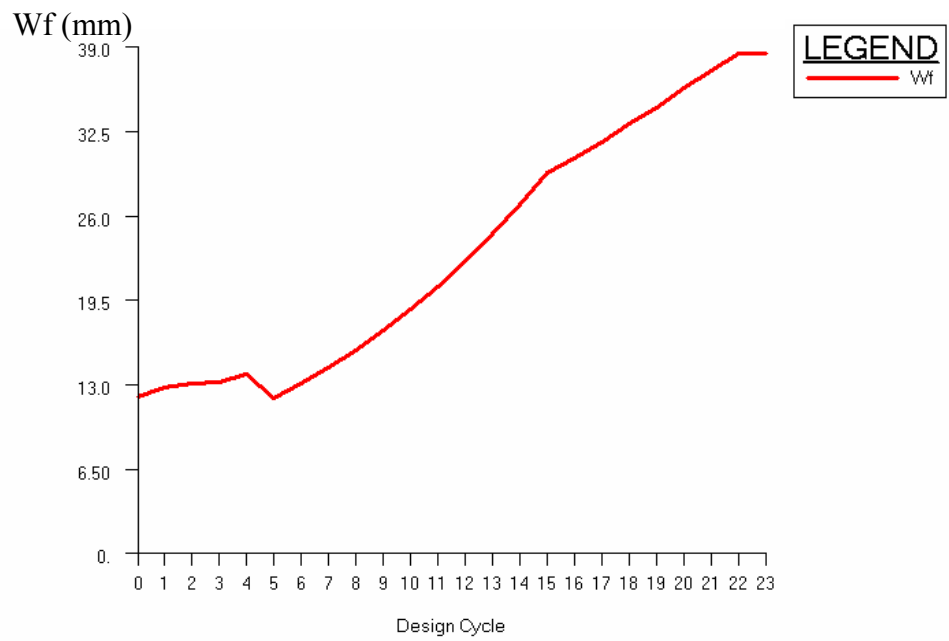


Figure 5.57 History of the design variable "Wf" (width of the flange)

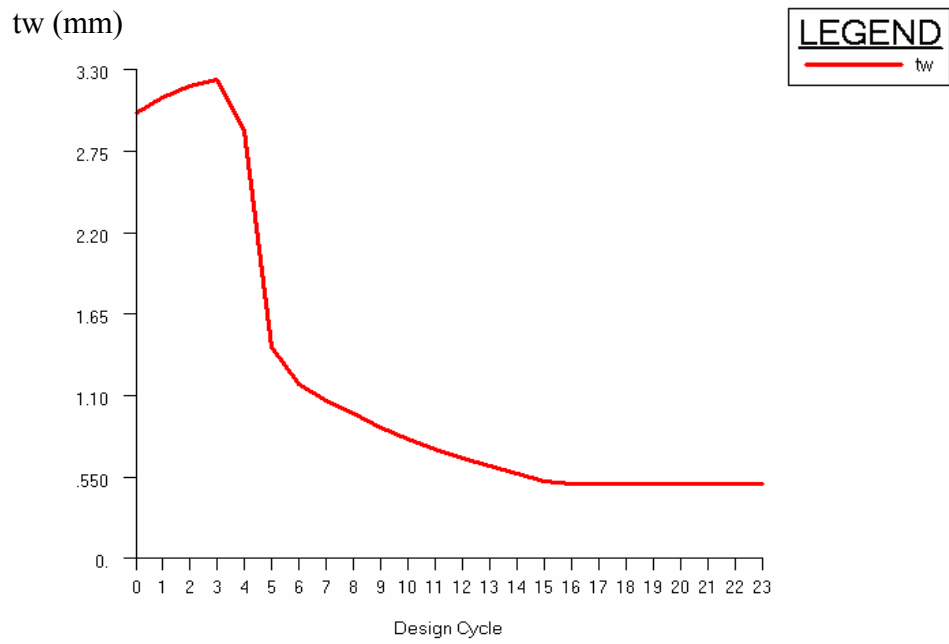


Figure 5.58 History of the design variable "tw" (thickness of the web)

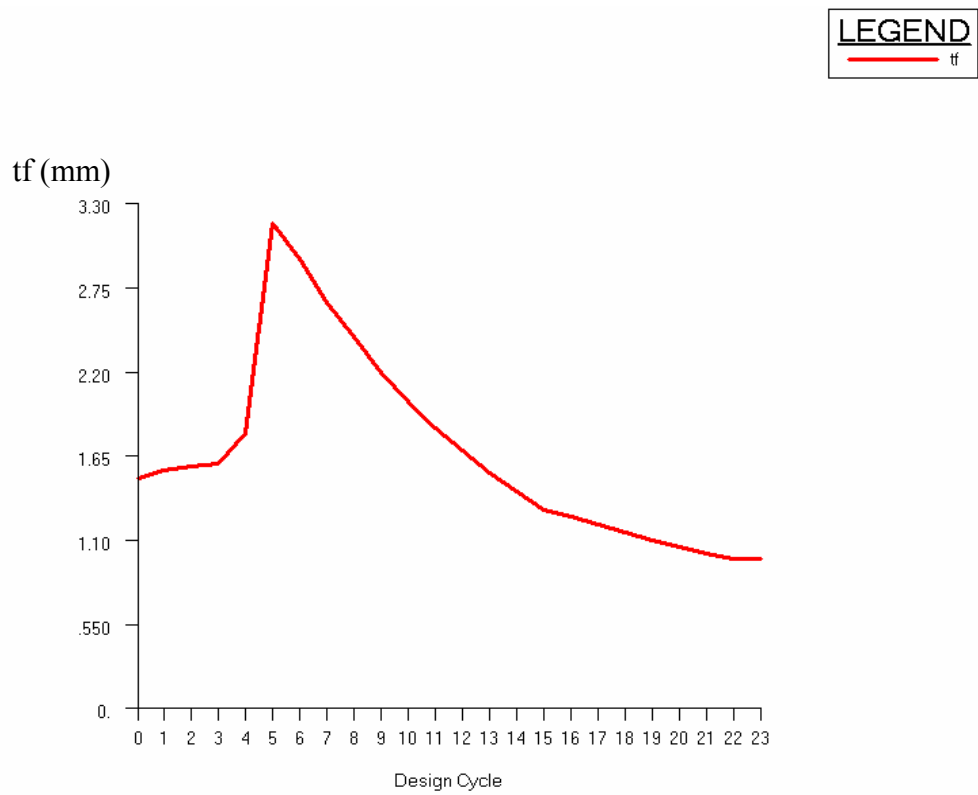


Figure 5.59 History of the design variable "tf" (thickness of the flange)

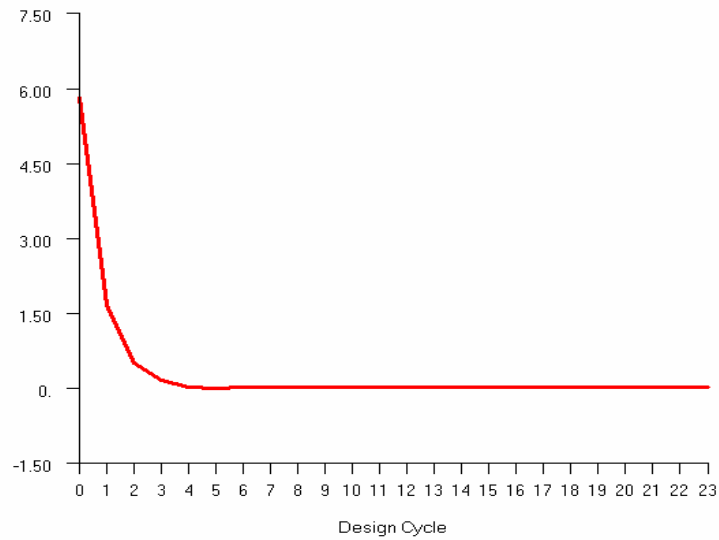


Figure 5.60 Cantilever beam problem history of the maximum constraint value

It is observed that in this problem history of the design variables do not show exactly the same similar behaviour as the history of the design variables in the other two optimization strategies. Results of the MSC.NASTRAN[®] optimization module are also tabulated and comparisons are made in section 5.2.4 with the results obtained by the other two methods. The effect of mesh density on results is presented in appendix C.2.

5.2.4. COMPARISON OF THE THREE DIFFERENT OPTIMIZATION STRATEGIES

In this section, results of the three different optimization strategies are compared with each other in Table 5.7.

For the first and second technique, number of iterations indicates evaluation of outer most loop of optimization process shown in figure 3.1. For the third technique, it indicates the evaluation of loop of optimization process shown in figure 4.1.

Table 5.7 Comparison of results for the I-Beam

| | | 1st Technique | 2nd Technique | 3rd Technique |
|---|----------------------|------------------|------------------|------------------|
| Number of iterations | | 71 | 75 | 23 |
| Beam Height, H (mm) | Initial value | 20 | 20.0 | 20 |
| | Final value | 39.983 | 40.0 | 40.0 |
| Flange Width, Wf (mm) | Initial value | 12.0 | 12.0 | 12.0 |
| | Final value | 39.974 | 38.43 | 38.43 |
| Web Thickness, tw (mm) | Initial value | 3.0 | 3.0 | 3.0 |
| | Final value | 0.50 | 0.50 | 0.50 |
| Flange Thickness, tf (mm) | Initial value | 1.5 | 1.5 | 1.5 |
| | Final value | 0.883 | 0.970 | 0.970 |
| Objective function, V (mm³) | Initial value | 43500 | 43500 | 43500 |
| | Final value | 44834 | 46820 | 46820 |
| Max. Stress at the root (MPa) | Initial value | 1448.4 | 1448.4 | 1448.4 |
| | Final value | 426.4 | 407.0 | 407.0 |
| Max. Shear Stress (MPa) | Initial value | 23.174 | 23.174 | 23.174 |
| | Final value | 65.938 | 65.826 | 65.826 |
| Max. deflection at tip (mm) | Initial value | 8.000 | 8.000 | 8.000 |
| | Final value | 25.39 | 25.474 | 25.474 |
| tf / tw | Initial value | 0.500 | 0.500 | 0.500 |
| | Final value | 1.765 | 1.939 | 1.939 |

It can be seen from Table 5.7 that there are slight differences in the converged design variables in the three solution strategies used. In the three approaches the

beam height and web thickness converges to almost the same value. However there are slight differences in flange width and flange thickness. Flange width obtained by using MSC.NASTRAN[®] is found a approximately 1 mm lower than the flange width obtained by the optimization code developed in MATLAB[®]. However, in the optimized solution the objective function value determined by the optimization by using MSC.NASTRAN[®] is slightly higher than the solution obtained by the optimization code which uses analytical functions as the solver. The difference is approximately 4.2 %. This slight difference is due to the higher flange thickness determined by the optimization by using MSC.NASTRAN[®]. It should also be noticed that in the optimum solution the value of the objective function is higher than its initial value. Such a situation occurs because the constraints of the problem drives the design variables into the feasible region and this process may end up with an increase in the optimized objective function value compared to its initial value.

Again the fastest solution is obtained with the optimization module of MSC.NASTRAN[®]. As it was discussed in the rectangular cross-section beam problem the second technique is very slow because of the frequent calling of MSC.NASTRAN[®] during the evaluation of the unconstrained function. Therefore, this approach should only be used for problems with complex geometry and loading conditions which require finite element analysis. In the future it is also recommended to improve the optimization code such that the optimum solution will be arrived at in less number of iteration steps.

It can be concluded that apart from the slight differences all three approaches converges to the same optimum, and this verifies that all three approaches work fine.

CHAPTER 6

OPTIMIZATION OF A WING TORQUE BOX

Weight saving is one of the most important issues in aerospace structures. Therefore, in this chapter structural optimization of a wing torque is performed by using the optimization module of MSC.NASTRAN[®]. As it was discussed before, the use of MSC.NASTRAN[®] as the solver only results in extremely long solution times with the optimization code developed in the thesis. To arrive at the solution within reasonable time in this section the optimization module of MSC.NASTRAN[®] is used and by the virtue of the sensitivity analysis feature of the optimization module of MSC.NASTRAN[®] the optimization of the torque box of a wing structure could be solved within a reasonable time period. The main objective is to design a suitable primary structure of least possible weight for the uniform cantilever wing while satisfying the constraints imposed. It should be noted that such an optimization study on an aerospace structure with the optimization module of a commercial finite element code is especially important for aerospace companies dealing with the design and manufacturing of aerospace systems. Commercial codes give the opportunity to perform structural optimization with many design variables within a reasonable time. In the particular study the sensitivity analysis capability and the building up of the approximate model by MSC.NASTRAN[®] allowed the optimization to be completed within a short time.

Two main types of optimization are performed on the torque box of the wing. In the first optimization study only property optimization is performed. In this type of optimization design variables are related to a property of an element such as shell element thickness or cross-sectional area of a rod element. Therefore

optimizer tries to reach the optimum solution by changing the properties of elements only. In this type of optimization grid locations are not changed, so initial shape of the wing is preserved. Two optimizations are performed within the scope of property optimization. In section 6.1, an equivalent aerodynamic lift force is applied at the tip of the wing, and optimization is performed for a constant tip force and tip bending moment. In section 6.2, a distributed aerodynamic lift force and pitching moment is applied to the torque box at the rib locations. Property optimization study has been performed with these two different external load cases.

The second type of optimization study performed involves shape optimization. In MSC.NASTRAN[®] shape optimization allows optimizer to modify grid locations, thus positions of structural elements can be changed to aid in arriving at the optimum solution. In section 6.3.1, only one variable which defines change of the location of rib 2 is used in a pure shape optimization study. This study is performed to verify that the optimization tool of MSC.NASTRAN[®] changes the location of the rib correctly so that desired constraint is satisfied. As it will be described in section 6.3.1, by performing static analysis with the rib 2 displaced to the left and right of its initial position, one can actually show that whether output of the optimizer is meaningful or not. In section 6.3.2, multi-variable shape and property optimization is performed simultaneously. This example can be regarded as the most complete optimization study which not only optimizes the properties but also allows location change of the ribs along the wing span to arrive at the optimum solution.

The uniform cantilever wing studied has a 1.524 m (5 ft) chord length and 4.572 m (15 ft) semispan. NACA 2412 type of airfoil defines the cross section of the wing. The geometry of the wing in rendered form is shown in Figure 6.1.

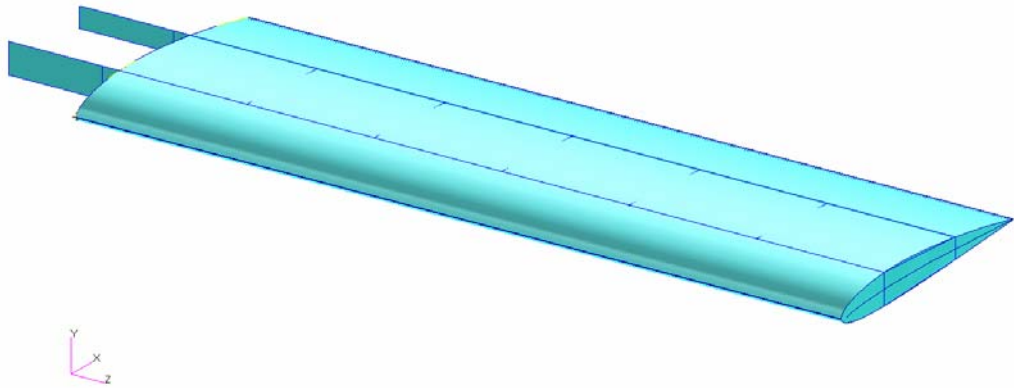


Figure 6.1 The wing model studied in optimization study

Wing is divided into 6 equal parts by the ribs. The rib located at the root is numbered 1 and the rib located at the tip is numbered 7. There are two spars on the wing, front and rear spar. Front spar is located at 25% of the chord and rear spar is located at 66% of the chord measured from the leading edge. Both spars have an extension at the root to connect the wing to the fuselage. Rib and spar locations are shown in detail in Figure 6.2.

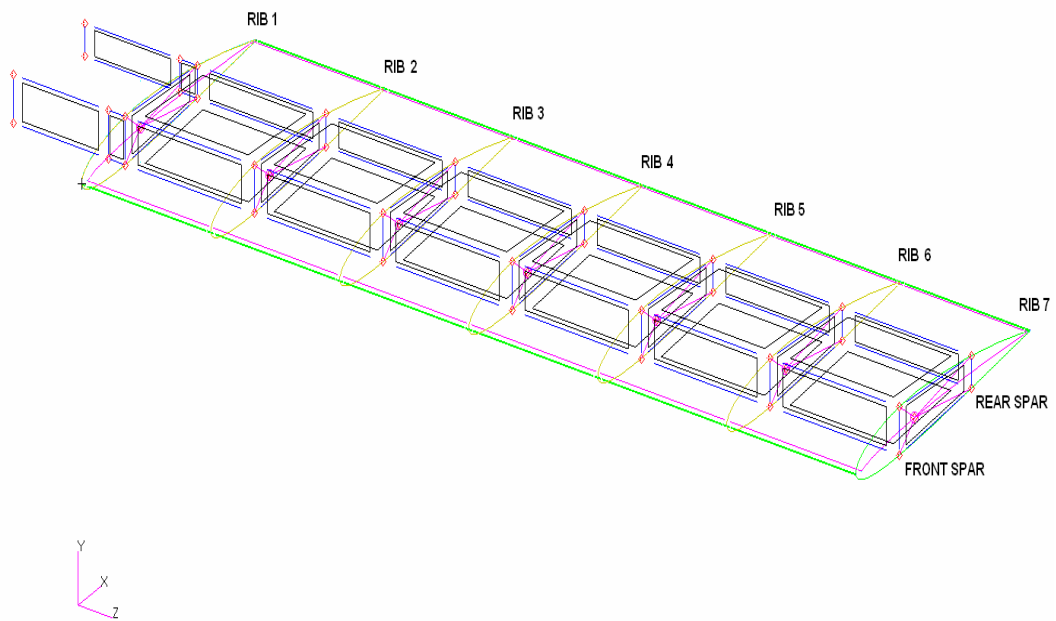


Figure 6.2 Geometry and finite element of the wing

In the finite element model rod elements are used to model the flanges of the spars and shell elements are used to model the webs and skin panels. Equivalent section option is used for the shell element properties to provide membrane effect only. For this purpose, a dummy material with relatively very low elastic modulus is chosen as the bending material. Finite element model of the wing is given in Figure 6.3. In the finite element model single shell elements are used between the ribs in the skins, and spar webs.

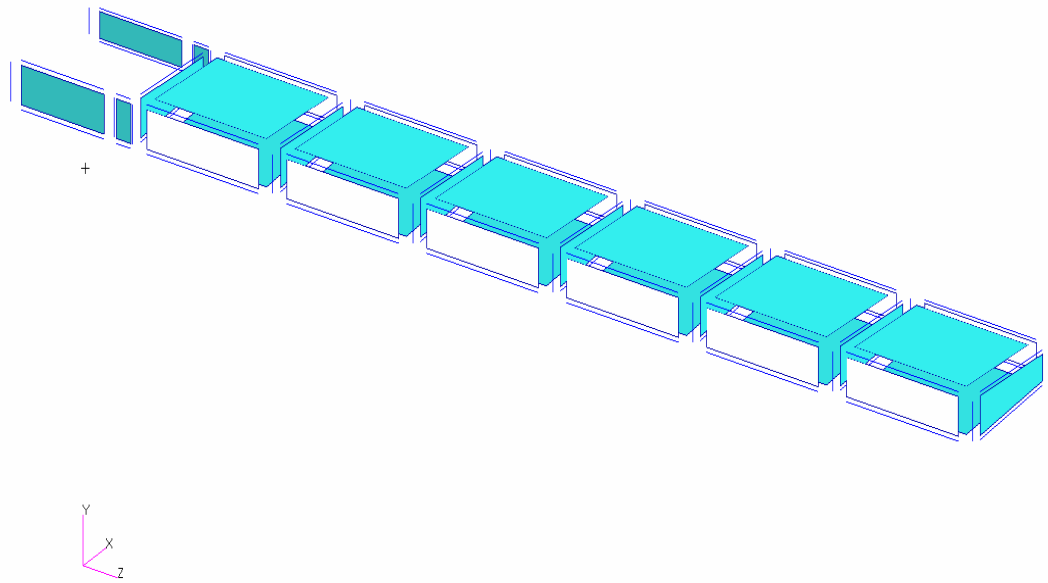


Figure 6.3 Elements of the wing model

Spars consist of a web, an upper flange and a lower flange. Element properties of front and rear spars are given in Tables 6.1 and 6.2, respectively. As it can be seen from Tables 6.1 and 6.2, the flange areas of the spars, web thicknesses and skin thicknesses change discretely between the rib stations. Thus, the flange areas, skin and web thicknesses are taken as the discrete design variables. The last three columns of the tables give the initial value, lower and upper bounds of the design variables. The thicknesses are given in mm, and the cap areas are given in mm^2 .

Table 6.1 Element properties and design variables of the front spar

| Front Spar | | | | | | |
|-----------------------|----------------|-----------------|--------------|----------------|-------------------|-------------------|
| Description | Element | Property | D. V. | Initial | Minimum | Maximum |
| Web Thickness | Number | Number | Name | Value | Value (mm) | Value (mm) |
| Rib 1 - Rib 2 | 110100 | 110100 | v001 | 1 | 0.8 | 5 |
| Rib 2 - Rib 3 | 210100 | 210100 | v002 | 1 | 0.8 | 5 |
| Rib 3 - Rib 4 | 310100 | 310100 | v003 | 1 | 0.8 | 5 |
| Rib 4 - Rib 5 | 410100 | 410100 | v004 | 1 | 0.8 | 5 |
| Rib 5 - Rib 6 | 510100 | 510100 | v005 | 1 | 0.8 | 5 |
| Rib 6 - Rib 7 | 610100 | 610100 | v006 | 1 | 0.8 | 5 |
| Upper Cap Area | | | | | | |
| Rib 1 - Rib 2 | 110200 | 110200 | v007 | 100 | 1 | 2000 |
| Rib 2 - Rib 3 | 210200 | 210200 | v008 | 100 | 1 | 2000 |
| Rib 3 - Rib 4 | 310200 | 310200 | v009 | 100 | 1 | 2000 |
| Rib 4 - Rib 5 | 410200 | 410200 | v010 | 100 | 1 | 2000 |
| Rib 5 - Rib 6 | 510200 | 510200 | v011 | 100 | 1 | 2000 |
| Rib 6 - Rib 7 | 610200 | 610200 | v012 | 100 | 1 | 2000 |
| Lower Cap Area | | | | | | |
| Rib 1 - Rib 2 | 110300 | 110300 | v013 | 100 | 1 | 2000 |
| Rib 2 - Rib 3 | 210300 | 210300 | v014 | 100 | 1 | 2000 |
| Rib 3 - Rib 4 | 310300 | 310300 | v015 | 100 | 1 | 2000 |
| Rib 4 - Rib 5 | 410300 | 410300 | v016 | 100 | 1 | 2000 |
| Rib 5 - Rib 6 | 510300 | 510300 | v017 | 100 | 1 | 2000 |
| Rib 6 - Rib 7 | 610300 | 610300 | v018 | 100 | 1 | 2000 |

Table 6.2 Element properties and design variables of the rear spar

| Rear Spar | | | | | | |
|-----------------------|----------------|-----------------|--------------|----------------|-------------------|-------------------|
| Description | Element | Property | D. V. | Initial | Minimum | Maximum |
| Web Thickness | Number | Number | Name | Value | Value (mm) | Value (mm) |
| Rib 1 - Rib 2 | 120100 | 120100 | v019 | 1 | 0.8 | 5 |
| Rib 2 - Rib 3 | 220100 | 220100 | v020 | 1 | 0.8 | 5 |
| Rib 3 - Rib 4 | 320100 | 320100 | v021 | 1 | 0.8 | 5 |
| Rib 4 - Rib 5 | 420100 | 420100 | v022 | 1 | 0.8 | 5 |
| Rib 5 - Rib 6 | 520100 | 520100 | v023 | 1 | 0.8 | 5 |
| Rib 6 - Rib 7 | 620100 | 620100 | v024 | 1 | 0.8 | 5 |
| Upper Cap Area | | | | | | |
| Rib 1 - Rib 2 | 120200 | 120200 | v025 | 100 | 1 | 2000 |
| Rib 2 - Rib 3 | 220200 | 220200 | v026 | 100 | 1 | 2000 |
| Rib 3 - Rib 4 | 320200 | 320200 | v027 | 100 | 1 | 2000 |
| Rib 4 - Rib 5 | 420200 | 420200 | v028 | 100 | 1 | 2000 |
| Rib 5 - Rib 6 | 520200 | 520200 | v029 | 100 | 1 | 2000 |
| Rib 6 - Rib 7 | 620200 | 620200 | v030 | 100 | 1 | 2000 |
| Lower Cap Area | | | | | | |
| Rib 1 - Rib 2 | 120300 | 120300 | v031 | 100 | 1 | 2000 |
| Rib 2 - Rib 3 | 220300 | 220300 | v032 | 100 | 1 | 2000 |
| Rib 3 - Rib 4 | 320300 | 320300 | v033 | 100 | 1 | 2000 |
| Rib 4 - Rib 5 | 420300 | 420300 | v034 | 100 | 1 | 2000 |
| Rib 5 - Rib 6 | 520300 | 520300 | v035 | 100 | 1 | 2000 |
| Rib 6 - Rib 7 | 620300 | 620300 | v036 | 100 | 1 | 2000 |

Finite element model and element numbering of front and rear spars are given in Figures 6.4 and 6.5 respectively.

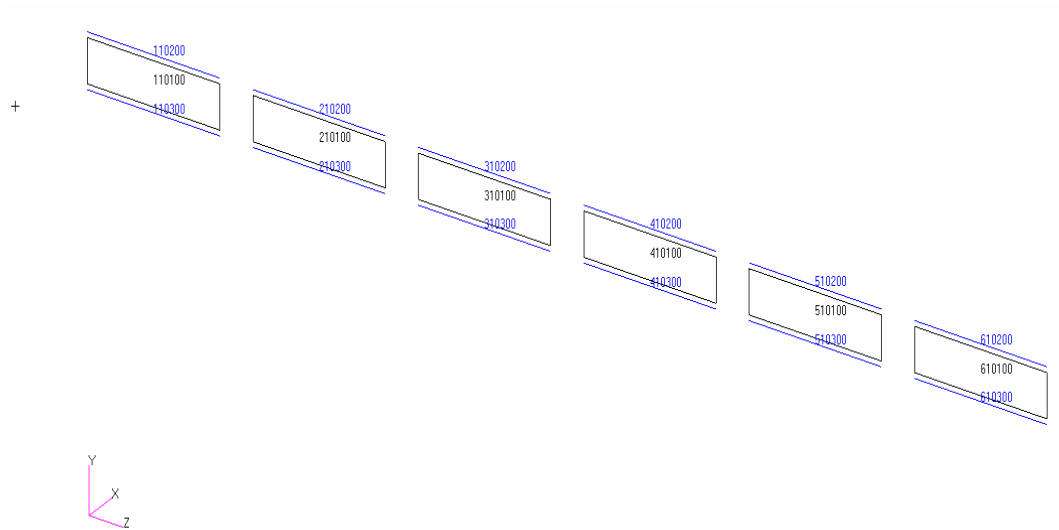


Figure 6.4 Elements of the front spar

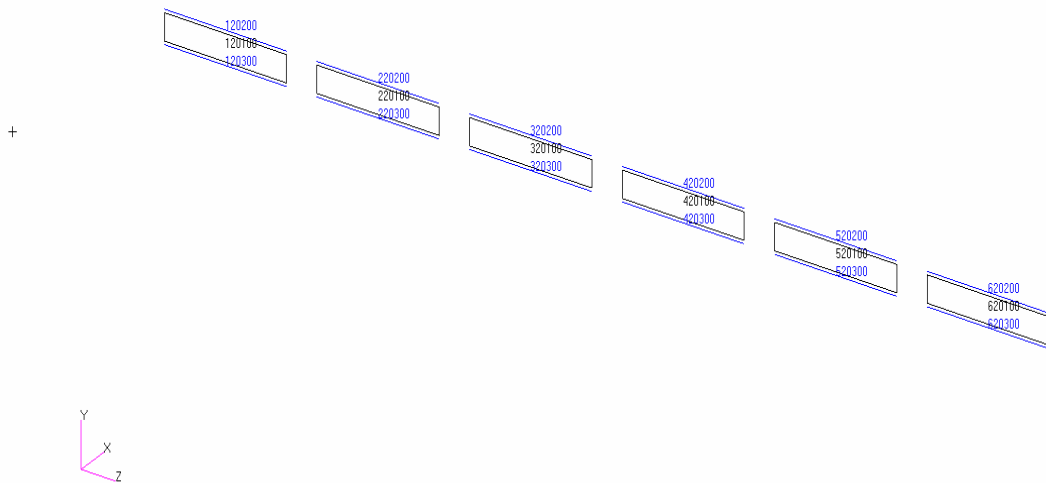


Figure 6.5 Elements of the rear spar

Skins consist of six panels. Element properties of upper and lower skin panels are given in Tables 6.3 and 6.4, respectively. The initial value of the thickness and the initial values of the lower and upper bounds are assigned arbitrarily based on experience.

Table 6.3 Element Properties and Design Variables of Upper Skin

| Upper Skin Thickness | | | | | | |
|----------------------|----------------|-----------------|------------|---------------|--------------------|--------------------|
| Description | Element Number | Property Number | D. V. Name | Initial Value | Minimum Value (mm) | Maximum Value (mm) |
| Rib 1 - Rib 2 | 110020 | 110020 | v037 | 1 | 0.8 | 5 |
| Rib 2 - Rib 3 | 210020 | 210020 | v038 | 1 | 0.8 | 5 |
| Rib 3 - Rib 4 | 310020 | 310020 | v039 | 1 | 0.8 | 5 |
| Rib 4 - Rib 5 | 410020 | 410020 | v040 | 1 | 0.8 | 5 |
| Rib 5 - Rib 6 | 510020 | 510020 | v041 | 1 | 0.8 | 5 |
| Rib 6 - Rib 7 | 610020 | 610020 | v042 | 1 | 0.8 | 5 |

Table 6.4 Element properties and design variables of lower skin

| Lower Skin Thickness | | | | | | |
|----------------------|----------------|-----------------|------------|---------------|--------------------|--------------------|
| Description | Element Number | Property Number | D. V. Name | Initial Value | Minimum Value (mm) | Maximum Value (mm) |
| Rib 1 - Rib 2 | 110030 | 110030 | v043 | 1 | 0.8 | 5 |
| Rib 2 - Rib 3 | 210030 | 210030 | v044 | 1 | 0.8 | 5 |
| Rib 3 - Rib 4 | 310030 | 310030 | v045 | 1 | 0.8 | 5 |
| Rib 4 - Rib 5 | 410030 | 410030 | v046 | 1 | 0.8 <td 5 | |
| Rib 5 - Rib 6 | 510030 | 510030 | v047 | 1 | 0.8 | 5 |
| Rib 6 - Rib 7 | 610030 | 610030 | v048 | 1 | 0.8 | 5 |

Finite element model and element numbering of upper and lower skins are given in Figures 6.6 and 6.7 respectively.

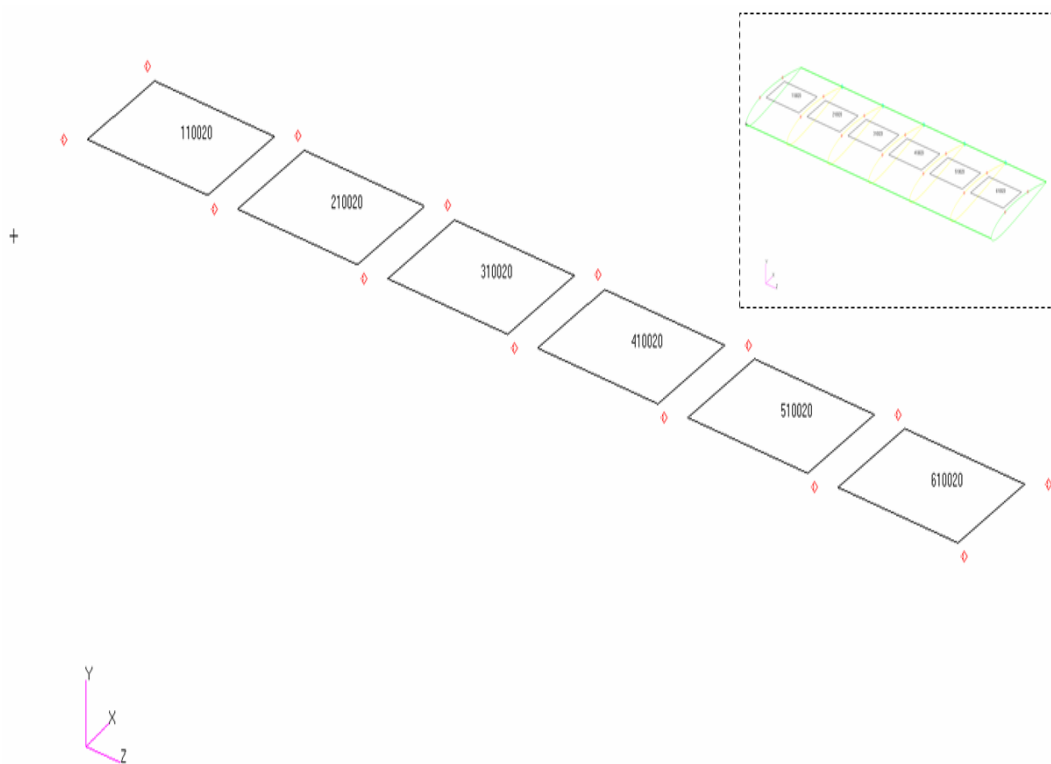


Figure 6.6 Upper skin elements

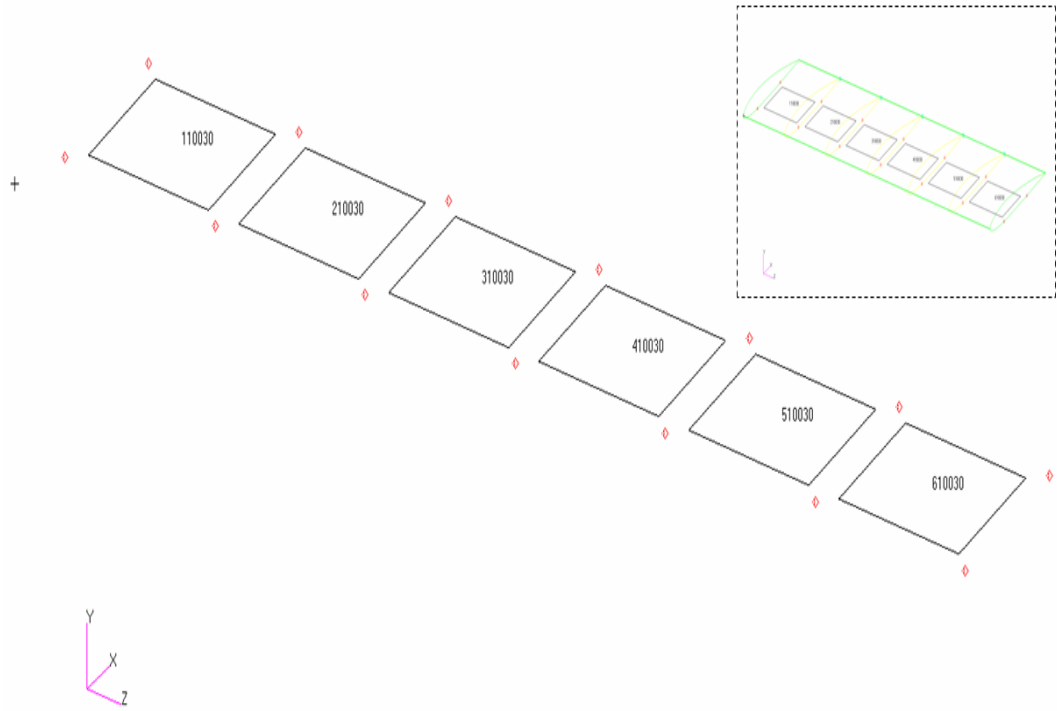


Figure 6.7 Lower skin elements

Ribs are assumed to consist of a web, an upper and a lower flange. Element properties of ribs from root to tip are given in Tables 6.5 - 6.11, respectively. Finite element model and element numbering of the ribs are given in Figures 6.8 - 6.14 from root to tip, respectively.

Table 6.5 Element properties and design variables of rib 1

| Rib 1 | | | | | | |
|-----------------------------------|----------------|-----------------|------------|---------------|---------------|---------------|
| Description | Element Number | Property Number | D. V. Name | Initial Value | Minimum Value | Maximum Value |
| Web Thickness (mm) | 111000 | 111000 | v049 | 1 | 0.8 | 5 |
| Upper Cap Area (mm ²) | 112000 | 112000 | v050 | 100 | 1 | 2000 |
| Lower Cap Area (mm ²) | 113000 | 113000 | v051 | 100 | 1 | 2000 |
| Front Cap Area (mm ²) | 114000 | 114000 | v052 | 100 | 1 | 2000 |
| Rear Cap Area (mm ²) | 124000 | 124000 | v053 | 100 | 1 | 2000 |

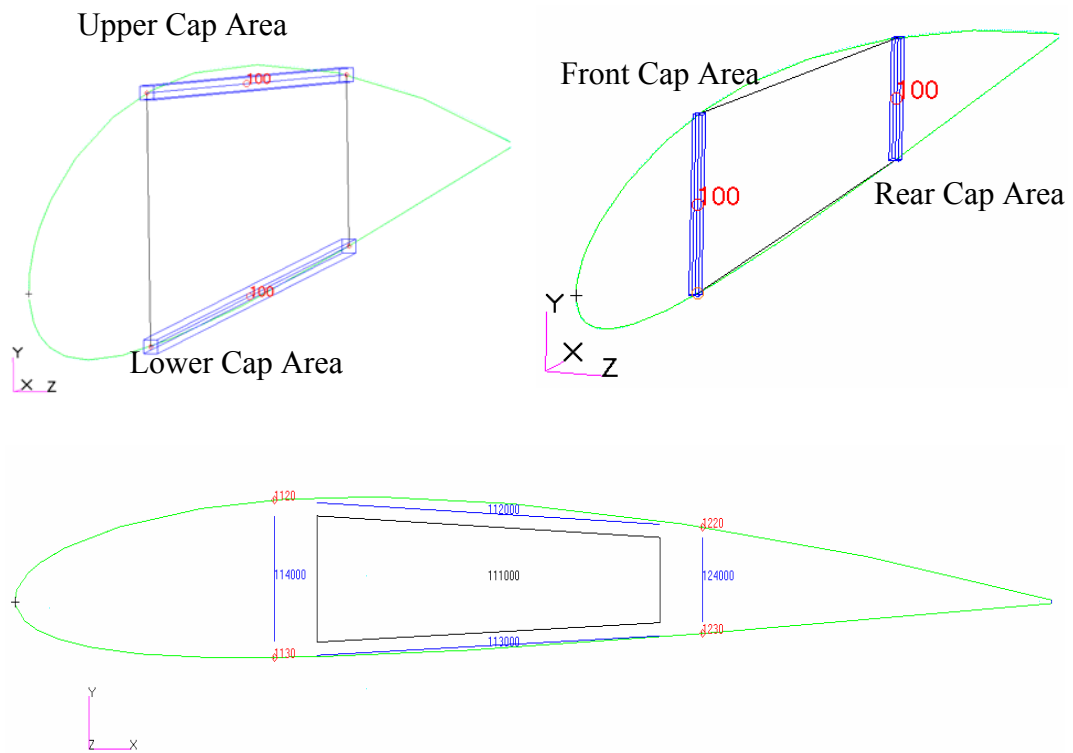


Figure 6.8 Elements of rib 1

Table 6.6 Element Properties and Design Variables of Rib 2

| Rib 2 | | | | | | |
|-----------------------------------|----------------|-----------------|------------|---------------|---------------|---------------|
| Description | Element Number | Property Number | D. V. Name | Initial Value | Minimum Value | Maximum Value |
| Web Thickness (mm) | 211000 | 211000 | v054 | 1 | 0.8 | 5 |
| Upper Cap Area (mm ²) | 212000 | 212000 | v055 | 100 | 1 | 2000 |
| Lower Cap Area (mm ²) | 213000 | 213000 | v056 | 100 | 1 | 2000 |
| Front Cap Area (mm ²) | 214000 | 214000 | v057 | 100 | 1 | 2000 |
| Rear Cap Area (mm ²) | 224000 | 224000 | v058 | 100 | 1 | 2000 |

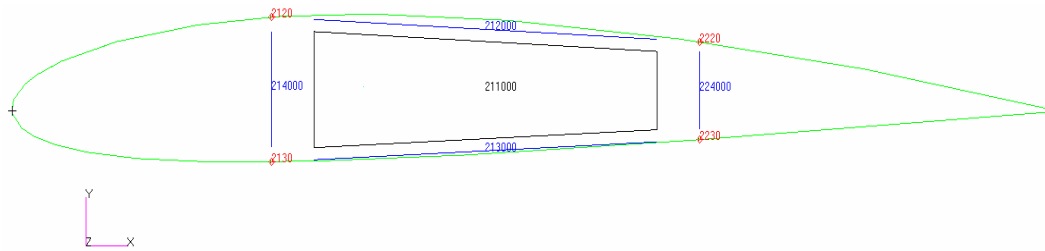


Figure 6.9 Elements of rib 2

Table 6.7 Element properties and design variables of rib 3

| Rib 3 | | | | | | |
|-----------------------------------|----------------|-----------------|------------|---------------|---------------|---------------|
| Description | Element Number | Property Number | D. V. Name | Initial Value | Minimum Value | Maximum Value |
| Web Thickness (mm) | 311000 | 311000 | v059 | 1 | 0.8 | 5 |
| Upper Cap Area (mm ²) | 312000 | 312000 | v060 | 100 | 1 | 2000 |
| Lower Cap Area (mm ²) | 313000 | 313000 | v061 | 100 | 1 | 2000 |
| Front Cap Area (mm ²) | 314000 | 314000 | v062 | 100 | 1 | 2000 |
| Rear Cap Area (mm ²) | 324000 | 324000 | v063 | 100 | 1 | 2000 |

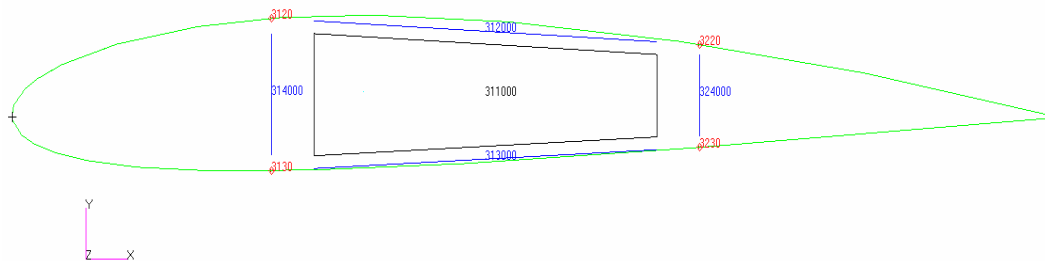


Figure 6.10 Elements of rib 3

Table 6.8 Element properties and design variables of rib 4

| Rib 4 | | | | | | |
|-----------------------------------|----------------|-----------------|------------|---------------|---------------|---------------|
| Description | Element Number | Property Number | D. V. Name | Initial Value | Minimum Value | Maximum Value |
| Web Thickness (mm) | 411000 | 411000 | v064 | 1 | 0.8 | 5 |
| Upper Cap Area (mm ²) | 412000 | 412000 | v065 | 100 | 1 | 2000 |
| Lower Cap Area (mm ²) | 413000 | 413000 | v066 | 100 | 1 | 2000 |
| Front Cap Area (mm ²) | 414000 | 414000 | v067 | 100 | 1 | 2000 |
| Rear Cap Area (mm ²) | 424000 | 424000 | v068 | 100 | 1 | 2000 |

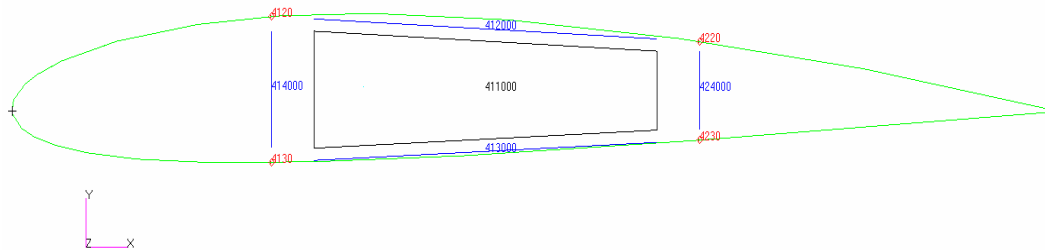


Figure 6.11 Elements of rib 4

Table 6.9 Element properties and design variables of rib 5

| Rib 5 | | | | | | |
|-----------------------------------|----------------|-----------------|------------|---------------|---------------|---------------|
| Description | Element Number | Property Number | D. V. Name | Initial Value | Minimum Value | Maximum Value |
| Web Thickness (mm) | 511000 | 511000 | v069 | 1 | 0.8 | 5 |
| Upper Cap Area (mm ²) | 512000 | 512000 | v070 | 100 | 1 | 2000 |
| Lower Cap Area (mm ²) | 513000 | 513000 | v071 | 100 | 1 | 2000 |
| Front Cap Area (mm ²) | 514000 | 514000 | v072 | 100 | 1 | 2000 |
| Rear Cap Area (mm ²) | 524000 | 524000 | v073 | 100 | 1 | 2000 |



Figure 6.12 Elements of rib 5

Table 6.10 Element properties and design variables of rib 6

| Rib 6 | | | | | | |
|-----------------------------------|----------------|-----------------|------------|---------------|---------------|---------------|
| Description | Element Number | Property Number | D. V. Name | Initial Value | Minimum Value | Maximum Value |
| Web Thickness (mm) | 611000 | 611000 | v074 | 1 | 0.8 | 5 |
| Upper Cap Area (mm ²) | 612000 | 612000 | v075 | 100 | 1 | 2000 |
| Lower Cap Area (mm ²) | 613000 | 613000 | v076 | 100 | 1 | 2000 |
| Front Cap Area (mm ²) | 614000 | 614000 | v077 | 100 | 1 | 2000 |
| Rear Cap Area (mm ²) | 624000 | 624000 | v078 | 100 | 1 | 2000 |



Figure 6.13 Elements of rib 6

Table 6.11 Element properties and design variables of rib 7

| Rib 7 | | | | | | |
|-----------------------------------|----------------|-----------------|------------|---------------|---------------|---------------|
| Description | Element Number | Property Number | D. V. Name | Initial Value | Minimum Value | Maximum Value |
| Web Thickness (mm) | 711000 | 711000 | v079 | 1 | 0.8 | 5 |
| Upper Cap Area (mm ²) | 712000 | 712000 | v080 | 100 | 1 | 2000 |
| Lower Cap Area (mm ²) | 713000 | 713000 | v081 | 100 | 1 | 2000 |
| Front Cap Area (mm ²) | 714000 | 714000 | v082 | 100 | 1 | 2000 |
| Rear Cap Area (mm ²) | 724000 | 724000 | v083 | 100 | 1 | 2000 |

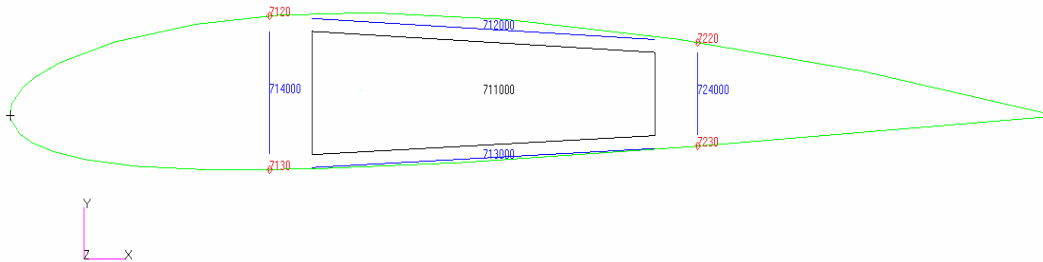


Figure 6.14 Elements of rib 7

Thus, there are 83 design variables as can be seen from Table 6.11 which lists the last five design variables.

Displacement boundary conditions are applied to nodes of extension part of the spars in all analyses and this part is not considered in the region to be optimized. Applied displacement boundary condition is shown in figure 6.15.

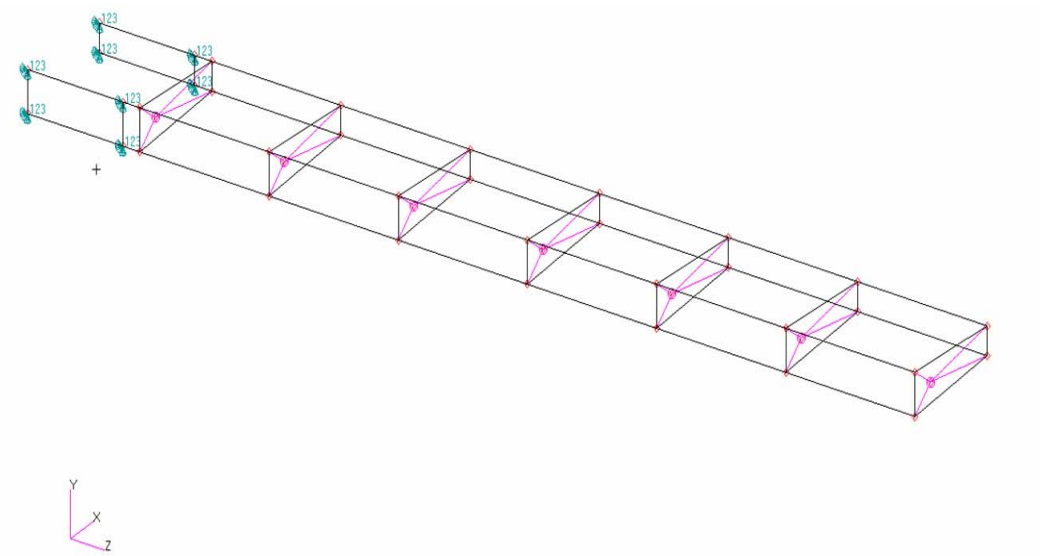


Figure 6.15 Applied displacement boundary condition

Elements to be optimized are shown in Figure 6.16 . The skin and web elements are shrunk by a certain percentage to allow one identify each structural element separately.

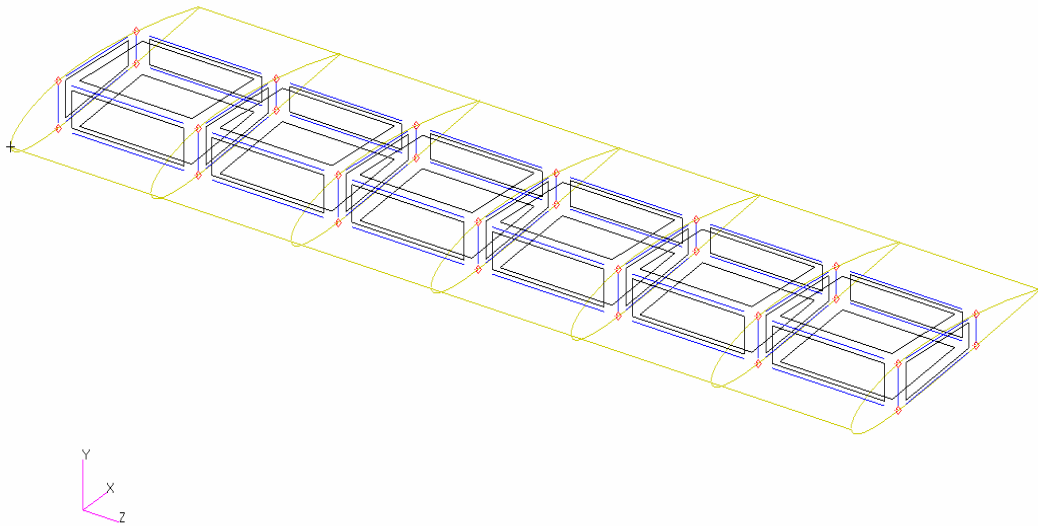


Figure 6.16 Elements to be optimized

The wing is designed for an aircraft having 1460 kg as the maximum takeoff weight, 861 kg minimum operating weight and a dive speed of 270 mile per hour. Based on this information span wise lift and pitching moment distribution is calculated in accordance with the ESDU document 95010 [12]. Span wise lift and pitching moment distributions are given in Figures 6.17 - 6.18.

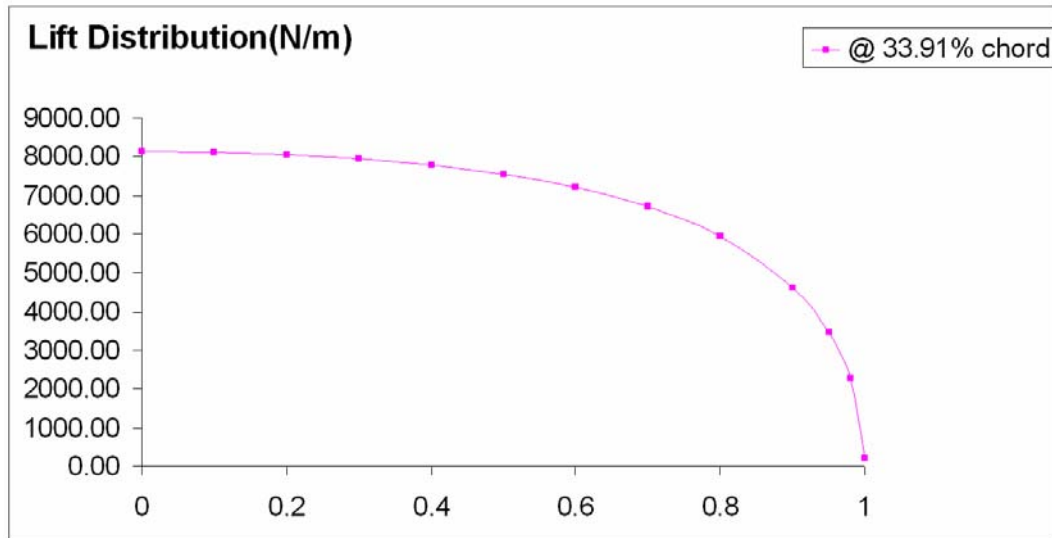


Figure 6.17 Spanwise aerodynamic lift force distribution

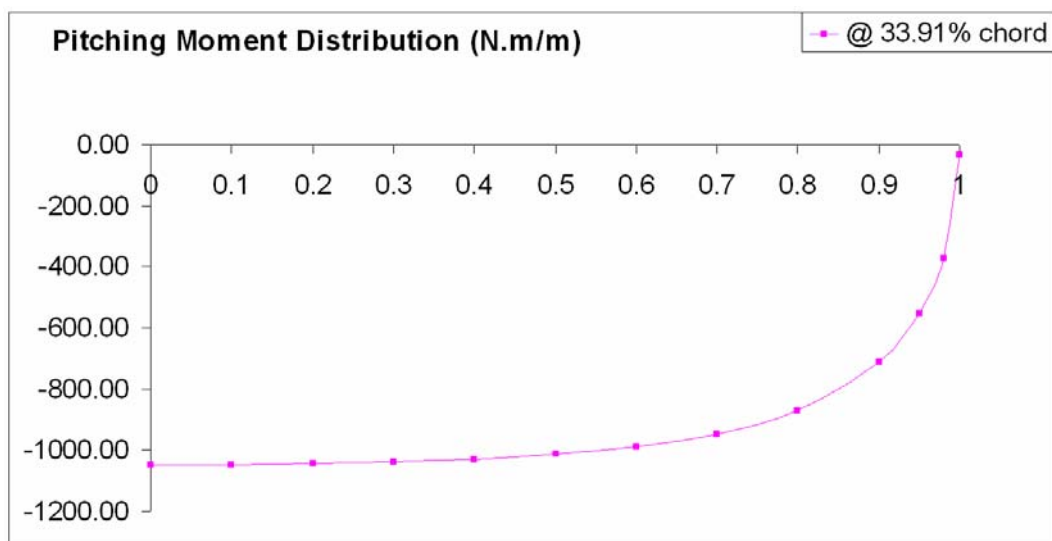


Figure 6.18 Spanwise aerodynamic pitching moment distribution

The optimization problem is defined such that the objective function is to minimize the weight of the wing subject to 87 constraints. Constraints are imposed on axial stresses in all flanges, Von Mises stresses in all webs and skins and displacements of nodes at the tip of the wing. All constraints are given in Tables 6.12 – 6.23.

Table 6.12 Design constraints related to front spar

| Front Spar | | | | | | | | |
|------------------------|----------------|-----------------|------------|------------|---------------|-------------|---------------|---------------|
| Description | Element Number | Property Number | D. R. Name | D. C. Name | Initial Value | | Minimum Value | Maximum Value |
| | | | | | Tip Loading | Distr. Load | | |
| Web Von Mises Stress | | | | | (MPa) | (MPa) | (MPa) | (MPa) |
| | 110100 | 110100 | s001 | AS001 | 224.8 | 203.3 | 0.01 | 300 |
| | 210100 | 210100 | s002 | AS002 | 218.3 | 153.9 | 0.01 | 300 |
| | 310100 | 310100 | s003 | AS003 | 219.6 | 113.5 | 0.01 | 300 |
| | 410100 | 410100 | s004 | AS004 | 219.9 | 73.5 | 0.01 | 300 |
| | 510100 | 510100 | s005 | AS005 | 216.1 | 37.5 | 0.01 | 300 |
| | 610100 | 610100 | s006 | AS006 | 237.9 | 10.2 | 0.01 | 300 |
| Upper Cap Axial Stress | | | | | | | | |
| | 110200 | 110200 | s007 | AS007 | -445.5 | -454.6 | -425 | 445 |
| | 210200 | 210200 | s008 | AS008 | -237.5 | -286.3 | -425 | 445 |
| | 310200 | 310200 | s009 | AS009 | -36.2 | -163.8 | -425 | 445 |
| | 410200 | 410200 | s010 | AS010 | 167.5 | -77.4 | -425 | 445 |
| | 510200 | 510200 | s011 | AS011 | 363.4 | -26.2 | -425 | 445 |
| | 610200 | 610200 | s012 | AS012 | 600.5 | -4.5 | -425 | 445 |
| Lower Cap Axial Stress | | | | | | | | |
| | 110300 | 110300 | s013 | AS013 | 445.5 | 454.7 | -425 | 445 |
| | 210300 | 210300 | s014 | AS014 | 237.5 | 286.3 | -425 | 445 |
| | 310300 | 310300 | s015 | AS015 | 36.2 | 163.9 | -425 | 445 |
| | 410300 | 410300 | s016 | AS016 | -167.5 | 77.4 | -425 | 445 |
| | 510300 | 510300 | s017 | AS017 | -363.5 | 26.2 | -425 | 445 |
| | 610300 | 610300 | s018 | AS018 | -600.5 | 4.5 | -425 | 445 |

Table 6.13 Design constraints related to rear spar

| Rear Spar | | | | | | | | |
|------------------------|----------------|-----------------|------------|------------|---------------|-------------|---------------|---------------|
| Description | Element Number | Property Number | D. R. Name | D. C. Name | Initial Value | | Minimum Value | Maximum Value |
| | | | | | Tip Loading | Distr. Load | | |
| Web Von Mises Stress | | | | | (MPa) | (MPa) | (MPa) | (MPa) |
| | 120100 | 120100 | s019 | AS019 | 120.5 | 107.4 | 0.01 | 300 |
| | 220100 | 220100 | s020 | AS020 | 134.7 | 96.1 | 0.01 | 300 |
| | 320100 | 320100 | s021 | AS021 | 131.8 | 67.8 | 0.01 | 300 |
| | 420100 | 420100 | s022 | AS022 | 131.3 | 44.3 | 0.01 | 300 |
| | 520100 | 520100 | s023 | AS023 | 139.6 | 22.6 | 0.01 | 300 |
| | 620100 | 620100 | s024 | AS024 | 92.0 | 6.6 | 0.01 | 300 |
| Upper Cap Axial Stress | | | | | | | | |
| | 120200 | 120200 | s025 | AS025 | -283.0 | -291.2 | -425 | 445 |
| | 220200 | 220200 | s026 | AS026 | -165.1 | -200.3 | -425 | 445 |
| | 320200 | 320200 | s027 | AS027 | -23.5 | -111.9 | -425 | 445 |
| | 420200 | 420200 | s028 | AS028 | 111.2 | -54.3 | -425 | 445 |
| | 520200 | 520200 | s029 | AS029 | 258.9 | -19.4 | -425 | 445 |
| | 620200 | 620200 | s030 | AS030 | 342.9 | -3.8 | -425 | 445 |
| Lower Cap Axial Stress | | | | | | | | |
| | 120300 | 120300 | s031 | AS031 | 283.1 | 291.3 | -425 | 445 |
| | 220300 | 220300 | s032 | AS032 | 165.2 | 200.3 | -425 | 445 |
| | 320300 | 320300 | s033 | AS033 | 23.5 | 111.9 | -425 | 445 |
| | 420300 | 420300 | s034 | AS034 | -111.3 | 54.3 | -425 | 445 |
| | 520300 | 520300 | s035 | AS035 | -258.9 | 19.4 | -425 | 445 |
| | 620300 | 620300 | s036 | AS036 | -343.0 | 3.8 | -425 | 445 |

Table 6.14 Design constraints related to upper skin

| Upper Skin Von Mises Stress | | | | | | | | |
|-----------------------------|----------------|-----------------|------------|------------|---------------|-------------|---------------|---------------|
| Description | Element Number | Property Number | D. R. Name | D. C. Name | Initial Value | | Minimum Value | Maximum Value |
| | | | | | Tip Loading | Distr. Load | | |
| | | | | | (MPa) | (MPa) | | |
| | 110020 | 110020 | s037 | AS037 | 370.1 | 378.9 | 0.01 | 281 |
| | 210020 | 210020 | s038 | AS038 | 207.9 | 249.9 | 0.01 | 281 |
| | 310020 | 310020 | s039 | AS039 | 38.8 | 141.3 | 0.01 | 281 |
| | 410020 | 410020 | s040 | AS040 | 144.2 | 67.9 | 0.01 | 281 |
| | 510020 | 510020 | s041 | AS041 | 319.6 | 23.8 | 0.01 | 281 |
| | 610020 | 610020 | s042 | AS042 | 479.7 | 4.6 | 0.01 | 281 |

Table 6.15 Design constraints related to lower skin

| Lower Skin Von Mises Stress | | | | | | | | |
|-----------------------------|----------------|-----------------|------------|------------|---------------|-------------|---------------|---------------|
| Description | Element Number | Property Number | D. R. Name | D. C. Name | Initial Value | | Minimum Value | Maximum Value |
| | | | | | Tip Loading | Distr. Load | | |
| | | | | | (MPa) | (MPa) | | |
| | 110030 | 110030 | s043 | AS043 | 370.1 | 379.0 | 0.01 | 281 |
| | 210030 | 210030 | s044 | AS044 | 207.9 | 250.0 | 0.01 | 281 |
| | 310030 | 310030 | s045 | AS045 | 38.8 | 141.4 | 0.01 | 281 |
| | 410030 | 410030 | s046 | AS046 | 144.2 | 67.9 | 0.01 | 281 |
| | 510030 | 510030 | s047 | AS047 | 319.7 | 23.8 | 0.01 | 281 |
| | 610030 | 610030 | s048 | AS048 | 479.8 | 4.6 | 0.01 | 281 |

Table 6.16 Design constraints related to rib 1

| Rib 1 | | | | | | | | |
|------------------------|----------------|-----------------|------------|------------|---------------|-------------|---------------|---------------|
| Description | Element Number | Property Number | D. R. Name | D. C. Name | Initial Value | | Minimum Value | Maximum Value |
| | | | | | Tip Loading | Distr. Load | | |
| | | | | | (MPa) | (MPa) | | |
| Web Von Mises Stress | 111000 | 111000 | s049 | AS049 | 10.3 | 8.5 | 0.01 | 300 |
| Upper Cap Axial Stress | 112000 | 112000 | s050 | AS050 | 82.7 | 83.4 | -425 | 445 |
| Lower Cap Axial Stress | 113000 | 113000 | s051 | AS051 | -82.7 | -83.4 | -425 | 445 |
| Front Cap Axial Stress | 114000 | 114000 | s052 | AS052 | 0.0 | 0.0 | -425 | 445 |
| Rear Cap Axial Stress | 124000 | 124000 | s053 | AS053 | 0.0 | 0.0 | -425 | 445 |

Table 6.17 Design constraints related to rib 2

| Rib 2 | | | | | | | | |
|------------------------|----------------|-----------------|------------|------------|---------------|-------------|---------------|---------------|
| Description | Element Number | Property Number | D. R. Name | D. C. Name | Initial Value | | Minimum Value | Maximum Value |
| | | | | | Tip Loading | Distr. Load | | |
| | | | | | (MPa) | (MPa) | | |
| Web Von Mises Stress | 211000 | 211000 | s054 | AS054 | 7.1 | 3.4 | 0.01 | 300 |
| Upper Cap Axial Stress | 212000 | 212000 | s055 | AS055 | 92.6 | 98.5 | -425 | 445 |
| Lower Cap Axial Stress | 213000 | 213000 | s056 | AS056 | -92.6 | -98.5 | -425 | 445 |
| Front Cap Axial Stress | 214000 | 214000 | s057 | AS057 | 0.0 | 0.0 | -425 | 445 |
| Rear Cap Axial Stress | 224000 | 224000 | s058 | AS058 | 0.0 | 0.0 | -425 | 445 |

Table 6.18 Design constraints related to rib 3

| Rib 3 Description | Element Number | Property Number | D. R. Name | D. C. Name | Initial Value | | Minimum Value | Maximum Value |
|------------------------|----------------|-----------------|------------|------------|---------------|-------------|---------------|---------------|
| | | | | | Tip Loading | Distr. Load | | |
| | | | | | (MPa) | (MPa) | | |
| Web Von Mises Stress | 311000 | 311000 | s059 | AS059 | 2.8 | 7.0 | 0.01 | 300 |
| Upper Cap Axial Stress | 312000 | 312000 | s060 | AS060 | 31.1 | 51.2 | -425 | 445 |
| Lower Cap Axial Stress | 313000 | 313000 | s061 | AS061 | -31.1 | -51.2 | -425 | 445 |
| Front Cap Axial Stress | 314000 | 314000 | s062 | AS062 | 0.0 | 0.0 | -425 | 445 |
| Rear Cap Axial Stress | 324000 | 324000 | s063 | AS063 | 0.0 | 0.0 | -425 | 445 |

Table 6.19 Design constraints related to rib 4

| Rib 4 Description | Element Number | Property Number | D. R. Name | D. C. Name | Initial Value | | Minimum Value | Maximum Value |
|------------------------|----------------|-----------------|------------|------------|---------------|-------------|---------------|---------------|
| | | | | | Tip Loading | Distr. Load | | |
| | | | | | (MPa) | (MPa) | | |
| Web Von Mises Stress | 411000 | 411000 | s064 | AS064 | 0.1 | 3.9 | 0.01 | 300 |
| Upper Cap Axial Stress | 412000 | 412000 | s065 | AS065 | -15.7 | 28.5 | -425 | 445 |
| Lower Cap Axial Stress | 413000 | 413000 | s066 | AS066 | 15.7 | -28.5 | -425 | 445 |
| Front Cap Axial Stress | 414000 | 414000 | s067 | AS067 | 0.0 | 0.0 | -425 | 445 |
| Rear Cap Axial Stress | 424000 | 424000 | s068 | AS068 | 0.0 | 0.0 | -425 | 445 |

Table 6.20 Design constraints related to rib 5

| Rib 5 Description | Element Number | Property Number | D. R. Name | D. C. Name | Initial Value | | Minimum Value | Maximum Value |
|------------------------|----------------|-----------------|------------|------------|---------------|-------------|---------------|---------------|
| | | | | | Tip Loading | Distr. Load | | |
| | | | | | (MPa) | (MPa) | | |
| Web Von Mises Stress | 511000 | 511000 | s069 | AS069 | 7.3 | 3.4 | 0.01 | 300 |
| Upper Cap Axial Stress | 512000 | 512000 | s070 | AS070 | -63.3 | 11.5 | -425 | 445 |
| Lower Cap Axial Stress | 513000 | 513000 | s071 | AS071 | 63.3 | -11.5 | -425 | 445 |
| Front Cap Axial Stress | 514000 | 514000 | s072 | AS072 | 0.0 | 0.0 | -425 | 445 |
| Rear Cap Axial Stress | 524000 | 524000 | s073 | AS073 | 0.0 | 0.0 | -425 | 445 |

Table 6.21 Design constraints related to rib 6

| Rib 6 Description | Element Number | Property Number | D. R. Name | D. C. Name | Initial Value | | Minimum Value | Maximum Value |
|------------------------|----------------|-----------------|------------|------------|---------------|-------------|---------------|---------------|
| | | | | | Tip Loading | Distr. Load | | |
| | | | | | (MPa) | (MPa) | | |
| Web Von Mises Stress | 611000 | 611000 | s074 | AS074 | 28.8 | 2.2 | 0.01 | 300 |
| Upper Cap Axial Stress | 612000 | 612000 | s075 | AS075 | -122.1 | 3.0 | -425 | 445 |
| Lower Cap Axial Stress | 613000 | 613000 | s076 | AS076 | 122.2 | -3.0 | -425 | 445 |
| Front Cap Axial Stress | 614000 | 614000 | s077 | AS077 | 0.0 | 0.0 | -425 | 445 |
| Rear Cap Axial Stress | 624000 | 624000 | s078 | AS078 | 0.0 | 0.0 | -425 | 445 |

Table 6.22 Design constraints related to rib 7

| Rib 7 Description | Element Number | Property Number | D. R. Name | D. C. Name | Initial Value | | Minimum Value (MPa) | Maximum Value (MPa) |
|------------------------|----------------|-----------------|------------|------------|----------------------|-------------------|---------------------|---------------------|
| | | | | | Tip Loading (MPa) | Distr. Load (MPa) | | |
| | | | | | Web Von Mises Stress | 711000 | | |
| Upper Cap Axial Stress | 712000 | 712000 | s080 | AS080 | -121.2 | 0.3 | -425 | 445 |
| Lower Cap Axial Stress | 713000 | 713000 | s081 | AS081 | 121.2 | -0.3 | -425 | 445 |
| Front Cap Axial Stress | 714000 | 714000 | s082 | AS082 | 0.0 | 0.0 | -425 | 445 |
| Rear Cap Axial Stress | 724000 | 724000 | s083 | AS083 | 0.0 | 0.0 | -425 | 445 |

Table 6.23 Design constraints related to displacements at rib 7

| Rib 7 | | | | | | |
|----------|------|-----|-----------|--------------------|------------------|------------------|
| D.R.Name | Node | DOF | D.C. Name | Initial Value (mm) | Upper Bound (mm) | Lower Bound (mm) |
| D201 | 7120 | Tz | D201 | 0.00 | -0.001 | -200 |
| D202 | 7220 | Tz | D202 | 0.00 | -0.001 | -200 |
| D203 | 7130 | Tz | D203 | 0.00 | -0.001 | -200 |
| D204 | 7230 | Tz | D204 | 0.00 | -0.001 | -200 |

6.1 OPTIMIZATION OF THE WING WITH TIP LOADING

This section describes the optimization of the wing subject to tip loading only. Equivalent aerodynamic lift force and pitching moment are applied on a node, which is created at 33.91% chord and on the camber line, at wing tip location as two concentrated loads. Rigid element RBE3 of MSC.NASTRAN[®] is used to distribute the applied load to the nodes of rib 7 which is the rib at the tip of the wing. Applied displacement boundary condition and distribution of the tip load are shown in Figure 6.19.

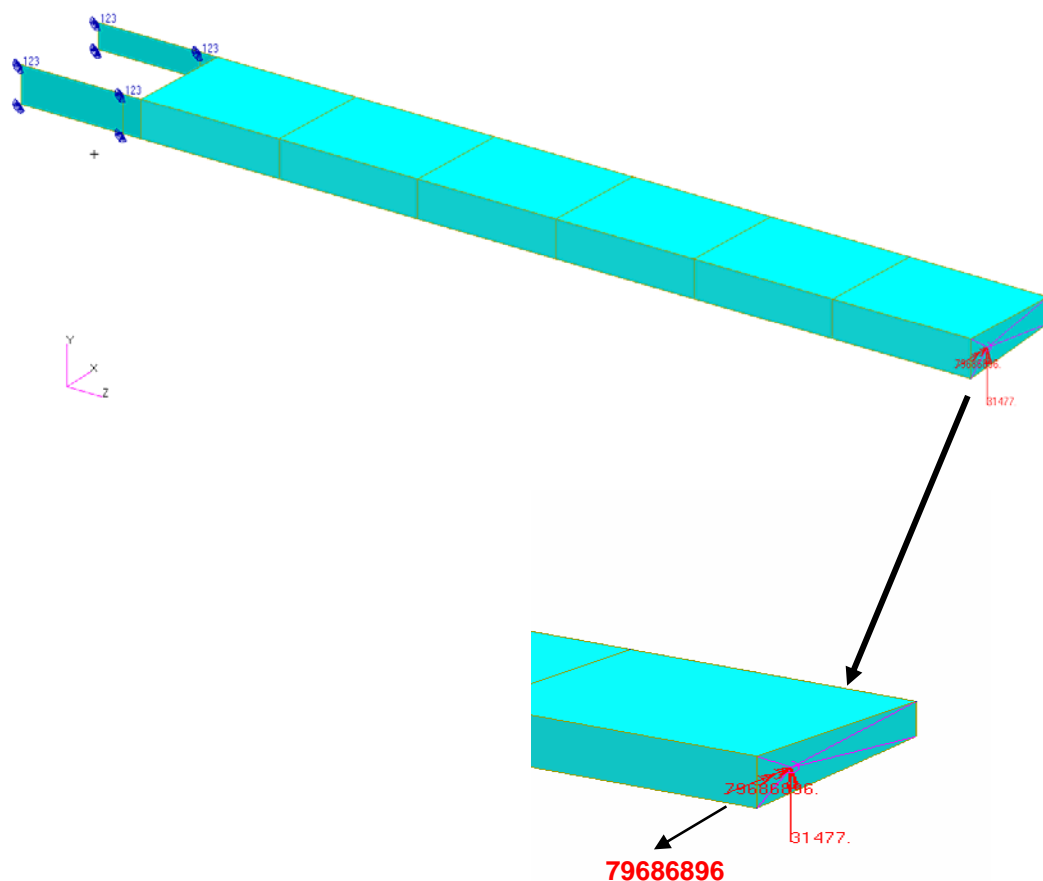


Figure 6.19 Initial wing model with tip loading

Initial analysis results are shown in Figures 6.20 – 6.23. These results belong to the wing with the initial values of the design variables.

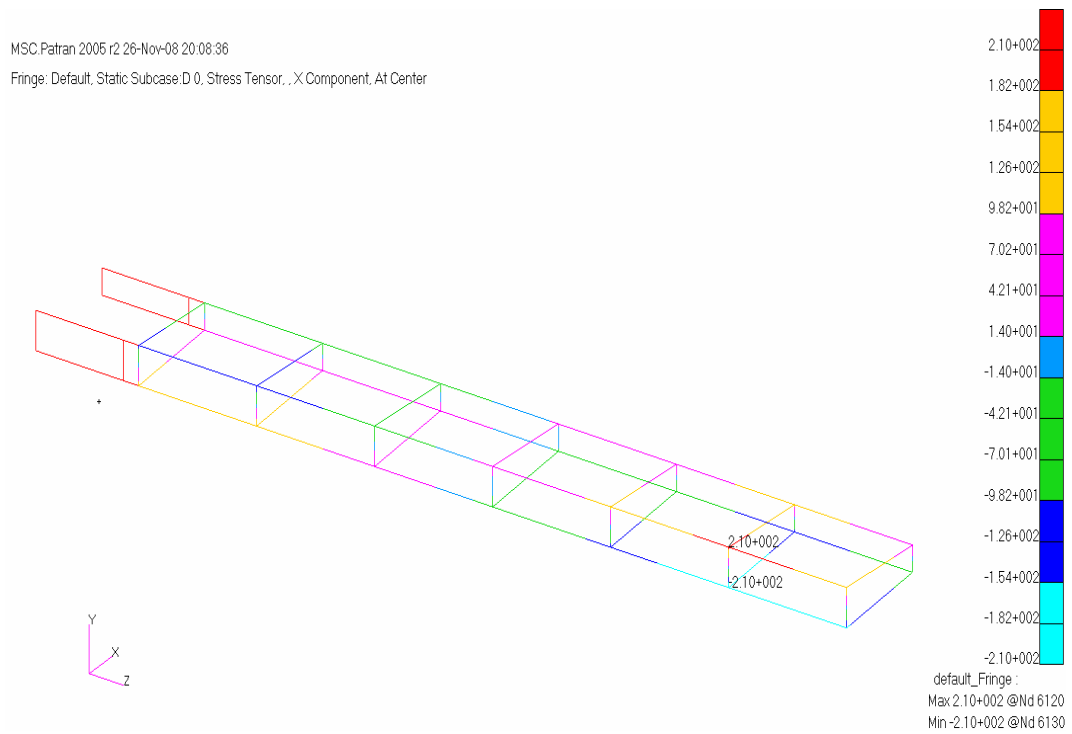


Figure 6.20 Initial axial stresses on the flanges

MSC.Patran 2005 r2 26-Nov-08 20:58:50

Fringe: Default, Static Subcase:D 0, Stress Tensor, von Mises, 2 of 3 layers (Maximum)

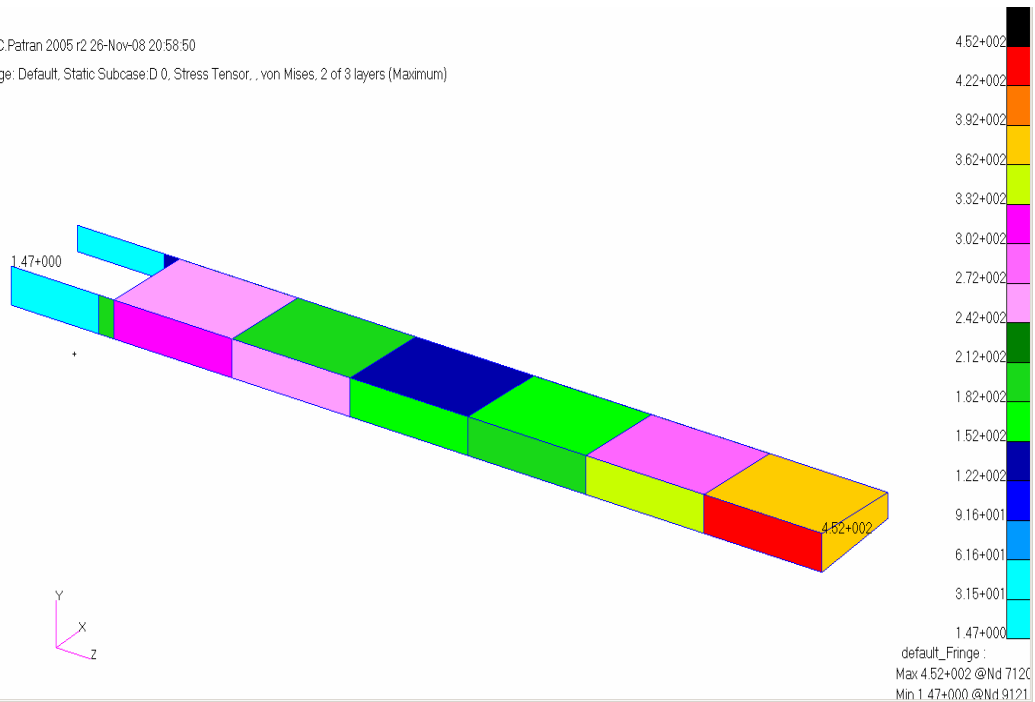


Figure 6.21 Initial Von Mises stresses on the skins and the webs

It should be noted that since the total external load is applied in a concentrated fashion at the wing tip, the stresses in the elements near the application point of the external force are found to be higher compared to the stresses in the rest of the elements of the wing. Axial stresses on the flanges also show similar behavior. Away from the wing tip, the stresses are seen to increase towards the root of the wing, as expected.

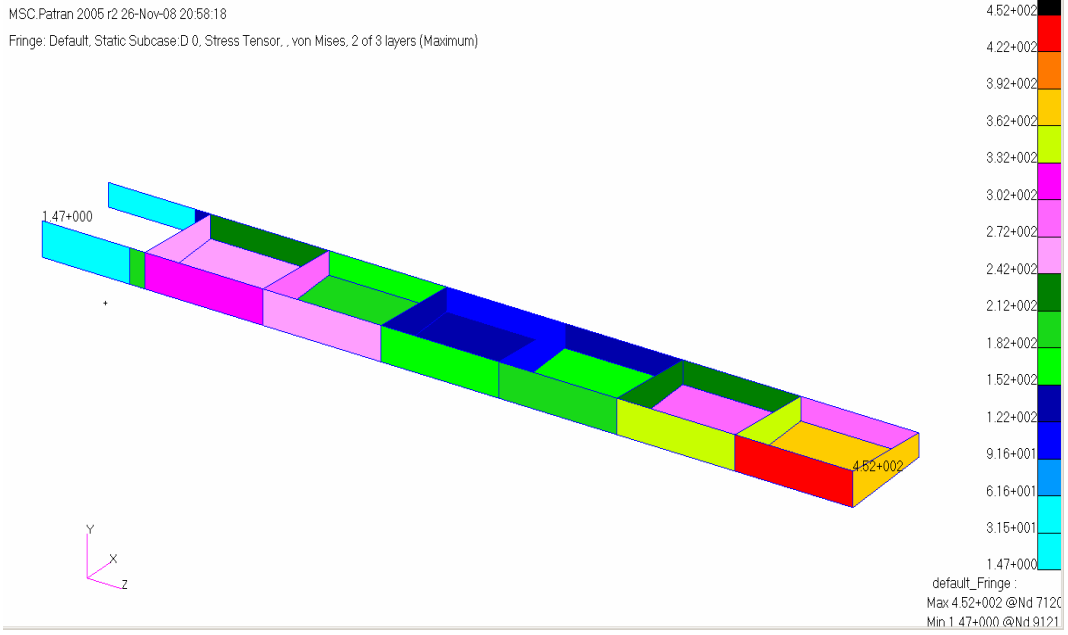


Figure 6.22 Initial Von Mises stresses on the skins and the webs interior view

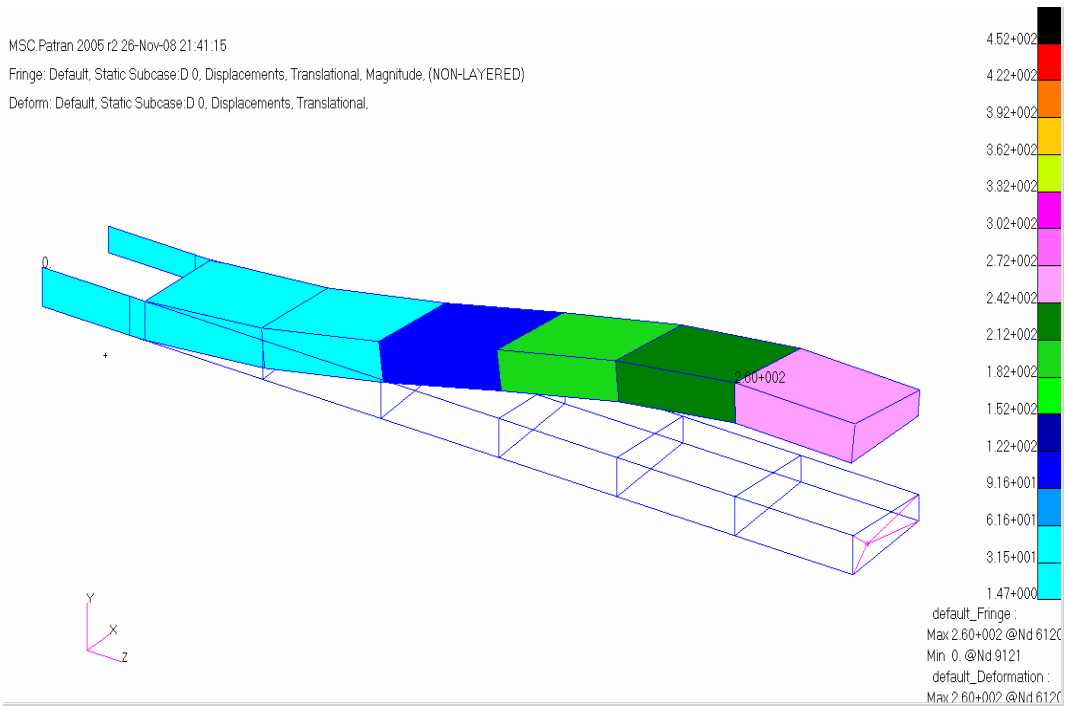


Figure 6.23 Initial deflection of the wing

The optimized element properties of the wing model are shown in Figures 6.24-6-29. These figures give the color plot representation of the final flange areas, skin, web and rib thicknesses. As it was discussed before, the element properties are allowed to change discretely between the rib stations. To reduce the number of design variables single elements were used to model the structure between the rib stations. Therefore, at the end of the solution single colors are assigned to the flange areas, skin and webs between the rib stations and ribs. Solution took 12.578 seconds of CPU time.

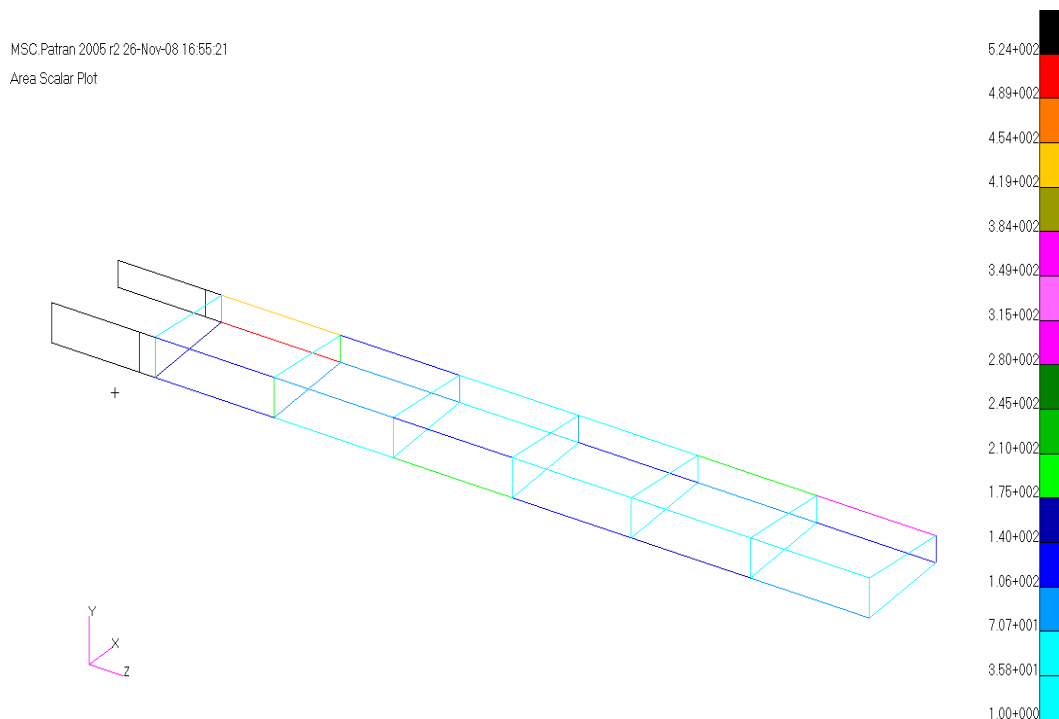


Figure 6.24 Final flange areas on the wing model

MSC Patran 2005 r2 26-Nov-08 21:46:10
Thickness Scalar Plot

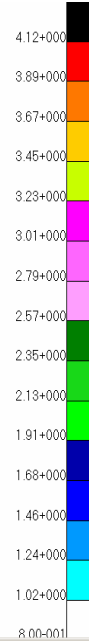
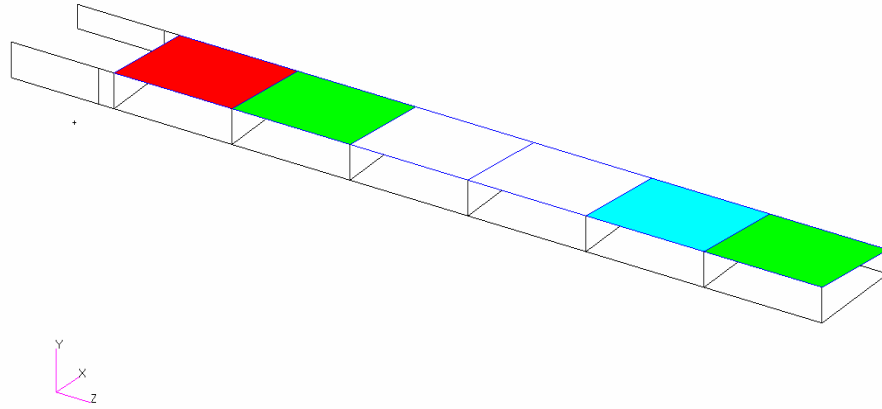


Figure 6.25 Final upper skin thicknesses of the wing model

MSC Patran 2005 r2 26-Nov-08 21:46:46
Thickness Scalar Plot

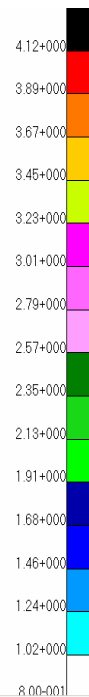
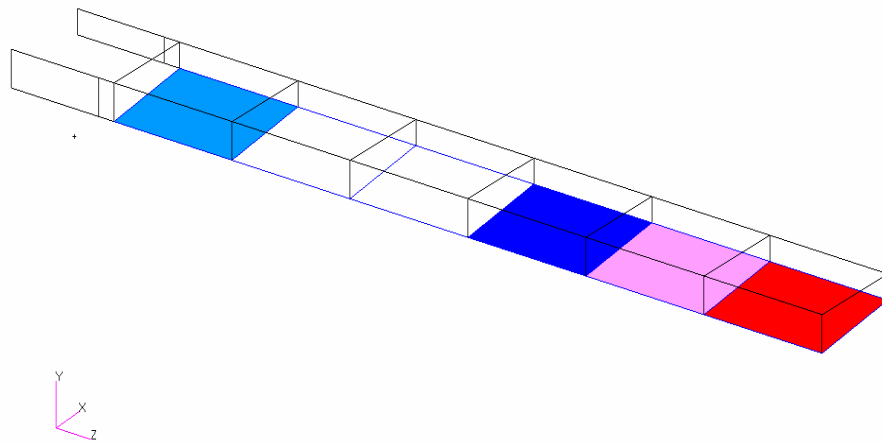


Figure 6.26 Final lower skin thicknesses of the wing model

MSC Patran 2005 r2 26-Nov-08 21:51:54
Thickness Scalar Plot

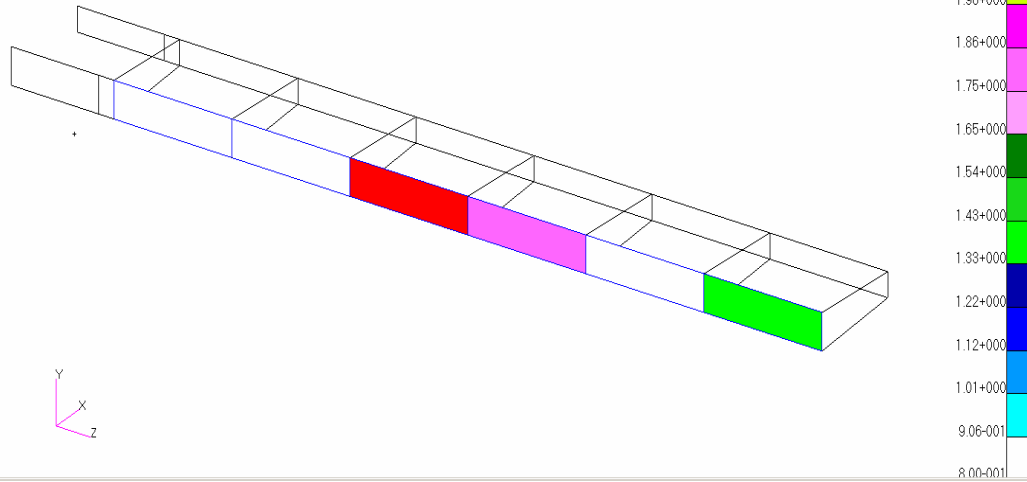


Figure 6.27 Final front spar thicknesses of the wing model

MSC Patran 2005 r2 26-Nov-08 21:53:10
Thickness Scalar Plot

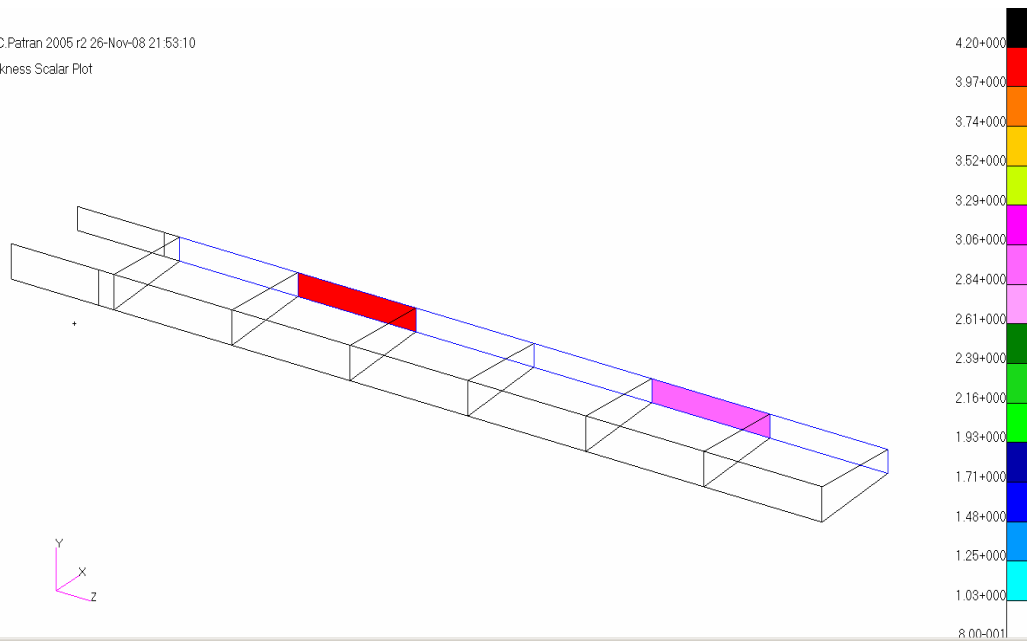


Figure 6.28 Final rear spar thicknesses of the wing model

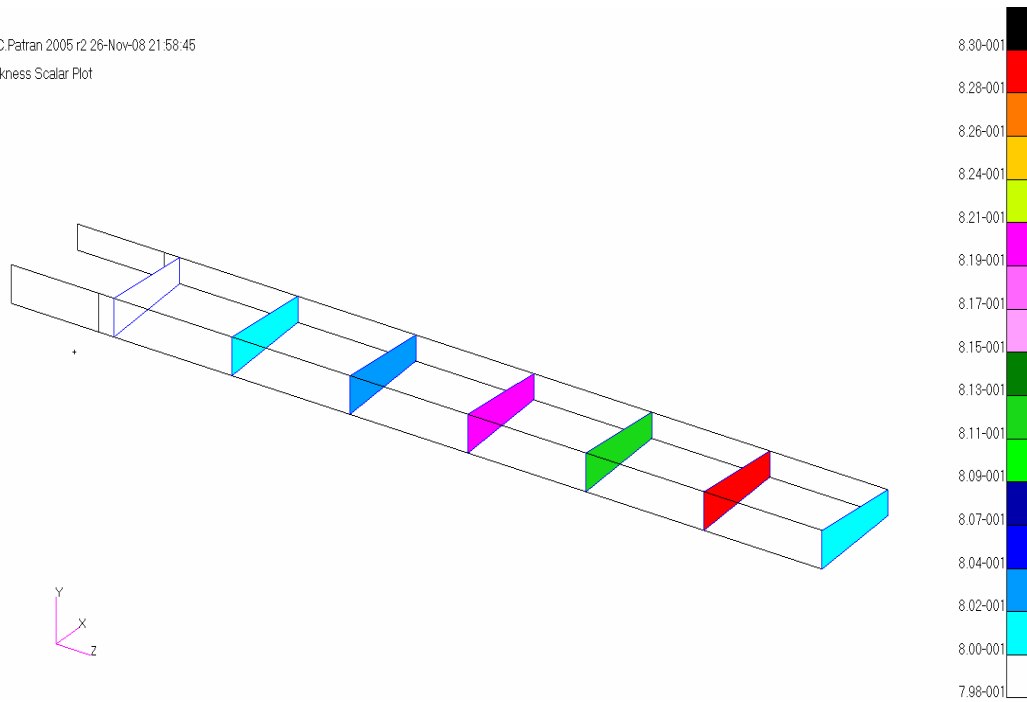


Figure 6.29 Final rib web thicknesses of the wing model

Final analysis results are shown in figures 6.30 – 6.33

MSC.Patran 2005 r2 26-Nov-08 20:07:23
Fringe: Default, Static Subcase:D 27, Stress Tensor, , X Component, At Center

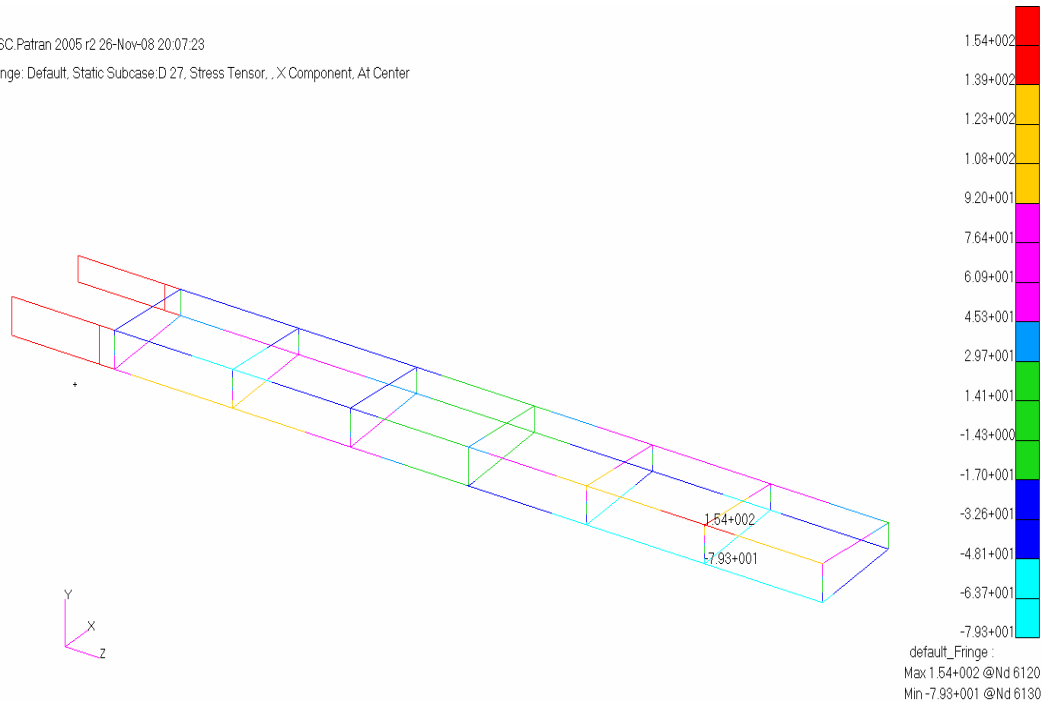


Figure 6.30 Final axial stresses on the flanges

MSC.Patran 2005 r2 26-Nov-08 20:59:23
Fringe: Default, Static Subcase:D 27, Stress Tensor, , von Mises, 2 of 3 layers (Maximum)

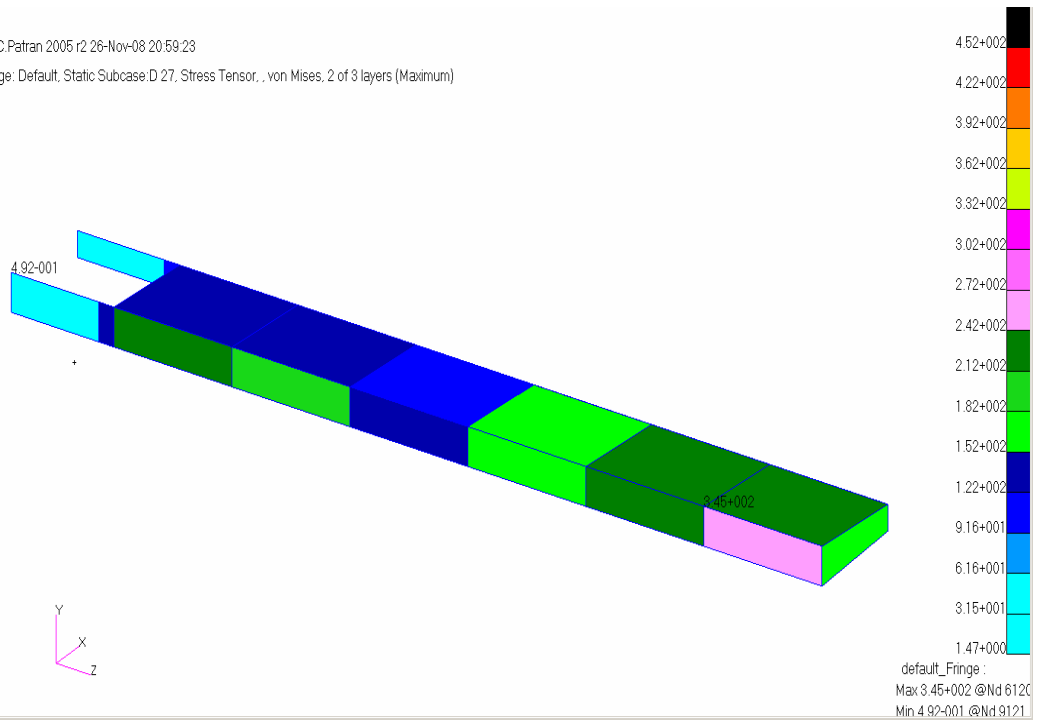


Figure 6.31 Final Von Mises stresses on the skins and the webs

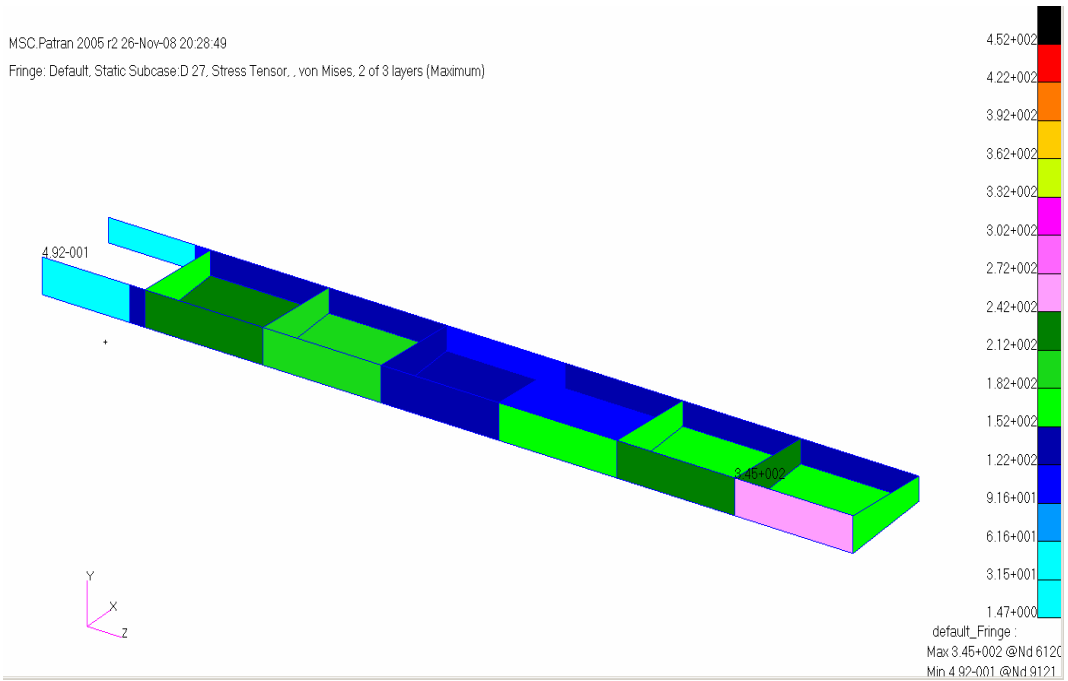


Figure 6.32 Final Von Mises stresses on the skins and the webs interior view

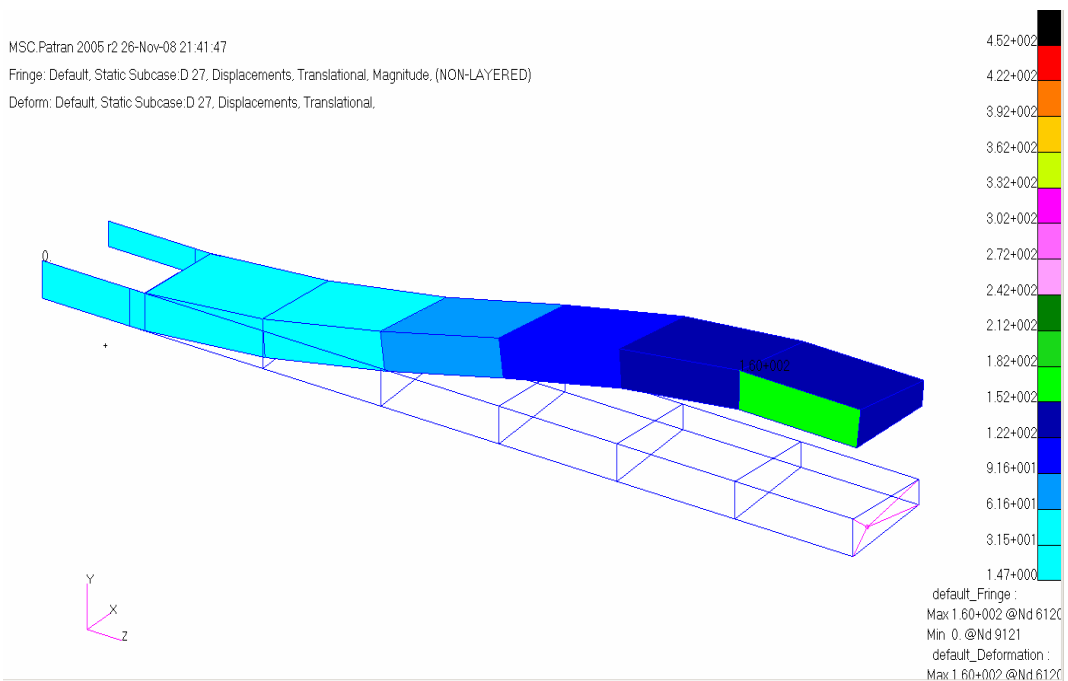


Figure 6.33 Final deflection of the wing

History of objective function which is the total weight of the wing is shown in Figure 6.34. The optimized weight is determined to be 57.7 kg, and it can be concluded that with the initial values of the design variables the constraints are not all satisfied and therefore the objective function increases until the constraints are satisfied.

Figures 6.35-6.50 show the history of all the design variables until the optimum solution is reached. It can be observed from these figures that except for the flange areas of the ribs most of the design variables increase compared to their initial values and this observation is in accordance with the variation of the objective function with the design cycle. In Figures 6.35-6.50 the thicknesses are given in mm and cap areas are given in mm².

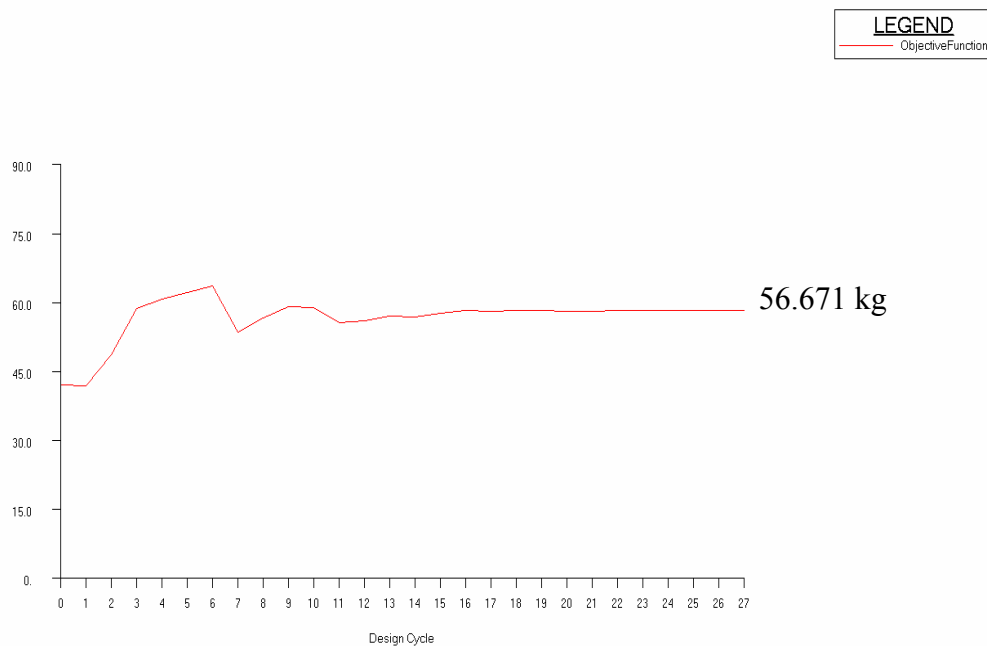


Figure 6.34 History of objective function (in kg)



for legend refer to table 6.4

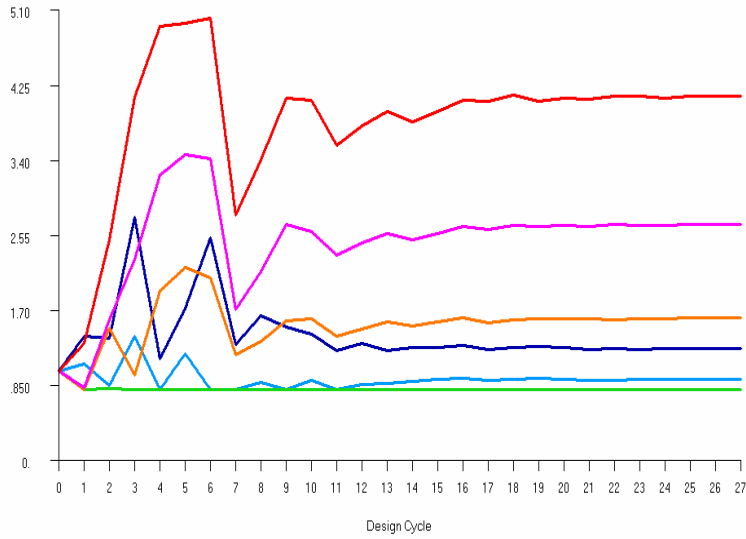


Figure 6.35 History of lower skin thicknesses (in mm)



for legend refer to table 6.3

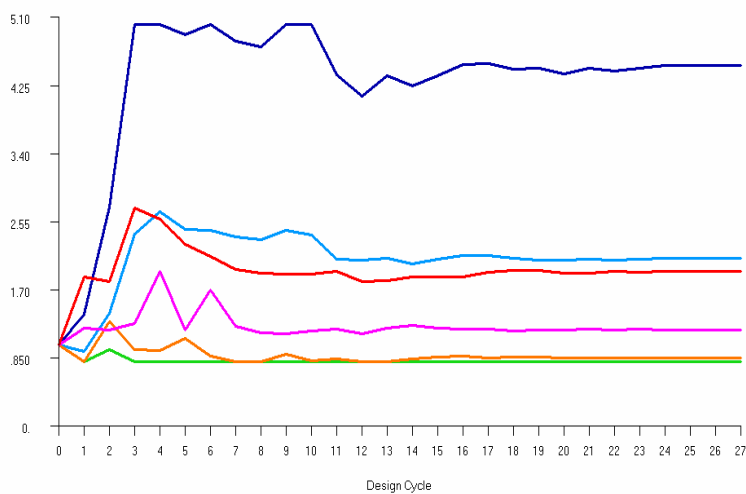


Figure 6.36 History of upper skin thicknesses (in mm)

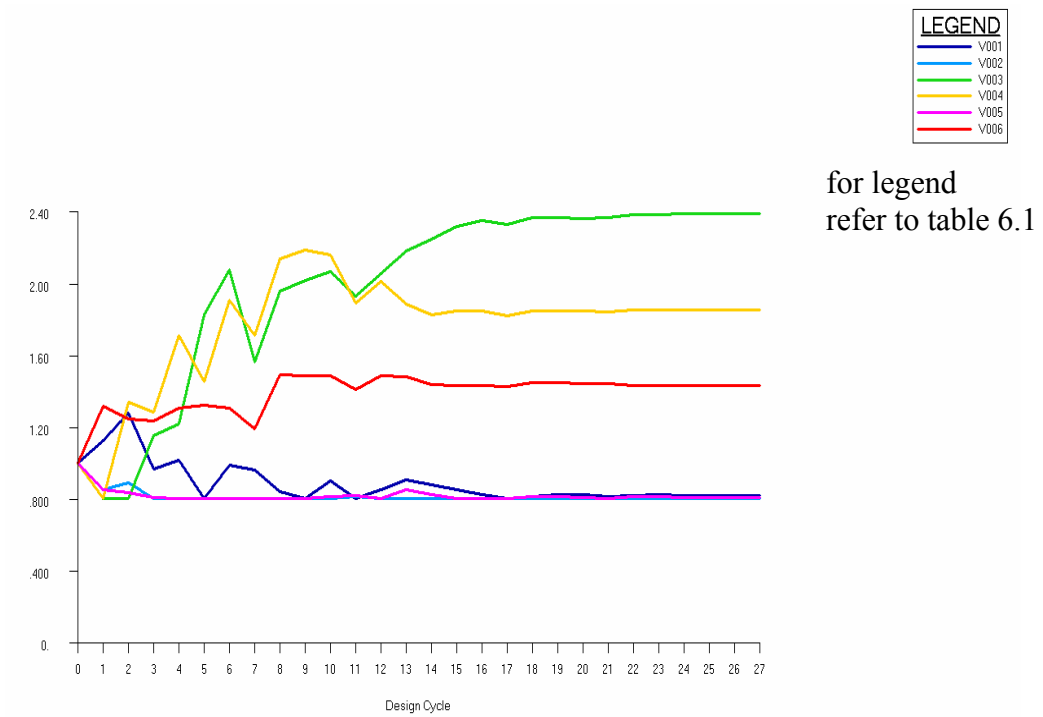


Figure 6.37 History of front spar web thicknesses (in mm)

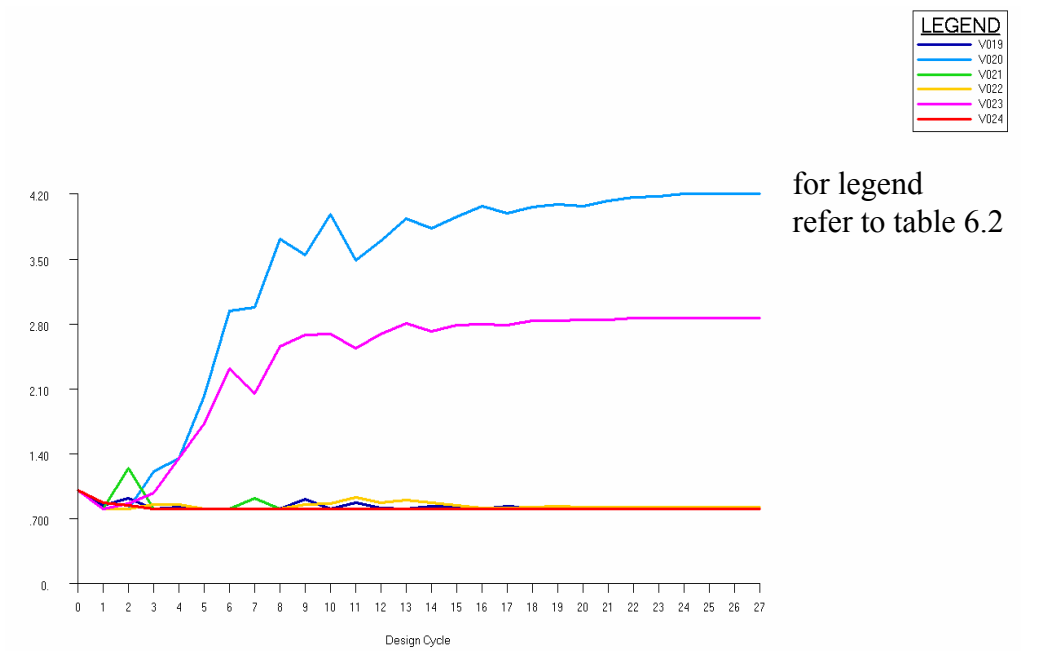


Figure 6.38 History of rear spar web thicknesses (in mm)

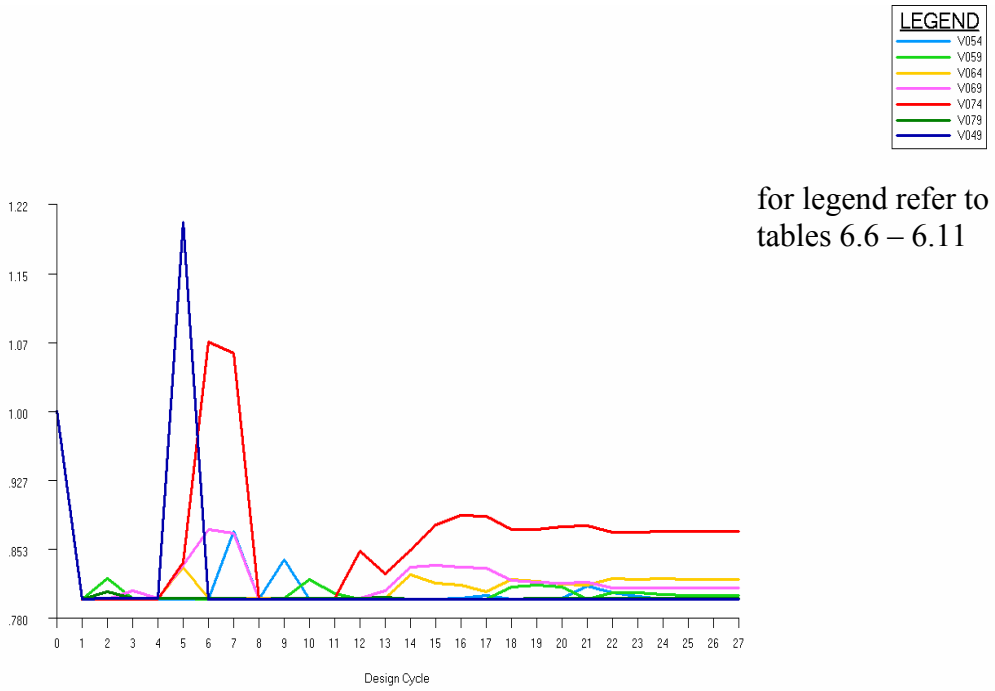


Figure 6.39 History of rib web thicknesses (in mm)

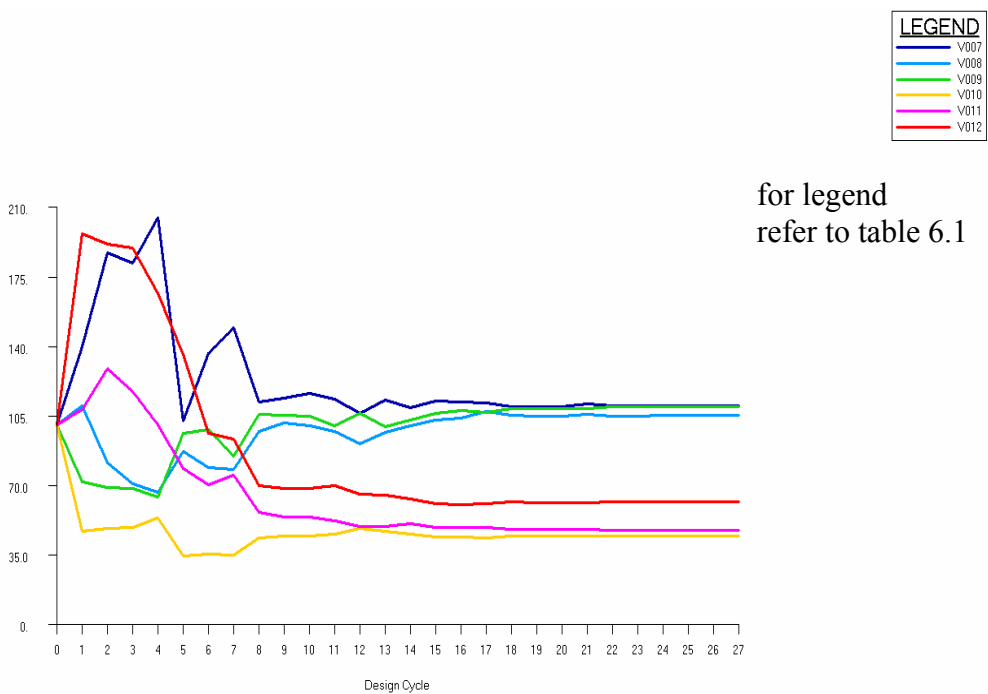


Figure 6.40 History of upper flange areas of front spar (in mm²)

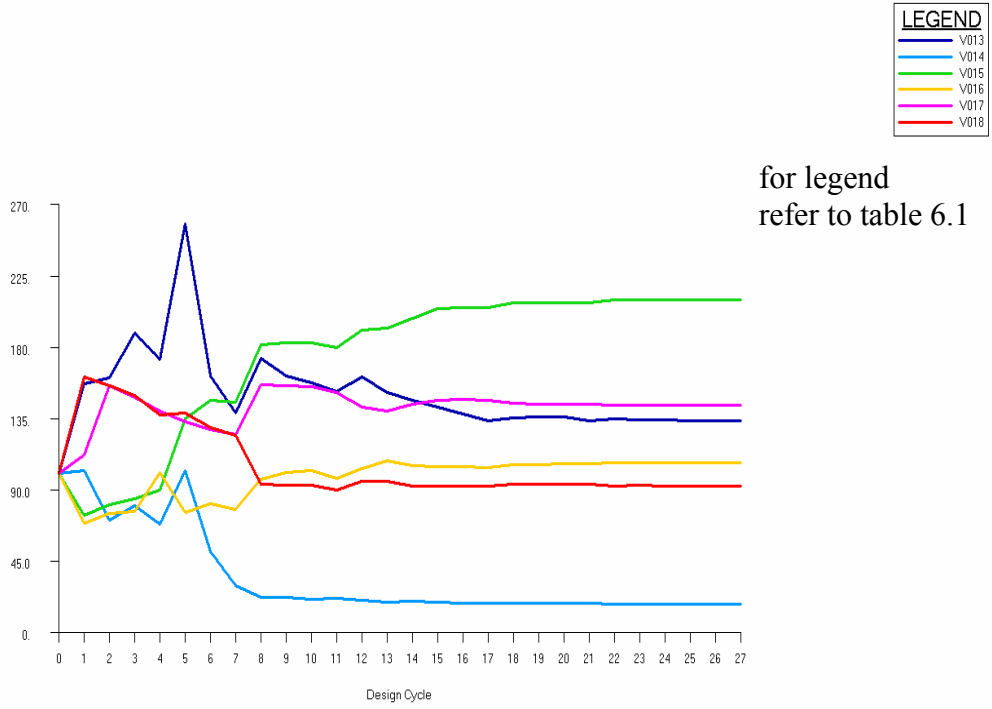


Figure 6.41 History of lower flange areas of front spar (in mm²)

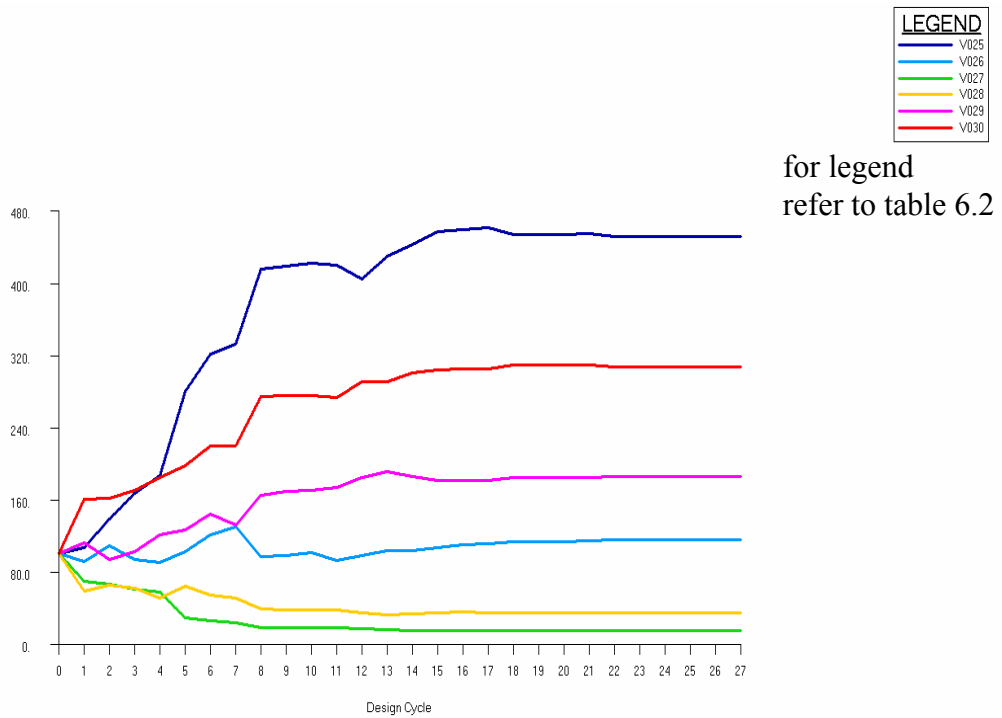


Figure 6.42 History of upper flange areas of rear spar (in mm²)

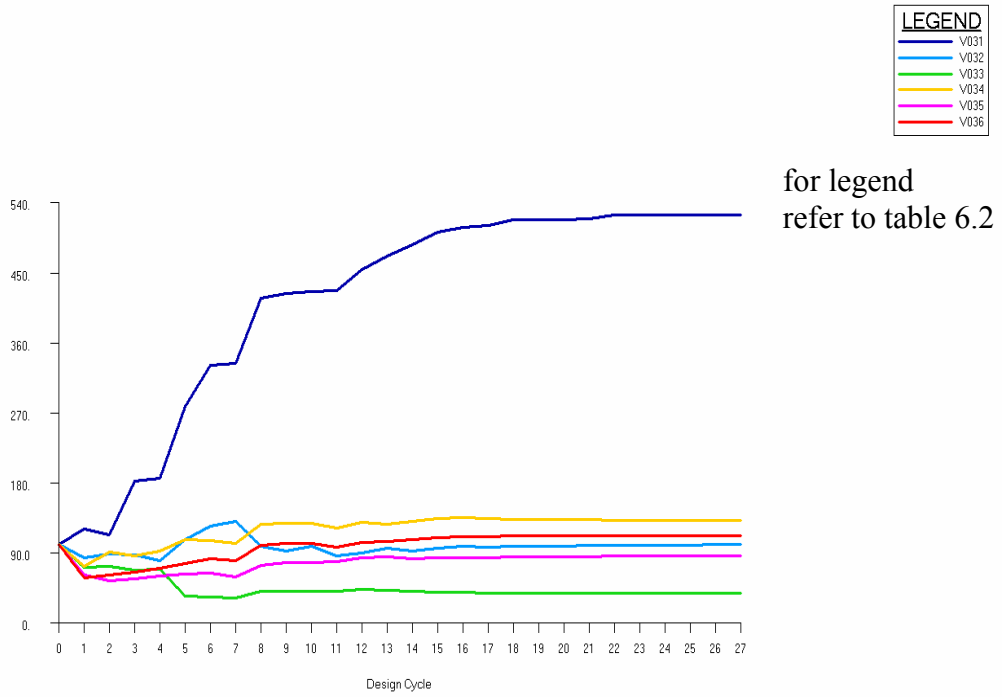


Figure 6.43 History of lower flange areas of rear spar (in mm²)

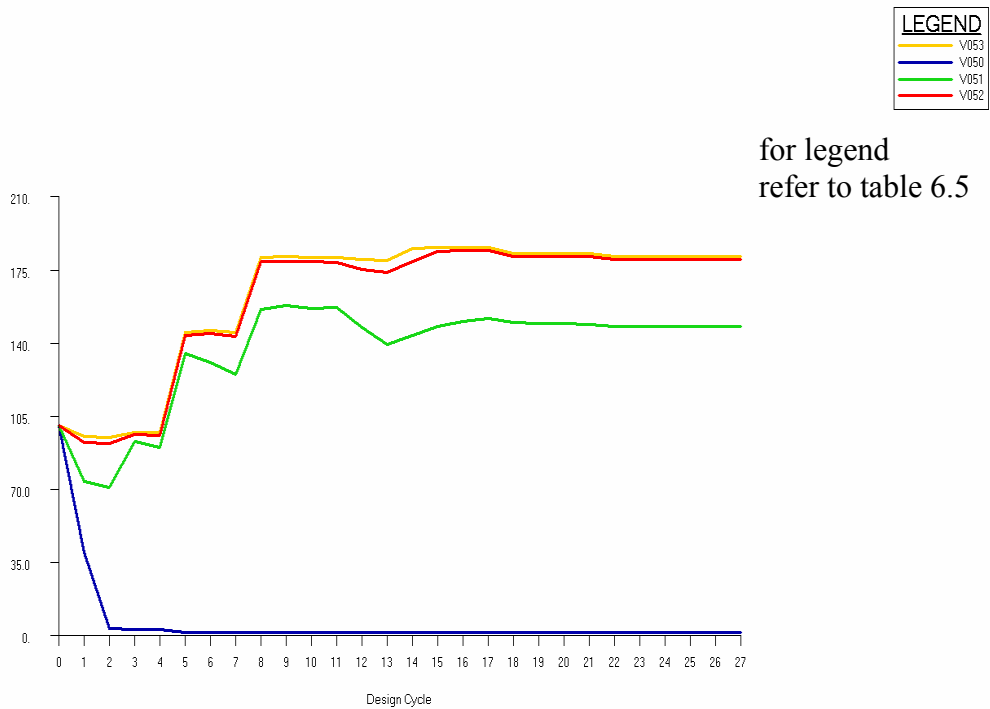


Figure 6.44 History of flange areas of rib 1 (in mm²)

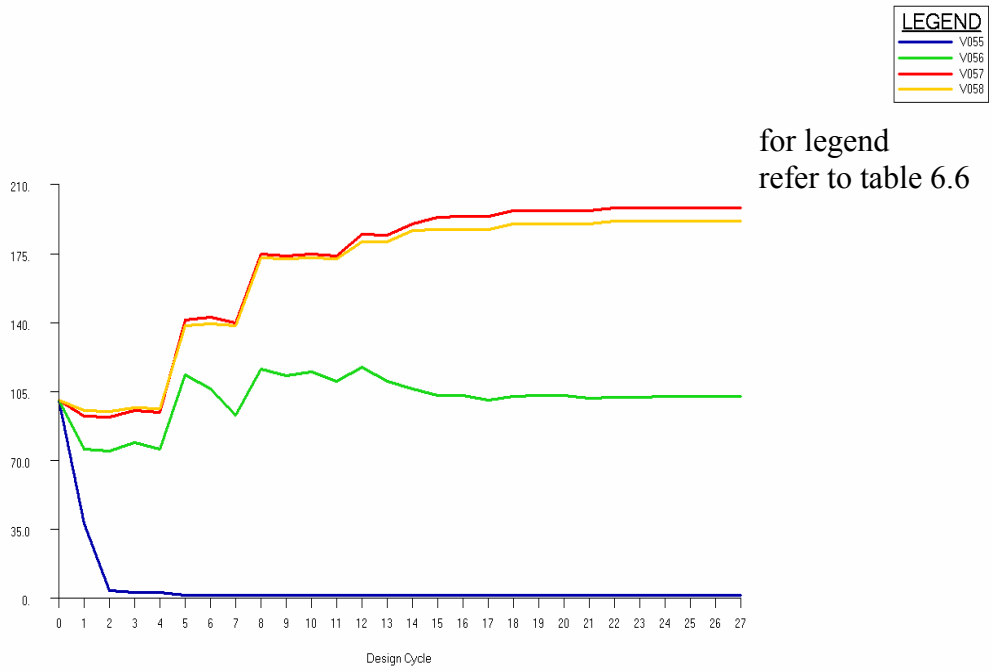


Figure 6.45 History of flange areas of rib 2 (in mm²)

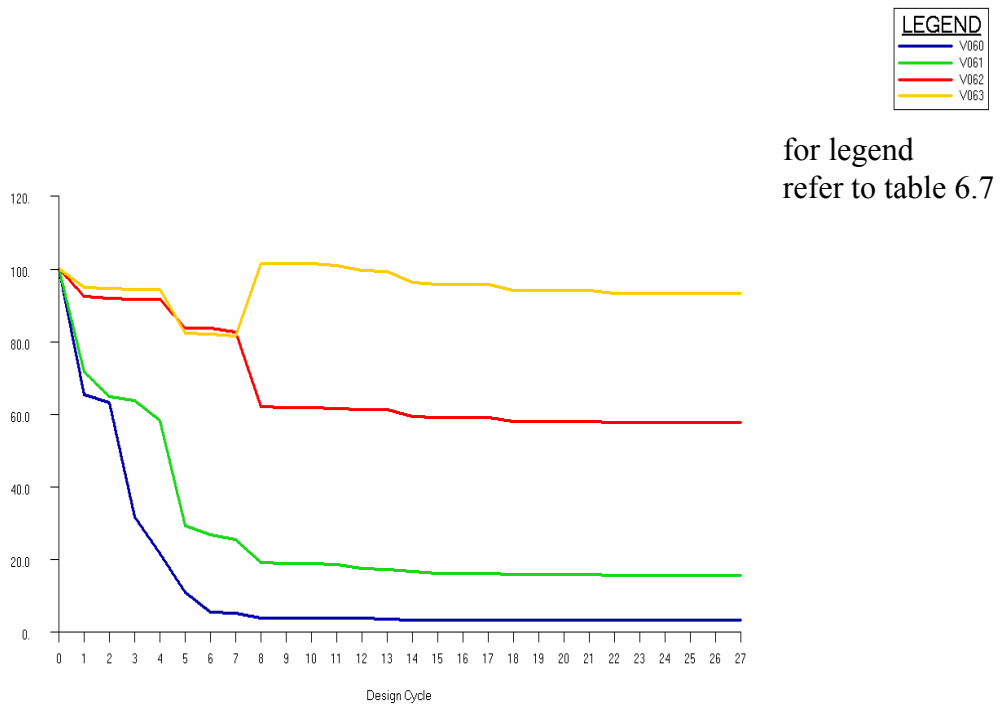


Figure 6.46 History of flange areas of rib 3 (in mm²)

| LEGEND | |
|--------|------|
| — | V065 |
| — | V066 |
| — | V067 |
| — | V068 |

for legend
refer to table 6.8

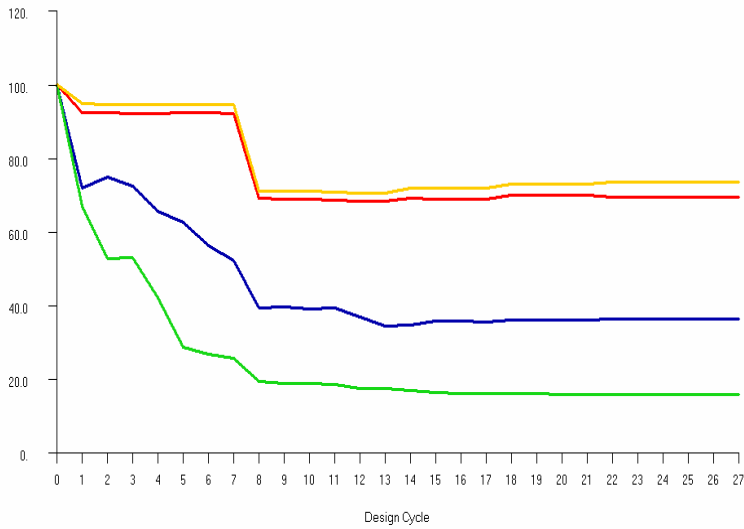


Figure 6.47 History of flange areas of rib 4 (in mm²)

| LEGEND | |
|--------|------|
| — | V070 |
| — | V071 |
| — | V072 |
| — | V073 |

for legend
refer to table 6.9

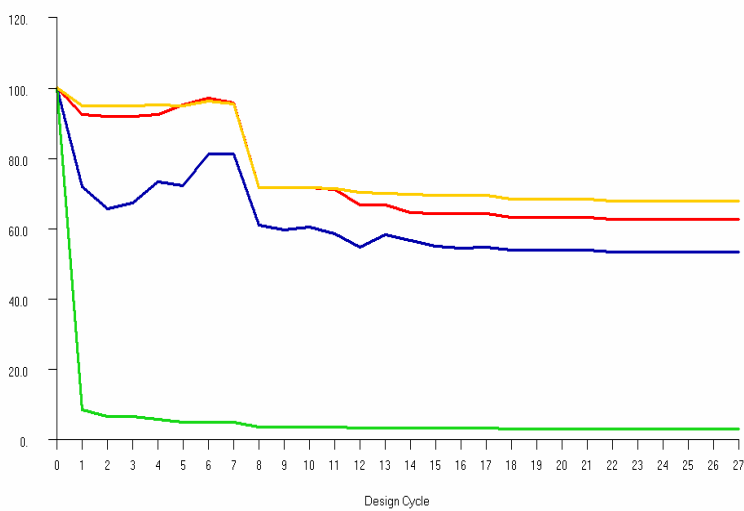


Figure 6.48 History of flange areas of rib 5 (in mm²)



for legend
refer to table 6.10

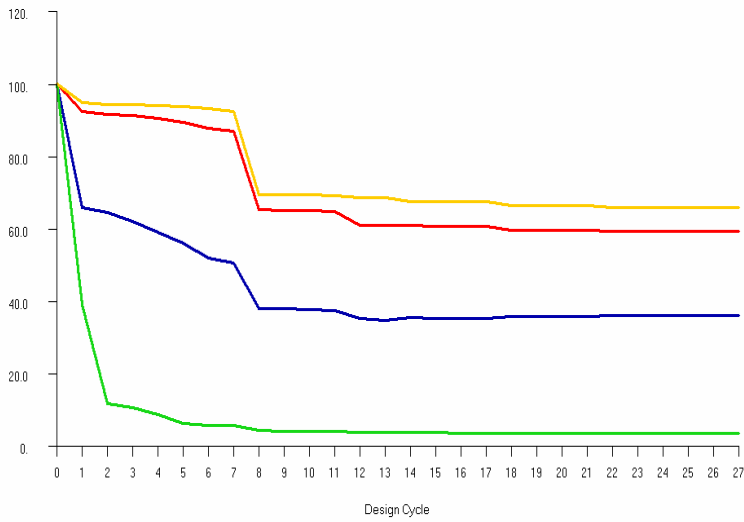


Figure 6.49 History of flange areas of rib 6 (in mm²)



for legend
refer to table 6.11

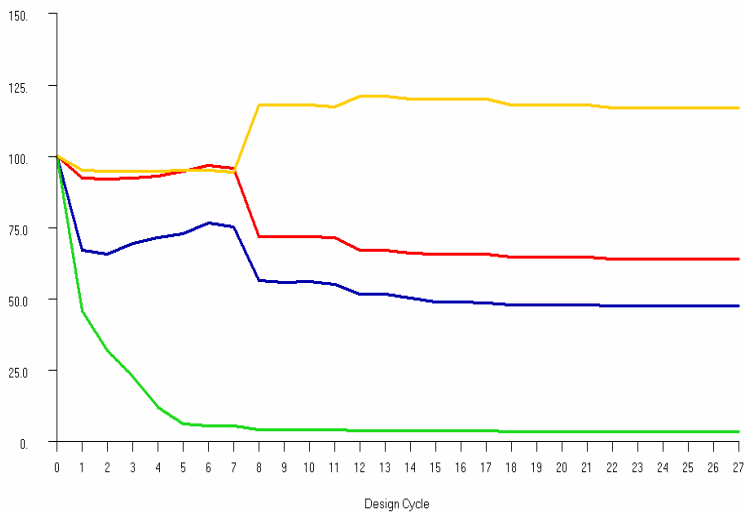


Figure 6.50 History of flange areas of rib 7 (in mm²)

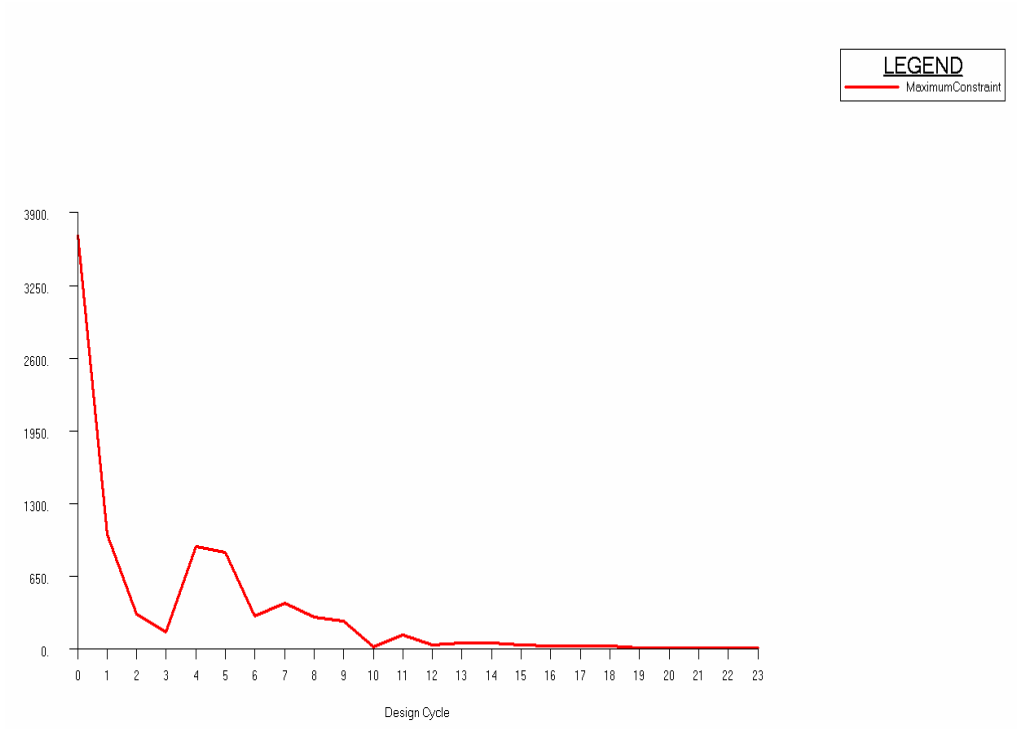


Figure 6.51 History of maximum constraint value

6.2 OPTIMIZATION OF THE WING WITH DISTRIBUTED LOADING

In this section the same torque box is optimized for the distributed load case. Aerodynamic lift force and pitching moment are applied on nodes which are created at 33.91% chord and on the camber line, as specified by the ESDU document [12], at each rib location. Rigid RBE3 element is then used to distribute applied load to the nodes of ribs similar to the tip load case. Displacement boundary condition applied and distributed load imposed are shown in Figure 6.52.

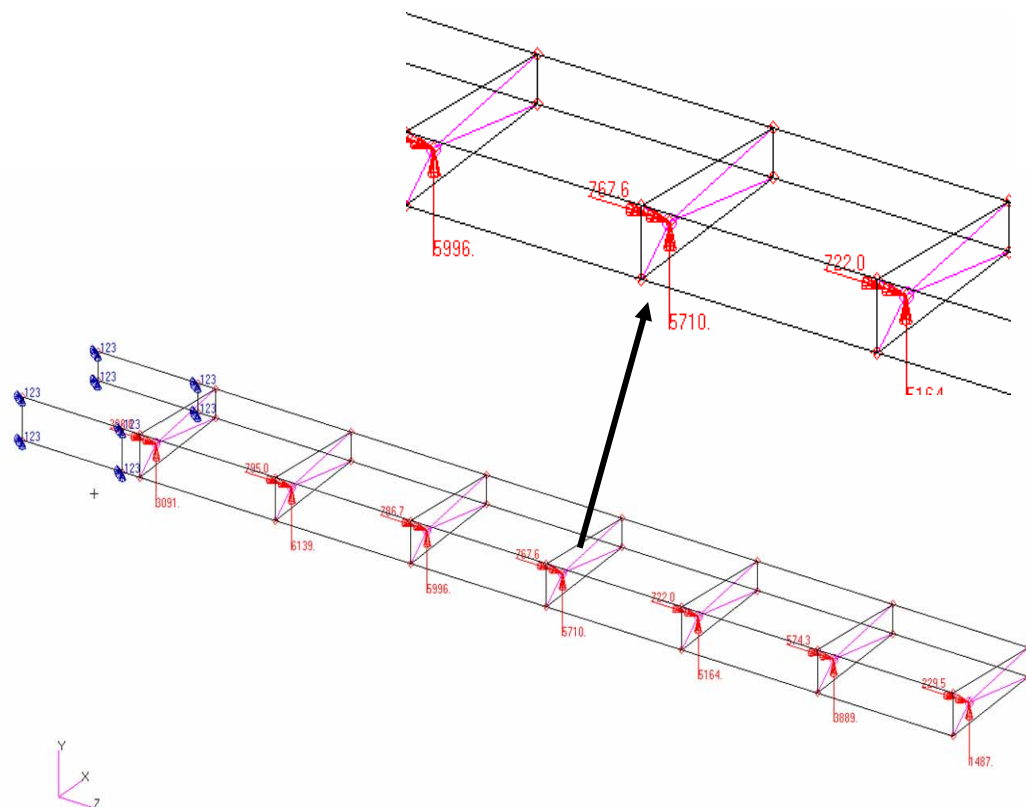


Figure 6.52 Initial wing model with distributed loading

Initial analysis results are shown in Figures 6.53 – 6.56. These results belong to the wing with the initial values of the design variables.

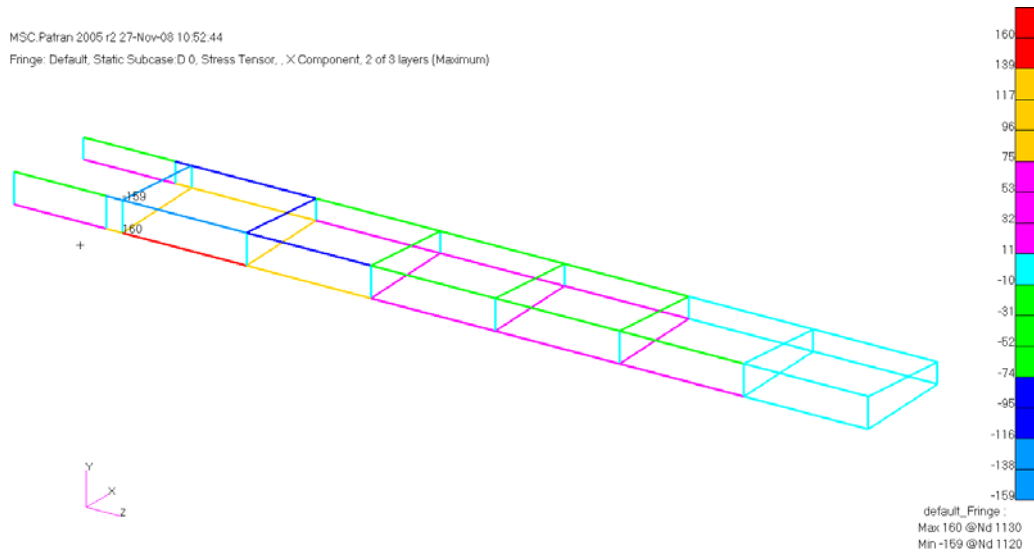


Figure 6.53 Initial axial stresses on the flanges

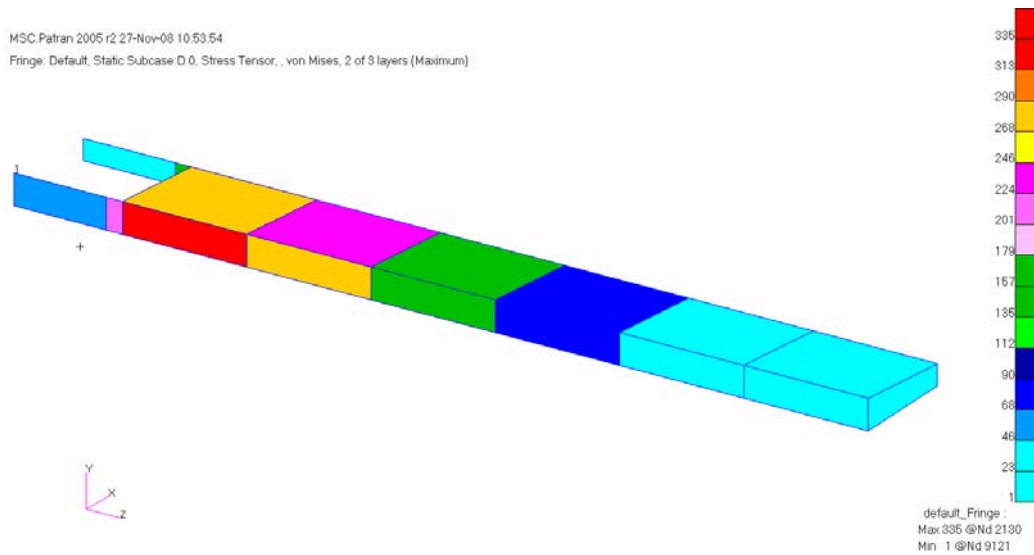


Figure 6.54 Initial Von Mises stresses on the skins and the webs

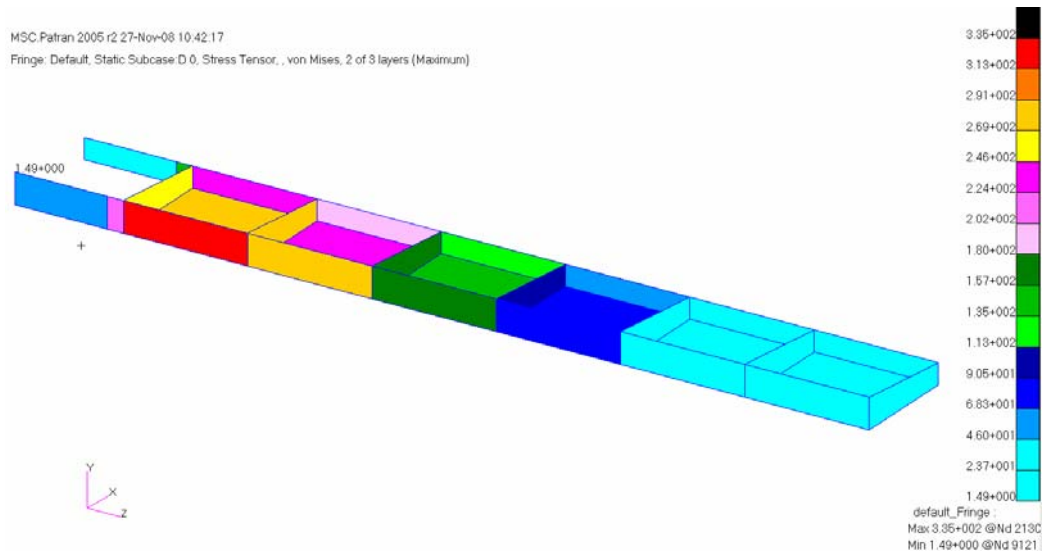


Figure 6.55 Initial Von Mises stresses on the skins and the webs interior view

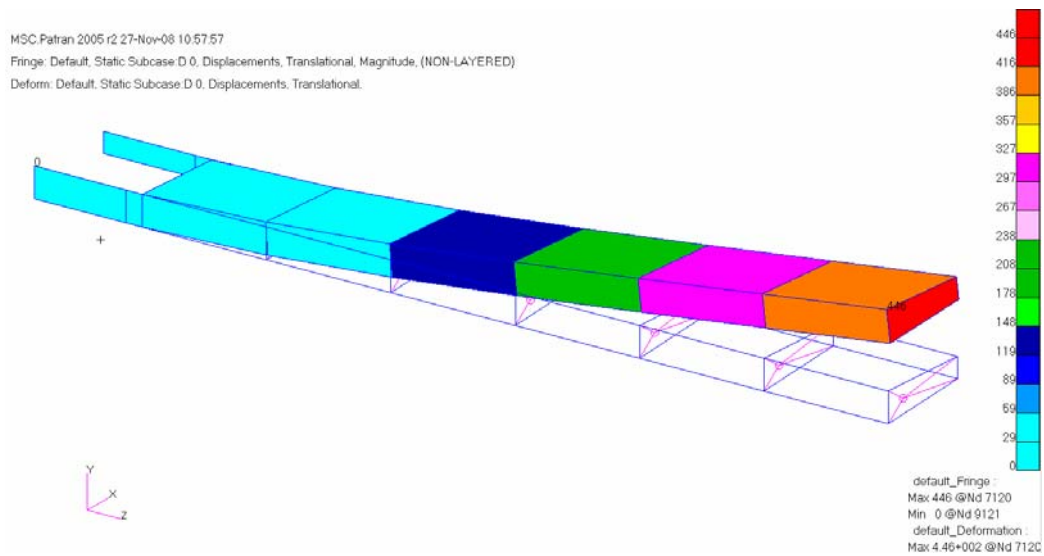


Figure 6.56 Initial deflection of the wing model

In this example it is observed that since the total load is applied on the wing in a distributed fashion the peak stresses occur towards the root of the wing contrary to the concentrated tip load case solved in the previous section.

The optimized element properties of the wing model are shown in Figures 6.57-6-64. These figures give the color plot representation of the final flange areas, skin, web and rib thicknesses. As it was discussed before, the element properties are allowed to change discretely between the rib stations. To reduce the number of design variables single elements were used to model the structure between the rib stations. Therefore, at the end of the solution single colors are assigned to the flange areas, skin and webs between the rib stations and ribs. Solution took 8.140 seconds of CPU time.

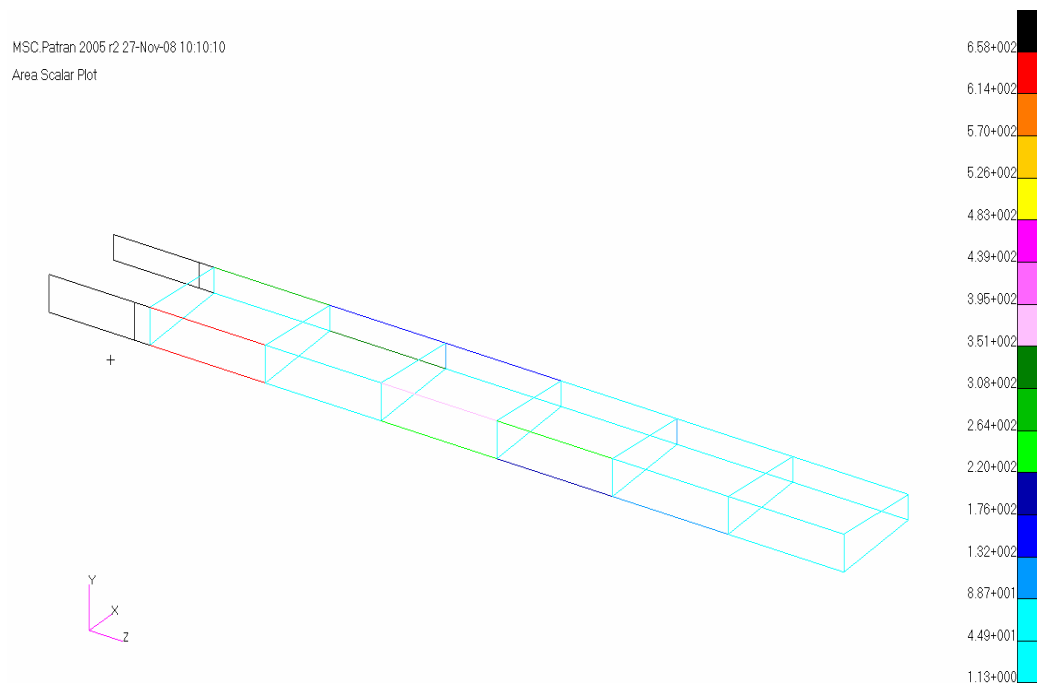


Figure 6.57 Final flange areas on the wing model

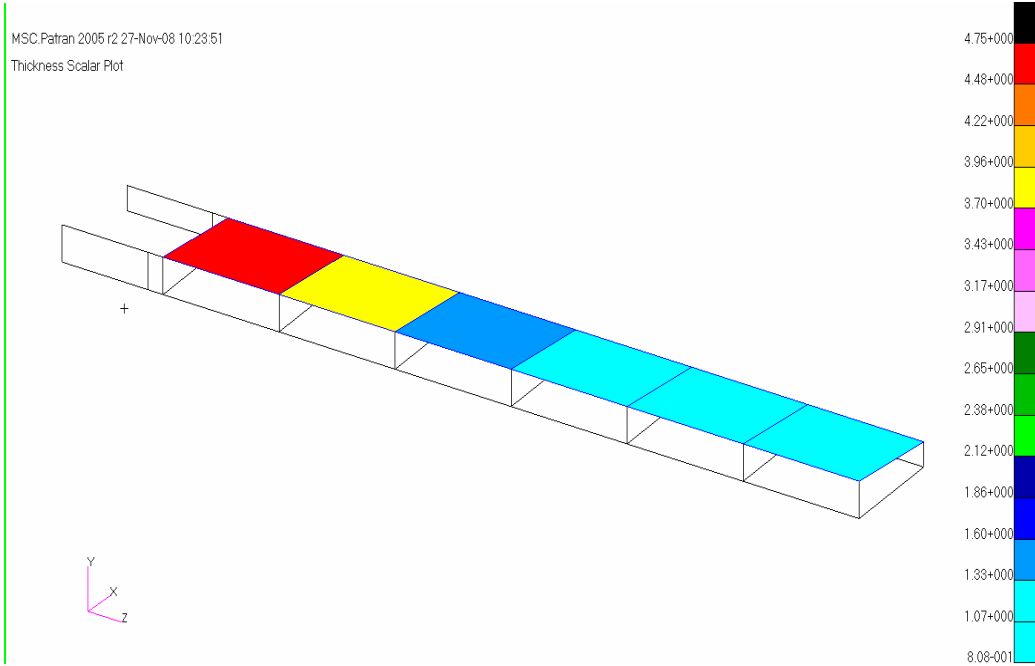


Figure 6.58 Final upper skin thicknesses of the wing model

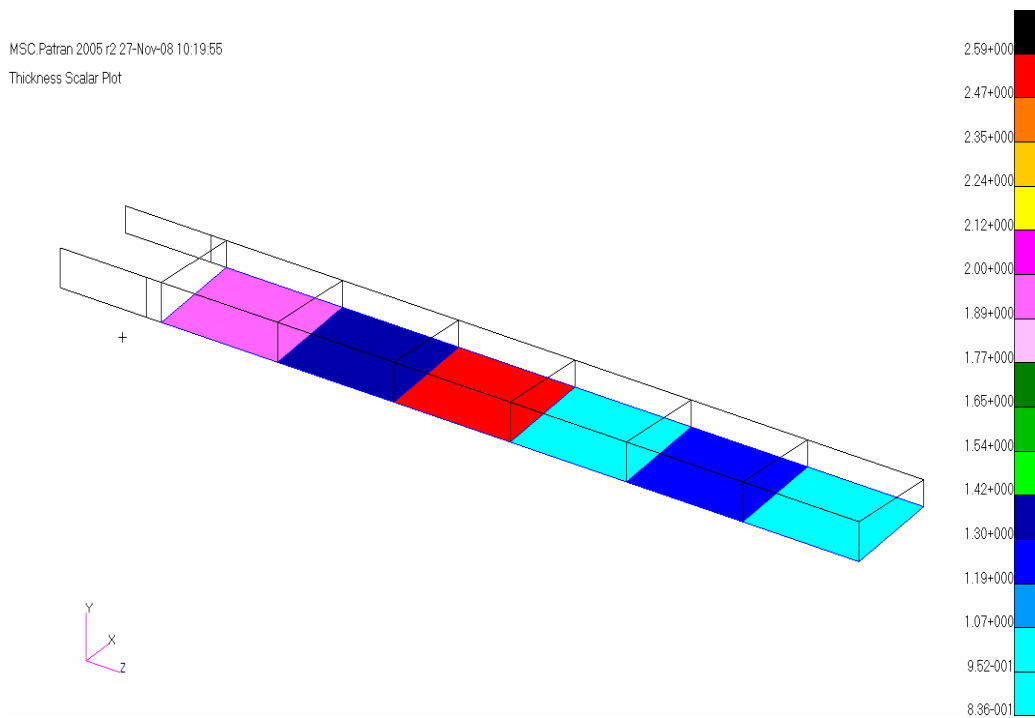


Figure 6.59 Final lower skin thicknesses of the wing model

MSC.Patran 2005 r2 27-Nov-08 10:26:30
Thickness Scalar Plot

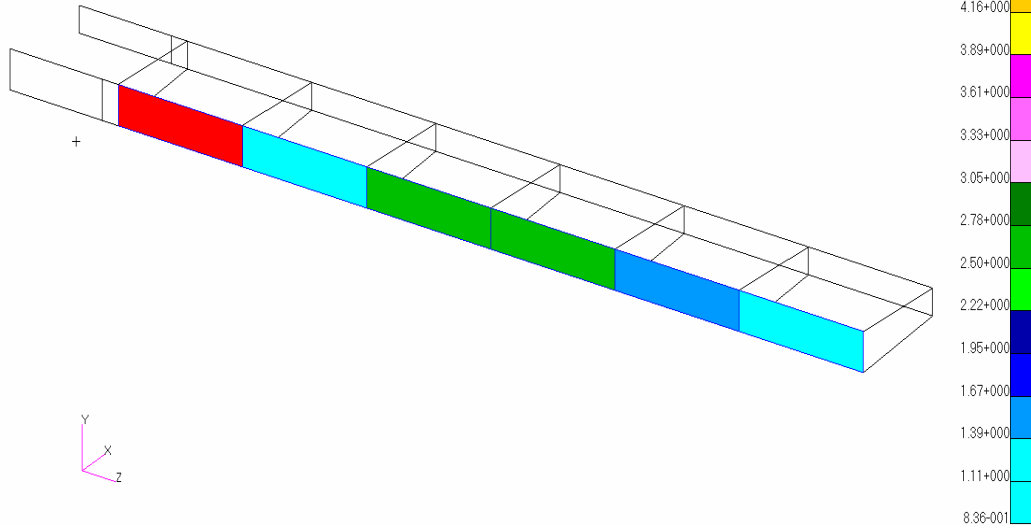


Figure 6.60 Final front spar thicknesses of the wing model

MSC.Patran 2005 r2 27-Nov-08 10:27:28
Thickness Scalar Plot

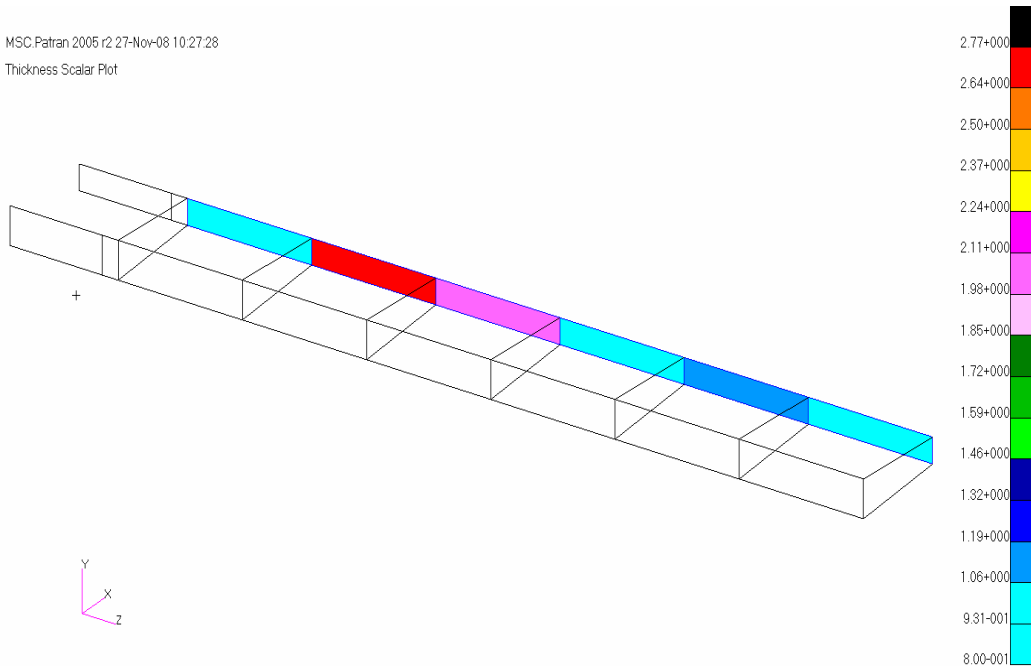


Figure 6.61 Final rear spar thicknesses of the wing model

MSC.Patran 2005 r2 27-Nov-08 10:32:42
Thickness Scalar Plot

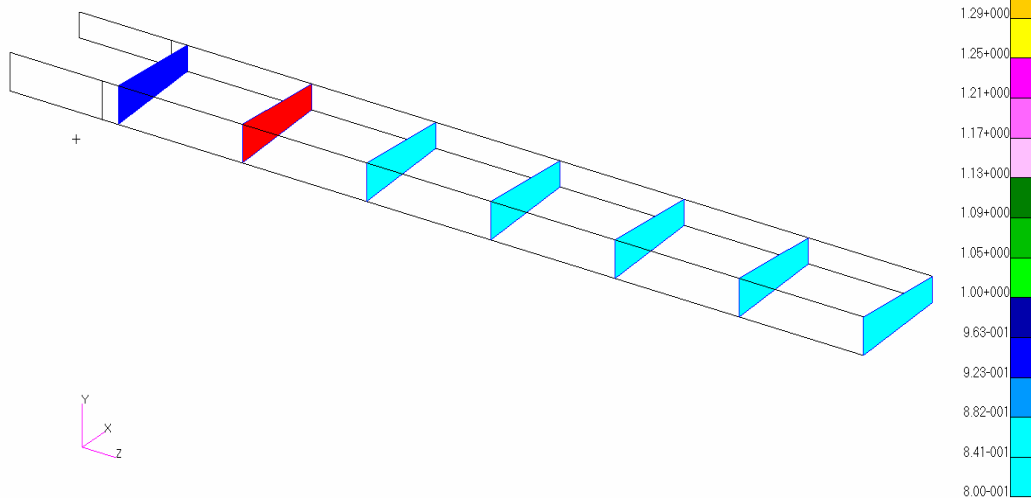


Figure 6.62 Final rib web thicknesses of the wing model

MSC.Patran 2005 r2 27-Nov-08 10:33:42
Thickness Scalar Plot

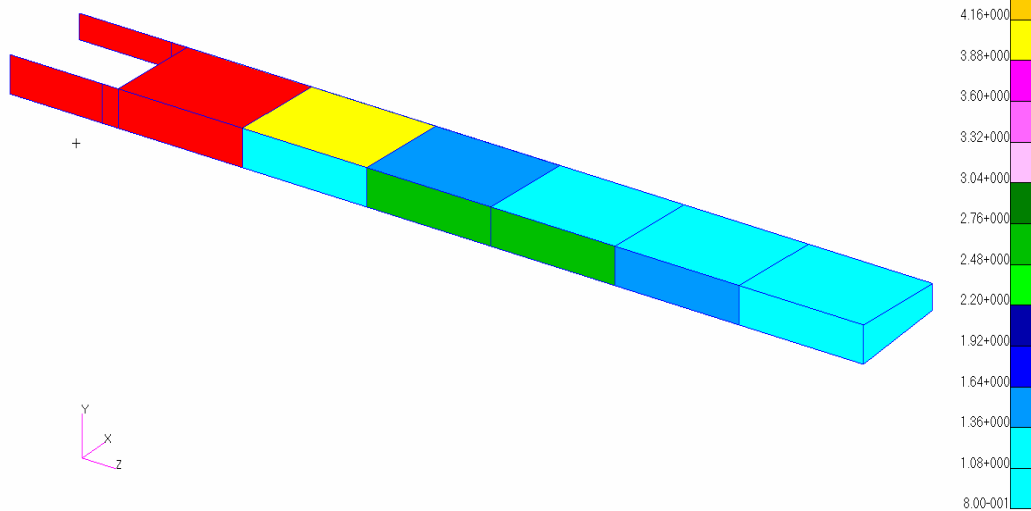


Figure 6.63 Final overall thicknesses of the wing model

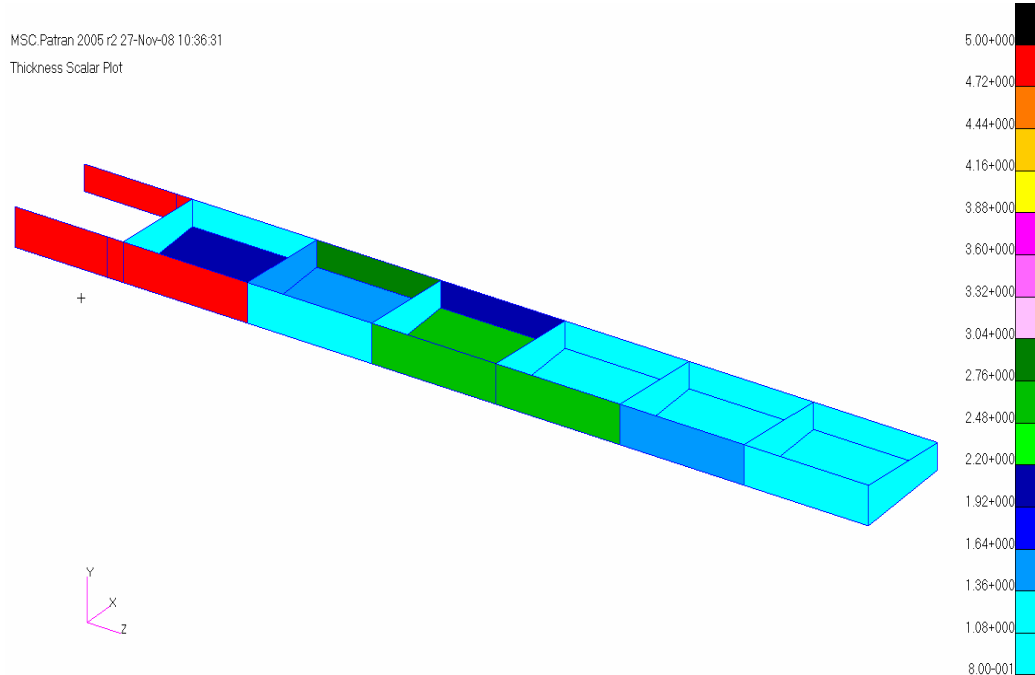


Figure 6.64 Final web thicknesses of the wing model interior view

Final analysis results of the optimized torque box are presented in Figures 6.65 – 6.68. It is observed that the final stresses are reduced from their initial values. This observation is based on the comparison of the initial stress analysis results given in Figures 6.53-6.55 with the stress analysis results of the optimized configuration given by Figures 6.65-6.67. Reduction in stress values would imply an increase in the weight of the final optimized configuration compared to the initial configuration. In order to check the validity of this conclusion the history of the objective function has to be checked.

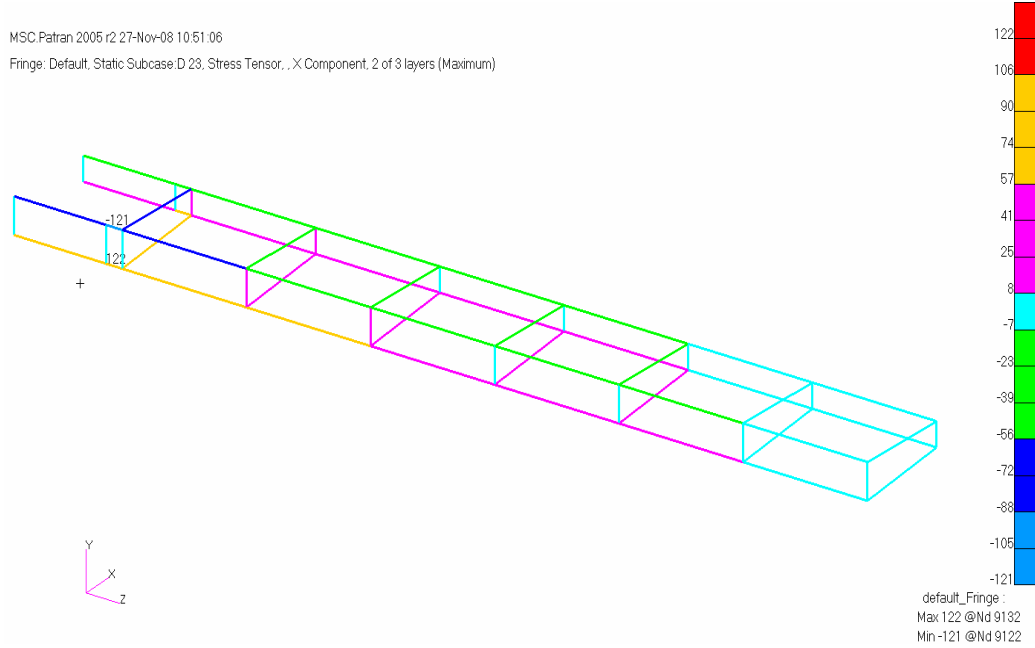


Figure 6.65 Final axial stresses on the flanges

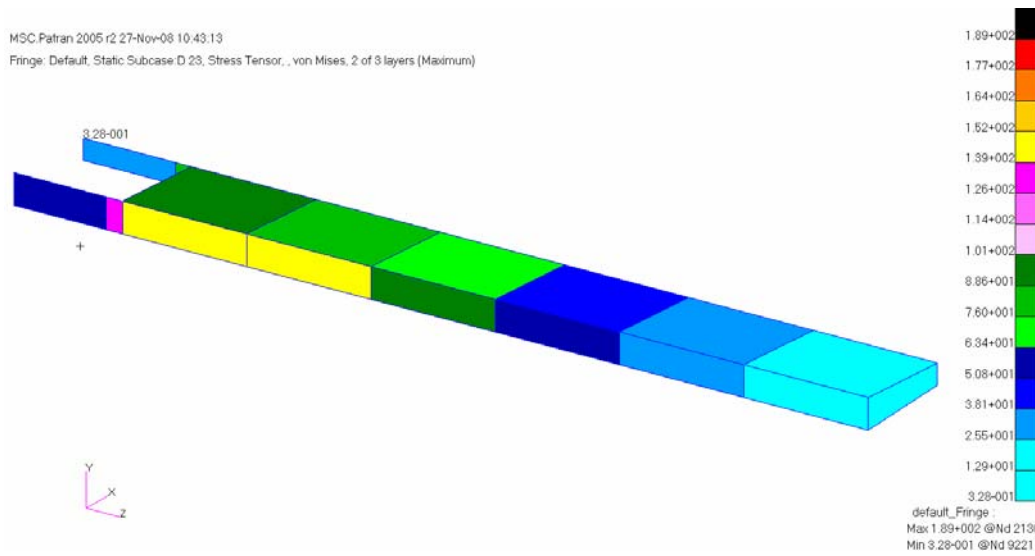


Figure 6.66 Final Von Mises stresses on the skins and the webs

MSC.Patran 2005 r2 27-Nov-08 10:42:52

Fringe: Default, Static Subcase:D 23, Stress Tensor, von Mises, 2 of 3 layers (Maximum)

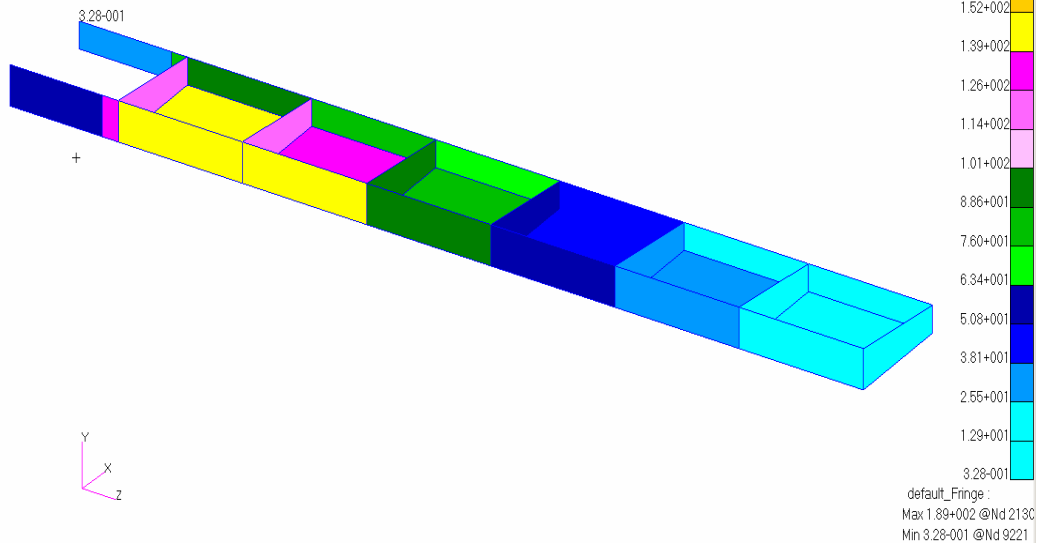


Figure 6.67 Final Von Mises stresses on the skins and the webs interior view

MSC.Patran 2005 r2 27-Nov-08 10:57:26

Fringe: Default, Static Subcase:D 23, Displacements, Translational, Magnitude, (NON-LAYERED)

Deform: Default, Static Subcase:D 23, Displacements, Translational

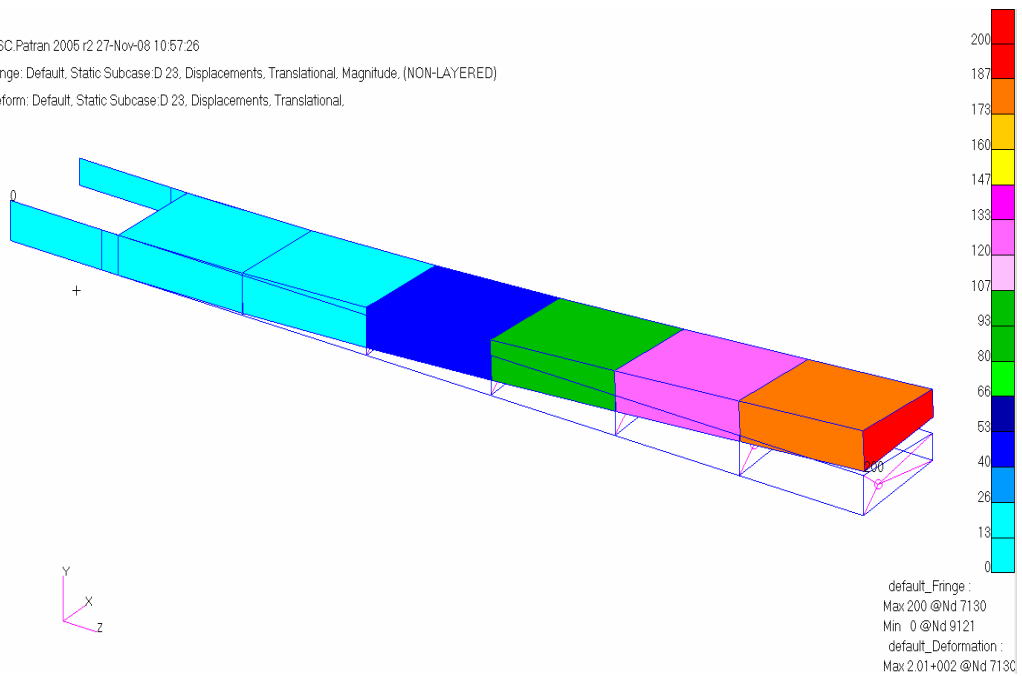


Figure 6.68 Final deflection of the wing model

History of objective function, design variables and constraints are shown in figures 6.69 – 6.86.

History of the objective function which is the total weight of the wing is shown in Figure 6.69. The optimized weight is determined to be about 60 kg. The increase of the weight of the wing in the optimized configuration justifies the increase of the stress values in most elements in the final configuration compared to the stresses analysis results in the initial configuration. It can be concluded that with the initial values of the design variables the constraints are not all satisfied and therefore the objective function increases until the constraints are satisfied.

Figures 6.70-6.85 show the history of all the design variables until the optimum solution is reached. It can be observed from these figures that except for the rib flange areas, most of the design variables increase compared to their initial values and this observation is in accordance with the variation of the objective function with the design cycle. In Figures 6.70-6.85 the thicknesses are given in mm and cap areas are given in mm².

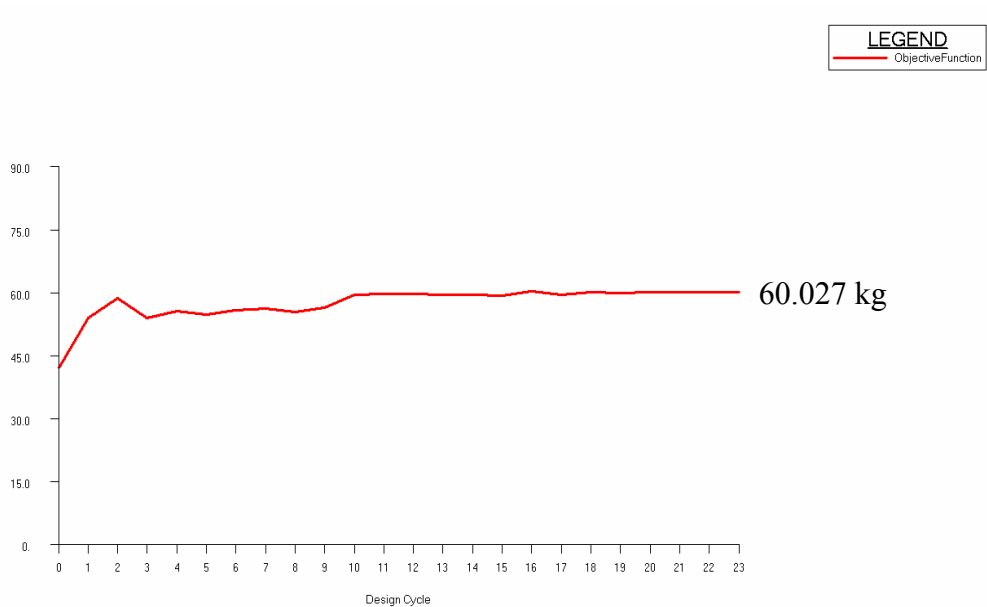


Figure 6.69 History of objective function (in kg)

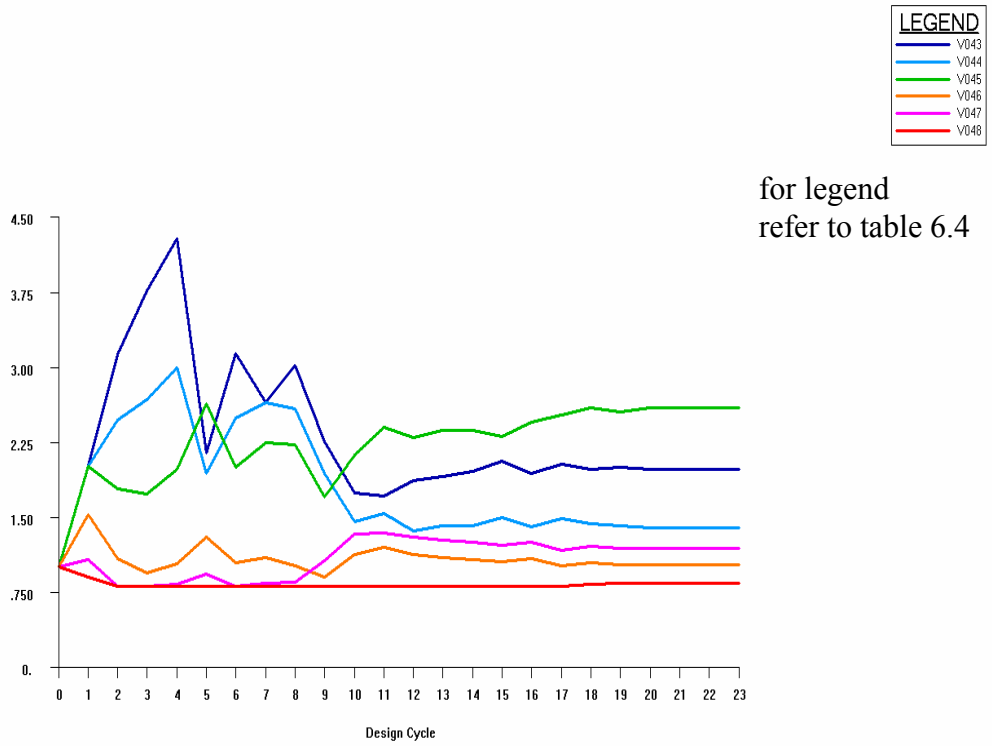


Figure 6.70 History of lower skin thicknesses (in mm)

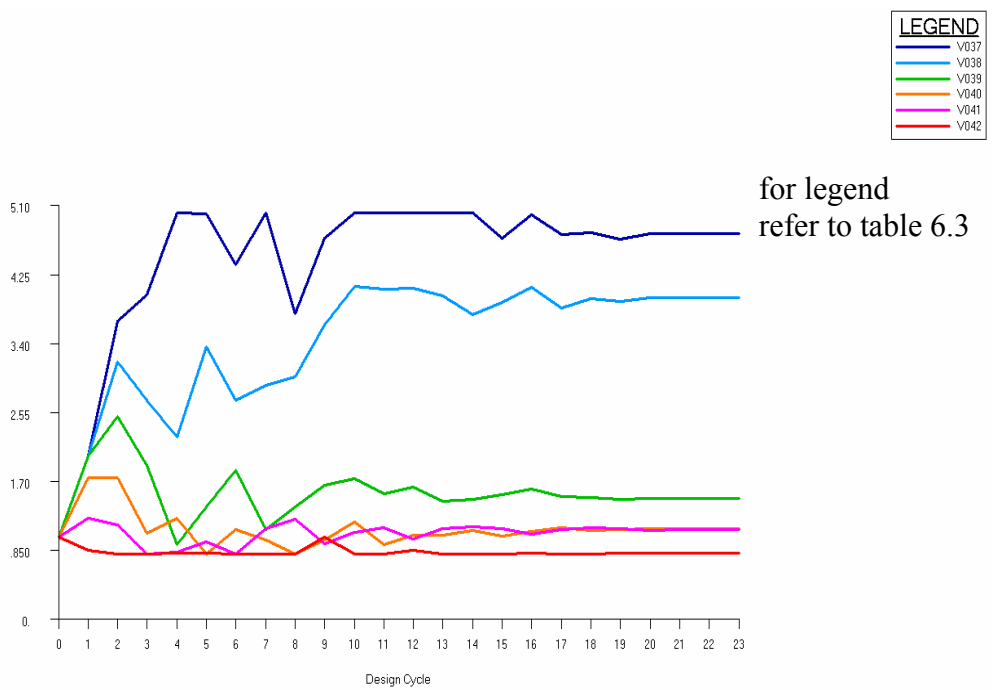


Figure 6.71 History of upper skin thicknesses (in mm)

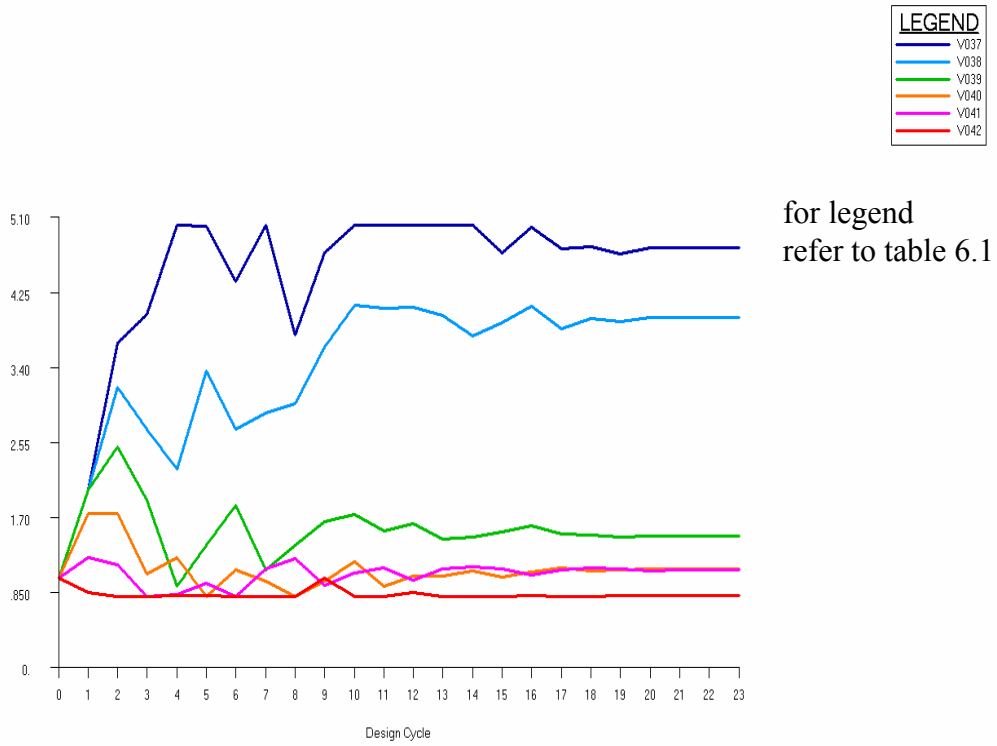


Figure 6.72 History of front spar web thicknesses (in mm)

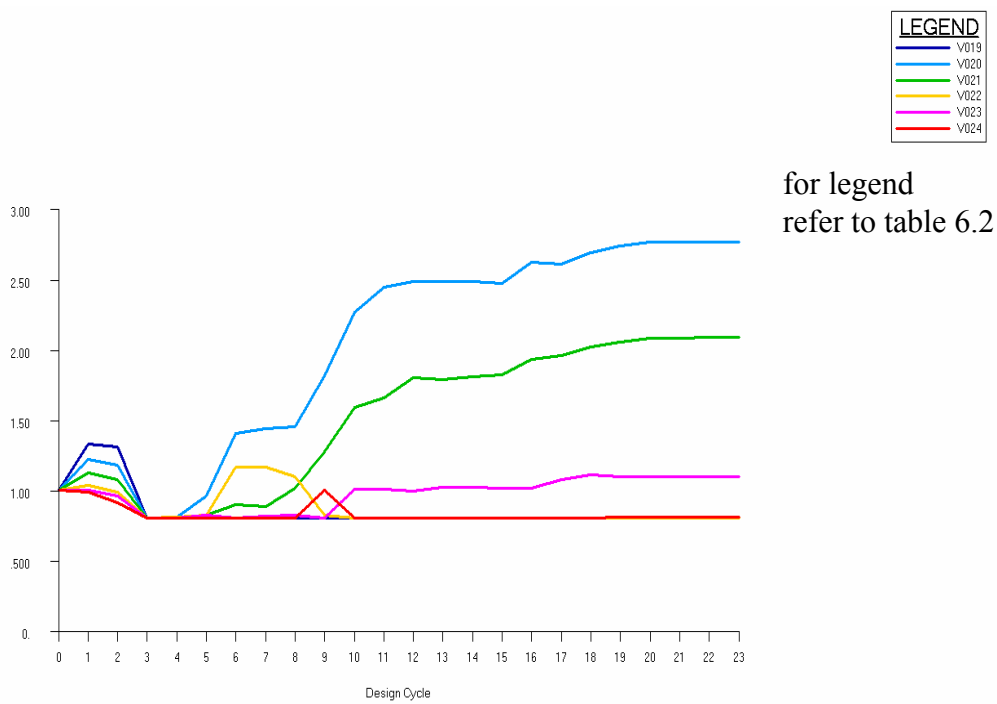


Figure 6.73 History of rear spar web thicknesses (in mm)

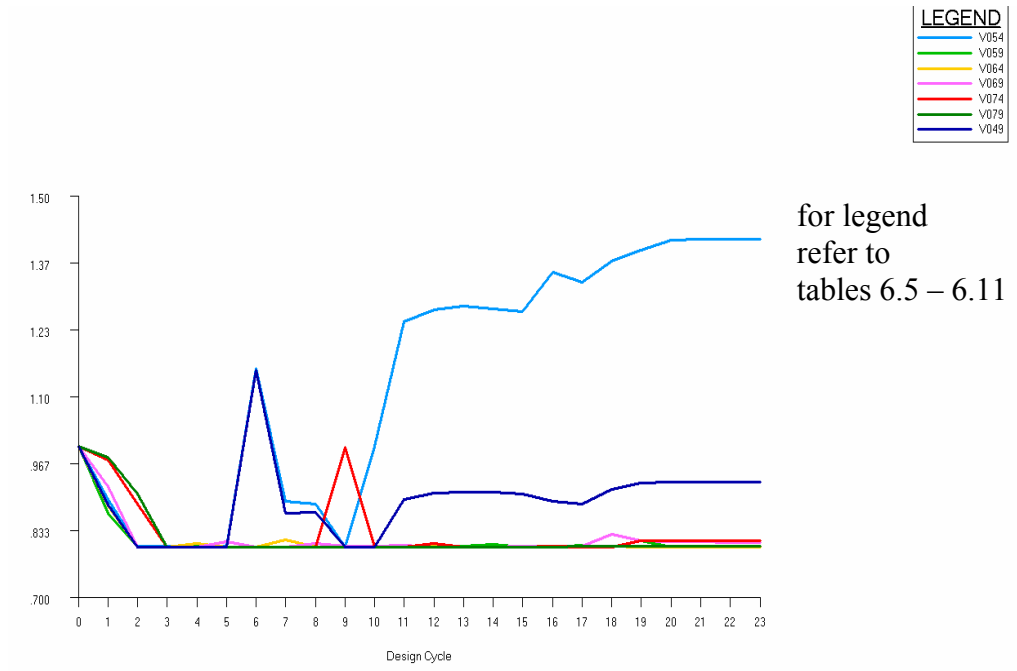


Figure 6.74 History of rib web thicknesses (in mm)

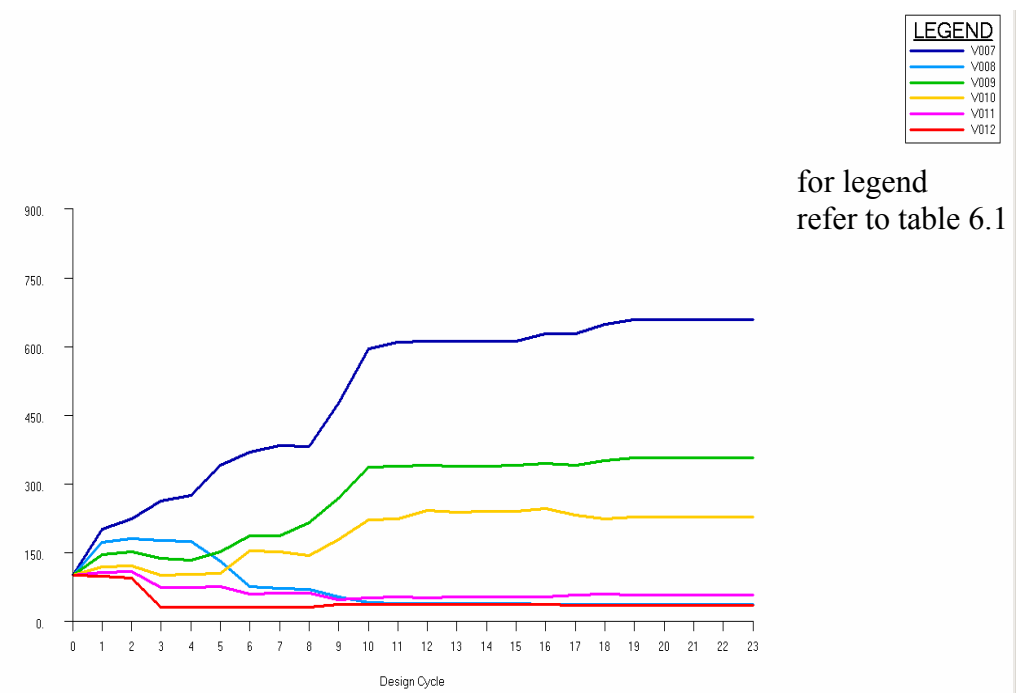


Figure 6.75 History of upper flange areas of front spar (in mm²)

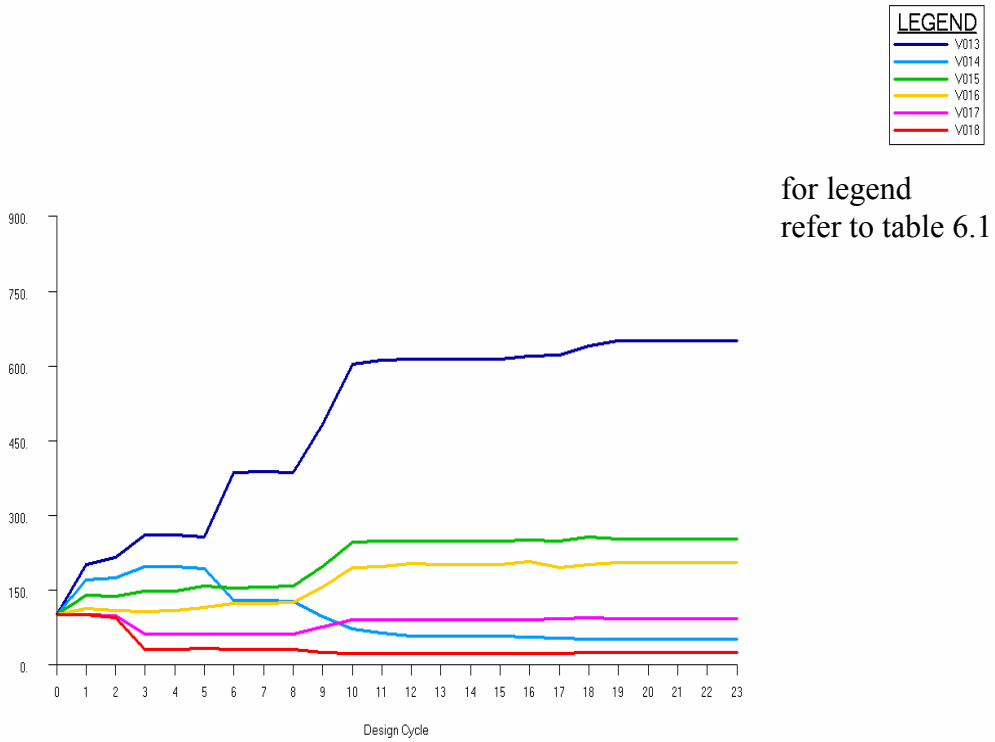


Figure 6.76 History of lower flange areas of front spar (in mm²)

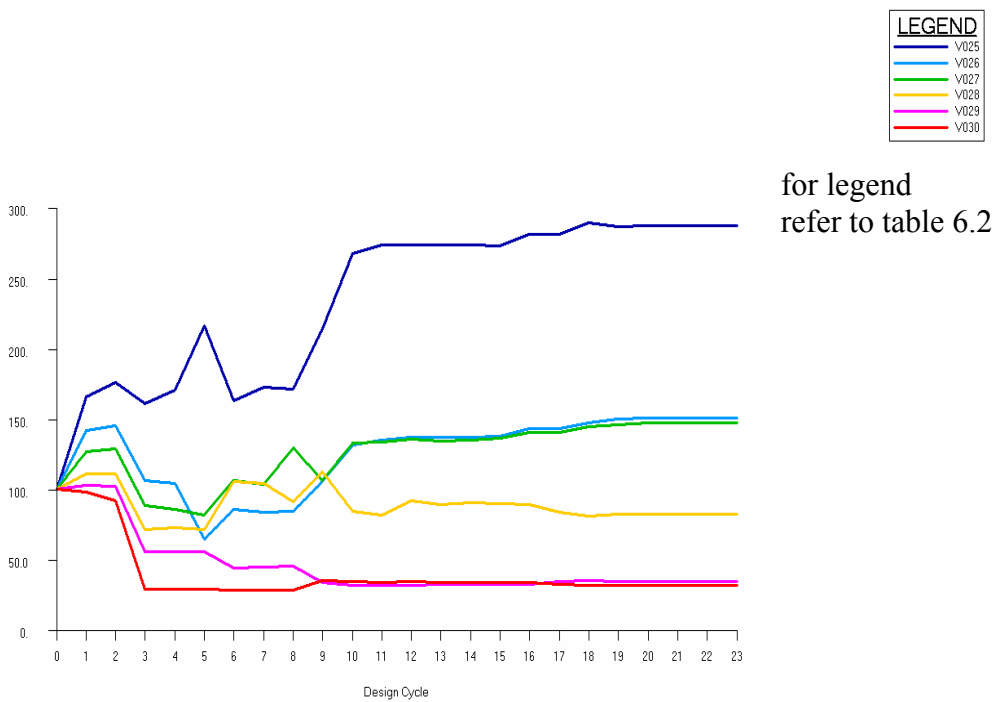


Figure 6.77 History of upper flange areas of rear spar (in mm²)

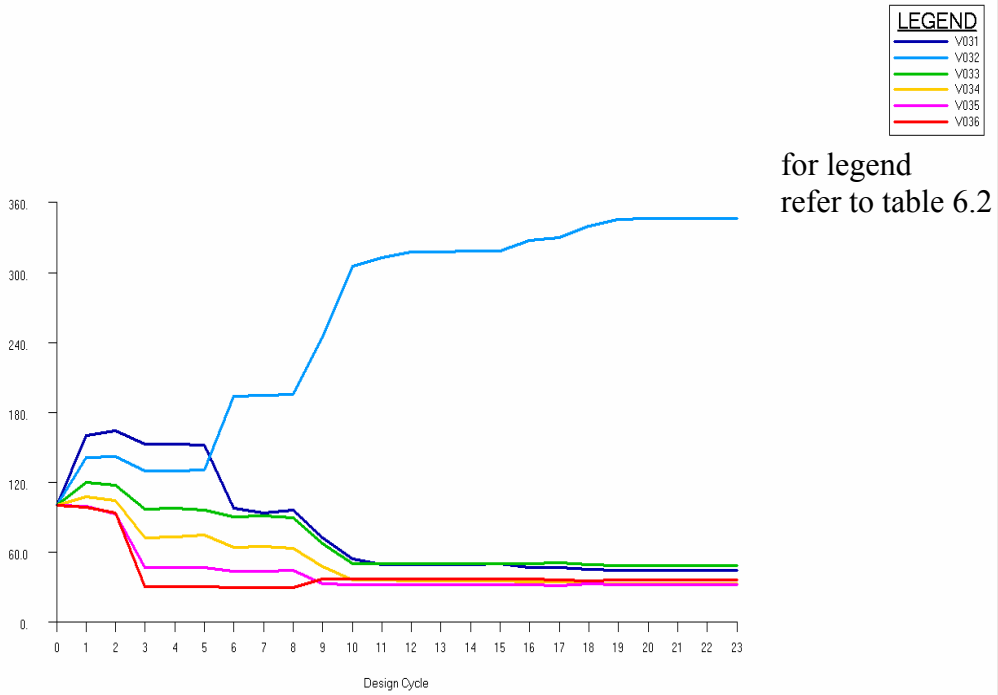


Figure 6.78 History of lower flange areas of rear spar (in mm²)

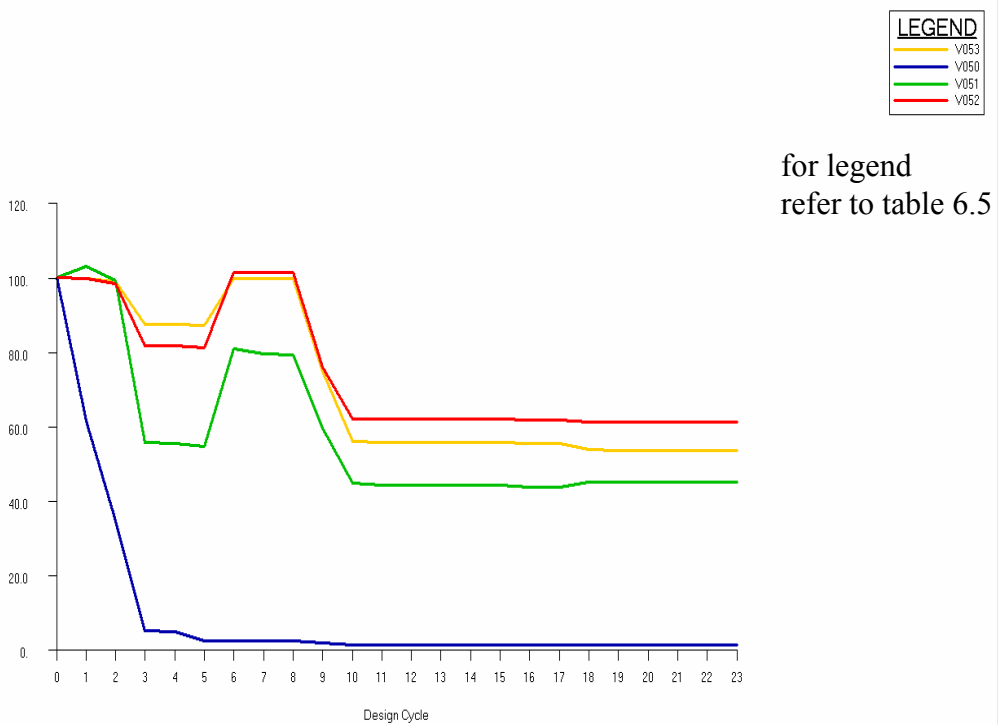


Figure 6.79 History of flange areas of rib 1 (in mm²)

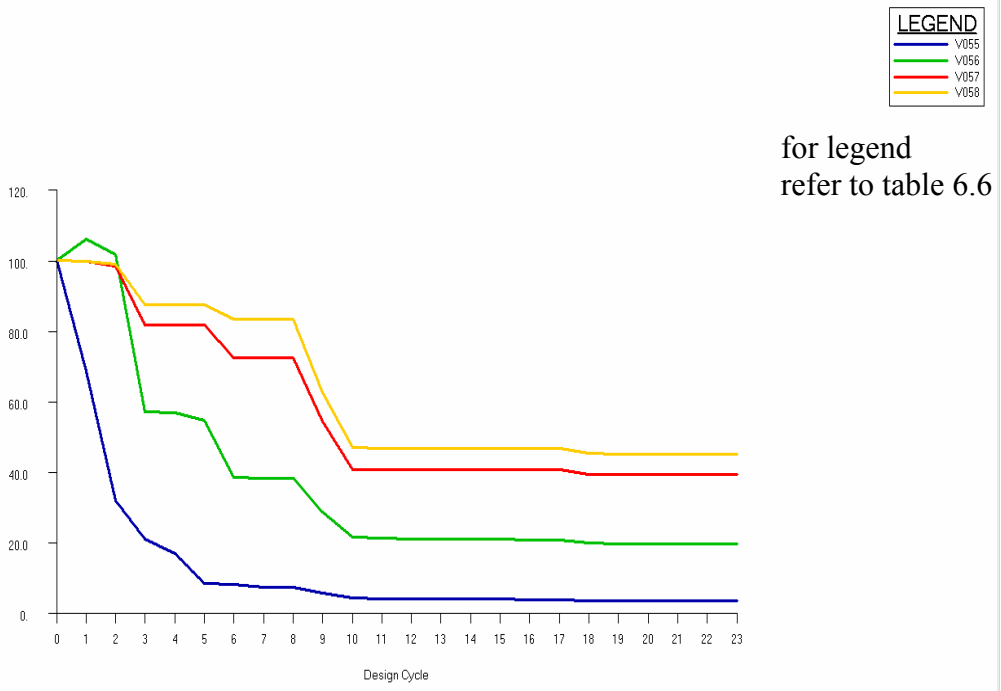


Figure 6.80 History of flange areas of rib 2 (in mm²)

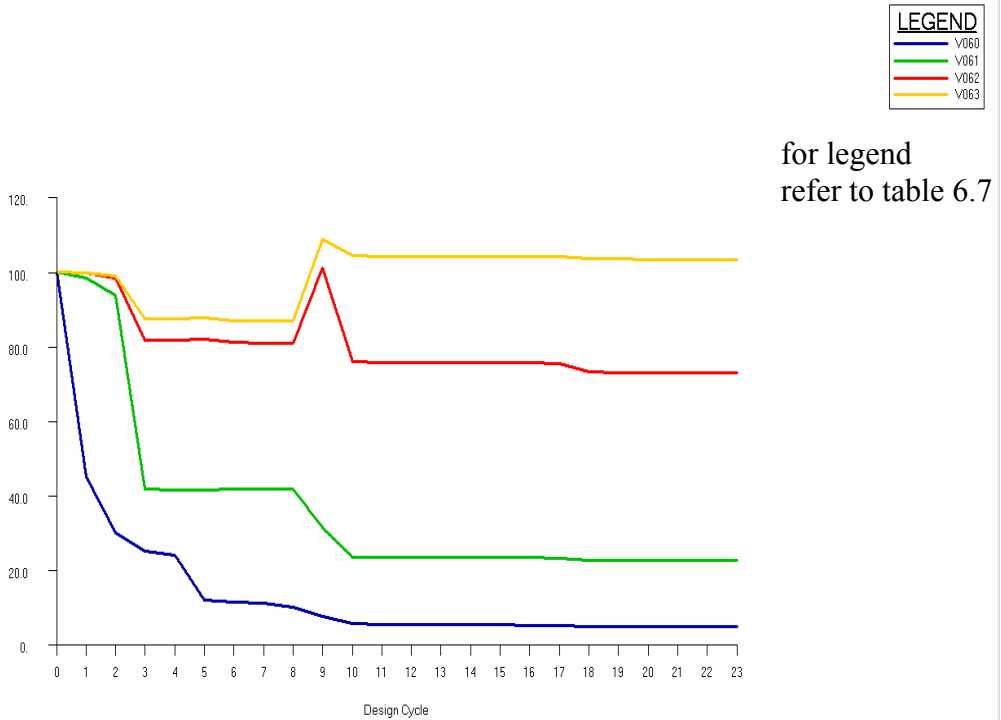
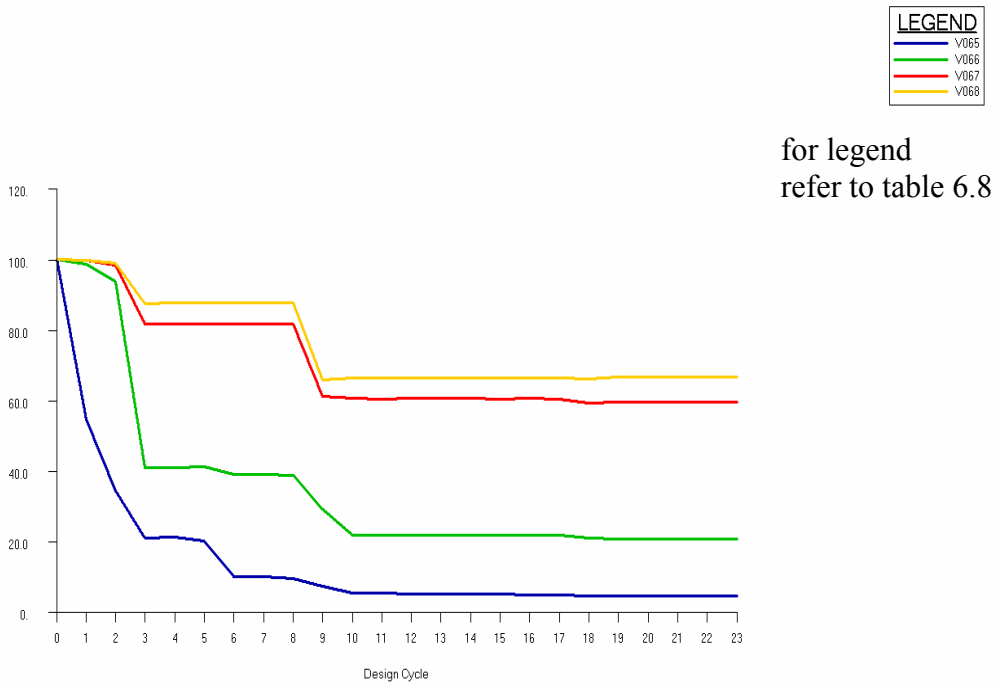
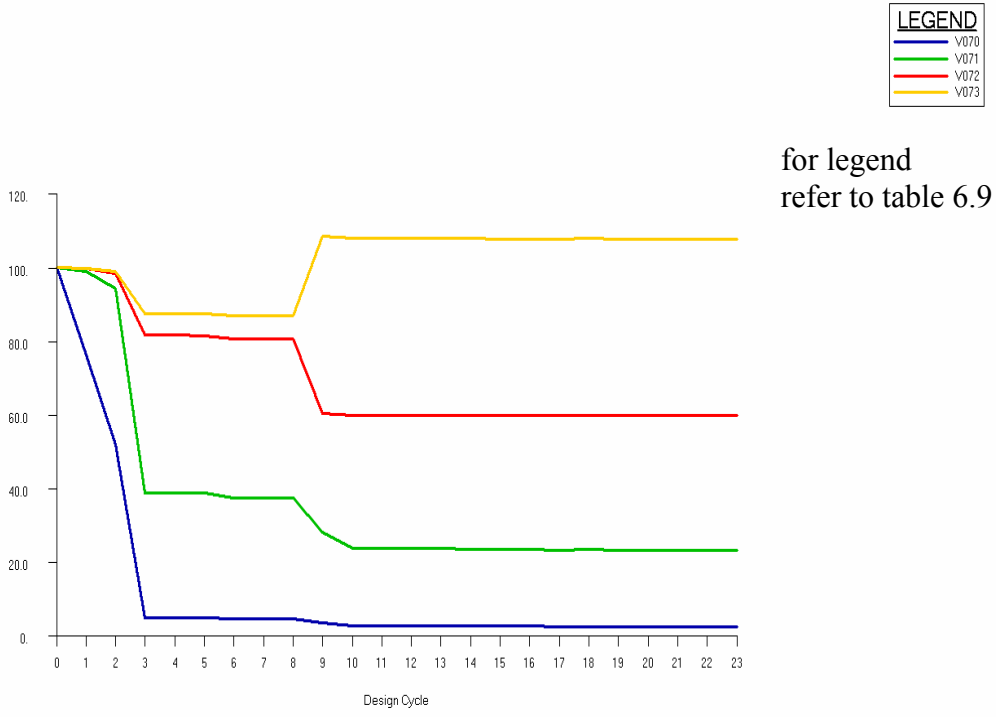


Figure 6.81 History of flange areas of rib 3 (in mm²)



for legend refer to table 6.8

Figure 6.82 History of flange areas of rib 4 (in mm²)



for legend refer to table 6.9

Figure 6.83 History of flange areas of rib 5 (in mm²)

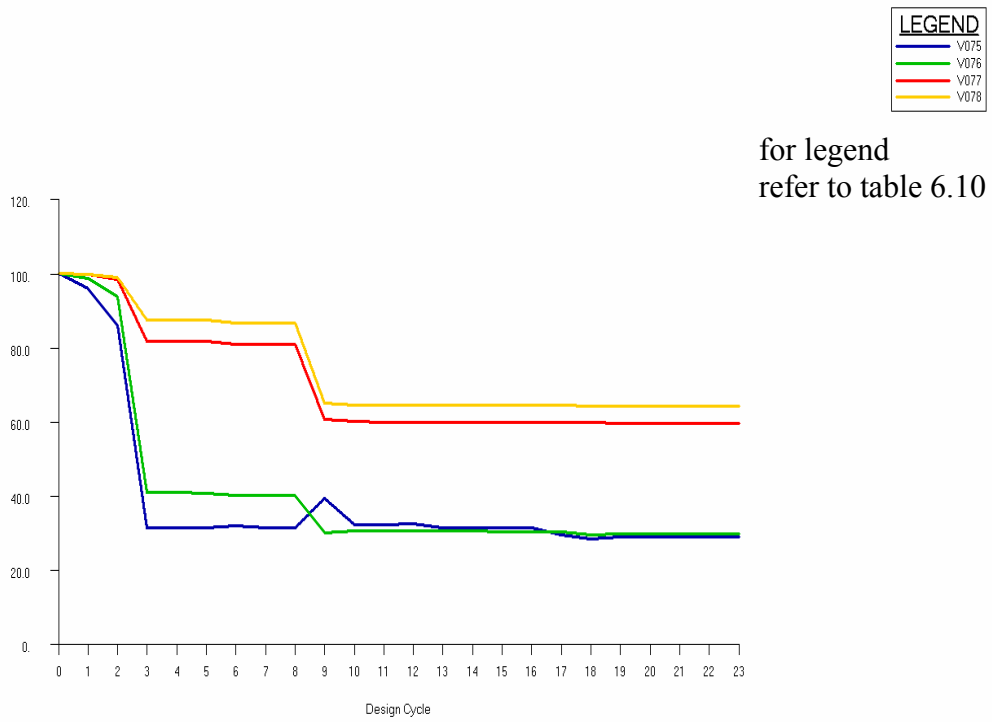


Figure 6.84 History of flange areas of rib 6 (in mm²)

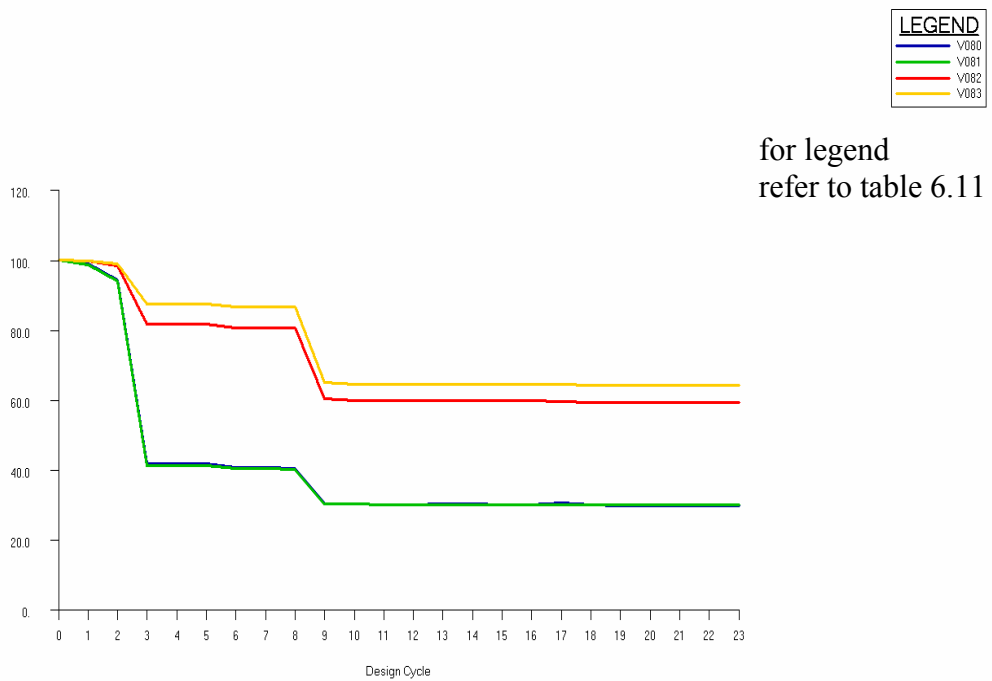


Figure 6.85 History of flange areas of rib 7 (in mm²)

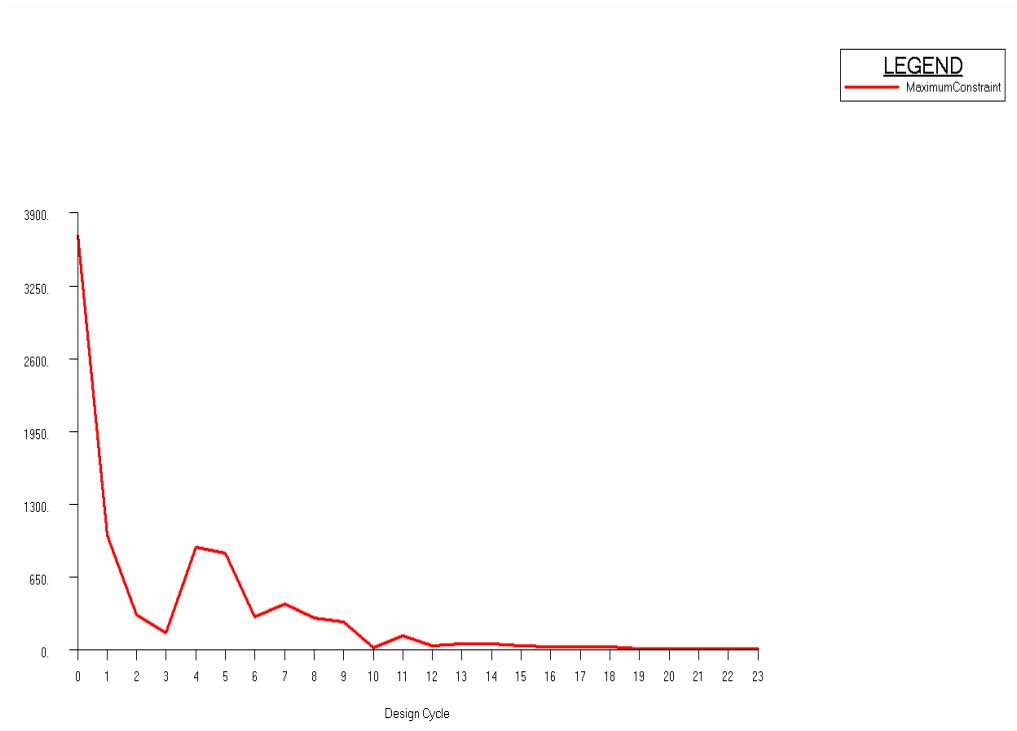


Figure 6.86 History of maximum constraint value

6.3 OPTIMIZATION OF THE WING TORQUE BOX WITH DISTRIBUTED LOADING INCLUDING SHAPE OPTIMIZATION

In this section the optimization of the wing torque box has been performed by incorporating the shape optimization feature of the optimization module of MSC.NASTRAN[®]. Within the context of the shape optimization the location of the ribs of the wing are chosen to be moveable. Each rib is allowed to move in-board and out-board by a distance equal to the half the distance between the rib and the neighboring in-board and out-board rib.

In order to carry out shape optimization, an auxiliary model is required to define shape basis vector in shape optimization. The optimizer requires a relation between shape design variables and changes of grid locations. This relation is defined as a linear combination of shape design variables times shape basis vectors, which results in the total change in grid locations. The auxiliary wing model is the same as the original one and it is used for both shape optimizations described in sections 6.3.1 and 6.3.2. Five different load cases are applied to the wing model. In each load case, a displacement vector, which is 10 mm towards the root, is applied to each rib located between the root and the tip rib of the wing and the other ribs are fixed. Linear static analysis is performed with these load cases. Resultant MASTER-file and DBALL-file are then introduced to the original .bdf-file. To ensure that MSC.NASTRAN[®] produces these result files “scr=no” command should be used. Load cases in auxiliary model are shown in Figures 6.87-6.91

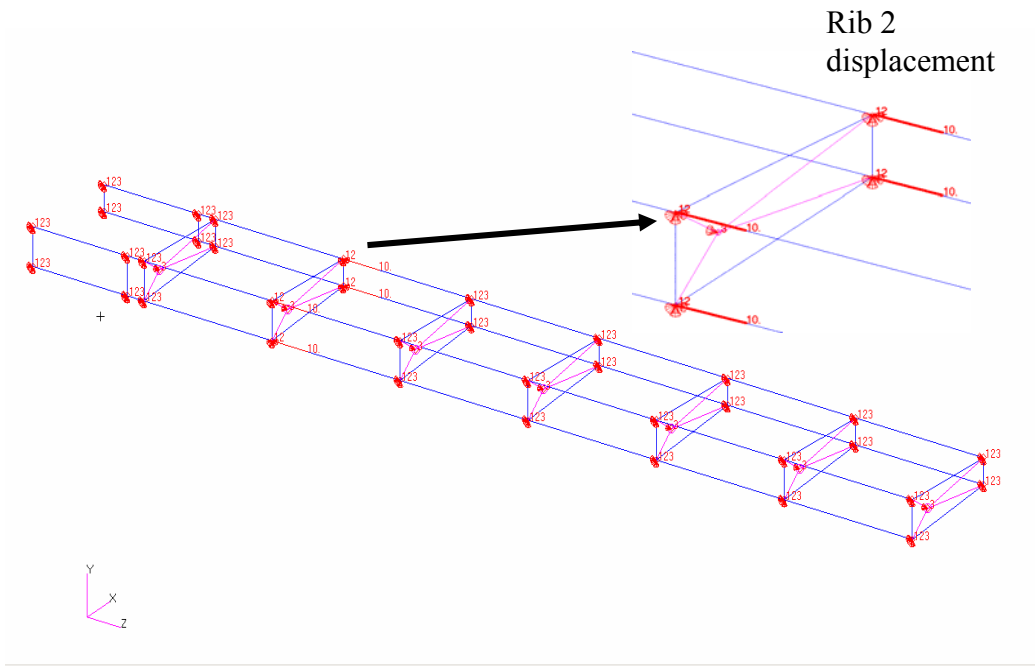


Figure 6.87 Load case 1 in auxiliary model

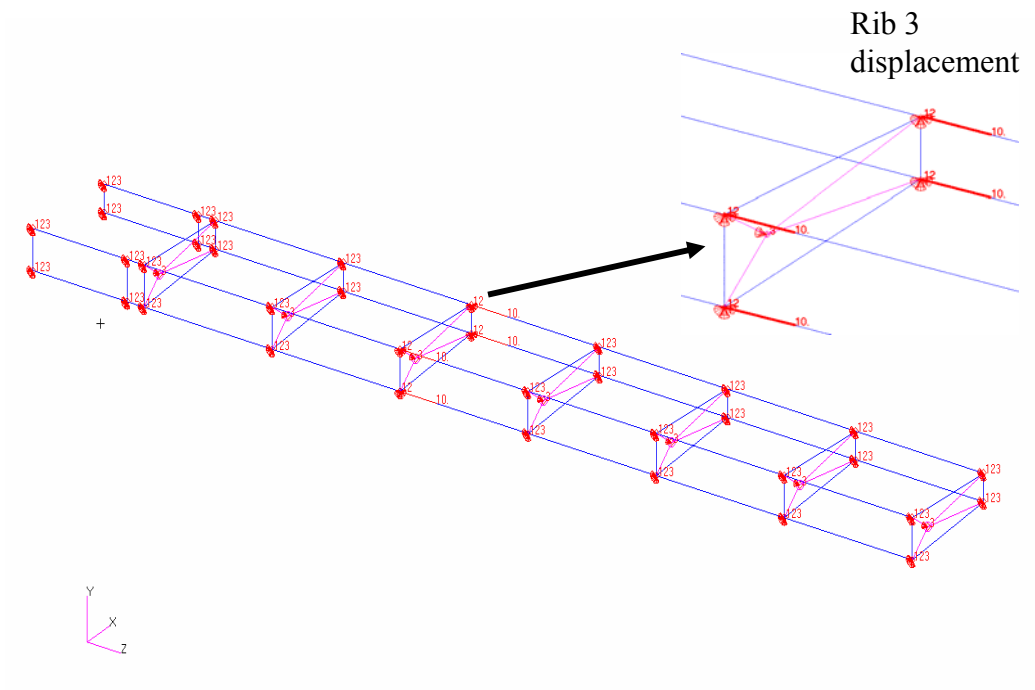


Figure 6.88 Load case 2 in auxiliary model

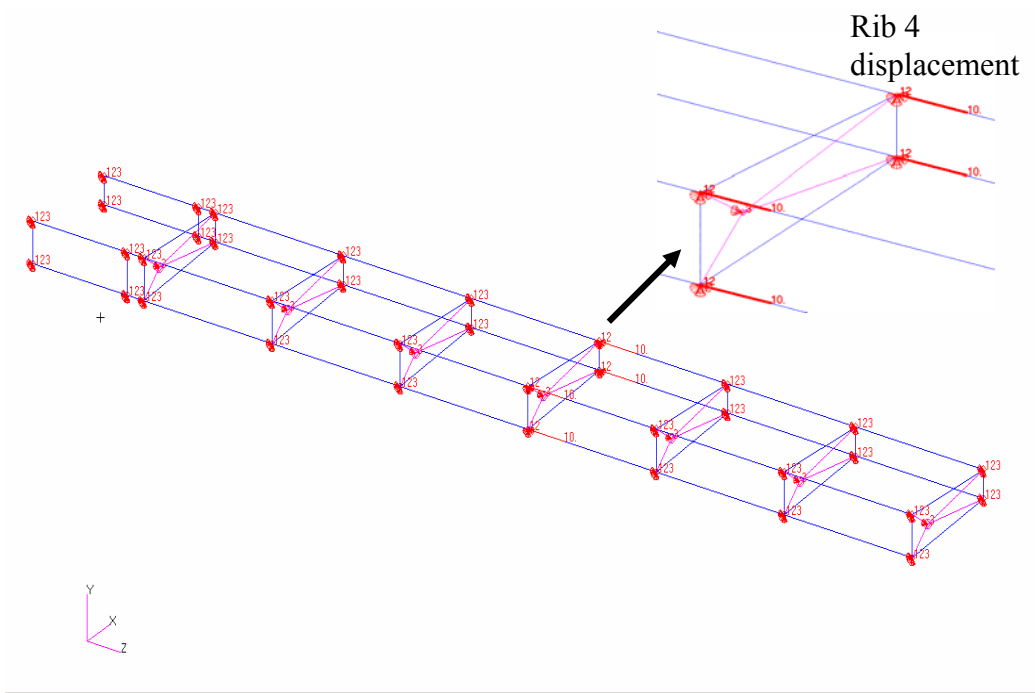


Figure 6.89 Load case 3 in auxiliary model

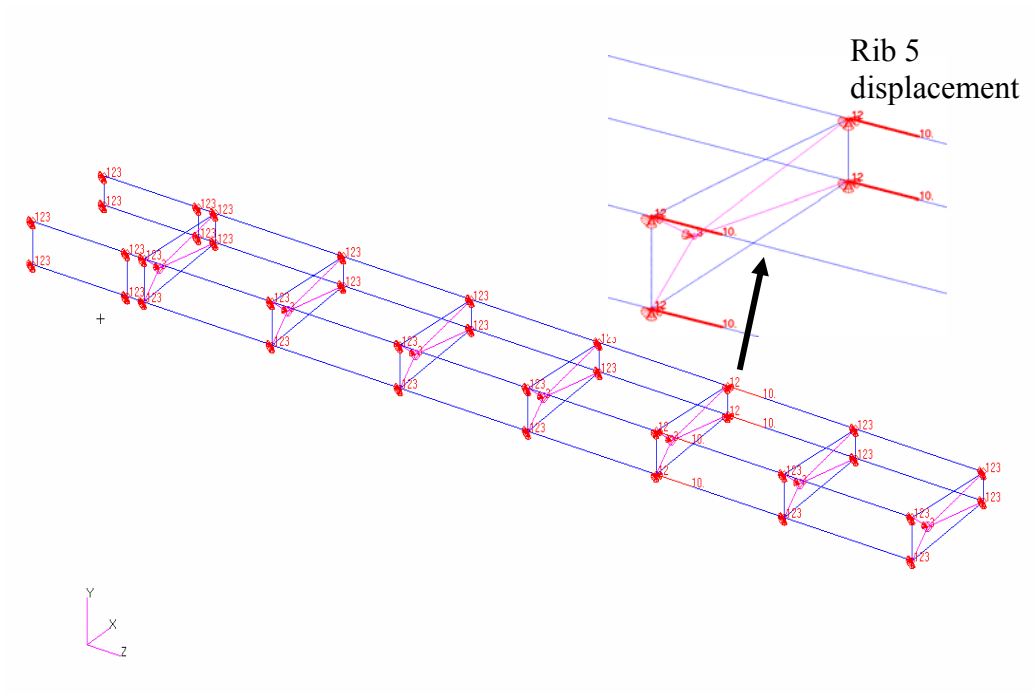


Figure 6.90 Load case 4 in auxiliary model

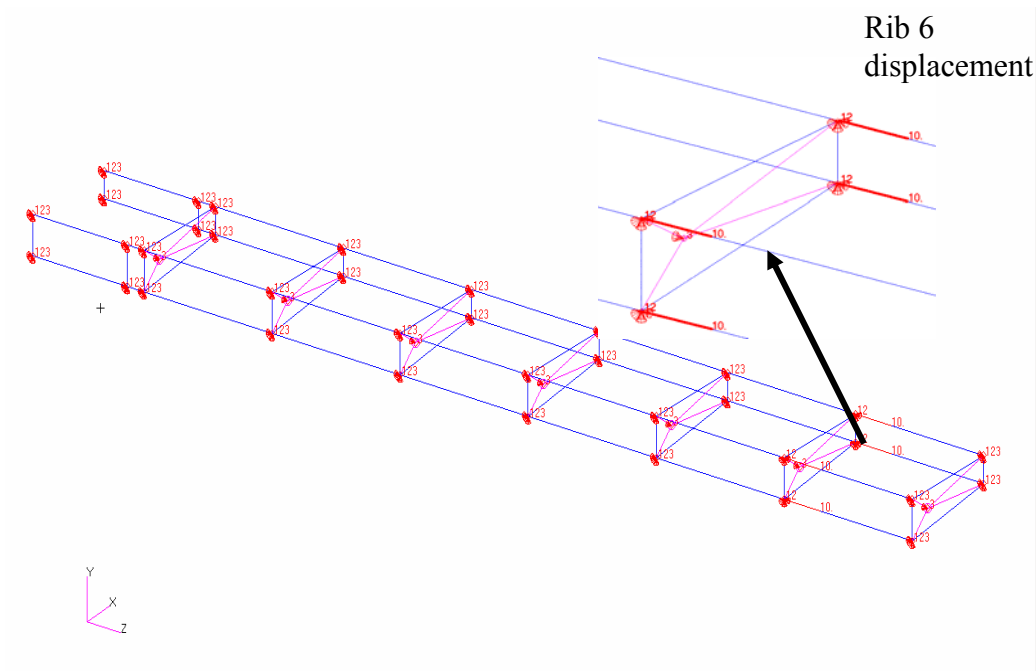


Figure 6.91 Load case 5 in auxiliary model

6.3.1. ONE VARIABLE OPTIMIZATION

In this section the shape optimization module is verified by performing a test optimization study involving the location change of a rib. For this purpose location of a single rib is selected as the main design parameter, and all the other design parameters are kept fixed. All property related design variables defined in the previous sections are taken as fixed quantities and except for rib 2, locations of all the rest of the ribs are also taken as fixed. Since element properties are not defined as design variables there is no objective function in this test case. To verify that the optimizer moves the rib in the correct direction a problem is defined. In the particular study a constraint is applied on the Von Mises stress of element 110030 and the position of rib 2 is taken as the only design variable. Initially, three static analyses are performed with the rib 2 in three different locations along the span of the wing. In the first static analysis rib is taken at its original position, and in the remaining two static analyses rib 2 is moved 300 mm in-board and out-board, respectively. At the end of the three static analyses Von Mises stress on element 110030 is recorded to see the effect of the rib position on the resulting stress on the element. The output of these three static analyses is given in Table 6.24.

Table 6.24 Comparison of linear static analyses of the wing with rib 2 at different spanwise locations

| | Rib 2 is moved towards the root | Rib 2 is in original position | Rib 2 is moved towards the tip |
|--|---------------------------------|-------------------------------|--------------------------------|
| Spanwise location of Rib 2 (mm) | 462.0 | 762.0 | 1062.0 |
| Von Mises Stress on Element 110030 (MPa) | 404.8 | 379.0 | 351.3 |

As it was pointed out above in the particular study there is no change in the objective function which is the weight of the wing because element properties are not assigned as design variables.

In the next analysis a shape optimization run is executed by imposing a constraint on the Von Mises stress on element 110030. Von Mises stress on element 110030 is constrained to be less than 360 MPa and this value is assigned as the single constraint of the optimization problem. This stress value is in between the stress determined by the static analysis with the rib 2 in the original position, and the stress determined by the static analysis with the rib 2 in its displaced position by a distance of 300 mm towards the wing tip. Based on the static analysis results presented in Table 6.24, it is clear that the shape optimizer has to move rib 2 towards the wing tip. The result of the shape optimization will be checked to see if the rib 2 is moved towards the wing tip or not.

Initial model of the wing is shown in Figure 6.92. Final rib 2 location and stress result of element 110030 are shown in Figures 6.93 and 6.94, respectively.

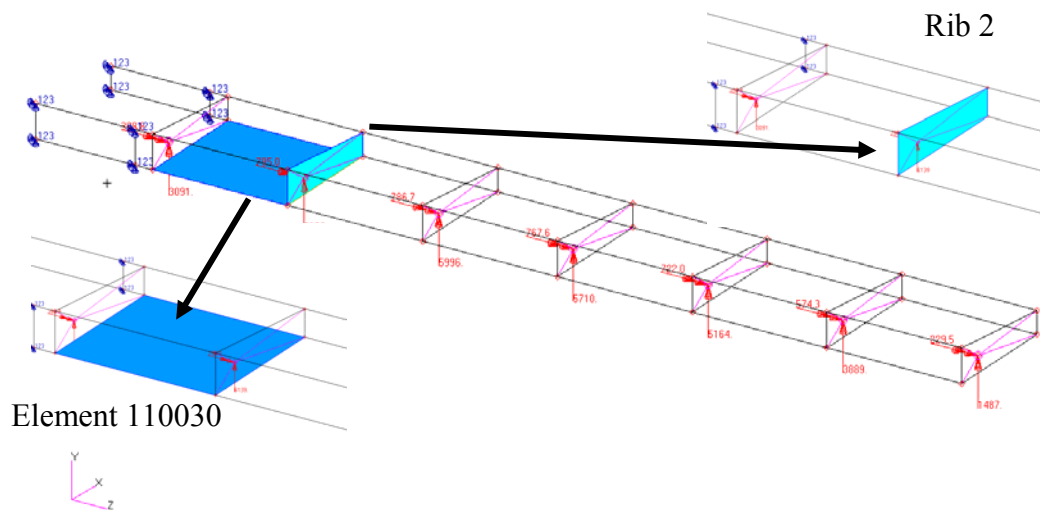


Figure 6.92 Initial wing model with distributed loading

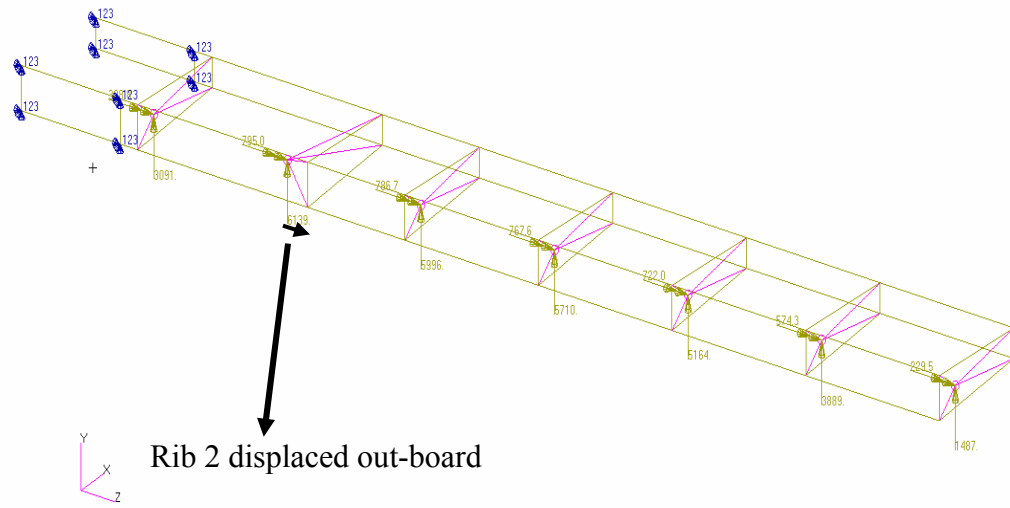


Figure 6.93 Final location of the rib 2 on the wing model

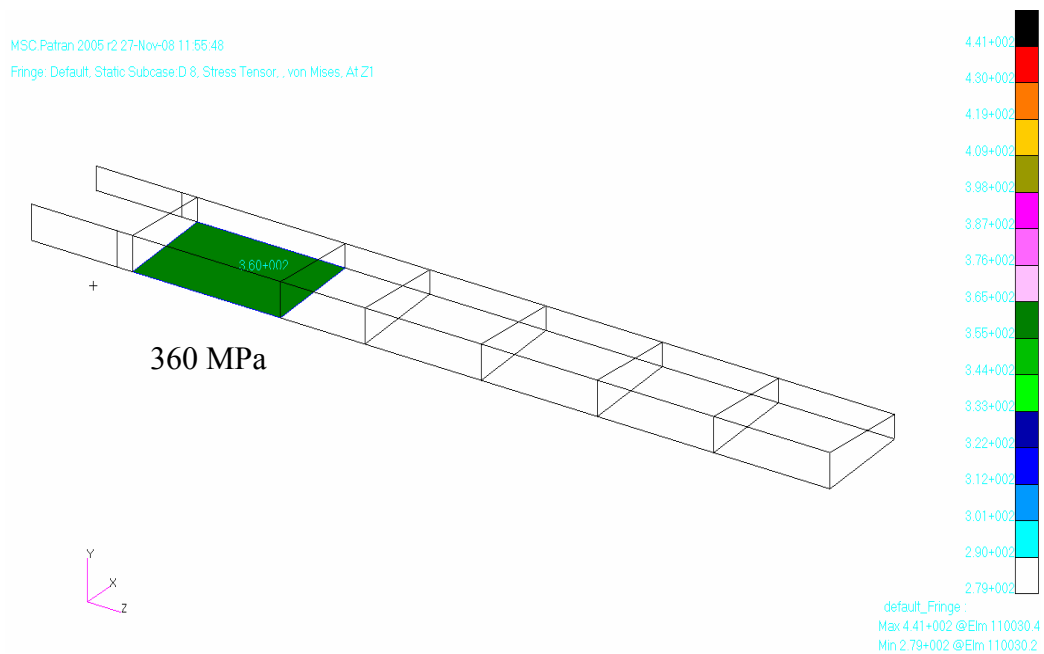


Figure 6.94 Final Von Mises stress on the element 110030

At the end of the shape optimization MSC.NASTRAN[®] shape optimizer has moved the rib 2 towards the tip by 208.4 mm so that Von Mises stress on the element 110030 became 360 MPa. The new position of rib 2 is between the original position of the rib 2 and the outboard displaced position of the of rib 2 given in Table 6.24, as expected. History of the objective function is given in Figure 6.95. Each design cycle indicates 1 iteration which is a complete loop described in figure 4.1. Since the element properties are not considered as the design variables the objective function which is the weight of the wing is kept constant. The initial weight is calculated based on the initial values of the element properties which were given in the previous section. The variation of the design variable, which is the position of rib 2, with respect to the design cycle is plotted in Figure 6.96. It is seen that in seven design cycles rib 2 moved out-board such that the constraint imposed on the Von Mises stress on element 110030 is satisfied. The history of the constraint function is shown in Figure 6.97. At the end of the seventh design cycle the constraint function becomes zero which means that the constraint is satisfied.

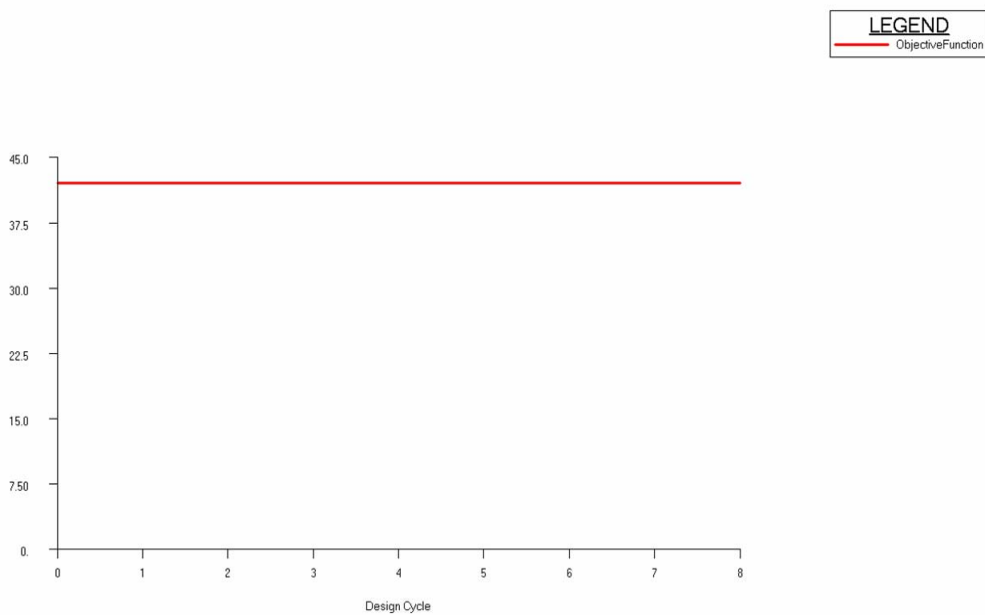


Figure 6.95 History of objective function (in kg)

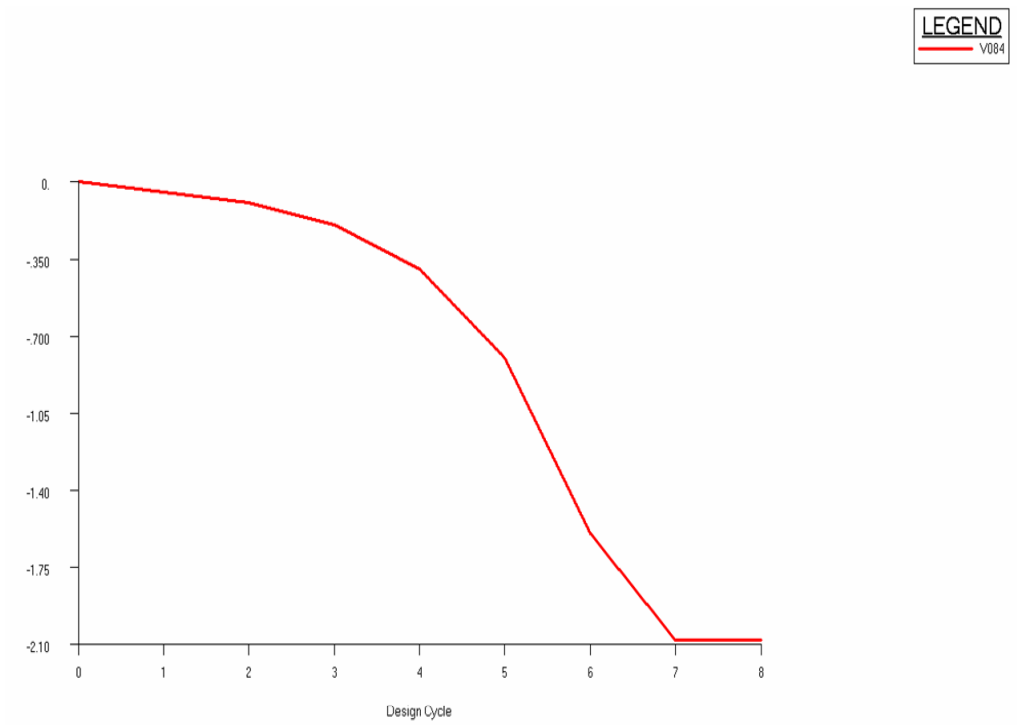


Figure 6.96 History of rib 2 location (in 100 mm)

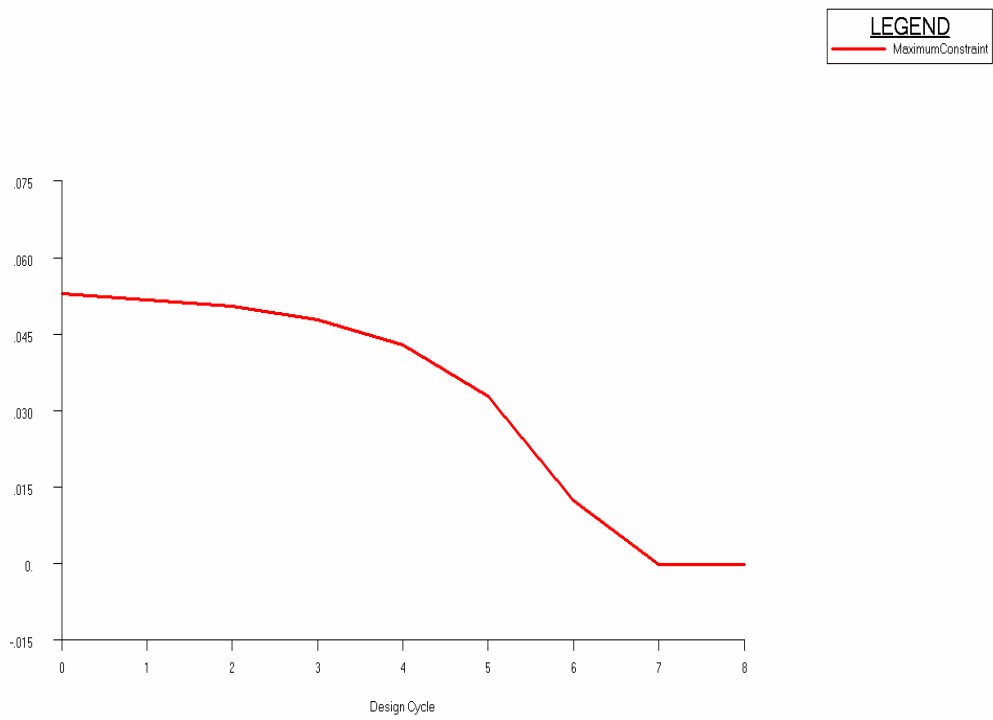


Figure 6.97 History of the maximum constraint value

6.3.2. MULTI VARIABLE OPTIMIZATION

In this section, property optimization and shape optimization are performed together for the wing torque box with distributed loading. Each rib is allowed to move in-board and out-board by a distance equal to the half the distance between the rib and the neighboring in-board and out-board rib. Since rib positions are also included in the design variables, the expectation is to end up with a final optimized configuration with less weight. The same finite element model is used as in the previous sections. Aerodynamic lift force and pitching moment are again applied on a node, which is created at 33.91% chord and on the camber line, at each rib location. The location of the load application nodes are not changed during the optimization process. Rigid RBE3 element of MSC.NASTRAN[®] is used to distribute the applied load to the nodes at the intersection of the ribs with the front and rear spar. Auxiliary model which was described in section 6.3 is used for constructing the shape basis vectors. Displacement boundary condition applied and distributed loading are shown in Figure 6.98.

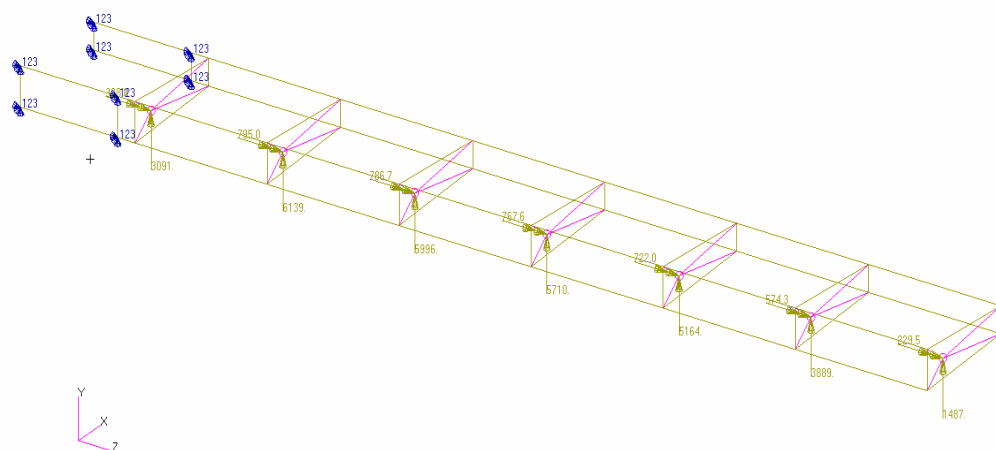


Figure 6.98 Initial wing model with distributed loading

Initial linear static run results are exactly same as in section 6.2. The element property optimization problem defined in section 6.2 is also same as the current problem with the addition of shape optimization. Solution took 35.437 seconds of CPU time.

In the optimized wing configuration, final rib locations and the element properties of the wing model are shown in Figures 6.99-6-107.

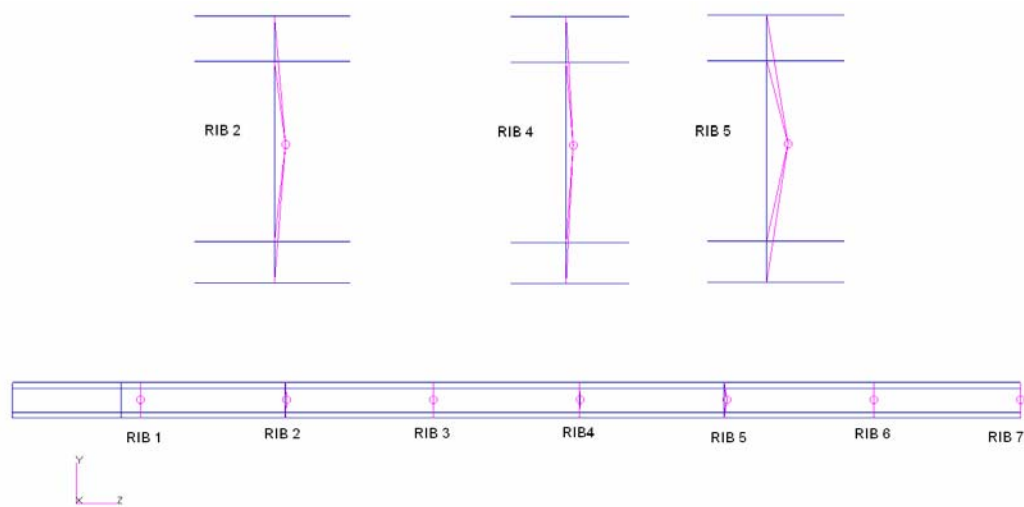


Figure 6.99 Final rib locations on the wing model

Figure 6.99 shows that rib positions in the optimized configuration are very close to the original rib positions. Ribs 2 , 4 and 5 are seen to displace most in the final configuration. In Figure 6.99, the location of the load application node is fixed, therefore the perpendicular distance from the load application point to the rib gives the distance by which the ribs move.

MSC.Patran 2005 r2 27-Nov-08 12:47:26
Area Scalar Plot

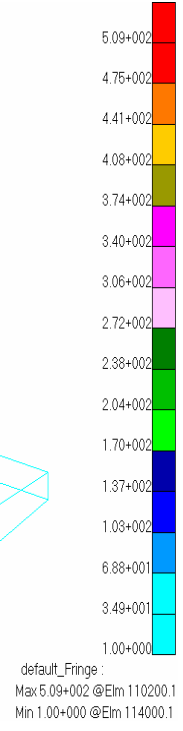
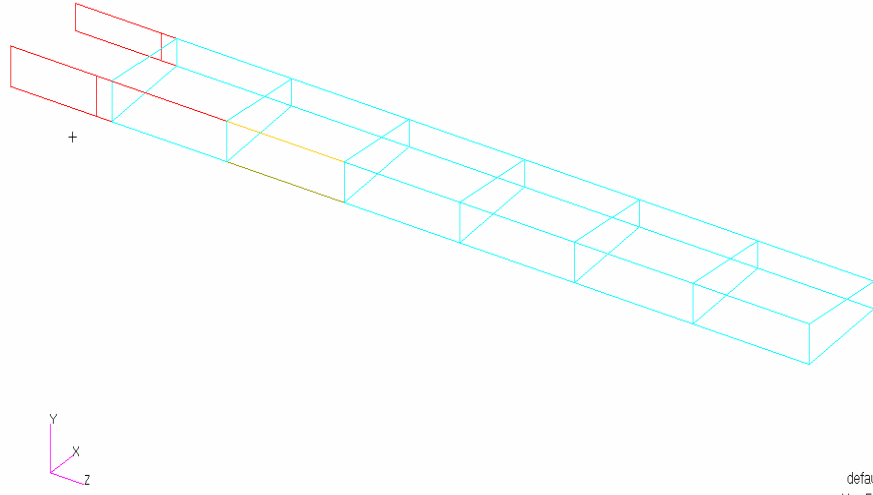


Figure 6.100 Final flange areas of the wing model

MSC.Patran 2005 r2 27-Nov-08 12:49:00
Thickness Scalar Plot

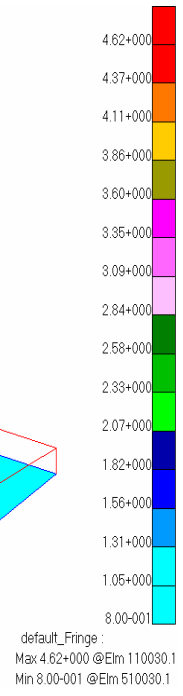
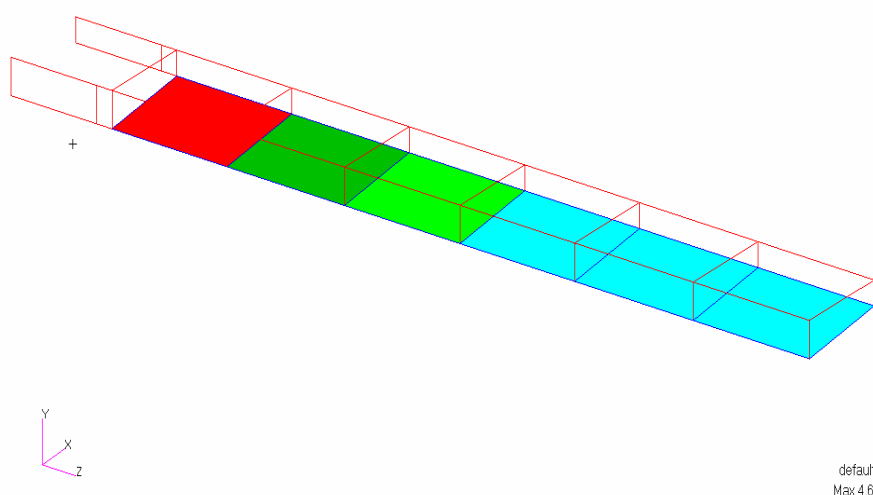


Figure 6.101 Final lower skin thicknesses of the wing model

MSC.Patran 2005 r2 27-Nov-08 12:50:39
Thickness Scalar Plot

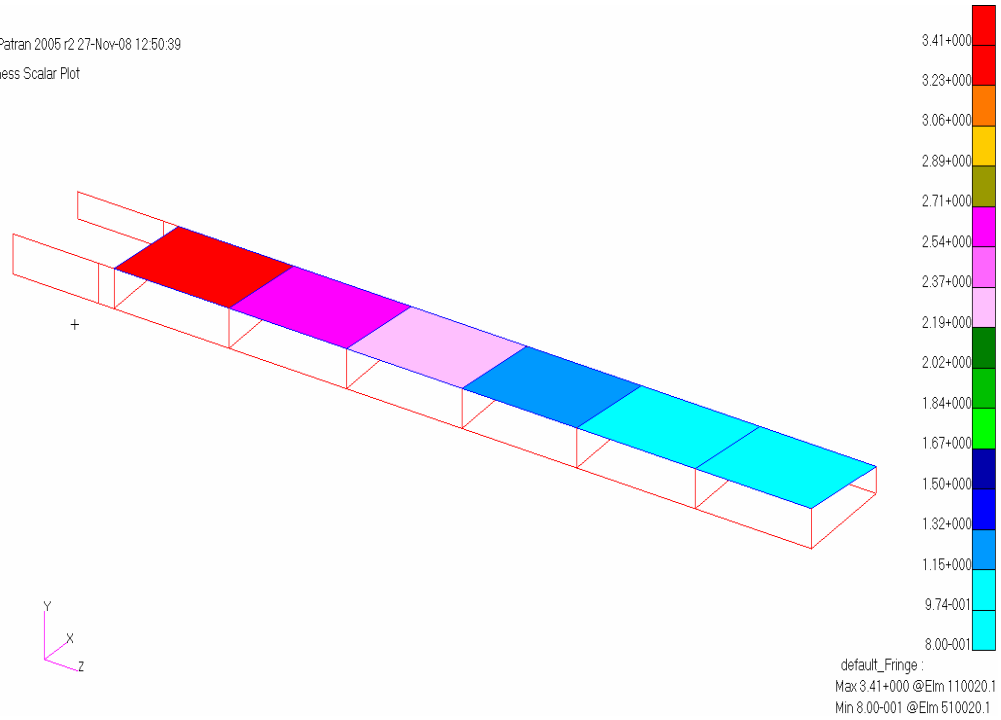


Figure 6.102 Final upper skin thicknesses of the wing model

MSC.Patran 2005 r2 27-Nov-08 12:52:42
Thickness Scalar Plot

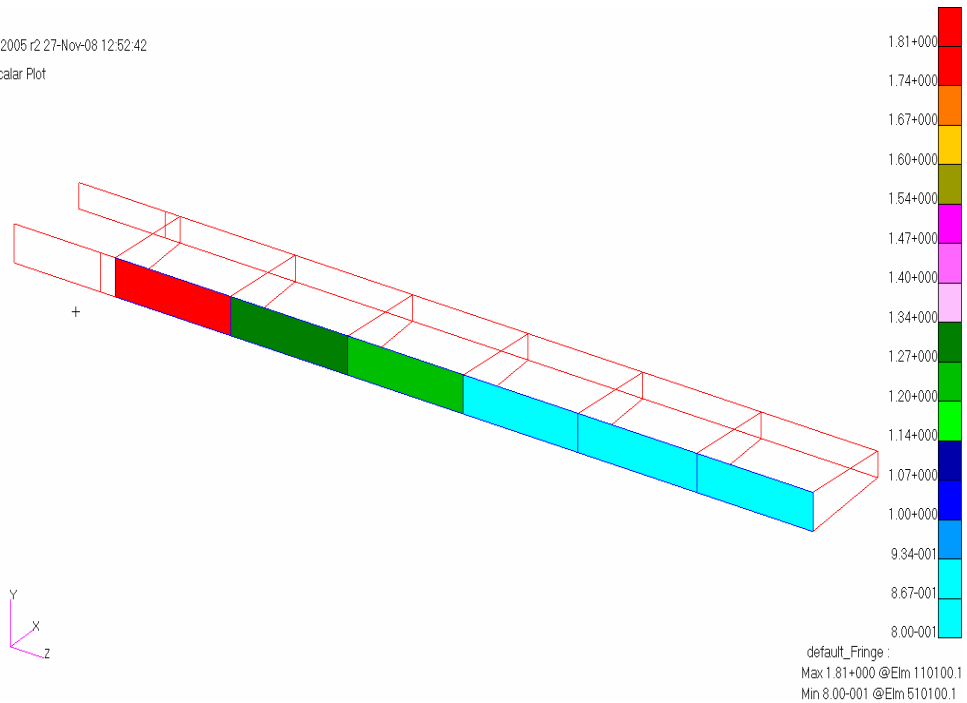


Figure 6.103 Final front spar thicknesses of the wing model

MSC.Patran 2005 r2 27-Nov-08 12:54:18
Thickness Scalar Plot

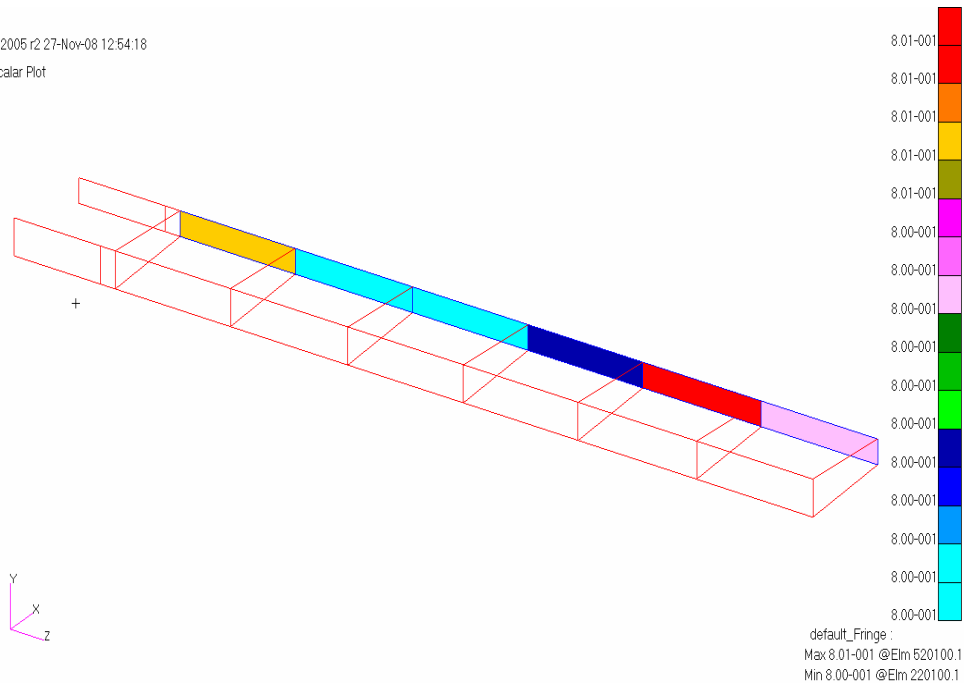


Figure 6.104 Final rear spar thicknesses of the wing model

MSC.Patran 2005 r2 27-Nov-08 12:55:38
Thickness Scalar Plot

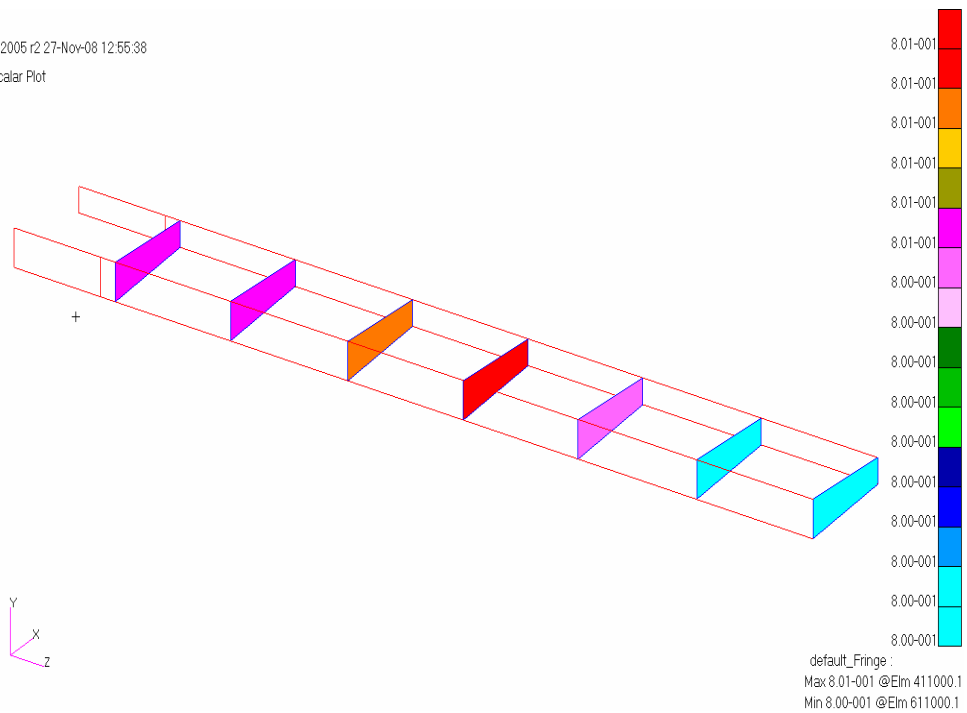


Figure 6.105 Final rib web thicknesses of the wing model

MSC.Patran 2005 r2 27-Nov-08 12:57:24
Thickness Scalar Plot

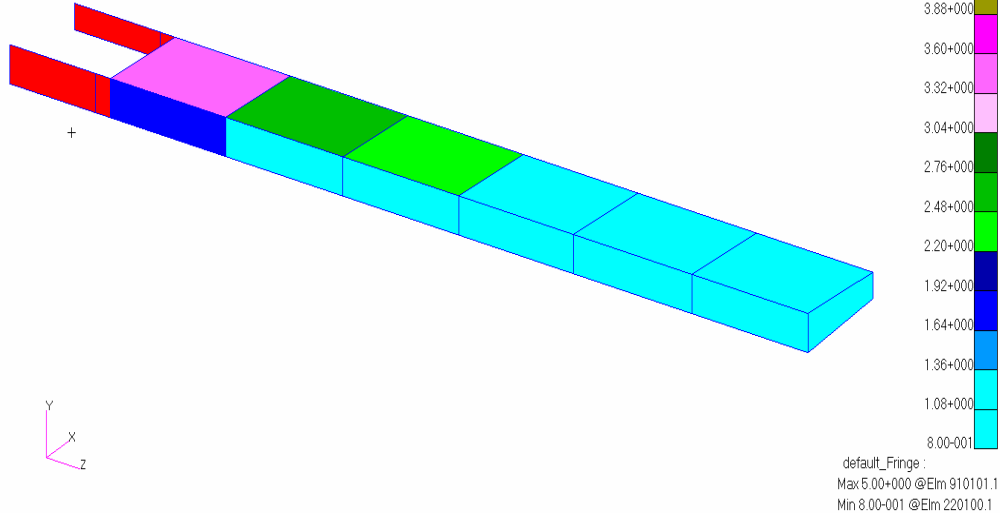


Figure 6.106 Final rib web thicknesses of the wing model

MSC.Patran 2005 r2 27-Nov-08 12:57:50
Thickness Scalar Plot

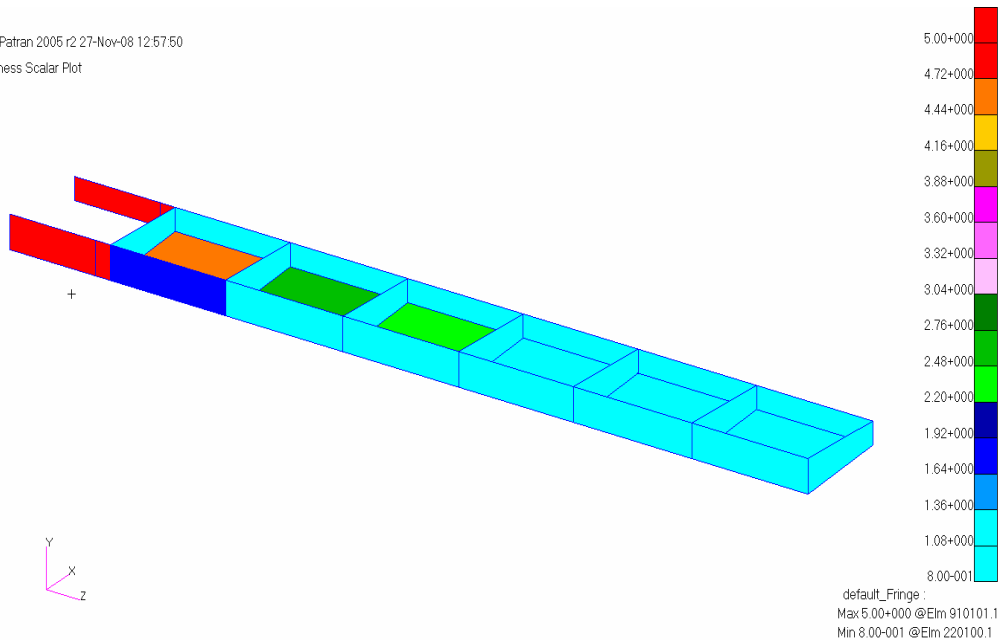


Figure 6.107 Final Rib web thicknesses of the wing model interior view

In the optimized configuration final analysis results are shown in Figures 6.108 – 6.111. Comparison of the stress analysis results given in Figures 6.108-6.110 with the stress analysis results of the element property optimization problem given in Figures 6.65-6.67 show that there is increase in the stress values, and this is an indication of weight reduction accomplished by shape optimization. Actually, in the original element property optimization problem there was a weight increase from the initial configuration to satisfy the constraints. In the current problem the initial configuration is again selected as the same initial configuration used in element property optimization. To be sure about the weight reduction the history of the objective function has to be checked, and this is done the subsequent pages.

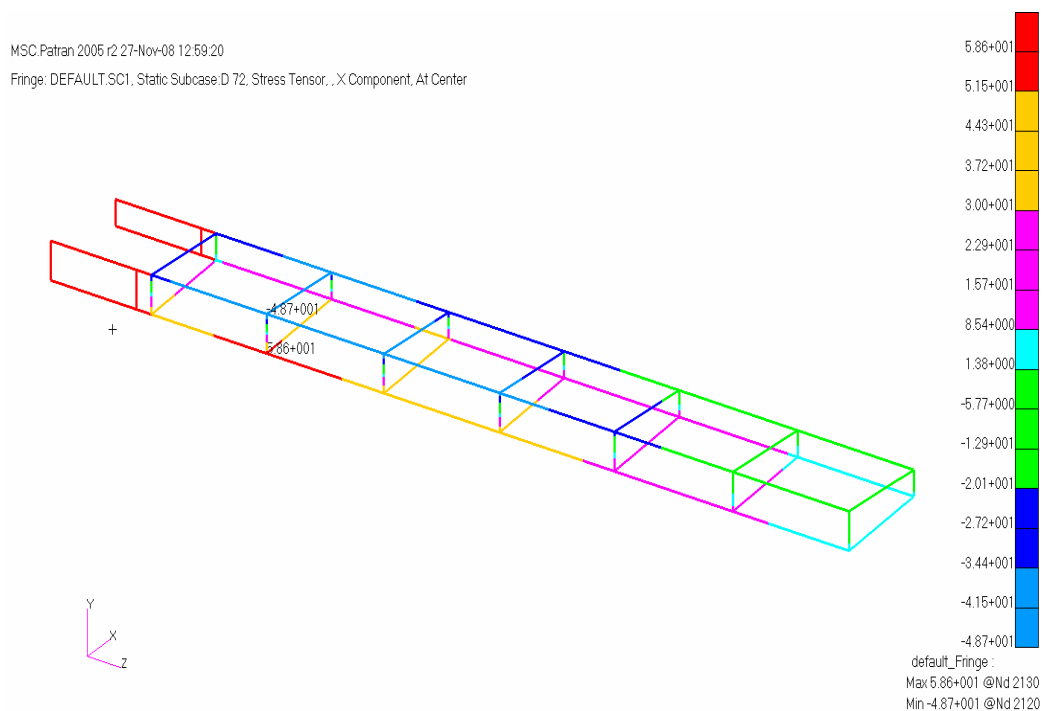


Figure 6.108 Final axial stresses on the flanges

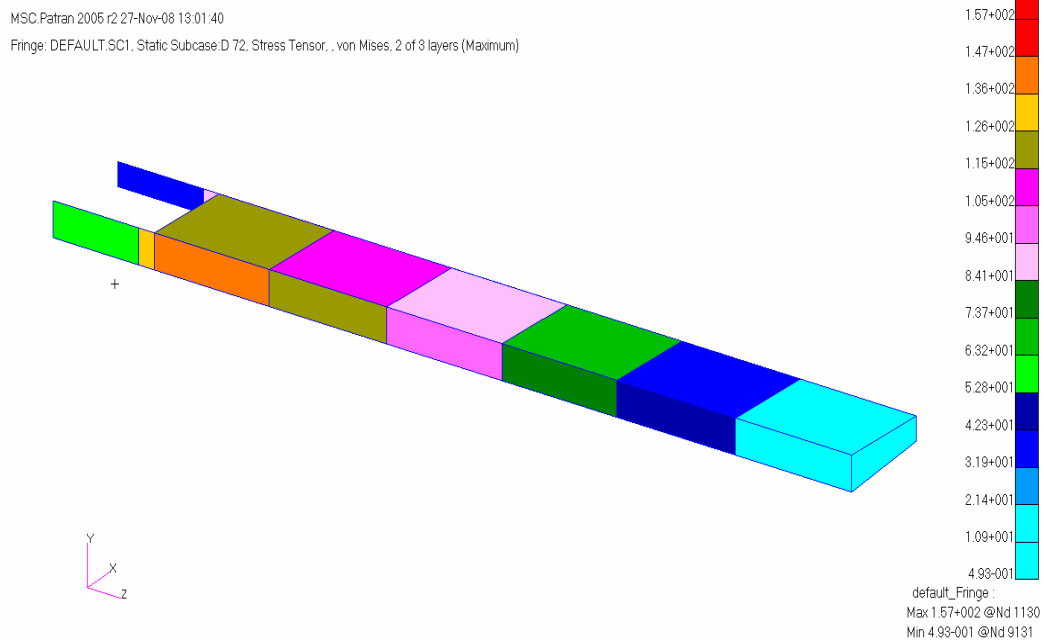


Figure 6.109 Final Von Mises stresses on the skins and the webs

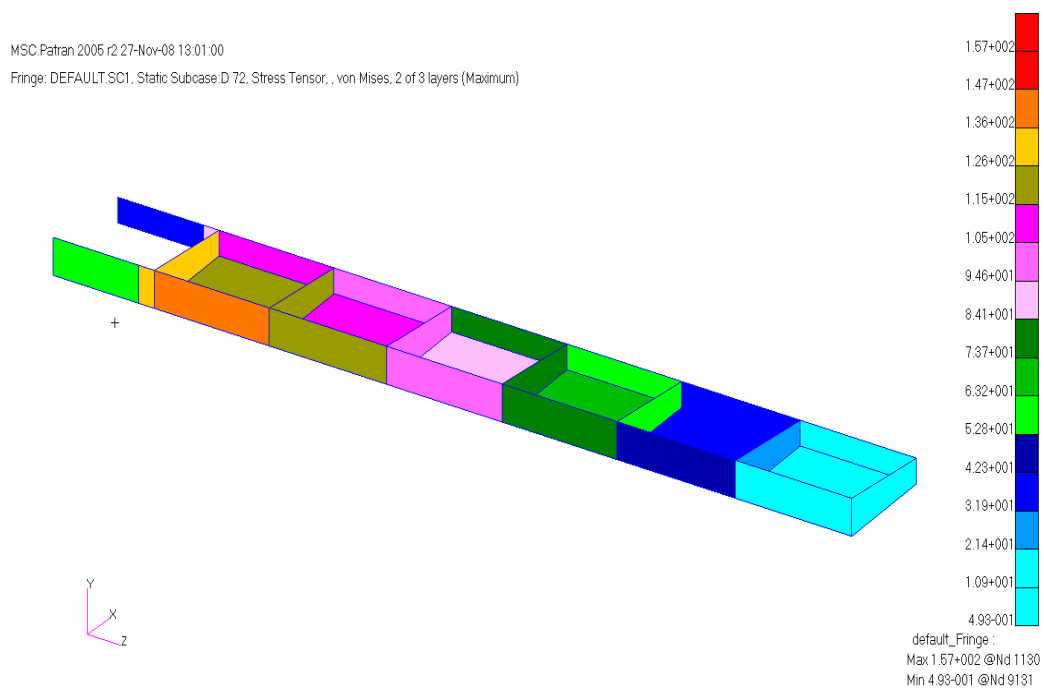


Figure 6.110 Final Von Mises stresses on the skins and the webs interior view

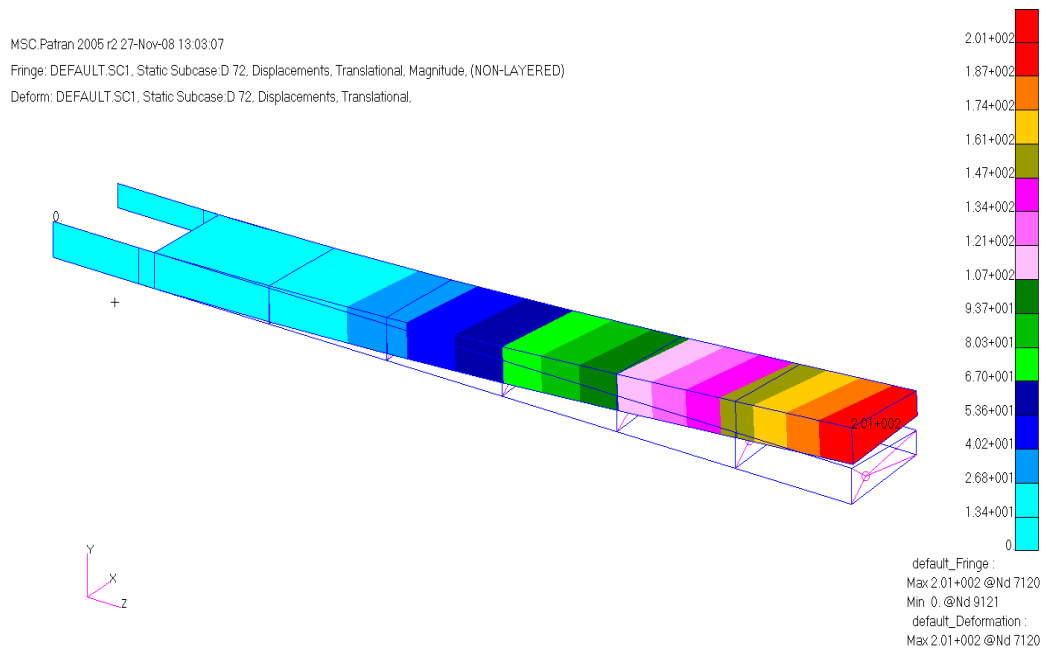


Figure 6.111 Final deflection of the wing model

History of objective function is given in Figure 6.112. Each design cycle indicates 12 iteration, therefore optimization process converged in 72 iterations. It can be seen from Figure 6.112 that the value of the objective function again increase compared to the value at of the objective function at the initial configuration. However, comparison of Figure 6.112 with Figure 6.69 reveals that the value of the objective function in the optimized configuration is less in the combined property and shape optimization solution. In the optimized configuration wing weighs about 51.5 kg which is 8.5 kg less compared to the final weight of the wing obtained in pure element property optimization. This results shows that shape optimization is also a very critical issue in optimizing aerospace structures because in aerospace structures there are many structural elements whose positions can be adjusted in the optimum way to achieve further weight reduction.

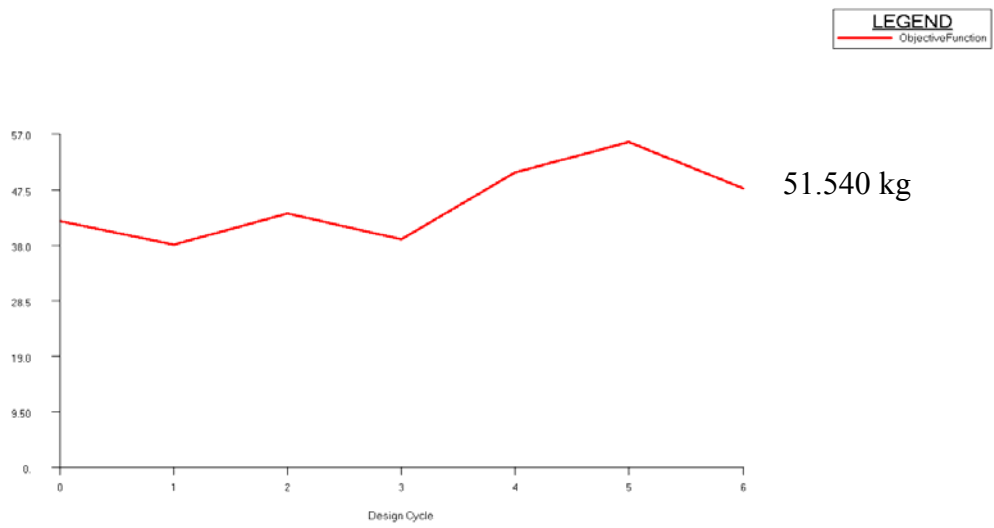


Figure 6.112 History of objective function

The history of the design variables are given in Figure 6.113-6.128.

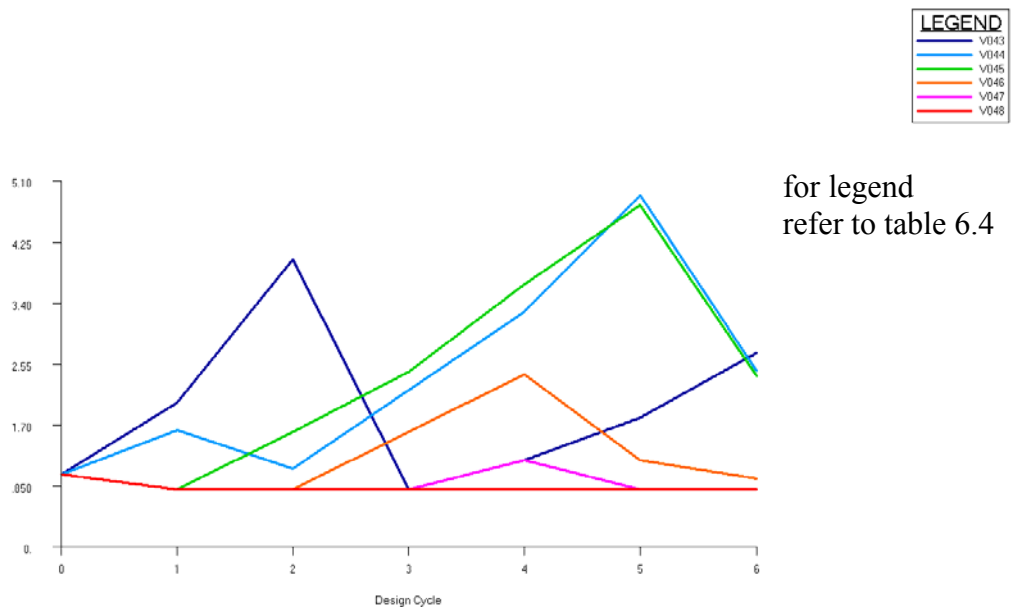


Figure 6.113 History of lower skin thicknesses (in mm)

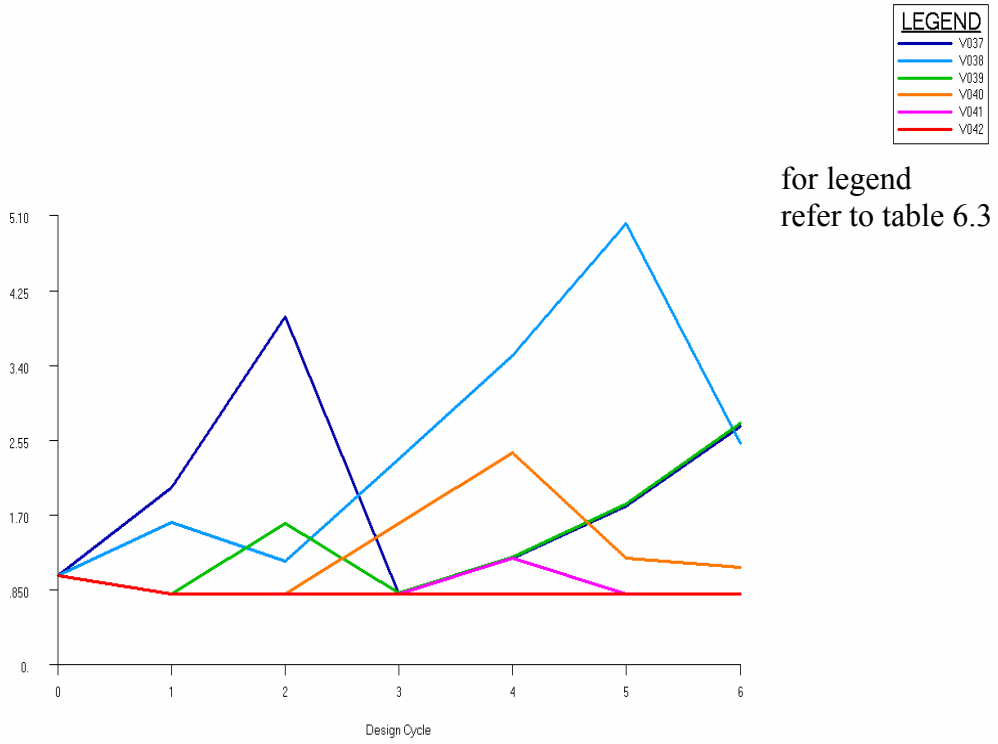


Figure 6.114 History of upper skin thicknesses (in mm)

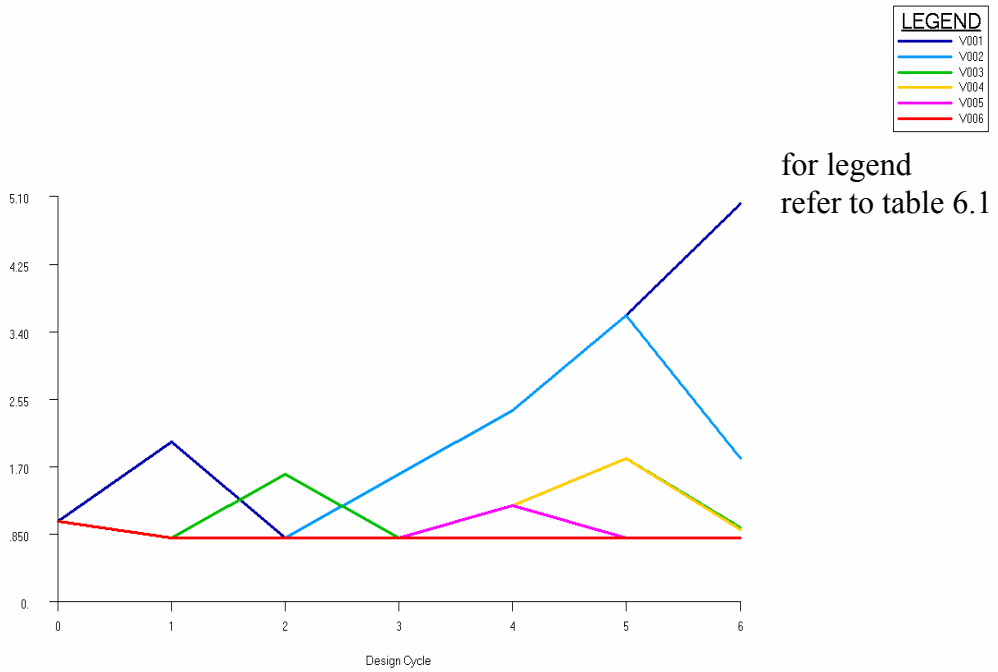


Figure 6.115 History of front spar web thicknesses (in mm)

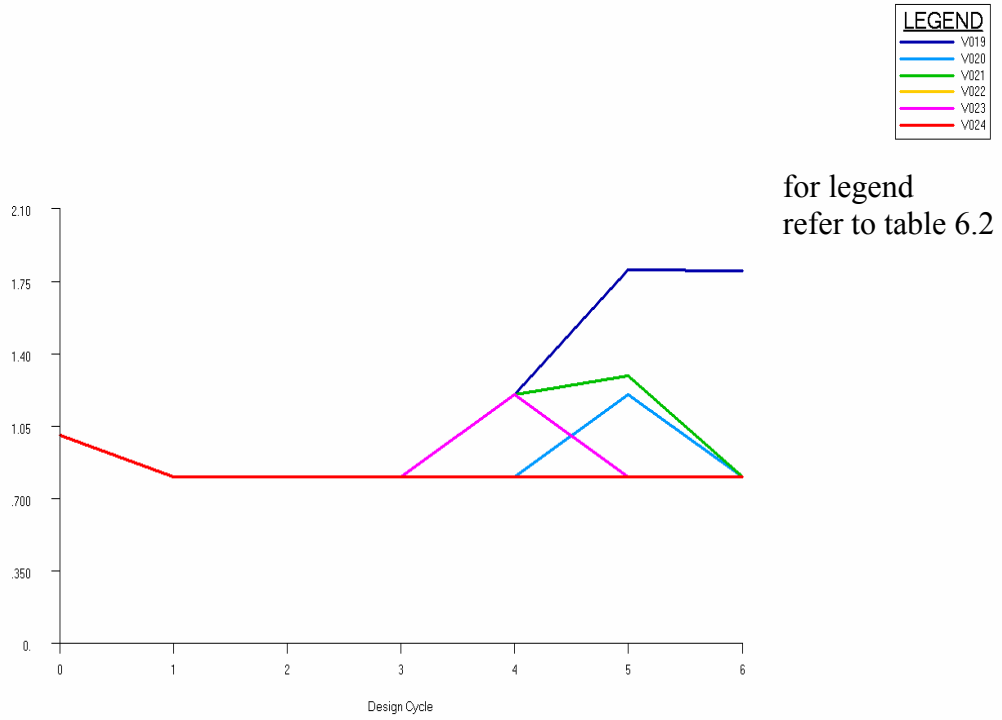


Figure 6.116 History of rear spar web thicknesses (in mm)

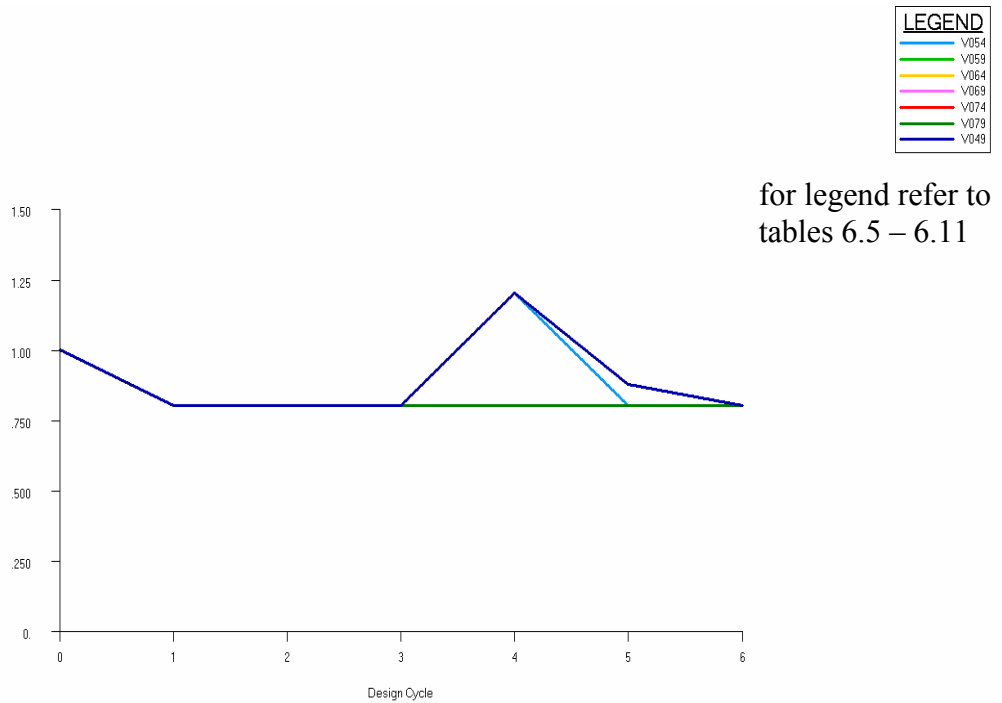


Figure 6.117 History of rib web thicknesses (in mm)

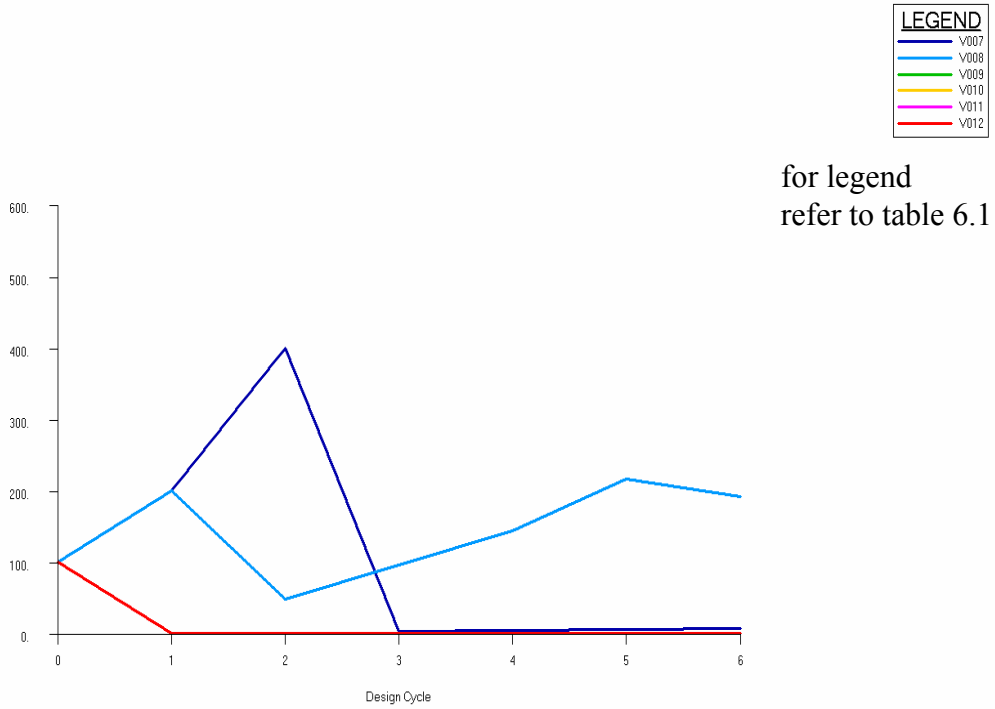


Figure 6.118 History of upper flange areas of front spar (in mm²)

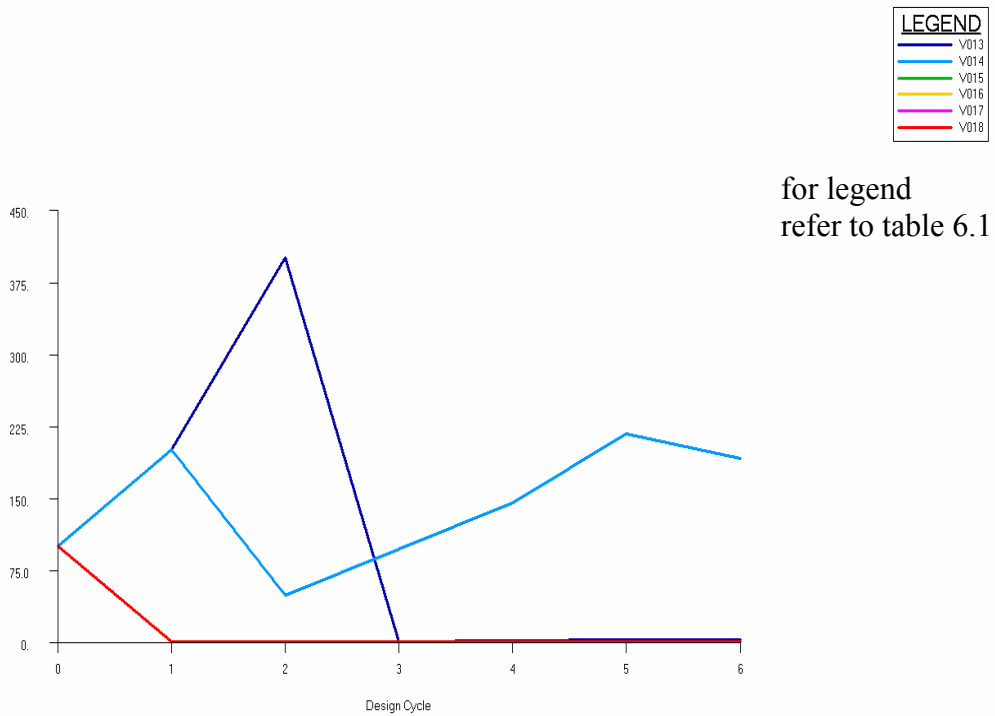


Figure 6.119 History of lower flange areas of front spar (in mm²)



for legend
refer to table 6.2

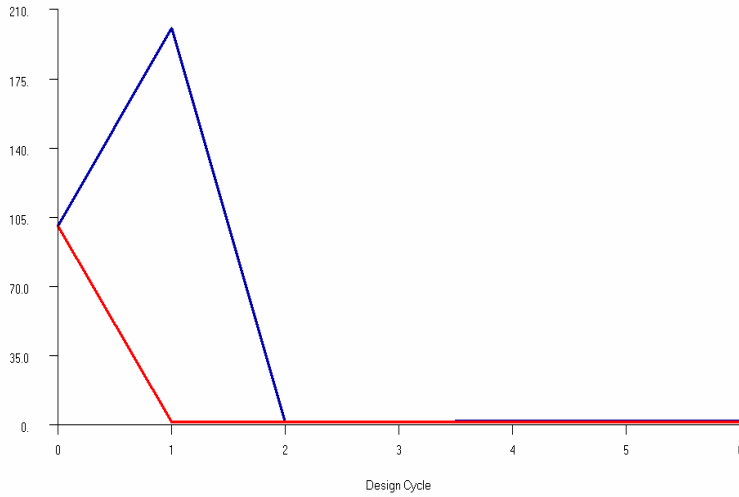


Figure 6.120 History of upper flange areas of rear spar (in mm²)



for legend
refer to table 6.2

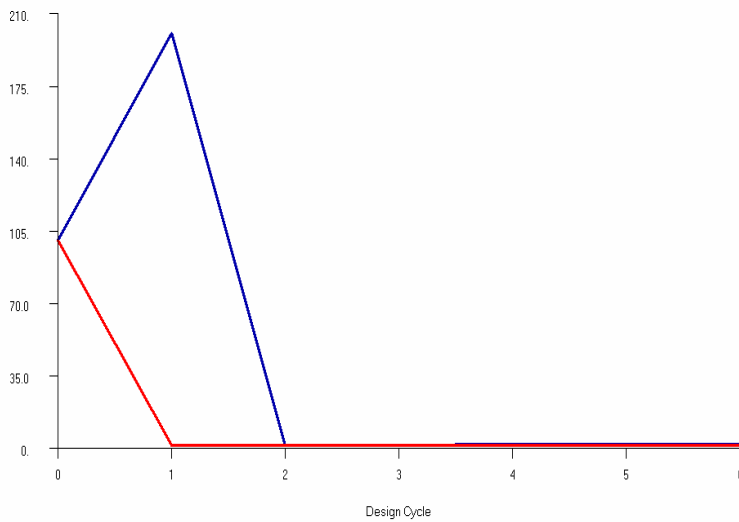


Figure 6.121 History of lower flange areas of rear spar (in mm²)



for legend
refer to table 6.5

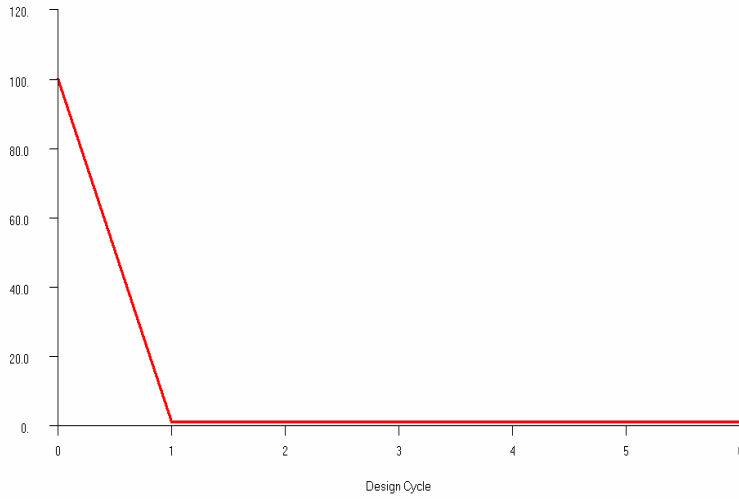


Figure 6.122 History of flange areas of rib 1 (in mm²)



for legend
refer to table 6.6

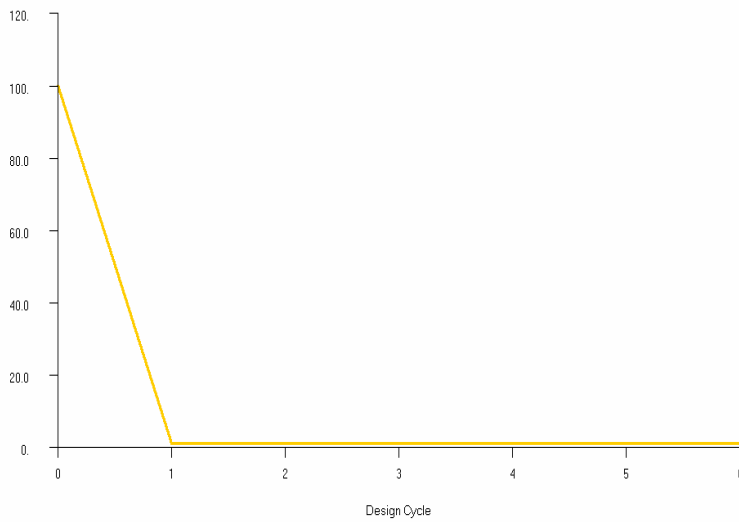


Figure 6.123 History of flange areas of rib 2 (in mm²)



for legend
refer to table 6.7

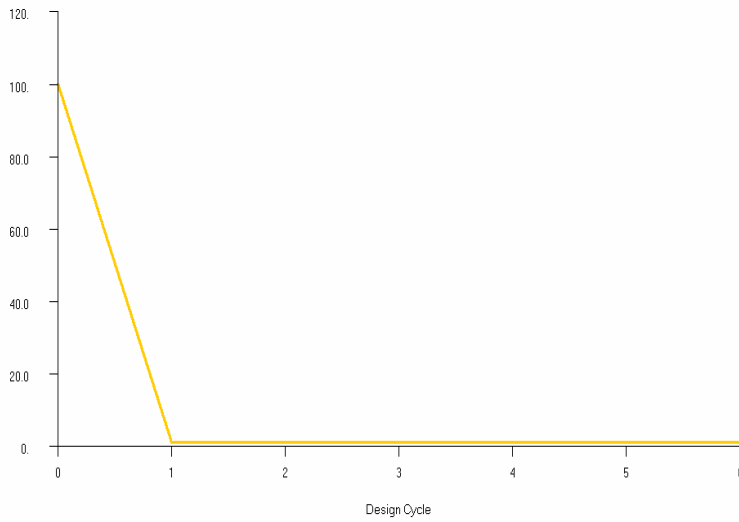


Figure 6.124 History of flange areas of rib 3 (in mm²)



for legend
refer to table 6.8

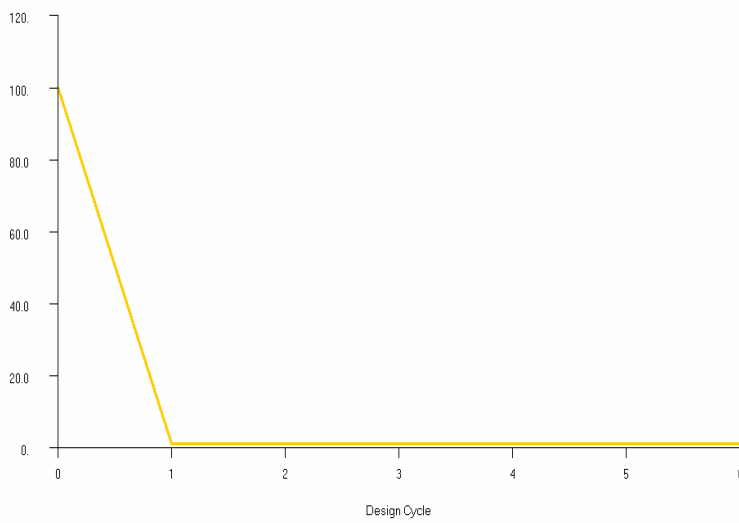


Figure 6.125 History of flange areas of rib 4 (in mm²)



for legend
refer to table 6.9

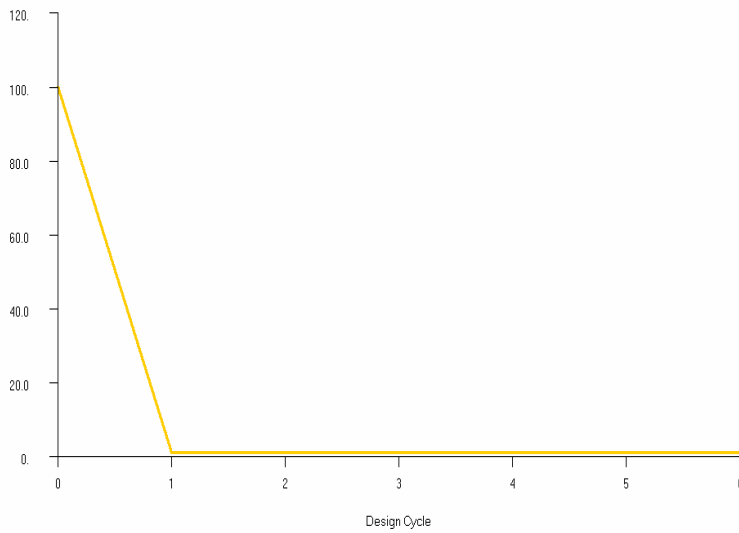


Figure 6.126 History of flange areas of rib 5 (in mm²)



for legend
refer to table 6.10

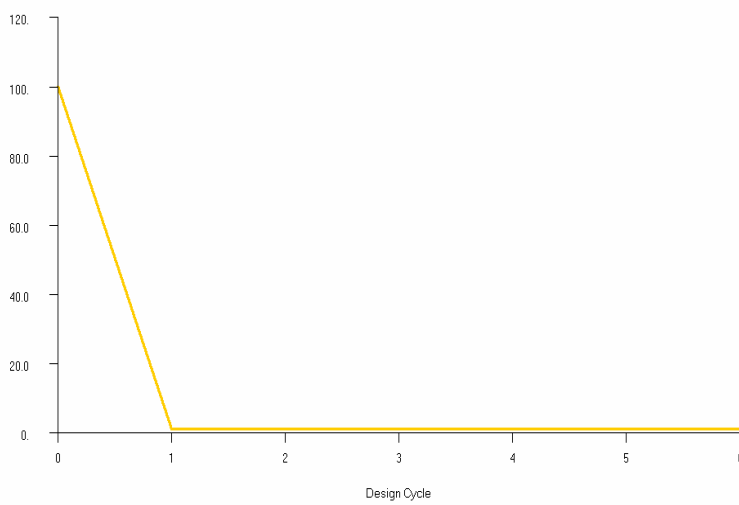


Figure 6.127 History of flange areas of rib 6 (in mm²)

| LEGEND | |
|--------|------|
| — | V080 |
| — | V081 |
| — | V082 |
| — | V083 |

for legend
refer to table 6.11

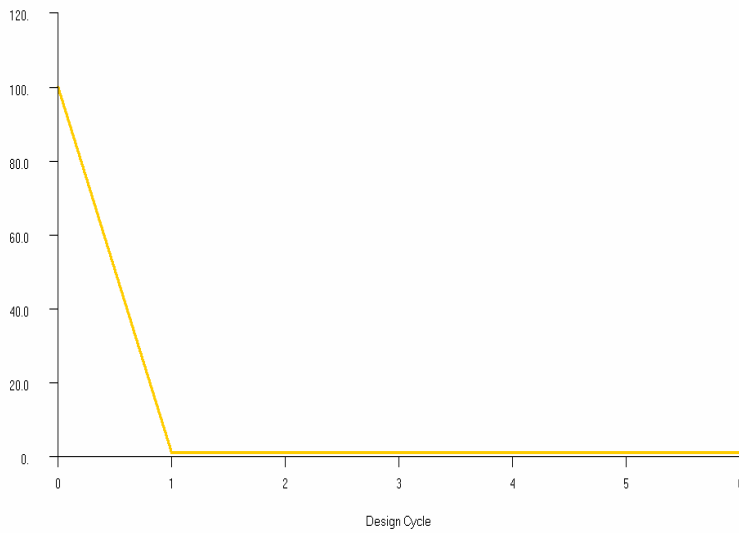


Figure 6.128 History of flange areas of rib 7 (in mm²)

| LEGEND | |
|--------|-------------------|
| — | MaximumConstraint |

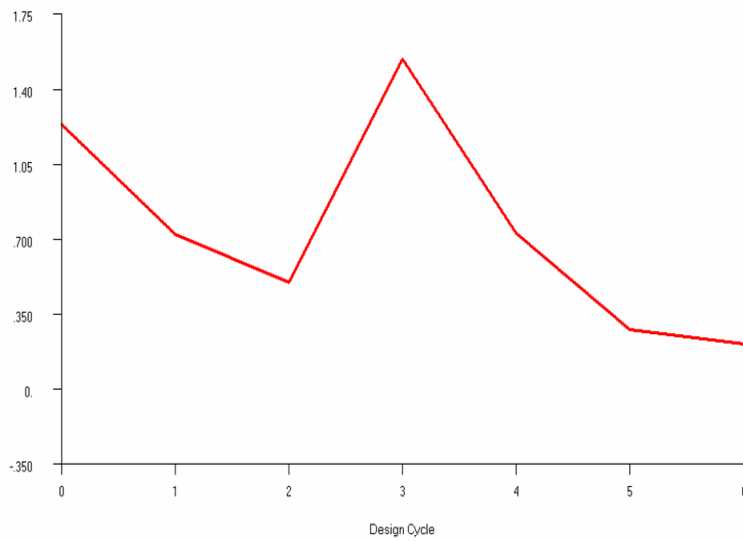


Figure 6.129 History of maximum constraint value

6.4 COMPARISON OF OPTIMIZATION STUDIES OF THE WING TORQUE BOX

In this section, the three optimization results are compared in Table 6.25. Detailed comparison tables for each constraint are in appendix C.3

Table 6.25 Comparison of results of three optimization processes

| | Lower Bound | Upper Bound | | Property Optimization | | Property & Shape Optimization |
|----------------------------------|-------------|-------------|---------|-----------------------|---------------------|-------------------------------|
| | | | | Tip Loading | Distributed Loading | Distributed Loading |
| Number of iterations | - | - | - | 27 | 23 | 72 |
| CPU time (second) | - | - | - | 12.578 | 8.140 | 35.437 |
| Objective function | - | - | Initial | 42.008 | 42.008 | 42.008 |
| | - | - | Final | 56.671 | 60.027 | 51.540 |
| Max. stress on the Skins (Mpa) | 0.01 | 281 | Initial | 480 | 379 | 379 |
| | | | Final | 277 | 178 | 123 |
| Max. stress on the Webs (Mpa) | 0.01 | 300 | Initial | 238 | 203 | 203 |
| | | | Final | 289 | 195 | 145 |
| Max. stress on the Flanges (Mpa) | 0.00 | 445 | Initial | 600 | 455 | 455 |
| | | | Final | 379 | 263 | 168 |
| Min. stress on the Flanges (Mpa) | -425 | 0.00 | Initial | -601 | -455 | -455 |
| | | | Final | -194 | -108 | -127 |
| Max. deflection at tip (mm) | 0.001 | 200 | Initial | 256 | 446 | 446 |
| | | | Final | 157 | 201 | 201 |

In all optimization processes weight is increased compared to the weight at the initial configuration without violating any constraint. Comparison of the property optimization results with the distributed loading with the results of the combined property and shape optimization shows that the maximum tip displacement condition is the more restricting condition. The final maximum

stress values are below their limits but the tip deflection reaches to the limit value. It can be seen that combined property and shape optimization results in significant weight reduction compared to just property optimization. This problem is a clear indication that shape optimization can play an important role in weight reduction. Shape optimization can be especially important in aerospace structures which is composed of many sub-elements whose positions can all be considered as a design variable to be used in the optimization process. However, the result of combined property/shape optimization may not be attributed to the rib location change only. It may be that when shape optimization is also incorporated in the solution of the optimization problem a better local minimum could have been obtained. Since in this example no multi-disciplinary optimization problem is defined, there might be many local minimums, and with combined property/shape optimization a different local minimum could be converged to. It should be expected that in a multi-disciplinary optimization problem, the number of local minimums may decrease significantly.

It should be noted that in the problem definition some of the constraints and upper and lower bounds of the design variables might not have been selected as reasonable figures. Therefore, results may not reflect a configuration that can be manufactured. However, in this chapter the aim was to demonstrate the use of element and shape optimization and to show the significant impact that the combined property and shape optimization might have on structural efficiency.

CHAPTER 7

CONCLUDING REMARKS AND FUTURE WORK

The main objective of the thesis was to demonstrate the application of three different strategies of structural optimization which are commonly used in the academic studies and industrial applications. Structural optimization requires an optimizer code working in conjunction with a solver code which mainly evaluates the constraint functions and calculates the objective function. For this purpose some people develop their own optimizer and solver codes, or some people develop only the optimizer and use a ready solver code which is typically a finite element code in structural analysis. In addition, nowadays there are many very efficient commercial finite element programs with embedded optimization modules, and especially in industrial work these commercial codes can be used very effectively to design optimum structures. In this thesis all three strategies of structural optimization are demonstrated. These approaches are listed below.

Approach 1: A gradient based optimization code is developed in MATLAB[®] environment and this code is used in conjunction with the analytical functions applicable in classical beam theory, to optimize two different beams with different cross-sections.

Approach 2: The same optimizer code developed is used in conjunction with a commercial finite element code MSC.NASTRAN[®] to demonstrate how one can take advantage of the available finite element solvers and use them with an optimization code of their own. For comparison purposes the two classical beam problems are solved with this approach.

Approach 3: The optimization module of the commercial finite element program MSC.NASTRAN[®] is used to solve the two beam problems with different number of design variables.

All three approaches are compared with each other by performing structural optimization of two different beams with different number of design variables. In the first case study a rectangular cross-section beam is optimized and only two design variables are used to verify that all three approaches converge to the true solution which can easily be demonstrated on a two dimensional space. In the second case study an I beam with four design variables is optimized. The results of the three approaches show that all of these techniques can be used to arrive at the same optimum solution. However, it was observed that the optimization module of MSC.NASTRAN[®] arrives at the optimum solution fastest. The high speed of convergence to the optimum solution by MSC NASTRAN[®] is due to the use of sensitivity analysis and construction of an approximate model in the search for the optimum. However, the I beam problem demonstrated that with the use of the analytical functions applicable for the beam theory in conjunction with the optimizer code developed resulted in a 4.5% more weight reduction. Thus, this example is a clear indication that in situations where weight reduction is very critical the use of different optimization approaches should be tried not only to cross-check the results but also to see if further weight reduction can be achieved or not. It is also noted that the calling of a commercial finite element solver from a used developed optimizer may not be a very effective method as far as solution times are concerned. Because of the frequent call of the commercial finite code and the need for some initial setup times used in checking the license file and like, the whole process takes extremely long time. However, in certain problems optimization modules of commercial finite element codes may not be used in arriving at the optimum solution. For instance, if the loads change with the deformation, then an external finite element solver could be incorporated to perform optimization instead of the optimization module of a commercial finite element program.

In the remaining part of the thesis a wing torque box is optimized by the optimization module of MSC.NASTRAN[®]. The fast convergence of the optimization module of MSC.NASTRAN[®] was the main reason to choose MSC.NASTRAN[®] in the optimization solution of the wing torque box. This section is intended to demonstrate the application of element property and shape optimization separately and combined element property and shape optimization. Element property optimization was performed with an almost equivalent tip load and distributed load. Within the context of shape optimization positions of the ribs were taken as the design variables. The shape optimizer was verified initially by performing a shape optimization with only a single rib location as the design variable and with all fixed quantities for the element properties. This solution showed that the rib was displaced in the right direction by the right amount. After verifying the result of the shape optimizer, the combined element property and shape optimization was performed and results of this study were compared with the results of the element property optimization. In both problems the final weight of the optimized configuration increased compared to the weight of the initial configuration to satisfy all the constraints. However, it was observed by incorporating shape optimizer in the optimization study weight reduction could be achieved compared to the just element property optimization. This study in a way demonstrated the significant impact that the shape optimization can have on the design of aerospace structures with higher structural efficiency.

As for the future work it is deemed that the optimization code developed could be improved to reduce the time spent in the search process to reach the optimum solution. For instance further improvement in the code could be made such as removing unnecessary function evaluations or reducing the pause time for MSC.NASTRAN[®] job to finish so that code can proceed to the subsequent operations faster. Especially more work needs to be done in reducing the time spent to reach to the optimum solution when the developed code works together with a commercial finite element solver. The main burden here is the pause time at each call to the finite element solver, and effort can be spent to optimize this

pause time to speed up the whole process. If the speeding up of the solution time can be accomplished then the wing torque box problem can be solved by using the optimization code developed in conjunction with the MSC.NASTRAN[®] solver. Furthermore, simplified structural analysis methodology could also be incorporated in the solver side to eliminate the need for finite element analysis. This way the optimizer code could be used with the simplified structural analysis relations which give direct stresses on flanges and shear stresses on the skins and the webs.

The gradient based optimizer code developed requires many evaluations of objective and constraint functions. When the code is used in conjunction with a commercial finite element code MSC.NASTRAN[®], the cost of the repeated finite element analysis is very high. As a further improvement, a module can be added to the optimization code which will produce an approximate model by using Taylor Series expansion of objective and constraint functions. In this manner, finite element analyses can be used in the construction of an approximate model. The optimization code can use the results coming from approximate model instead of performing finite element analysis whenever evaluation of the objective and constraint functions is required. In this way, high cost of the repeated finite element analyses can be avoided.

In addition, multi-disciplinary optimization problems can be performed in MSC.NASTRAN[®] and the wing torque box analyzed can be optimized in all aspects. For instance constraints on the fundamental frequency can be incorporated into the problem definition. In addition, the skin and web panels can be checked from local buckling point of view. For this purpose local buckling relations can be added as other constraints and these can relations can be linked to the axial stresses occurring in the panels for the calculation of the local buckling margins of safety. A further study could be to incorporate aeroelastic constraints on flutter speed or divergence speed to see how restrictive these constraints might be. A further work could be on making a finer mesh but using the same number of design variables. In such a study the properties of the critical elements between the rib stations can be selected as the design variables

and the element properties of all the other elements between the rib stations can be linked to the critical element. This study may be required to see the effect of mesh density on the optimum structural configuration. A further work could be made on using a more accurate distribution of the external load acting on the wing structure. Output from a CFD code could be incorporated into MSC.NASTRAN[®] and property and shape optimization studies can be performed with a more realistic load case.

REFERENCES

- [1] Bector C.R., Chandra S., Dutta J., Principles of Optimization Theory, Alpha Science, 2005
- [2] Sarker R.A. and Newton C.S., “Optimization Modelling, A Practical Approach”, CRC Press, 2007
- [3] Chambers, L.D., Practical Handbook of Genetic Algorithms, CRC Press, 1999
- [4] Standford University Web Site,
<http://adg.stanford.edu/aa241/structures/structuraldesign.html>, Last accessed date August 2008
- [5] University of Southampton Web Site
<http://www.soton.ac.uk/~ajk/truss/welcome.html>, Last accessed date August 2008
- [6] Valencia Sailing Web Site,
http://valenciasailing.blogspot.com/2007_03_01_archive.html, Last accessed date August 2008
- [7] Chong E.K.P and Zak S.H., “An Introduction to Optimization”, John Wiley and Sons, 2008
- [8] Venkataraman P., “Applied Optimization with MATLAB® Programming”, John Wiley and Sons, 2002

- [9] Greig D.M., "Optimization", Longman Group Limited, 1980
- [10] MSC.NASTRAN®, "MSC.Nastran Quick Reference Guide" MSC Software Corp., 2003
- [11] MSC.NASTRAN® 2004, "Design Sensitivity and Optimization User's Guide", MSC Software Corp., 2003
- [12] ESDU 95010 'Computer program for estimation of spanwise loading of wings with camber and twist in subsonic attached flow', www.esdu.com, June 1995.
- [13] Bertsekas D.P., "Constrained Optimization and Lagrange Multiplier Methods", Academic Press, 1982
- [14] Luenberger D.G., "Linear and Nonlinear Programming", Addison-Wesley, 2005
- [15] MSC/France & MSC/UK Paper 1998 Web Site, http://www.ipek.uni-karlsruhe.de/medien/veroeffentlichungen/fed_mscconf98/paper_final_980528.htm, Last accessed date August 2008
- [16] Cuthbert Jr. T.R., Optimization Using Personal Computers, Wiley-Interscience, 1987
- [17] Conley W., Computer Optimization Techniques, PBI, 1980
- [18] Laporte E., Le Tallec P., Numerical Methods in Sensitivity Analysis and Shape Optimization, Birkhauser, 2003

APPENDIX A.1

NEWTON-RAPHSON METHOD

Following is the algorithm for Newton-Raphson Method [8]:

- Step 1 assume α
- Step 2 calculate $\Delta\alpha$
- Step 3 update $\bar{\alpha} = \alpha + \Delta\alpha$
 - if $\Phi(\bar{\alpha}) = 0$ exit
 - if $\Phi(\bar{\alpha}) \neq 0$ $\alpha \leftarrow \bar{\alpha}$
 - go to step 2

Calculation of $\Delta\alpha$

$$\Phi(\bar{\alpha}) = \Phi(\alpha + \Delta\alpha) = \Phi(\alpha) + \frac{d\Phi}{d\alpha} \Delta\alpha = 0$$

$$\Delta\alpha = -\frac{\Phi(\alpha)}{d\Phi/d\alpha} = -\left[\frac{d\Phi}{d\alpha}\right]^{-1} \Phi(\alpha)$$

APPENDIX A.2

BISECTION METHOD

Following is the algorithm for Bisection Method [8]:

Step 1 choose α_a and α_b $\alpha_a < \alpha_b$
Step 2 set $\alpha = \alpha_a + (\alpha_b - \alpha_a)/2$
Step 3 if $\Phi(\alpha) = 0.0$ exit
 Else if $\Phi(\alpha_b - \alpha_a) \leq 10^{-4}$ exit
 Else if $\Phi(\alpha) * \Phi(\alpha_a) \geq 0$ then $\alpha_a \leftarrow \alpha$
 Else $\alpha_b \leftarrow \alpha$
 go to step 2

APPENDIX A.3

GOLDEN SECTION METHOD

Following is the algorithm for Golden Section Method [8]:

Step 1 Choose $\alpha^{\text{low}}, \alpha^{\text{up}}$
 $\tau=0.38197$
 $\varepsilon=\text{tolerance} = (\Delta\alpha)_{\text{final}}/(\alpha^{\text{up}} - \alpha^{\text{low}})$
 N number of iterations= $-2.078 \ln \varepsilon$
 $i=1$

Step 2 $\alpha_1=(1-\tau)\alpha^{\text{low}}+\tau\alpha^{\text{up}}$ $f_1=f(\alpha_1)$
 $\alpha_2=\tau\alpha^{\text{low}}+(1-\tau)\alpha^{\text{up}}$ $f_2=f(\alpha_2)$

Step 3 if ($i < N$)
 if ($f_1 > f_2$)
 $\alpha^{\text{low}} \leftarrow \alpha_1$ $\alpha_1 \leftarrow \alpha_2$ $f_1 \leftarrow f_2$
 $\alpha_2 = \tau\alpha^{\text{low}} + (1-\tau)\alpha^{\text{up}}$ $f_2 = f(\alpha_2)$
 $i \leftarrow i+1$
 Go to Step 3
 if ($f_2 > f_1$)
 $\alpha^{\text{up}} \leftarrow \alpha_2$ $\alpha_2 \leftarrow \alpha_1$ $f_2 \leftarrow f_1$
 $\alpha_1 = (1-\tau)\alpha^{\text{low}} + \tau\alpha^{\text{up}}$ $f_1 = f(\alpha_1)$
 $i \leftarrow i+1$
 Go to Step 3

APPENDIX A.4

STEEPEST DESCENT METHOD

Following is the algorithm for Steepest Descent Method [8]:

- Step 1 Choose \mathbf{x}_1 , N (number of iterations)
 $f_s(1) = f(\mathbf{x}_1)$; $\mathbf{x}_s(1) = \mathbf{x}_1$ (store values)
 $\varepsilon_1, \varepsilon_2, \varepsilon_3$ (tolerance for stopping criteria)
 Set $i=1$ (initialize iteration counter)
- Step 2 $\mathbf{s}_i = -\nabla f(\mathbf{x}_i)$ (this is computed in step 3)
 $\mathbf{x}_{i+1} = \mathbf{x}_i + \alpha_i \mathbf{s}_i$
 α_i is determined by minimizing $f(\mathbf{x}_{i+1})$
 $\mathbf{x}_s(i+1) \leftarrow \mathbf{x}_{i+1}$; $f_s(i+1) = f(\mathbf{x}_{i+1})$ (store values)
- Step 3 $\Delta f = f_s(i+1) - f_s(i)$
 $\Delta \mathbf{x} = \mathbf{x}_s(i+1) - \mathbf{x}_s(i)$
 If $|\Delta f| \leq \varepsilon_1$ stop (function not changing)
 If $\Delta \mathbf{x}^T \Delta \mathbf{x} \leq \varepsilon_2$ stop (design not changing)
 $i+1 = N$ stop
 $\nabla f(\mathbf{x}_{i+1})^T \nabla f(\mathbf{x}_{i+1}) \leq \varepsilon_3$ converged
 $i \leftarrow i+1$
 Go to Step 2

APPENDIX A.5

CONJUGATE GRADIENT METHOD

Following is the algorithm for Conjugate Gradient Method [8]:

Step 1 Choose \mathbf{x}_1 , N (number of iterations)
 $f_s(1) = f(\mathbf{x}_1)$; $\mathbf{x}_s(1) = \mathbf{x}_1$ (store values)
 $\varepsilon_1, \varepsilon_2, \varepsilon_3$ (tolerance for stopping criteria)
 set $i=1$ (initialize iteration counter)

Step 2 if $i=1$, $\mathbf{s}_i = -\nabla f(\mathbf{x}_i)$
 else, $\beta = \frac{\nabla f(\mathbf{x}_i)^T \nabla f(\mathbf{x}_i)}{\nabla f(\mathbf{x}_{i-1})^T \nabla f(\mathbf{x}_{i-1})}$
 $\mathbf{s}_i = -\nabla f(\mathbf{x}_i) + \beta \mathbf{s}_{i-1}$
 $\mathbf{x}_{i+1} = \mathbf{x}_i + \alpha_i \mathbf{s}_i$
 α_i is determined by minimizing $f(\mathbf{x}_{i+1})$
 $\mathbf{x}_s(i+1) \leftarrow \mathbf{x}_{i+1}$; $f_s(i+1) = f(\mathbf{x}_{i+1})$ % (store values)

Step 3 $\Delta f = f_s(i+1) - f_s(i)$
 $\Delta \mathbf{x} = \mathbf{x}_s(i+1) - \mathbf{x}_s(i)$
 If $|\Delta f| \leq \varepsilon_1$ stop (function not changing)
 If $\Delta \mathbf{x}^T \Delta \mathbf{x} \leq \varepsilon_2$ stop (design not changing)
 If $i+1 = N$ stop
 If $\nabla f(\mathbf{x}_{i+1})^T \nabla f(\mathbf{x}_{i+1}) \leq \varepsilon_3$ converged
 $i \leftarrow i+1$
 go to step 2

APPENDIX A.6

DAVIDON-FLETCHER-POWELL METHOD

Following is the algorithm for Davidon-Fletcher-Powell Method [8]:

- Step 1 Choose \mathbf{x}_1 , $[\mathbf{A}_1]$ (initial metric), N
 ε_1 , ε_2 , ε_3 (tolerance for stopping criteria)
 Set $i=1$ (initialize iteration counter)
- Step 2 $\mathbf{s}_i = -[\mathbf{A}_i] \nabla f(\mathbf{x}_i)$
 $\mathbf{x}_{i+1} = \mathbf{x}_i + \alpha_i \mathbf{s}_i$; $\Delta \mathbf{x} = \alpha_i \mathbf{s}_i$
 α_i is determined by minimizing $f(\mathbf{x}_{i+1})$
- Step 3 If $\nabla f(\mathbf{x}_{i+1})^T \nabla f(\mathbf{x}_{i+1}) \leq \varepsilon_3$; converged
 If $|f(\mathbf{x}_{i+1}) - f(\mathbf{x}_i)| \leq \varepsilon_1$; stop (function not changing)
 If $\Delta \mathbf{x}^T \Delta \mathbf{x} \leq \varepsilon_2$; stop (design variable \mathbf{x} is not changing)
 If $i+1 = N$, stop (iteration limit)
 Else
 $\mathbf{Y} = \nabla f(\mathbf{x}_{i+1}) - \nabla f(\mathbf{x}_i)$
 $\mathbf{Z} = [\mathbf{A}_i] \mathbf{Y}$
 $[\mathbf{B}] = \frac{\Delta \mathbf{x} \Delta \mathbf{x}^T}{\Delta \mathbf{x}^T \mathbf{Y}}$
 $[\mathbf{C}] = -\frac{\mathbf{Z} \mathbf{Z}^T}{\mathbf{Y}^T \mathbf{Z}}$
 $[\mathbf{A}_{i+1}] = [\mathbf{A}_i] + [\mathbf{B}] + [\mathbf{C}]$
 $i \leftarrow i+1$
 Go to Step 2

APPENDIX A.7

PENALTY FUNCTION METHOD

Following is the algorithm for Penalty Function Method [8]:

- Step 1 Choose \mathbf{x}^1 , N_s (Maximum number of Penalty Function Method iterations)
 N_u (number of DFP iterations)
 ε_i 's (for convergence and stopping)
 r_h^1, r_g^1 (initial penalty multipliers)
 c_h, c_g (scaling value for multipliers)
 $q = 1$ (Penalty Function Method iteration counter)
- Step 2 Call DFP to minimize $F(\mathbf{x}^q, r_h^q, r_g^q)$
 Output: \mathbf{x}^{q*}
- Step 3 Convergence for Penalty Function Method
 If $h_k = 0$, for $k = 1, 2, \dots, l$;
 If $g_j \leq 0$, for $j = 1, 2, \dots, m$;
 If all side constraints are satisfied
 Then converged, Stop
 Stopping criteria:
 $\Delta F = F_q - F_{q-1}$, $\Delta \mathbf{x} = \mathbf{x}^{q*} - \mathbf{x}^{(q-1)*}$
 If $(\Delta F)^2 \leq \varepsilon_1$: stop (function not changing)
 Else If $\Delta \mathbf{x}^T \Delta \mathbf{x} \leq \varepsilon_1$: stop (design variable \mathbf{x} is not changing)
 Else If $q = N_s$: stop (maximum iterations reached)
 Continue
 $q \leftarrow q+1$

$$r_h^q \leftarrow r_h^{q*} C_h; r_g^q \leftarrow r_g^{q*} C_g$$

$$\mathbf{x}^q \leftarrow \mathbf{x}^{q*}$$

go to step 2

APPENDIX A.8

AUGMENTED LAGRANGE MULTIPLIER METHOD

Following is the algorithm for Augmented Lagrange Multiplier (ALM) Method [8].

- Step 1 Choose \mathbf{x}^1 , N_s (Maximum number of ALM iterations)
 N_u (Maximum number of DFP iterations)
 ε_i 's (for convergence and stopping criteria)
 r_h^1, r_g^1 (initial penalty multipliers)
 c_h, c_g (scaling value for multipliers)
 $\boldsymbol{\lambda}^1, \boldsymbol{\beta}^1$ (initial multiplier vectors)
 $q = 1$ (ALM iteration counter)
- Step 2 Call DFP to minimize unconstrained objective function $F(\mathbf{x}^q, \boldsymbol{\lambda}^q, \boldsymbol{\beta}^q, r_h^q, r_g^q)$
 Output: \mathbf{x}^{q*}
- Step 3 Convergence for ALM
 If $h_k = 0$, for $k = 1, 2, \dots, l$;
 If $g_j \leq 0$, for $j = 1, 2, \dots, m$;
 (If $\beta_j > 0$ for $g_j = 0$)
 (If $\nabla f + \sum \lambda_k \nabla h_k + \sum \beta_j \nabla g_j = 0$)
 Then converged, Stop
 Stopping criteria:
 $\Delta F = F_q - F_{q-1}$, $\Delta \mathbf{x} = \mathbf{x}^{q*} - \mathbf{x}^{(q-1)*}$
 If $(\Delta F)^2 \leq \varepsilon_1$: stop (function not changing)
 Else If $\Delta \mathbf{x}^T \Delta \mathbf{x} \leq \varepsilon_1$: stop (design variable \mathbf{x} not changing)

Else If $q = N_s$: stop (maximum number of iterations reached)

Continue

$q \leftarrow q+1$

$\lambda^q \leftarrow \lambda^q + 2 r_h \mathbf{h}(\mathbf{x}^{q*})$

$\beta^q \leftarrow \beta^q + 2 r_g (\max [\mathbf{g}(\mathbf{x}^{q*}), -\beta^q/2r_g])$

$r_h^q \leftarrow r_h^{q*} C_h; r_g^q \leftarrow r_g^{q*} C_g$

$\mathbf{x}^q \leftarrow \mathbf{x}^{q*}$

go to step 2

APPENDIX B.1

USER INTERFACE OF MATLAB® CODE DEVELOPED FOR OPTIMIZATION

Optimization of cantilever beam with rectangular cross section using optimization code developed in MATLAB® is presented here.

- Open MATLAB® in the computer and select the directory, which includes “AugLagMet.m”, “DFP.m”, “golden.m”, “gradfunction.m”, “FALM.m”, “Ofun.m”, “Gfun.m” and “Hfun.m” files, as current directory.
- Type “AugLagMet” in the MATLAB® command window as shown in figure B.1 and press enter. This command starts optimization.

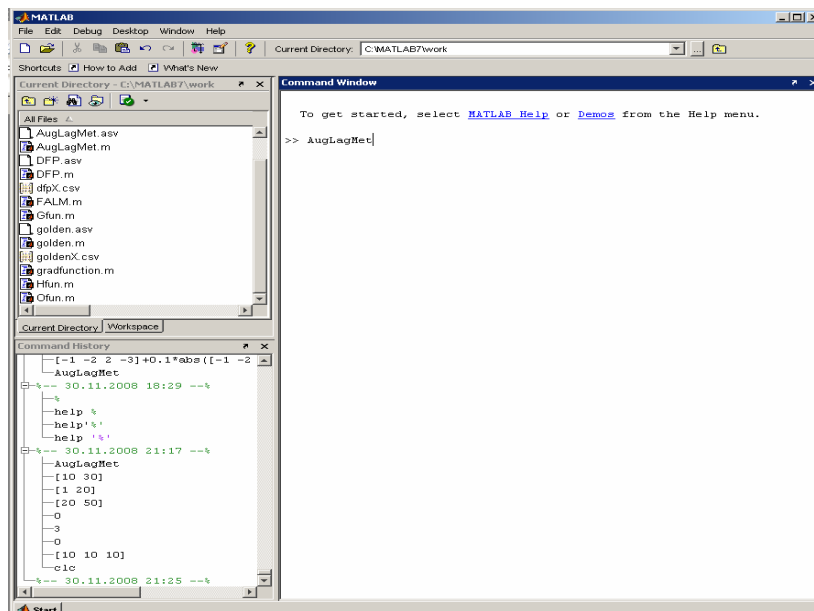


Figure B.1 Starting AugLagMet in MATLAB® command window

- Enter asked inputs in the MATLAB[®] command window as shown in figure B.2.

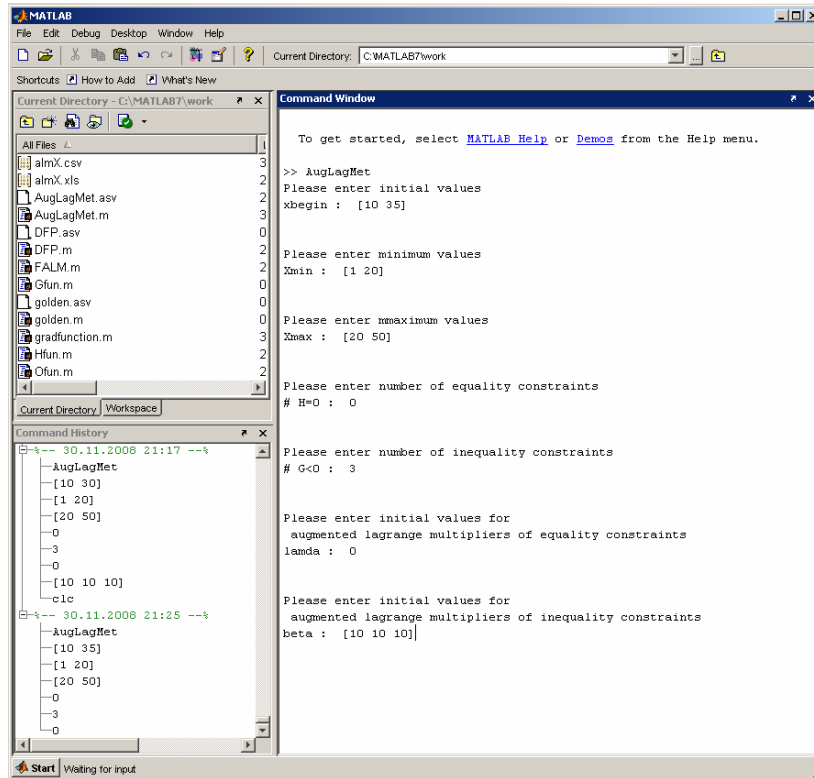


Figure B.2 Entering initial values in MATLAB[®] command window

Result will appear in MATLAB[®] command window shown in figure B.3. History of the design variables, objective function and constraints are written in ac comma separated value (csv) file called “almX.csv”.

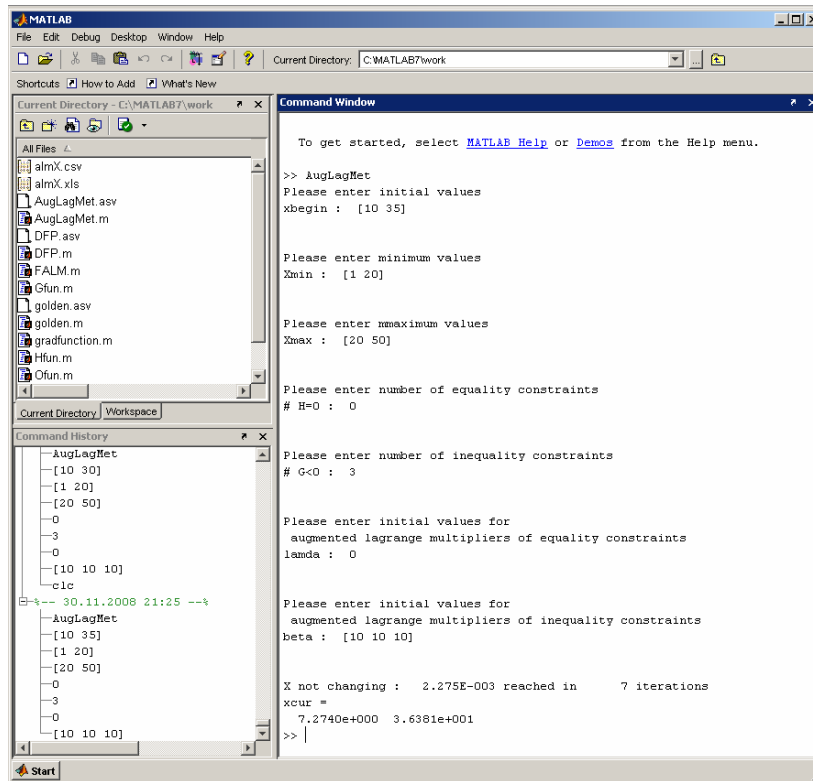


Figure B.3 Result in MATLAB[®] command window

APPENDIX B.2

MATLAB[®] TO MSC.NASTRAN[®] INTERFACE

The objective “nastfunc.m” file calculates the objective function value with new design variables. First requirement is that the folder should contain “cantbeam1.bdf” file. This file is created by MSC.PATRAN[®] as input for the finite element analysis using MSC.NASTRAN[®]. Second requirement is an arrangement in Microsoft WINDOWS[®] and this will be explained later.

Objective function is composed of three main parts.

First part is main objective function without constraints which is volume of the beam. It is a very simple function of design variables and can be calculated analytically. Therefore there is no need to perform an finite element analysis.

Second part is a penalty function for equality constraints. For the beam example there is no equality constraints. This part is skipped.

Third part is a penalty function for inequality constraints. For the beam example these constraints are related with the displacements and the stresses which are obtained from finite element analysis.

“nastfunc.m” first performs the finite element analysis using MSC.NASTRAN[®], then calculates the objective function value.

There are three steps to perform finite element analysis.

First step is modifying input file. In other words, the values of the design variables should be changed. Initial “cantbeam1.bdf” file is renamed as “dummy.bdf” and a new empty “cantbeam1.bdf” is created. Each line of the “dummy.bdf” file is directly copied to the “cantbeam1.bdf” file until 23rd line which includes the design variable. This line is rewritten to the “cantbeam1.bdf”

file with the new values of design variables. From line 24 to end of file, each line is copied from “dummy.bdf” to “cantbeam1.bdf”.

Second step is performing finite element analysis. For finite element analysis, MSC.NASTRAN[®] is used. To call MSC.NASTRAN[®] from MATLAB[®] “winopen” function is used. This function is same as double clicking on a file in Microsoft WINDOWS[®]. Second requirement explained below is necessary for this step. After starting MSC.NASTRAN[®] job, program waits until the end of the job. When the job is finished all unnecessary files are deleted.

Third step is reading stresses and displacements from “cantbeam1.f06” file. This file is an output of MSC.NASTRAN[®] job. The displacement is stored in the 265th line and the stress is stored in the 325th line. After opening “cantbeam1.f06” file, each line is read until the end of file. Using “sscanf” command, line 265 and 325 are stored in Ascan and Bscan matrices respectively. 4th element of the Ascan matrix is the displacement and 8th element of the Bscan matrix is the stress for the constraints. Next “cantbeam1.f06” file is closed and deleted.

At the end, the value of the objective function is calculated in accordance with Augmented Lagrange Multipliers (ALM) Method.

Second requirement for this process is an arrangement in Microsoft WINDOWS[®].

In MATLAB[®], “winopen” function performs double clicking in Microsoft WINDOWS[®]. What is required at this step is that, if a “bdf” file is double clicked, this “bdf” file must be opened with MSC.NASTRAN[®]. Therefore, following steps has to be performed in Microsoft WINDOWS[®]:

- Right click on a bdf file.
- Choose “Open With > Choose Program...” as shown in figure B.4

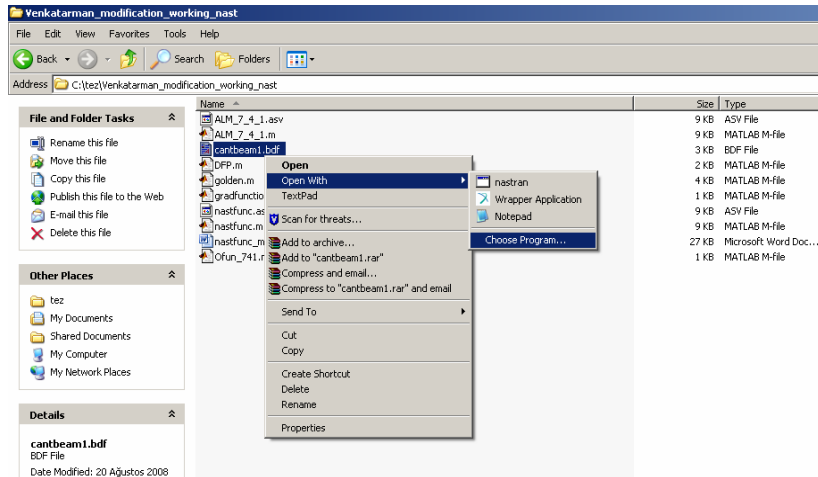


Figure B.4 Open with a bdf-file in Microsoft.WINDOWS®

- Click on “Browse...” , then choose “C:\MSC.Software\MSC.Nastran\bin\” as shown in figure B.5

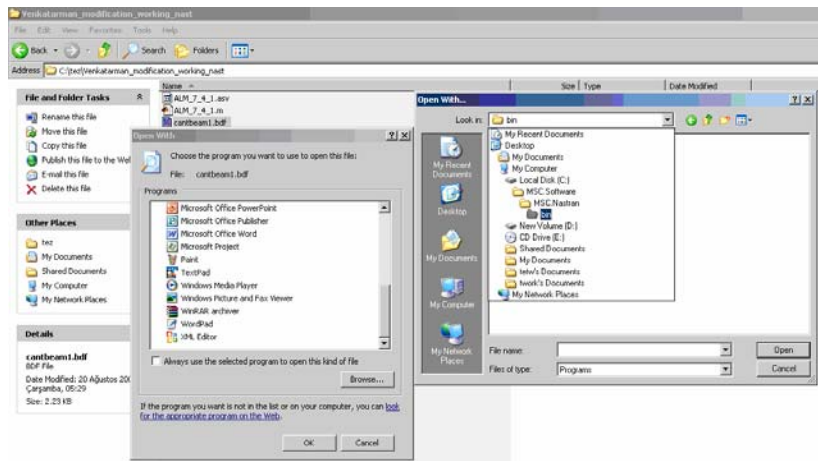


Figure B.5 Location of “nastran.exe”

- Choose “nastran.exe” and click on “Open” as shown in figure B.6

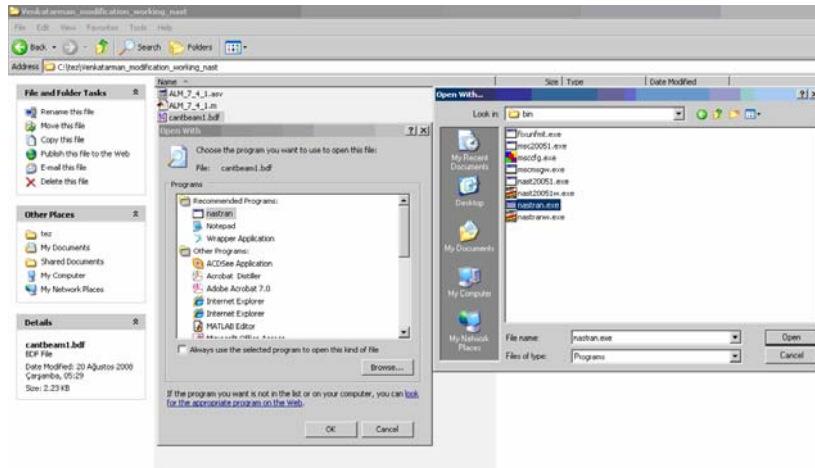


Figure B.6 “nastran.exe” file in ./bin/ directory

- Toggle “Always use the selected program to open this kind of file” as shown in figure B.7

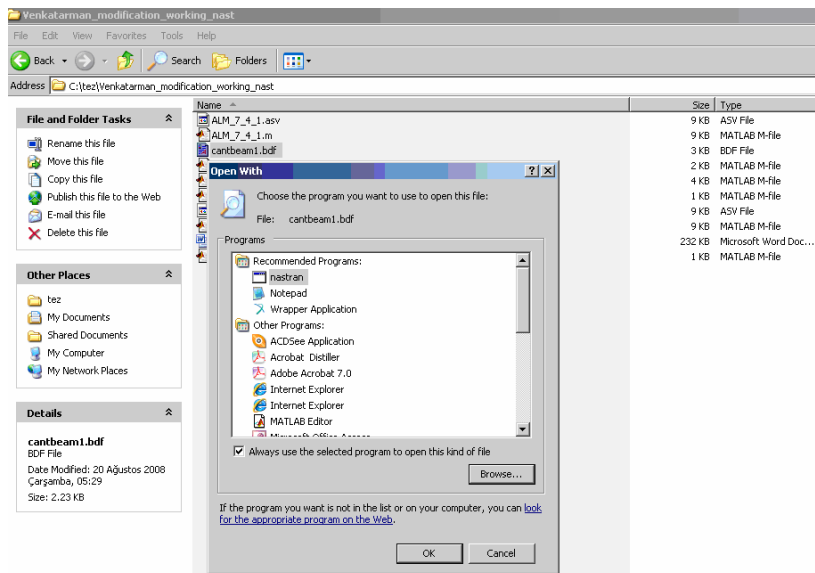


Figure B.7 Open a “bdf-file” allways with “nastran.exe”

- Click on “OK”

Second requirement is fulfilled now.

How to use nastfunc.m is explained below;

- Open MATLAB®
- Choose a folder containing “nastfunc.m” and “cantbeam1.bdf” as the current directory .
- Type `nastfunc([15 35])` and press enter as shown in figure B.8. [15 35] is the design variable vector for rectangular cross section beam. For this example, it is a row vector with two variables.

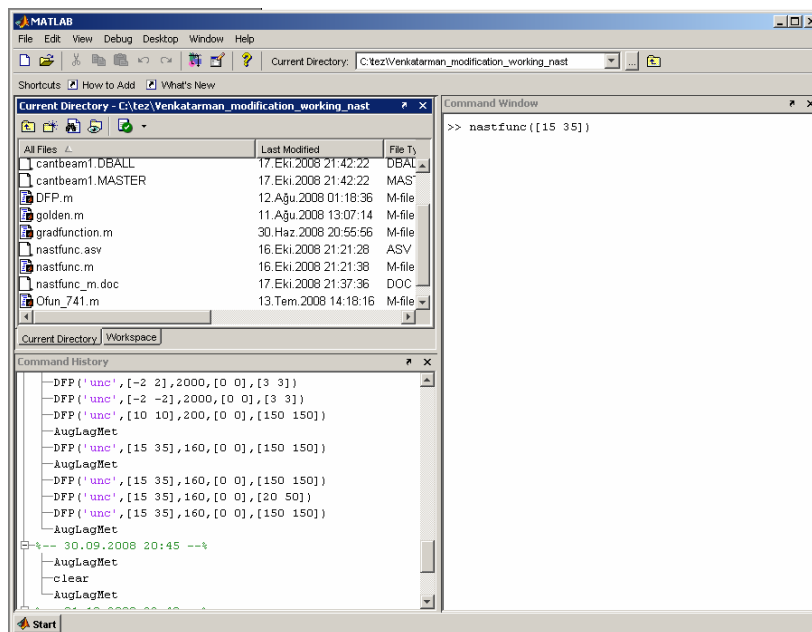


Figure B.8 MATLAB® command window

MSC.NASTRAN® starts and the screen presented in figure B.9 appears until the end of the job.

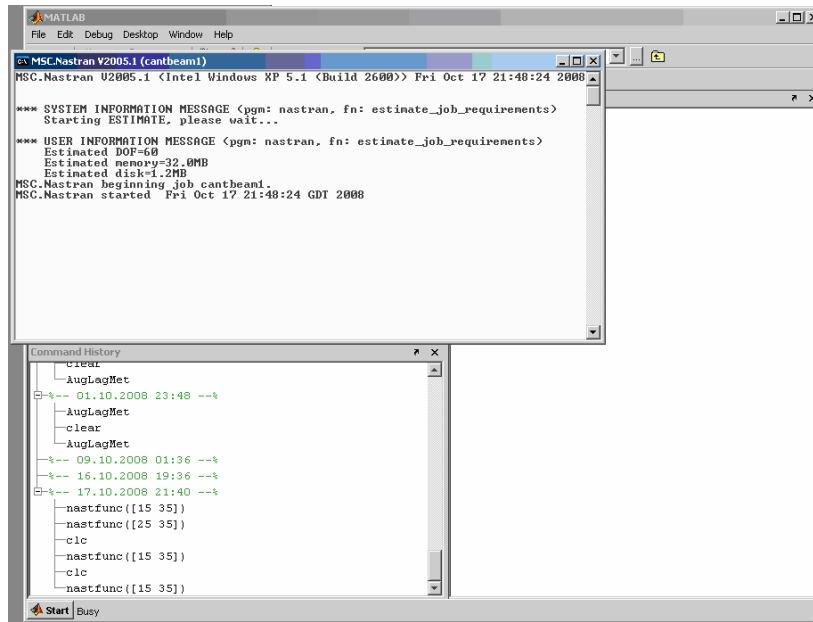


Figure B.9 MSC.NASTRAN[®] run window

At the end, the value of the objective function appears on the MATLAB[®] screen.

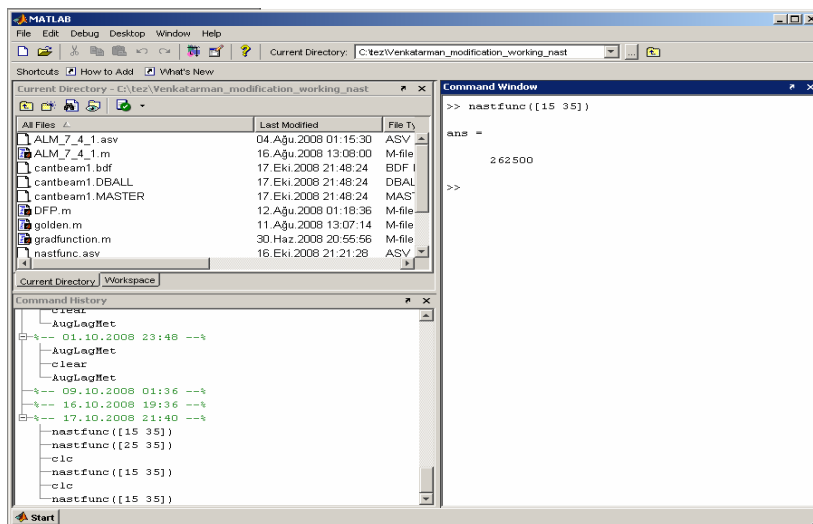


Figure B.10 MATLAB[®] command window

APPENDIX C.1

MESH DENSITY COMPARISON FOR RECTANGULAR CROSS SECTION CANTILEVER BEAM

To investigate the effect of mesh density on optimization problem of rectangular cross section cantilever beam, five identical models are built with 2, 5, 10, 20 and 50 elements, respectively. The initial models are shown in figure C.1.

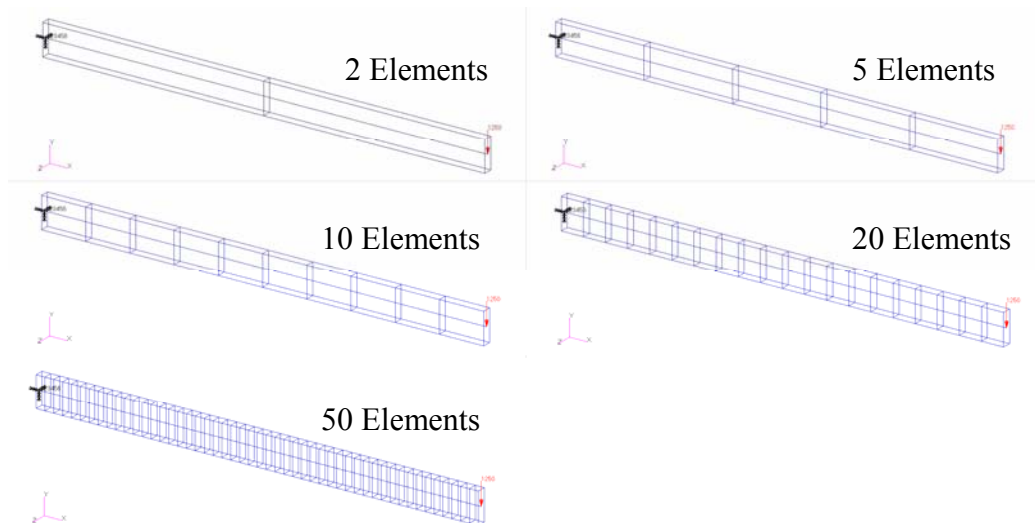


Figure C.1 Finite element models for rectangular cross section cantilever beam with different mesh densities

Optimization is performed by using MSC.NASTRAN[®] for all five models and results are tabulated in table C.1.

Table C.1 Comparison of optimization results of rectangular cross section cantilever beam with different mesh densities

| | | 2 | 5 | 10 | 20 | 50 |
|--|----------------------|----------------|----------------|----------------|----------------|----------------|
| | | Element | Element | Element | Element | Element |
| Number of iterations | | 6 | 6 | 6 | 6 | 6 |
| B (mm) | Initial value | 10 | 10 | 10 | 10 | 10 |
| | Final value | 7.290 | 7.290 | 7.290 | 7.290 | 7.290 |
| H (mm) | Initial value | 35 | 35 | 35 | 35 | 35 |
| | Final value | 36.448 | 36.448 | 36.448 | 36.448 | 36.448 |
| Objective function, Volume (mm³) | Initial value | 175000 | 175000 | 175000 | 175000 | 175000 |
| | Final value | 132849 | 132849 | 132849 | 132849 | 132849 |
| Max axial stress at the root (Mpa) | Initial value | 306.1 | 306.1 | 306.1 | 306.1 | 306.1 |
| | Final value | 387.2 | 387.2 | 387.2 | 387.2 | 387.2 |
| Max. tip deflection (mm) | Initial value | 20.825 | 20.906 | 20.906 | 20.906 | 20.906 |
| | Final value | 25.402 | 25.402 | 25.402 | 25.402 | 25.402 |
| H/B | Initial value | 3.500 | 3.500 | 3.500 | 3.500 | 3.500 |
| | Final value | 5.000 | 5.000 | 5.000 | 5.000 | 5.000 |

It is observed that mesh density has no effect on this particular problem. Objective function, design variables and constraints converged to the same values after 6 iterations in each analysis. Therefore using 10 element provides reliable results.

APPENDIX C.2

MESH DENSITY COMPARISON FOR I SHAPED CROSS SECTION CANTILEVER BEAM

Five identical models are built with 2, 5, 10, 20 and 50 elements, respectively. To investigate the effect of mesh density on optimization problem of I shaped cross section cantilever beam, the initial models are shown in figure C.2.

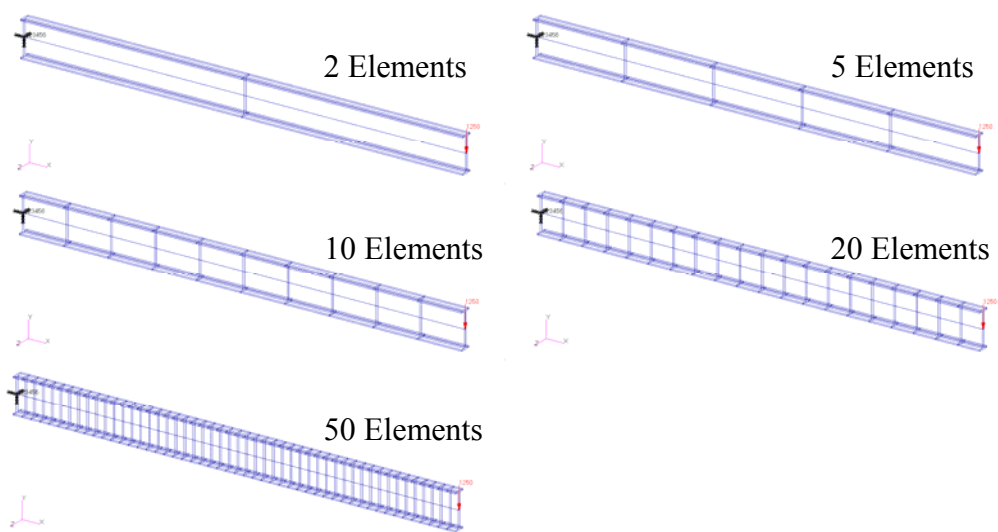


Figure C.2 Finite element models for I shaped cross section cantilever beam with different mesh densities

Optimization is performed by using MSC.NASTRAN[®] for all five models and results are tabulated in table C.2.

Table C.2 Comparison of optimization results of shaped cross section cantilever beam with different mesh densities

| | | 2 | 5 | 10 | 20 | 50 |
|---|----------------------|----------------|----------------|----------------|----------------|----------------|
| | | Element | Element | Element | Element | Element |
| Number of iterations | | 21 | 23 | 23 | 23 | 23 |
| Beam Height, H (mm) | Initial value | 20.0 | 20.0 | 20.0 | 20.0 | 20.0 |
| | Final value | 40.0 | 40.0 | 40.0 | 40.0 | 40.0 |
| Flange Width, Wf (mm) | Initial value | 12.0 | 12.0 | 12.0 | 12.0 | 12.0 |
| | Final value | 35.83 | 38.43 | 38.43 | 38.43 | 38.43 |
| Web Thickness, tw (mm) | Initial value | 3.0 | 3.0 | 3.0 | 3.0 | 3.0 |
| | Final value | 0.50 | 0.50 | 0.50 | 0.50 | 0.50 |
| Flange Thickness, tf (mm) | Initial value | 1.5 | 1.5 | 1.5 | 1.5 | 1.5 |
| | Final value | 1.05 | 0.97 | 0.97 | 0.97 | 0.97 |
| Objective function, V (mm³) | Initial value | 43500 | 43500 | 43500 | 43500 | 43500 |
| | Final value | 46967 | 46820 | 46820 | 46820 | 46820 |
| Max. Stress at the root (MPa) | Initial value | 1448.4 | 1448.4 | 1448.4 | 1448.4 | 1448.4 |
| | Final value | 406.9 | 407.0 | 407.0 | 407.0 | 407.0 |
| Max. Shear Stress (MPa) | Initial value | 23.174 | 23.174 | 23.174 | 23.174 | 23.174 |
| | Final value | 65.884 | 65.826 | 65.826 | 65.826 | 65.826 |
| Max. deflection at tip (mm) | Initial value | 8.000 | 8.000 | 8.000 | 8.000 | 8.000 |
| | Final value | 25.476 | 25.474 | 25.474 | 25.474 | 25.474 |
| tf / tw | Initial value | 0.500 | 0.500 | 0.500 | 0.500 | 0.500 |
| | Final value | 2.090 | 1.939 | 1.939 | 1.939 | 1.939 |

It is observed that if the number of elements is greater or equal to 5 then mesh density has no effect on this problem. Objective function, design variables and constraints converged to the same values after 23 iterations in the analyses with 5 or more elements. But they converged to slightly different values in 21 iterations with 2 elements. Therefore using 10 element provides reliable results.

APPENDIX C.3

COMPARISON TABLES FOR WING TORQUE BOX OPTIMIZATION

The results of optimizations performed in chapter 6 are compared in tables C3-13 for all stress constraints. Initial and final stress values on each element and corresponding upper and lower bounds are tabulated.

Table C.3 Comparison of front spar results of three optimization processes

| Front Spar | | | | | | | | |
|---------------------------------|-----------|---------------|---------------------|-------------|-------------|-----------------------|---------------------|-------------------------------|
| Web Von Mises Stress (MPa) | | | | | | | | |
| Description | D.C. Name | Initial Value | | Lower Bound | Upper Bound | Property Optimization | | Property & Shape Optimization |
| | | Tip Loading | Distributed Loading | | | Tip Loading | Distributed Loading | |
| Between Rib 1 - Rib 2 | AS001 | 224.8 | 203.3 | 0.01 | 300 | 288.9 | 50.9 | 112.9 |
| Between Rib 2 - Rib 3 | AS002 | 218.3 | 153.9 | 0.01 | 300 | 260.6 | 194.6 | 126.5 |
| Between Rib 3 - Rib 4 | AS003 | 219.6 | 113.5 | 0.01 | 300 | 93.4 | 40.6 | 95.8 |
| Between Rib 4 - Rib 5 | AS004 | 219.9 | 73.5 | 0.01 | 300 | 122.7 | 29.2 | 84.5 |
| Between Rib 5 - Rib 6 | AS005 | 216.1 | 37.5 | 0.01 | 300 | 264.8 | 27.7 | 47.0 |
| Between Rib 6 - Rib 7 | AS006 | 237.9 | 10.2 | 0.01 | 300 | 200.4 | 12.1 | 12.7 |
| Upper Flange Axial Stress (MPa) | | | | | | | | |
| Description | D.C. Name | Initial Value | | Lower Bound | Upper Bound | Property Optimization | | Property & Shape Optimization |
| | | Tip Loading | Distributed Loading | | | Tip Loading | Distributed Loading | |
| Between Rib 1 - Rib 2 | AS007 | -445.5 | -454.6 | -425 | 445 | -118.1 | -103.7 | -126.7 |
| Between Rib 2 - Rib 3 | AS008 | -237.5 | -286.3 | -425 | 445 | -123.7 | -108.1 | -101.4 |
| Between Rib 3 - Rib 4 | AS009 | -36.2 | -163.8 | -425 | 445 | -35.3 | -74.3 | -110.7 |
| Between Rib 4 - Rib 5 | AS010 | 167.5 | -77.4 | -425 | 445 | 185.7 | -60.4 | -77.7 |
| Between Rib 5 - Rib 6 | AS011 | 363.4 | -26.2 | -425 | 445 | 350.5 | -29.3 | -44.3 |
| Between Rib 6 - Rib 7 | AS012 | 600.5 | -4.5 | -425 | 445 | 379.3 | -5.9 | -7.0 |
| Lower Flange Axial Stress (MPa) | | | | | | | | |
| Description | D.C. Name | Initial Value | | Lower Bound | Upper Bound | Property Optimization | | Property & Shape Optimization |
| | | Tip Loading | Distributed Loading | | | Tip Loading | Distributed Loading | |
| Between Rib 1 - Rib 2 | AS013 | 445.5 | 454.7 | -425 | 445 | 317.6 | 136.6 | 168.1 |
| Between Rib 2 - Rib 3 | AS014 | 237.5 | 286.3 | -425 | 445 | 295.9 | 262.8 | 107.6 |
| Between Rib 3 - Rib 4 | AS015 | 36.2 | 163.9 | -425 | 445 | 31.3 | 63.2 | 111.9 |
| Between Rib 4 - Rib 5 | AS016 | -167.5 | 77.4 | -425 | 445 | -122.5 | 62.5 | 77.8 |
| Between Rib 5 - Rib 6 | AS017 | -363.5 | 26.2 | -425 | 445 | -148.8 | 26.2 | 44.3 |
| Between Rib 6 - Rib 7 | AS018 | -600.5 | 4.5 | -425 | 445 | -193.8 | 6.0 | 7.0 |

Table C.4 Comparison of rear spar results of three optimization processes

| Rear Spar | | | | | | | | |
|---------------------------------|-----------|---------------|---------------------|-------------|-------------|-----------------------|---------------------|-------------------------------|
| Web Von Mises Stress (MPa) | | | | | | | | |
| Description | D.C. Name | Initial Value | | Lower Bound | Upper Bound | Property Optimization | | Property & Shape Optimization |
| | | Tip Loading | Distributed Loading | | | Tip Loading | Distributed Loading | Distributed Loading |
| Between Rib 1 - Rib 2 | AS019 | 120.5 | 107.4 | 0.01 | 300 | 163.6 | 71.6 | 144.9 |
| Between Rib 2 - Rib 3 | AS020 | 134.7 | 96.1 | 0.01 | 300 | 49.3 | 34.5 | 101.4 |
| Between Rib 3 - Rib 4 | AS021 | 131.8 | 67.8 | 0.01 | 300 | 156.3 | 46.2 | 64.4 |
| Between Rib 4 - Rib 5 | AS022 | 131.3 | 44.3 | 0.01 | 300 | 165.4 | 41.1 | 61.7 |
| Between Rib 5 - Rib 6 | AS023 | 139.6 | 22.6 | 0.01 | 300 | 66.0 | 17.3 | 27.8 |
| Between Rib 6 - Rib 7 | AS024 | 92.0 | 6.6 | 0.01 | 300 | 71.4 | 8.4 | 8.4 |
| Upper Flange Axial Stress (MPa) | | | | | | | | |
| Description | D.C. Name | Initial Value | | Lower Bound | Upper Bound | Property Optimization | | Property & Shape Optimization |
| | | Tip Loading | Distributed Loading | | | Tip Loading | Distributed Loading | Distributed Loading |
| Between Rib 1 - Rib 2 | AS025 | -283.0 | -291.2 | -425 | 445 | -86.1 | -53.3 | -113.2 |
| Between Rib 2 - Rib 3 | AS026 | -165.1 | -200.3 | -425 | 445 | -108.6 | -55.6 | -100.9 |
| Between Rib 3 - Rib 4 | AS027 | -23.5 | -111.9 | -425 | 445 | -34.0 | -81.0 | -52.4 |
| Between Rib 4 - Rib 5 | AS028 | 111.2 | -54.3 | -425 | 445 | 154.6 | -38.2 | -60.9 |
| Between Rib 5 - Rib 6 | AS029 | 258.9 | -19.4 | -425 | 445 | 183.3 | -16.0 | -29.8 |
| Between Rib 6 - Rib 7 | AS030 | 342.9 | -3.8 | -425 | 445 | 159.4 | -6.1 | -6.7 |
| Lower Flange Axial Stress (MPa) | | | | | | | | |
| Description | D.C. Name | Initial Value | | Lower Bound | Upper Bound | Property Optimization | | Property & Shape Optimization |
| | | Tip Loading | Distributed Loading | | | Tip Loading | Distributed Loading | Distributed Loading |
| Between Rib 1 - Rib 2 | AS031 | 283.1 | 291.3 | -425 | 445 | 163.2 | 183.8 | 49.8 |
| Between Rib 2 - Rib 3 | AS032 | 165.2 | 200.3 | -425 | 445 | 156.9 | 85.9 | 98.8 |
| Between Rib 3 - Rib 4 | AS033 | 23.5 | 111.9 | -425 | 445 | 35.9 | 60.3 | 53.4 |
| Between Rib 4 - Rib 5 | AS034 | -111.3 | 54.3 | -425 | 445 | -72.2 | 46.3 | 61.0 |
| Between Rib 5 - Rib 6 | AS035 | -258.9 | 19.4 | -425 | 445 | -140.1 | 16.2 | 29.9 |
| Between Rib 6 - Rib 7 | AS036 | -343.0 | 3.8 | -425 | 445 | -111.3 | 5.7 | 6.7 |

Table C.5 Comparison of upper skin results of three optimization processes

| Upper Skin Von Mises Stress (MPa) | | | | | | | | |
|-----------------------------------|-----------|---------------|---------------------|-------------|-------------|-----------------------|---------------------|-------------------------------|
| Description | D.C. Name | Initial Value | | Lower Bound | Upper Bound | Property Optimization | | Property & Shape Optimization |
| | | Tip Loading | Distributed Loading | | | Tip Loading | Distributed Loading | Distributed Loading |
| Between Rib 1 - Rib 2 | AS037 | 370.1 | 378.9 | 0.01 | 281 | 105.1 | 81.1 | 123.1 |
| Between Rib 2 - Rib 3 | AS038 | 207.9 | 249.9 | 0.01 | 281 | 122.2 | 84.3 | 104.1 |
| Between Rib 3 - Rib 4 | AS039 | 38.8 | 141.3 | 0.01 | 281 | 42.7 | 82.1 | 83.9 |
| Between Rib 4 - Rib 5 | AS040 | 144.2 | 67.9 | 0.01 | 281 | 175.7 | 50.7 | 71.7 |
| Between Rib 5 - Rib 6 | AS041 | 319.6 | 23.8 | 0.01 | 281 | 277.0 | 23.4 | 38.4 |
| Between Rib 6 - Rib 7 | AS042 | 479.7 | 4.6 | 0.01 | 281 | 276.4 | 6.5 | 7.5 |

Table C.6 Comparison of lower skin results of three optimization processes

| Lower Skin Von Mises Stress (MPa) | | | | | | | | |
|-----------------------------------|-----------|---------------|---------------------|-------------|-------------|-----------------------|---------------------|-------------------------------|
| Description | D.C. Name | Initial Value | | Lower Bound | Upper Bound | Property Optimization | | Property & Shape Optimization |
| | | Tip Loading | Distributed Loading | | | Tip Loading | Distributed Loading | Distributed Loading |
| Between Rib 1 - Rib 2 | AS043 | 370.1 | 379.0 | 0.01 | 281 | 245.2 | 165.5 | 112.0 |
| Between Rib 2 - Rib 3 | AS044 | 207.9 | 250.0 | 0.01 | 281 | 239.2 | 177.7 | 106.1 |
| Between Rib 3 - Rib 4 | AS045 | 38.8 | 141.4 | 0.01 | 281 | 43.0 | 65.4 | 85.1 |
| Between Rib 4 - Rib 5 | AS046 | 144.2 | 67.9 | 0.01 | 281 | 101.1 | 55.3 | 71.8 |
| Between Rib 5 - Rib 6 | AS047 | 319.7 | 23.8 | 0.01 | 281 | 149.9 | 22.0 | 38.4 |
| Between Rib 6 - Rib 7 | AS048 | 479.8 | 4.6 | 0.01 | 281 | 157.0 | 6.3 | 7.5 |

Table C.7 Comparison of rib 1 results of three optimization processes

| Rib 1 | | | | | | | | |
|---------------------------------|-----------|---------------|---------------------|-------------|-------------|-----------------------|---------------------|-------------------------------|
| Description | D.C. Name | Initial Value | | Lower Bound | Upper Bound | Property Optimization | | Property & Shape Optimization |
| | | Tip Loading | Distributed Loading | | | Tip Loading | Distributed Loading | Distributed Loading |
| Web Von Mises Stress (MPa) | AS049 | 10.3 | 8.5 | 0.01 | 300 | 24.4 | 42.8 | 17.7 |
| Upper Flange Axial Stress (MPa) | AS050 | 82.7 | 83.4 | -425 | 445 | 30.2 | 24.2 | 37.2 |
| Lower Flange Axial Stress (MPa) | AS051 | -82.7 | -83.4 | -425 | 445 | -49.4 | -40.3 | -33.6 |
| Front Flange Axial Stress (MPa) | AS052 | 0.0 | 0.0 | -425 | 445 | -10.2 | -2.3 | -5.2 |
| Rear Flange Axial Stress (MPa) | AS053 | 0.0 | 0.0 | -425 | 445 | -2.0 | -8.3 | 5.8 |

Table C.8 Comparison of rib 2 results of three optimization processes

| Rib 2 | | | | | | | | |
|---------------------------------|-----------|---------------|---------------------|-------------|-------------|-----------------------|---------------------|-------------------------------|
| Description | D.C. Name | Initial Value | | Lower Bound | Upper Bound | Property Optimization | | Property & Shape Optimization |
| | | Tip Loading | Distributed Loading | | | Tip Loading | Distributed Loading | Distributed Loading |
| Web Von Mises Stress (MPa) | AS054 | 7.1 | 3.4 | 0.01 | 300 | 50.4 | 41.5 | 11.0 |
| Upper Flange Axial Stress (MPa) | AS055 | 92.6 | 98.5 | -425 | 445 | 37.0 | 27.1 | 38.1 |
| Lower Flange Axial Stress (MPa) | AS056 | -92.6 | -98.5 | -425 | 445 | -75.8 | -59.0 | -36.4 |
| Front Flange Axial Stress (MPa) | AS057 | 0.0 | 0.0 | -425 | 445 | -20.3 | -7.6 | -4.8 |
| Rear Flange Axial Stress (MPa) | AS058 | 0.0 | 0.0 | -425 | 445 | -6.2 | -6.1 | 5.9 |

Table C.9 Comparison of rib 3 results of three optimization processes

| Rib 3 | | | | | | | | |
|---------------------------------|-----------|---------------|---------------------|-------------|-------------|-----------------------|---------------------|-------------------------------|
| Description | D.C. Name | Initial Value | | Lower Bound | Upper Bound | Property Optimization | | Property & Shape Optimization |
| | | Tip Loading | Distributed Loading | | | Tip Loading | Distributed Loading | Distributed Loading |
| Web Von Mises Stress (MPa) | AS059 | 2.8 | 7.0 | 0.01 | 300 | 48.6 | 23.2 | 9.0 |
| Upper Flange Axial Stress (MPa) | AS060 | 31.1 | 51.2 | -425 | 445 | 36.0 | 26.9 | 29.0 |
| Lower Flange Axial Stress (MPa) | AS061 | -31.1 | -51.2 | -425 | 445 | -48.1 | -33.5 | -30.3 |
| Front Flange Axial Stress (MPa) | AS062 | 0.0 | 0.0 | -425 | 445 | -4.6 | -5.9 | 0.5 |
| Rear Flange Axial Stress (MPa) | AS063 | 0.0 | 0.0 | -425 | 445 | -5.3 | 0.0 | -1.1 |

Table C.10 Comparison of rib 4 results of three optimization processes

| Rib 4 | | | | | | | | |
|---------------------------------|-----------|---------------|---------------------|-------------|-------------|-----------------------|---------------------|-------------------------------|
| Description | D.C. Name | Initial Value | | Lower Bound | Upper Bound | Property Optimization | | Property & Shape Optimization |
| | | Tip Loading | Distributed Loading | | | Tip Loading | Distributed Loading | Distributed Loading |
| Web Von Mises Stress (MPa) | AS064 | 0.1 | 3.9 | 0.01 | 300 | 6.4 | 36.4 | 13.4 |
| Upper Flange Axial Stress (MPa) | AS065 | -15.7 | 28.5 | -425 | 445 | -22.4 | 21.5 | 24.9 |
| Lower Flange Axial Stress (MPa) | AS066 | 15.7 | -28.5 | -425 | 445 | 19.4 | -15.0 | -24.9 |
| Front Flange Axial Stress (MPa) | AS067 | 0.0 | 0.0 | -425 | 445 | -0.9 | 2.1 | -0.3 |
| Rear Flange Axial Stress (MPa) | AS068 | 0.0 | 0.0 | -425 | 445 | -4.5 | 2.1 | 0.2 |

Table C.11 Comparison of rib 5 results of three optimization processes

| Rib 5 | | | | | | | | |
|---------------------------------|-----------|---------------|---------------------|-------------|-------------|-----------------------|---------------------|-------------------------------|
| Description | D.C. Name | Initial Value | | Lower Bound | Upper Bound | Property Optimization | | Property & Shape Optimization |
| | | Tip Loading | Distributed Loading | | | Tip Loading | Distributed Loading | Distributed Loading |
| Web Von Mises Stress (MPa) | AS069 | 7.3 | 3.4 | 0.01 | 300 | 45.1 | 2.7 | 8.9 |
| Upper Flange Axial Stress (MPa) | AS070 | -63.3 | 11.5 | -425 | 445 | -71.9 | 11.1 | 18.7 |
| Lower Flange Axial Stress (MPa) | AS071 | 63.3 | -11.5 | -425 | 445 | 43.5 | -12.9 | -18.7 |
| Front Flange Axial Stress (MPa) | AS072 | 0.0 | 0.0 | -425 | 445 | -14.6 | -0.6 | 0.1 |
| Rear Flange Axial Stress (MPa) | AS073 | 0.0 | 0.0 | -425 | 445 | -6.9 | -0.7 | 0.0 |

Table C.12 Comparison of rib 6 results of three optimization processes

| Rib 6 | | | | | | | | |
|---------------------------------|-----------|---------------|---------------------|-------------|-------------|-----------------------|---------------------|-------------------------------|
| Description | D.C. Name | Initial Value | | Lower Bound | Upper Bound | Property Optimization | | Property & Shape Optimization |
| | | Tip Loading | Distributed Loading | | | Tip Loading | Distributed Loading | Distributed Loading |
| Web Von Mises Stress (MPa) | AS074 | 28.8 | 2.2 | 0.01 | 300 | 98.0 | 0.8 | 2.4 |
| Upper Flange Axial Stress (MPa) | AS075 | -122.1 | 3.0 | -425 | 445 | -87.9 | 3.8 | 5.7 |
| Lower Flange Axial Stress (MPa) | AS076 | 122.2 | -3.0 | -425 | 445 | 50.1 | -2.9 | -5.7 |
| Front Flange Axial Stress (MPa) | AS077 | 0.0 | 0.0 | -425 | 445 | -24.7 | 0.5 | 0.0 |
| Rear Flange Axial Stress (MPa) | AS078 | 0.0 | 0.0 | -425 | 445 | -2.7 | 0.0 | 0.0 |

Table C.13 Comparison of rib 7 results of three optimization processes

| Rib 7 | | | | | | | | |
|---------------------------------|-----------|---------------|---------------------|-------------|-------------|-----------------------|---------------------|-------------------------------|
| Description | D.C. Name | Initial Value | | Lower Bound | Upper Bound | Property Optimization | | Property & Shape Optimization |
| | | Tip Loading | Distributed Loading | | | Tip Loading | Distributed Loading | Distributed Loading |
| Web Von Mises Stress (MPa) | AS079 | 11.7 | 1.1 | 0.01 | 300 | 47.9 | 1.7 | 1.5 |
| Upper Flange Axial Stress (MPa) | AS080 | -121.2 | 0.3 | -425 | 445 | -78.6 | 0.8 | 0.3 |
| Lower Flange Axial Stress (MPa) | AS081 | 121.2 | -0.3 | -425 | 445 | 50.4 | -1.1 | -0.3 |
| Front Flange Axial Stress (MPa) | AS082 | 0.0 | 0.0 | -425 | 445 | -18.7 | -0.1 | 0.0 |
| Rear Flange Axial Stress (MPa) | AS083 | 0.0 | 0.0 | -425 | 445 | 2.3 | 0.1 | 0.0 |

APPENDIX D.1

SAMPLE BDF-FILE FOR PROPERTY OPTIMIZATION

The bdf-file used in rectangular beam optimization is presented here. Original bdf-file entries are in bold characters.

At the beginning of the file descriptive information is given. A “\$” sign is used in the beginning of comments.

**\$ NASTRAN input file created by the MSC MSC.Nastran input file
\$ translator (MSC.Patran 13.1.116) on June 19, 2008 at 22:02:49.
\$ Direct Text Input for Nastran System Cell Section**

For this example there is no need for File Management Section . Therefore it is skipped. Only a comment is given to indicate its location.

\$ Direct Text Input for File Management Section

Next Executive Control Section takes place. Only SOL 200 statement is used in this section to indicate that optimization process will be performed.

**\$ Design Sensitivity and Optimization Analysis
SOL 200
\$ Direct Text Input for Executive Control
CEND**

Case Control Section starts here with title of the job.

TITLE = MSC.Nastran job created on 19-Jun-08 at 19:43:29

“ECHO= SORT,PUNCH(NEWBULK)” command provides initial bulkdata written in f06-file and final (optimized) bulk data in pch-file.

ECHO = SORT,PUNCH(NEWBULK)

“DESOBJ(MIN) = 1” indicates that the objective function is given in DRESP1 card with number 1. This card is in the design response section of the design model.

DESOBJ(MIN) = 1

“DESSUB = 21” indicates the active constraints group which is 21. Constraints are defined with DCONSTR” cards in the design constraints section of the design model

DESSUB = 21

In this optimization task linear static analyses are performed.

ANALYSIS = STATICS

\$ Direct Text Input for Global Case Control Data

At the end of the case control section applied load case is defined. In this example only one load case is implemented.

SUBCASE 1

\$ Subcase name : Default

SUBTITLE=Default

SPC = 2

LOAD = 2

DISPLACEMENT(SORT1,REAL)=ALL

SPCFORCES(SORT1,REAL)=ALL

STRESS(SORT1,REAL,VONMISES,BILIN)=ALL

Bulk Data Section is the last section .

BEGIN BULK

Following parameters are used to control output of analysis

PARAM POST -1

PARAM PRTMAXIM YES

PARAM NASPRT 1

\$ Direct Text Input for Bulk Data

Description of analysis model starts here.

Element property is defined first. PBARL card allows one to introduce cross section of bar element to MSC.NASTRAN®. “BAR” in this card indicates rectangular cross section. 10 and 35 are width (DIM1) and height (DIM2) of the cross section respectively.

\$ Elements and Element Properties for region : beam

**PBARL 1 1 BAR
10. 35.**

\$ Pset: "beam" will be imported as: "pbarl.1"

Elements are defined next.

**CBAR 1 1 1 2 0. 1. 0.
CBAR 2 1 2 3 0. 1. 0.
CBAR 3 1 3 4 0. 1. 0.
CBAR 4 1 4 5 0. 1. 0.
CBAR 5 1 5 6 0. 1. 0.
CBAR 6 1 6 7 0. 1. 0.
CBAR 7 1 7 8 0. 1. 0.
CBAR 8 1 8 9 0. 1. 0.
CBAR 9 1 9 10 0. 1. 0.
CBAR 10 1 10 11 0. 1. 0.**

Material definition is given in “MAT1” card. For weight optimization a value for density must be entered. For this example, elastic modulus is 7000. MPa, poissons ratio is 0.33 and density is 1. kg/mm³. In this case the value of the weight is equal to the value of volume in mm³.

\$ Referenced Material Records

\$ Material Record : al

\$ Description of Material : Date: 19-Jun-08 Time: 19:39:44

MAT1 1 70000. .33 1.

“GRID” cards are used to define the node locations

\$ Nodes of the Entire Model

**GRID 1 0. 0. 0.
GRID 2 50. 0. 0.
GRID 3 100. 0. 0.
GRID 4 150. 0. 0.
GRID 5 200. 0. 0.
GRID 6 250. 0. 0.**

```

GRID 7      300.  0.  0.
GRID 8      350.  0.  0.
GRID 9      400.  0.  0.
GRID 10     450.  0.  0.
GRID 11     500.  0.  0.

```

At the end of the analysis model definition loads and boundary conditions are defined.

```

$ Loads for Load Case : Default
SPCADD 2 1
LOAD 2 1. 1. 1
$ Displacement Constraints of Load Set : disproof
SPC1 1 123456 1
$ Nodal Forces of Load Set : yforce
FORCE 1 11 0 1250. 0. -1. 0.
$ Referenced Coordinate Frames

```

After end of the analysis model definition, design model description starts.

First design variables are defined. “DESVAR” card includes the number, name, initial value, upper bound and lower bound information of a design variable.

```

$ ...DESIGN VARIABLE DEFINITION
$ rect_W
DESVAR 1 rect_W:110. 1. 20. 1.
$ rect_H
DESVAR 2 rect_H:235. 20. 50. 1.

```

Design variable must be related to a property of elements in analysis model or shape basis vectors in shape optimization. “DVPREL1” card is used to relate a design variable to a element property in analysis model. Initial value of a design variable overwrites the corresponding value. DIM1 is the width of the rectangular cross section. Therefore, design variable 1 is related to the width of the rectangular cross section.

```

$ ...DEFINITION OF DESIGN VARIABLE TO ANALYSIS MODEL
PARAMETER RELATIONS
DVPREL1 1 PBARL 1 DIM1
1 1.
DVPREL1 2 PBARL 1 DIM2
2 1.

```

Design responses indicates which results are important for the optimization task.

\$...STRUCTURAL RESPONSE IDENTIFICATION

In this example total weight, y displacement of tip node and maximum stress at the root element are used as first type of response. Design response number 1 is the weight and chosen as objective function in case control section.

```
DRESP1 1 W WEIGHT  
DRESP1 27 U2 DISP 2 11  
DRESP1 37 S1 STRESS PBAR 7 1
```

An equation which is the height to width ratio of the cross section is used as the second type of design response.

```
DRESP2 15 BH 230  
DESVAR 1 2  
DEQATN 230 BH(W,H)= H/W
```

Next step is definition of constraints. “DCONSTR” card includes the constraint group number , which is 21 in this example, related design response number, upper and lower bounds for the design response.

```
$ ...CONSTRAINTS  
DCONSTR 21 27 -25.4 25.4  
DCONSTR 21 37 -700.0 700.0  
DCONSTR 21 15 0.1 5.0
```

Finally, maximum iteration number, number of fully stressed design cycles, frequency of the output, design quantities to be printed, convergence criteria and move limits on approximate optimization are defined by using “DOPTPRM” card [3].

```
$ ...OPTIMIZATION CONTROL  
DOPTPRM DESMAX 100 FSDMAX 0 P1 1 P2 1  
CONV1 .001 CONV2 1.-20 CONVDV .001 CONVPR .01  
DELP .2 DELX 1. DPMIN .01 DXMIN .05  
ENDDATA e4f673bf
```

This is the end of bdf-file

APPENDIX D.2

SAMPLE BDF-FILE FOR SHAPE OPTIMIZATION

The bdf-file used in wing torque box shape and property optimization is presented here. Original bdf-file entries are in bold characters. Repeated cards are omitted and replaced by "...".

At the beginning of the file descriptive information is given. A "\$" sign is used in the beginning of comments.

```
$ NASTRAN input file created by the MSC MSC.Nastran input file  
$ translator ( MSC.Patran 13.1.116 ) on October 21, 2008 at 20:43:46.  
$ Direct Text Input for Nastran System Cell Section  
$ Direct Text Input for File Management Section  
$ Design Sensitivity and Optimization Analysis
```

In File Management Section, result of auxiliary model analysis which is used to built shape basis vectors for shape optimization is introduced. The extensions of necessary result files are "MASTER" and "DBALL". Therefore, both files must exist in the folder where optimization is performed, but only MASTER-file is introduced in the bdf-file.

```
ASSIGN F1_AUX='wing_aux.MASTER'  
DBLOCATE DATABLK=(ug/ugd,geom1/geom1d,geom2/geom2d) ,  
LOGICAL=F1_AUX
```

Next Executive Control Section takes place. SOL 200 statement is used in this section to indicate that optimization process will be performed.

```
SOL 200  
TIME 600  
$ Direct Text Input for Executive Control  
CEND
```

Case Control Section starts here with title of the job.

TITLE = MSC.Nastran job created on 05-Oct-08 at 13:53:10

“ECHO= SORT,PUNCH(NEWBULK)” command provides initial bulkdata written in f06-file and final (optimized) bulk data in pch-file. Limitation is set by “MAXLINES” command.

**ECHO = SORT,PUNCH(NEWBULK)
MAXLINES = 999999999**

“DESOBJ(MIN) = 1” indicates that the objective function is given in DRESP1 card with number 1. This card is in the design response section of the design model.

DESOBJ(MIN) = 1

“DESSUB = 21” indicates the active constraints group which is 21. Constraints are defined with DCONSTR” cards in the design constraints section of the design model.

DESSUB = 21

In this optimization task linear static analyses are performed.

**ANALYSIS = STATICS
\$ Direct Text Input for Global Case Control Data**

At the end of the case control section applied load case is defined. In this example only one load case is implemented.

**SUBCASE 1
\$ Subcase name : Default
SUBTITLE=Default
SPC = 2
LOAD = 2
DISPLACEMENT(SORT1,REAL)=ALL
SPCFORCES(SORT1,REAL)=ALL
GPFORCE=ALL
STRESS(SORT1,REAL,VONMISES,BILIN)=ALL**

Bulk Data Section is the last section .

BEGIN BULK

Following parameters are used to control output of analysis “PARAM NASPRT 50” indicates that outputs of finite element analyses are recorded in every 50th iteration during optimization process.

```
PARAM POST -1  
PARAM PRTMAXIM YES  
PARAM NASPRT 50  
$ Direct Text Input for Bulk Data
```

Description of analysis model starts here. Element, property and material definitions, grid locations, multipoint constraints, load and boundary conditions are defined in this section.

```
$ Elements and Element Properties for region : 110020  
PSHELL 110020 1 1. 2 1  
$ Pset: "110020" will be imported as: "pshell.110020"  
CQUAD4 110020 110020 1120 1220 2220 2120  
...  
...  
...  
$ Elements and Element Properties for region : 711000  
PSHELL 711000 3 1. 2 3  
$ Pset: "711000" will be imported as: "pshell.711000"  
CQUAD4 711000 711000 7120 7220 7230 7130  
$ Elements and Element Properties for region : 112000  
PROD 112000 3 100.  
$ Pset: "112000" will be imported as: "prod.112000"  
CROD 112000 112000 1120 1220  
...  
...  
...  
$ Elements and Element Properties for region : 620300  
PROD 620300 3 100.  
$ Pset: "620300" will be imported as: "prod.620300"  
CROD 620300 620300 6230 7230  
$ Elements and Element Properties for region : 900000  
PSHELL 900000 3 5. 3 3  
$ Pset: "900000" will be imported as: "pshell.900000"  
CQUAD4 910101 900000 9121 9122 9132 9131
```

CQUAD4 910102 900000 9122 1120 1130 9132
CQUAD4 920101 900000 9221 9222 9232 9231
CQUAD4 920102 900000 9222 1220 1230 9232
\$ Elements and Element Properties for region : 900001
PBARL 900001 3 BAR
50. 20.
\$ Pset: "900001" will be imported as: "pbarl.900001"
CBAR 910201 900001 9121 9122 0. 1. 1.
...
...
...
CBAR 924002 900001 9222 9232 0. 1. 1.
\$ Referenced Material Records
\$ Material Record : AL2024
\$ Description of Material : Date: 04-Oct-08 Time: 20:45:10
MAT1 1 72000. .33 2.8E-6
\$ Material Record : AL7050
\$ Description of Material : Date: 04-Oct-08 Time: 20:45:10
MAT1 3 70000. .33 2.8E-6
\$ Material Record : dummy
\$ Description of Material : Date: 04-Oct-08 Time: 20:45:10
MAT1 2 1. .33 2.8E-6
\$ Multipoint Constraints of the Entire Model
RBE3 1 1000 123456 1. 123 1120 1130
1220 1230
...
...
...
RBE3 7 7000 123456 1. 123 7120 7130
7220 7230
\$ Nodes of the Entire Model
GRID 1000 516.788 29.6729 0.
GRID 1120 381.115 116.891 0.
...
...
...
GRID 9231 1010.6 -36.4019-662.
GRID 9232 1010.6 -36.4019-100.
\$ Loads for Load Case : Default
SPCADD 2 1
LOAD 2 1. 1. 1 1. 3 1. 4
1. 5 1. 6 1. 7 1. 8
1. 9 1. 10 1. 11 1. 12
1. 13 1. 14 1. 15
\$ Displacement Constraints of Load Set : root
SPC1 1 123 9121 9122 9131 9132 9221 9222

```

          9231  9232
$ Nodal Forces of Load Set : Rib_1
FORCE  1   1000  0  3091.16  0.  1.  0.
$ Nodal Forces of Load Set : Rib_1
MOMENT 3   1000  0  398.76  0.  0.  1.
...
...
...
FORCE 14   7000  0  1486.88  0.  1.  0.
$ Nodal Forces of Load Set : Rib_7
MOMENT 15   7000  0  229.46  0.  0.  1.
$ Referenced Coordinate Frames

```

After end of the analysis model definition, design model description starts.

First design variables are defined. “DESVAR” card includes the number, name, initial value, upper bound and lower bound information of a design variable.

```

$ ...DESIGN VARIABLE DEFINITION
$ v001
DESVAR 11  v001  1.  .8  5.
$ v002
DESVAR 12  v002  1.  .8  5.
...
...
...
$ v082
DESVAR 92  v082 100.  1.  2000.
$ v083
DESVAR 93  v083 100.  1.  2000.
$
$ Shape Optimization variables
$ v084
DESVAR 94  v084  1. -30.  30.
...
...
...
$ v088
DESVAR 98  v088  1. -30.  30.
$
$

```

Design variable must be related to a property of elements in analysis model or shape basis vectors in shape optimization. “DVPREL1” card is used to relate a

design variable to a element property in analysis model. Initial value of a design variable overwrites the corresponding value. “DVSHAP” card is used to relate a design variable to a shape basis vector which is constructed by using single load case result of analysis auxiliary model. For example, “DVSHAP 95 2 1.0” card indicates that design variable with number 95 is related with the shape basis vector which is constructed by using the result of second load case in auxiliary model analysis. “1.0” is the multiplication factor.

**\$...DEFINITION OF DESIGN VARIABLE TO ANALYSIS MODEL
PARAMETER RELATIONS**

**DVPREL1 11 PSHELL 110100 T
11 1.**

**DVPREL1 12 PSHELL 210100 T
12 1.**

...

...

...

**DVPREL1 92 PROD 714000 A
92 1.**

**DVPREL1 93 PROD 724000 A
93 1.**

\$

\$ A DVSHAP entry defines a shape basis vector by associating one design variable to a dblocated displacement vector.

\$

DVSHAP 94 1 1.0

DVSHAP 95 2 1.0

DVSHAP 96 3 1.0

DVSHAP 97 4 1.0

DVSHAP 98 5 1.0

\$

\$

\$

Design responses indicates which results are important for the optimization task.

\$...STRUCTURAL RESPONSE IDENTIFICATION

In this example total weight, y displacement of tip nodes, Von Mises stress at all shell element and axial stress at rod elements are used as first type of response.

Design response number 1 is the weight and chosen as objective function in case control section.

```

DRESP1 1 MinWeigh WEIGHT
$ Stress Responce
DRESP1 101 S101 STRESS PSHELL 11 110100
DRESP1 102 S102 STRESS PSHELL 11 210100
...
...
...
DRESP1 182 S182 STRESS PROD 2 714000
DRESP1 183 S183 STRESS PROD 2 724000
$ Displacement Responce
DRESP1 201 D201 DISP 2 7120
DRESP1 202 D202 DISP 2 7130
DRESP1 203 D203 DISP 2 7220
DRESP1 204 D204 DISP 2 7230

```

Next step is definition of constraints. “DCONSTR” card includes the constraint group number , which is 21 in this example, related design response number, upper and lower bounds for the design response.

```

$ ...CONSTRAINTS
DCONSTR 21 101 0.01 300.0
DCONSTR 21 102 0.01 300.0
...
...
...
DCONSTR 21 182 -425.0 445.0
DCONSTR 21 183 -425.0 445.0
$
DCONSTR 21 201 0.001 200.0
DCONSTR 21 202 0.001 200.0
DCONSTR 21 203 0.001 200.0
DCONSTR 21 204 0.001 200.0
$
$

```

Finally, maximum iteration number, number of fully stressed design cycles, frequency of the output, design quantities to be printed, convergence criteria and

move limits on approximate optimization are defined by using “DOPTPRM” card [3].

```
$ ...OPTIMIZATION CONTROL  
DOPTPRM DESMAX 5000 FSDMAX 0 P1 50 P2 5  
CONV1 .001 CONV2 1.-20 CONVDV .001 CONVPR .01  
DELP .2 DELX 1. DPMIN .01 DXMIN .05  
ENDDATA e0fc0b62
```

This is the end of bdf-file